Electrical Breakdown and Mechanical Ageing in Dielectric Elastomers

Zakaria, Shamsul Bin

Publication date:
2016

Document Version
Publisher's PDF, also known as Version of record

Electrical Breakdown and Mechanical Ageing in Dielectric Elastomers

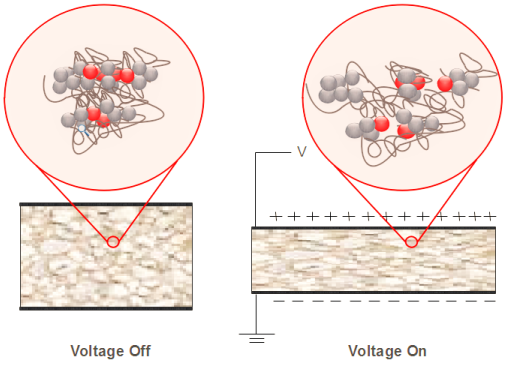

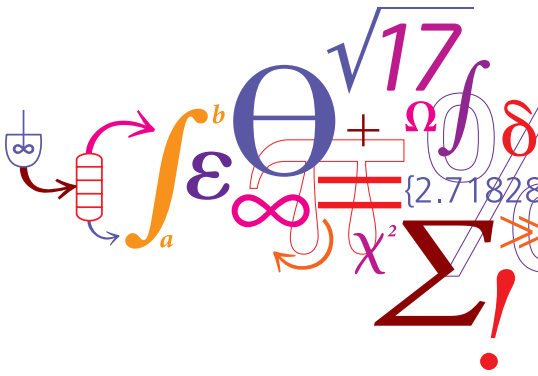

Shamsul Bin Zakaria

PhD Thesis

January 2016

DTU Chemical Engineering
Department of Chemical and Biochemical Engineering

Electrical Breakdown and Mechanical Ageing in Dielectric Elastomers

Shamsul Bin Zakaria
January, 2016
Supervisor: Anne Ladegaard Skov

PhD Thesis
Danish Polymer Centre, Department of Chemical and Biochemical Engineering,
Technical University of Denmark, Kongens Lyngby

PREFACE

This thesis presents the results of my Ph.D project carried out at the Danish Polymer Centre (DPC), Department of Chemical and Biochemical Engineering, Technical University of Denmark (DTU). This work was performed during the period from January 2013 to January 2016 under supervision of Professor Dr. Anne Ladegaard Skov. This Ph.D project was funded by the Ministry of Education, Malaysia and Universiti Malaysia Pahang. Danfoss PolyPower A/S is also acknowledged for financial support.

I would like to express my sincere gratitude to my supervisor for her full support throughout this project. Her guidance, support and encouragement during these three years were extremely fortunate for me. I am really blessed to have a very committed supervisor correcting my articles very patiently.

I am grateful to all the people at the Danish Polymer Centre. I would like to thank to Dr. Liyun Yu for her help and useful suggestion on my experiments. I would to thank to Kim Chi Szabo for running TGA and DSC for my samples.

I also would like to thank to the people from the workshop for technical support. I thank to Ivan H. Pedersen and the entire worker for designing and making the static stretch frame for me which significantly improved my experiments.

I would also like to thank to Associate Professor Dr. Peter Morshuis from University Technology of Delft, Dr. Mohammed Benslimane Yahia from Danfoss Polypower A/S, Dr. Guggi Kofod from Inmold A/S, Dr. Frederikke Bahrt Madsen and all the co-authors for the pleasant collaboration of our joint papers.

Finally, I wish to thank my parents and parents in law, my beloved wife, my adorable son, my siblings and siblings in law, and my fellow friends for their loving support and encouragement.

Shamsul Bin Zakaria
January, 2016

"In the name of Allah, most Gracious, most Compassionate"

Untuk Siti dan Hakeem yang tersayang

CONTENTS

ABSTRACT

Dielectric elastomers (DE) are used in various applications, such as artificial eye lids, pressure sensors and human motion energy generators. For many applications, one of the major factors that limits the DE performance is premature electrical breakdown. There are many approaches that have been reported to increase the breakdown strength of DEs such as compositing and pre-stretching. Some of the techniques, however, affect other parameters related to DEs negatively. For instance, the elastomers with *hard* filler particles (e.g. metal oxides) used as DEs experience difficulties to maintain their long-term mechanical reliability as they are susceptible to Mullins effects as the results of pre-stretching. Therefore, two strategies are developed in this thesis in order to produce DEs with high electrical performance and long-term electromechanical reliability. The first strategy is to study the mechanisms behind the electrical breakdown of DEs and the second strategy is to investigate the long-term electromechanical reliability of DEs. In the first strategy, the electrothermal breakdown in polydimethylsiloxane (PDMS) elastomers was modelled in order to evaluate the thermal mechanisms behind the electrical failures. From the modelling based on the fitting of experimental data, it showed that the electrothermal breakdown of the PDMS elastomers was strongly influenced by the increase in both relative permittivity and conductivity. In addition to that, a methodology in determining the parameters that affect the breakdown strength of the pre-stretched DEs was developed. Breakdown strength was determined for samples with and without volume conservation and was found to depend strongly on the strain and the thickness of the samples.

In order for DEs to be fully implementable in commercial products, the lifetime of elastomer materials needs further investigation. Therefore, in the second strategy, several DE parameters such as Young's moduli, breakdown strengths and dielectric permittivities of PDMS elastomers filled with *hard* filler particles were investigated after being subjected to pre-stretching for various timespans. The study showed that electromechanical reliability when pre-stretching was difficult to achieve with PDMS elastomers filled with *hard* filler particles. Subsequently, the long-term mechanical and electrical reliability was further investigated to the PDMS elastomers filled with the *soft* fillers (e.g. oils). Interestingly, the results also showed that *soft* fillers significantly influence the long-term electromechanical reliability of PDMS elastomers. However, despite the pre-stretched PDMS elastomers filled with *hard* and *soft* filler experience difficulties to maintain their long-term electromechanical reliability, the study paves the way for electromechanically reliable DEs by indicating that simply post-curing PDMS elastomers before use.

Therefore in the last part of this thesis, the effect of post-curing was investigated for PDMS elastomer thin-films as a means of improving the long-term elastomer film electromechanical reliability. The PDMS elastomers were found to contain less than 2% of volatiles but nevertheless a strong effect from post-curing was observed. Furthermore, the determined electrical breakdown parameters from Weibull analyses showed that greater electrical reliability could be achieved by post-curing the PDMS elastomers before usage, and this method therefore paves a way towards more electromechanically reliable DEs.

RESUME PÅ DANSK

Dielektriske elastomerer (DE'er) bliver anvendt i mange forskellige applikationer såsom kunstige øjenlåg, tryksensorer og bevægelsesenergi-generatorer. For de fleste applikationer er en af de største hindringer præmatur elektrisk sammenbrud. Der er mange tiltag til at løse dette problem, herunder kompositfremstilling og præstræk. Mange af disse løser problemet med præmaturt sammenbrud, men samtidigt ødelægger de andre favorable egenskaber. For eksempel oplever elastomerer med "hårde" fyldstoffer såsom metaloxider en kraftig reduktion i mekanisk stabilitet over tid. Derfor udvikledes to strategier i dette arbejde til produktion af DE'er med høj elektrisk performance og langtidsstabilitet. Den første strategi var at studere mekanismerne bag elektrisk sammenbrud af polydimethylsiloxan (PDMS) elastomerer, og den anden strategi var at undersøge den mekaniske langtidsstabilitet af dielektriske elastomerer. I den første strategi blev eksperimentelle data analyseret med hensyn til en udviklet model, der kunne redegøre for termiske effekter, der kunne være bevirkende til elektrisk sammenbrud. Det blev vist, at elektrotermisk sammenbrud var stærkt afhængigt af både dielektrisk permittivitet og konduktivitet. Desuden blev der udviklet en metode til at separere forskellige effekter af præstræk på elektrisk sammenbrud. Dette blev vist ved hjælp af målinger med og uden volumebevarelse. Det blev vist, at præstræk har en fundamental og positiv indflydelse på det elektriske sammenbrud.

For at DE'er skal være implementerbare i kommercielle produkter er det vigtigt at undersøge den mekaniske livstid under stræk nøjere, hvis præstræk ønskes anvendt. Derfor blev der i anden del af afhandlingen fokuseret på at studere adskillige relevante DE parametre, såsom dielektrisk permittivitet, sammenbrudsstyrke og Young's modul, af elastomerer med både hårde fyldstoffer og bløde fuldstoffer såsom olier. Begge typer af fyldstoffer forårsagede reduktion i langtidsstabiliteten af elastomererne over tid. Det blev dog vist, at disse stabilitetsproblemer kunne undgås, hvis elastomererne blev post-hærdet inden brug. Derfor blev sidste del af afhandlingen fokuseret på at undersøge indvirkningen af post-hærdning på de elektromekaniske egenskaber over tid. Elastomererne blev undersøgt til maksimalt at have 2% flygtige stoffer efter traditionel hærdning men alligevel sås der en kraftig, positiv effekt af post-hærdning. Efter post-hærdningen kunne det konkluderes efter Weibull analyse, at der var specifikt opnået en større elektrisk pålidelighed af elastomererne, og fundet af denne simple procedure forventes at kunne bevirke pålidelige dielektriske elastomerer i fremtiden.

1 INTRODUCTION

Discovered in the early 1990s, dielectric elastomers (DEs) constitute an aspiring and advanced material technology. The DE technology is evolving quickly, whether measured by the number of research studies published or the variety of potential applications developed, which, undoubtedly, attracts many researchers with diverse scientific backgrounds and disciplines.

Early development of DE technology was inspired by work done by Kornbluh et al. [1] as they presented at the 4th world conference on robotics research in Pittsburgh, emphasised to the investigation into new actuation technology that can mimic natural soft muscle. This class of actuation technology gave a new perspective in the robotic fields at that time. The fundamental work done by Pelrine et al. [2] and Kornbluh et al. [3] at the SRI International showed a thin elastomer film sandwiched between compliant electrodes giving an actuation response inspired to the rapid growth of soft actuation technology at that time.

At present, as the DEs field matures, the fundamental understanding of materials is very important as a greater demand on elastomers to be synthesized and optimized specifically as DE is crucial. It seems likely in the near future, DEs will be recognised with a performance far superior than in the past since the DE research and development has tremendously grown from in the early 1990s to become one of important advanced material today.

1.1 THESIS OBJECTIVES AND OUTLINES

In the present thesis, the electrical breakdown and the mechanical ageing of DEs were investigated. A better understanding of these two aspects may help in designing and developing of mechanically and electrically reliable DE based devices.

The objectives of this PhD project are as follows:

1) To predict the electrothermal breakdown of polydimethylsiloxane (PDMS) elastomers with respect to the DEs at a given electric field.
2) To characterize several parameters related to breakdown measurements of the pre-stretched PDMS elastomers, namely the specimen volume, specimen thickness, specimen strain and electrode configuration.
3) To investigate long-term mechanical and electrical reliability of pre-stretched PDMS elastomers with different permittivity enhancing techniques; compositing, covalent grafting of high-permittivity moieties and blending in of high-permittivity oils.
4) To investigate the effects of post-curing on the mechanical and electrical reliability of PDMS elastomers with and without additional permittivity enhancing fillers.

The thesis is divided into two main parts, where Part I comprises Chapters 2 and 3 which focus on electrical breakdown occurrences in DEs. Chapter 2 deals with electrothermal breakdown phenomenon in DEs. The modelling based on the fitting of the experimental data of this phenomenon was implemented and discussed in context of DE electrical breakdown. Chapter 3 involves the characterisation of parameters related to electrical breakdown measurements of DEs. In order to understand the mechanisms behind the electrical breakdown of DEs, the methodology involved in determination of the parameters that affect the breakdown strength of the pre-stretched DEs such as volume, thickness and strain of the elastomeric specimen, as well as electrode configuration.

Secondly, Part II comprises Chapters 4, 5 and 6 which focus on the factors and strategies in order to produce a DE with long-term mechanical and electrical reliable. Chapters 4 and 5 discuss the mechanical ageing of several PDMS elastomer systems which were formulated by different permittivity enhancing techniques. In order to understand the intrinsic mechanical ageing in the systems, these elastomers were pre-stretched for various timespans. The expected change of mechanical properties due to the pre-stretching thus affected the other DEs related parameters such as the breakdown strength and relative permittivity. Chapter 6 presents a discussion of strategy for a long-term mechanical and electrical reliability of the DEs through an effective thermal post-treatment approach of the cured PDMS elastomers, commonly known as post-curing.

A conclusion and an outlook for future work can be found in Chapter 7.

The thesis is based on the manuscripts listed below, which can be found in the following appendices:

Appendix A:
Zakaria S, Morshuis PHF, Benslimane MY, Gernaey KV, Skov AL, (2014) ***The electrical breakdown of thin dielectric elastomers: thermal effects.*** Proceeding of SPIE, Electroactive Polymer Actuators and Devices (EAPAD) California, USA 90562V–1–10.

Appendix B:
Zakaria S, Morshuis PHF, Benslimane MY, Yu L, Skov AL, (2015) ***The breakdown strength of pre-stretched elastomers, with and without sample volume conservation.*** Smart Materials and Structures 24:055009.

Appendix C:
Zakaria S, Yu L, Kofod G, Skov AL, (2015) ***The influence of static pre-stretching on the mechanical ageing of filled silicone rubbers for dielectric elastomer applications.*** Material Today Communication 4: 204-215.

Appendix D:
Madsen FB, Zakaria S, Yu L, Skov AL, (2015) ***Mechanical and electrical ageing effects upon long-term stretching of silicone dielectric elastomers with soft fillers***.
Submitted to Smart Structures and Materials.

Appendix E:
Zakaria S, Madsen FB, Skov AL, (2015) ***Post-curing as an effective means for a long-term mechanical reliability of PDMS thin-films for dielectric elastomer applications.*** Submitted to Macromolecular Materials and Engineering.

Other publications (not included in the thesis):

Yu L, Vudayagiri S, Zakaria S, Benslimane MY, Skov AL, (2014) ***Filled liquid silicone rubbers: possibilities and challenges.*** Proceeding of SPIE, Electroactive Polymer Actuators and Devices (EAPAD) California, USA: 90560S.

Vudayagiri S, Zakaria S, Yu L, Hassouneh SS, Benslimane M, Skov AL, (2014) ***High breakdown-strength composites from liquid silicone rubbers.*** Smart Materials and Structures 23: 105017.

1.2 DIELECTRIC ELASTOMERS (DEs)

When a DE sandwiched between two compliant electrodes is subjected to a voltage, Maxwell stress is generated. The electrostatic pressure is formed when charge flows through an external conducting connector from one electrode to the other and creates opposite charges on the two electrodes. For the DE to deform, the electrodes must be compliant to the DE deformation. The electrostatic pressure then squeezes the elastomer in thickness and as the elastomer is incompressible, the pressure consequently results in a lateral expansion as shown in **Figure** 1.1. This operation of the transducer converts electrical energy into mechanical energy. When the external voltage is switched off, the elastomer film then returns to its original shape due to the elasticity. This working principle shows how a DE can be used as an actuator.

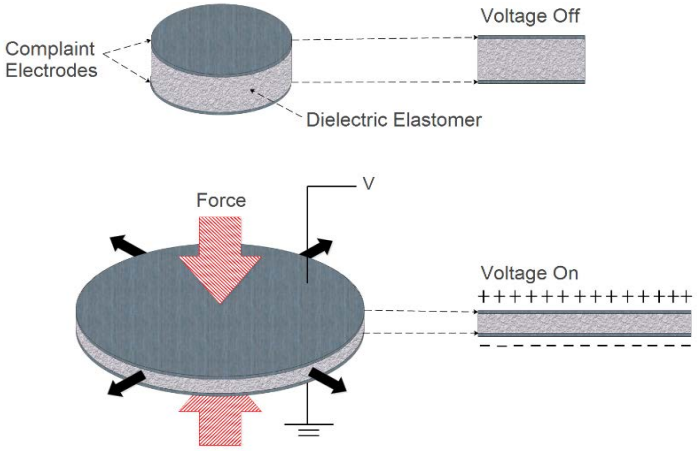

Figure 1.1: Schematic illustration of the actuation working principle of DEs.

Interestingly, DEs can also be used as a generator to create electrical energy as the working principle is the inverse of an actuator, which can be explained as follows. A thin elastomer sandwiched between two compliant electrodes is stretched by an external mechanical force and electrical charges are placed on the elastomer film. When the film is allowed to contract, opposite charges on the two electrodes are pushed further apart as the thickness of elastomer increases, while similar charges are brought closer together as the area of the elastomer is decreasing (charge density increases), thus increasing electrical energy [4]. Therefore, in this case, mechanical energy is converted to electrical energy. The generator's working principle can be seen in **Figure** 1.2.

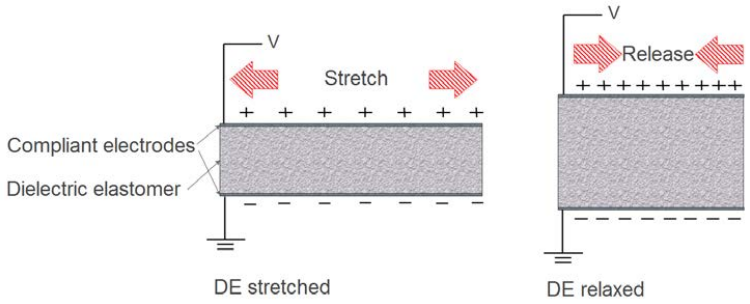

Figure 1.2: The basic mechanism of DE generator mode.

DEs can also be used as a sensor. When an elastomer sandwiched between two compliant electrodes through which a constant current is flowing, any external force that deforms (e.g. stretching) the DE, changes the capacitance of the elastomer. As the change in capacitance is proportional to the square of the DE strain ratio [5], thus the signal can be measured to be used as a sensor.

1.3 ELASTOMERS

In this thesis, PDMS elastomers were chosen as the investigated elastomer as they have outstanding properties such as high in efficiency and fast response times [6]. One prominent advantage over other elastomers is lower viscous loss, which means that it can maintain the mechanical stability and integrity of the elastomer even it subjected at higher frequencies. In addition to that, PDMS elastomers can be operated at a broader temperature range [6]. The example of performance of PDMS elastomers as DEs is shown in **Table** 1.1 which was adapted from [5, 6].

Table 1.1: Performance of the best PDMS elastomers (including pre-stretched PDMS elastomer films).

Parameter	Value	Comment
Maximum actuation strain (%)	120	-
Maximum frequency response (Hz)	>50 000	-
Maximum electric field (V/µm)	350	Maximum fields are attainable only in uniform pre-stretched films with few defects
Relative dielectric constant	2.5–3.0	Measured at 1 kHz
Dielectric loss factor	<0.005	Measured at 1 kHz
Elastic modulus (MPa)	0.1–2.0	-
Mechanical loss factor	0.05	-
Lifetime (cycles)	>10 000 000	Lifetime is highly dependent on how close the driving voltage is to the maximum field
Temperature operating range (°C)	-100 to 260	-

Despite of many excellent properties, PDMS elastomers are intrinsically weak as their tear and tensile strength are relatively low compared to e.g. the acrylic-based elastomer VHB^{TM} from 3M^{TM}. Therefore, in order to get a better performance, usually micro/nano-particles are added as fillers in the PDMS elastomers. The most common and efficient mechanical reinforcing filler for PDMS elastomers is silica (SiO_2).

1.4 ELECTRICAL BREAKDOWN

In DEs, there are several categories of mechanisms that lead to the electrical breakdown which can generally be classified by the range of electric fields and timescales by which they occur. **Figure** 1.3 presents the electrical breakdown regions that normally occur in power cable polymers (e.g. polyethylene). Cross-linked polymers with very soft and elastic properties such as PDMS elastomers used in this thesis are generally physically and chemically different from non-crosslinked or lightly crosslinked polyethylenes which are commonly used as power cable polymers. Therefore, directly adapting and translatingelectrical breakdown mechanisms of polyethylene to PDMS elastomers is not possible. However, several studies to investigate the electrical breakdown mechanisms of DEs have been successfully performed where the electrical breakdown mechanisms in power cable polymers are used as reference. For example, through comparison of electromechanical breakdown mechanisms in polyethylene to a thermoplastic dielectric elastomer, it was found that breakdown strength of DEs depends on the Young's modulus [7].

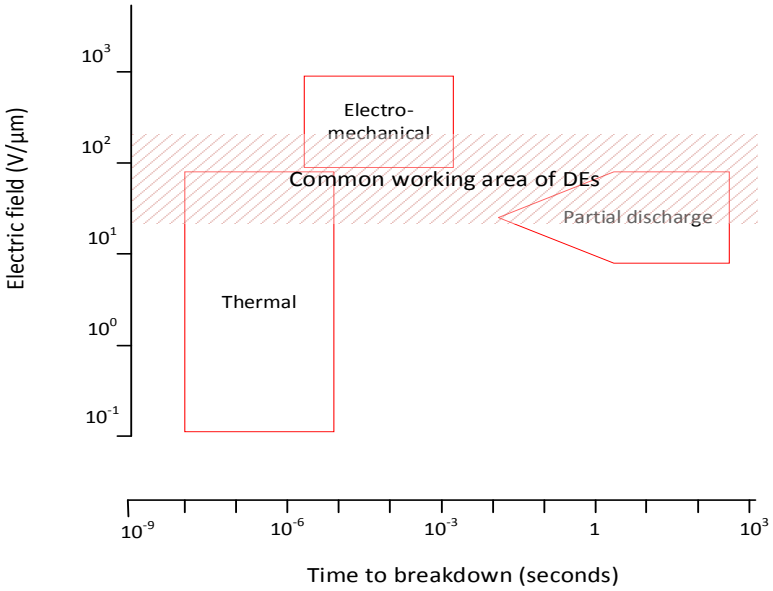

Figure 1.3: The electric fields and timescales in which the electrical breakdowns occur.[8]

For DEs, high breakdown strength is desirable so that premature failure as shown in **Figure** 1.4 can be prevented. Therefore, a thorough study on the electrical breakdown of DEs should be done in order to understand the mechanisms behind this electrical failure. Several examples of the electrical breakdown mechanisms in power cable polymers are discussed in the next subsections (1.4.1-1.4.3).

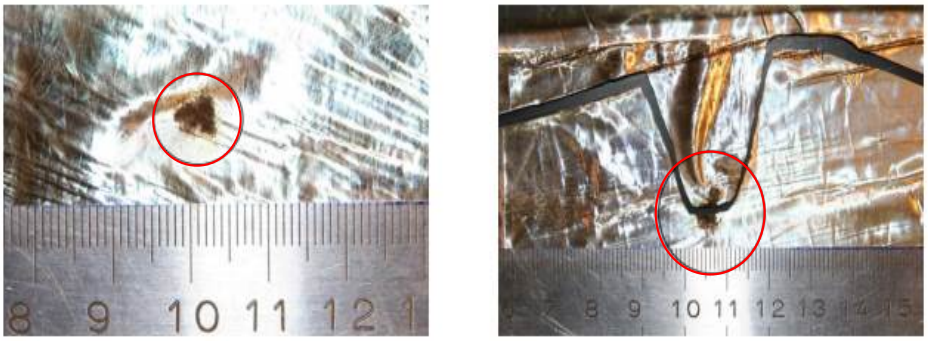

Figure 1.4: Electrical breakdown causes a pinhole formation on DEs film leading to major damage of the DE based devices. [9].

1.4.1 Electromechanical breakdown

Stark and Garton [10] reported that the electrical stress at the local regions of a DE may give rise to a localized thinning (now well-known as the Stark and Garton thinning process) due to its softness. Subsequently, the electric field increases locally due to that the DE decreases in thickness, and thereby increases the electrostatic forces further. In addition to that, Blok and LeGrand [11] considered the local regions that are subjected to higher-than-average electric fields and experienced a shear stress have a tendency to form an indentation. The indentation generates an inhomogeneous field creating a sharp notch causing the material to push radially away by an amount depending on the DE's Young's modulus. If the voltage exceeds the critical voltage, the DE will short-circuit due to cavity formation.

1.4.2 Electrothermal breakdown

Electrothermal breakdown occurs when the heat generated inside the DE cannot be balanced by heat lost to the surrounding.[8] The electrical power dissipation causes heating of at least part of the elastomer to higher than a critical temperature which results in failure [8]. In other words, when a voltage is applied to a DE, electrical power will be dissipated, and the temperature will increase. This local heating causes the electrical power dissipation increases causing a further increase in temperature (thermal runaway) [12]. If the temperature exceeds the critical temperature, electrothermal breakdown will occur.

1.4.3 Partial discharge

The formation of small voids is inevitable in DEs, even in the most carefully prepared elastomers. The gas inside the voids has lower permittivity and breakdown strength than the polymer matrix. When the applied voltage is raised, low relative permittivity gas inside the voids will give rise to electric field [8]. Subsequently, the gas in the void will breaks down before the polymer matrix. These discharges that formed due to electrical breakdown inside the voids erode the void's walls and eventually result in DE failure. The condition which partial discharges can be initiated depends on several factors such as the gas pressure, void shape as well as void size [8]. This phenomenon is called partial discharge as this condition does not necessarily cause the whole polymer to breakdown immediately. However, for a very thin DE, partial discharge may rapidly lead to failure [8].

1.5 OTHER IMPORTANT ELASTOMER PARAMETERS

In elastomer optimisation, the modification of one parameter often affects other parameter(s) in negative way. Therefore, several other important DE parameters should be carefully considered during elastomer optimisations.

1.5.1 Relative permittivity and dielectric loss

Relative permittivity (ε_r) is the ratio of the storage permittivity of a dielectric to the storage permittivity of vacuum (8.854×10^{-12} F/m). When an electric field is applied, the dielectric is polarized, where the dipoles inside of a dielectric will align with the field as shown in **Figure** 1.5. A PDMS elastomer typically have relative permittivity at around 2.0-3.0.

Dielectric loss can be expressed in terms of the loss tangent, as $\tan \delta = \varepsilon''/\varepsilon'$, where ε' is the storage permittivity and ε'' is the loss permittivity. The ε'' can be attributed to dipole relaxation phenomena, which give rise to energy loss.

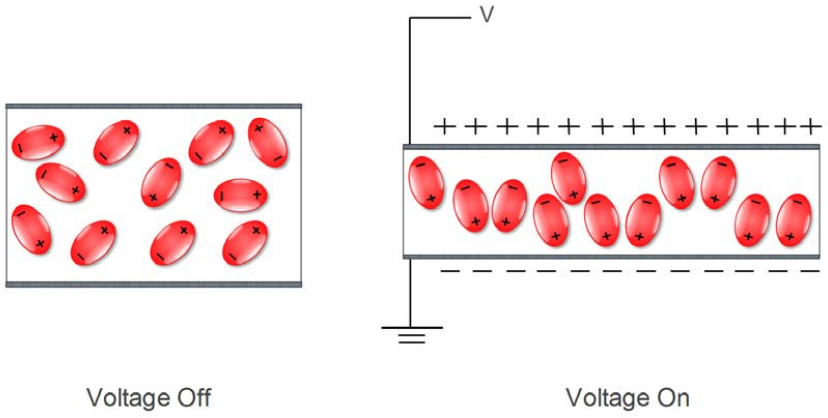

Figure 1.5: Schematic illustration of dipoles alignment in a dielectric when not subjected (left) and subjected to an electrical field (right).

1.5.2 Young's modulus and viscous loss

The elastic and viscous properties of PDMS elastomers are well expressed by

$$G^* = G'(\omega) + iG''(\omega) \qquad \text{Eq. 1.1}$$

where G* is the shear complex modulus and ω is the frequency, *G'* is the shear storage modulus, and *G''* is the shear loss modulus which attributed to the viscous

properties of the elastomers. Poisson's ratio (ν) of PDMS elastomers is close to 0.5 due to incompressibility [13]. The Young's modulus can be determined as $Y = 2(1+\nu)G$, where $G = G'(\omega \to 0)$.

The Young's modulus can also be determined by the gradient of the stress-strain graph in the linear regime of viscoelasticity of a polymer (where Hooke's law is obeyed), $Y = \partial\sigma/\partial s$.

The viscous loss which can be expressed in terms of the loss tangent, tan δ, as tan $\delta = G''/G'$.

1.6 ELASTOMER OPTIMISATION

Elastomer optimisation for DEs is usually performed on the basis of the equation for actuation strain developed by Pelrine et al. [14]. In this equation, the DEs related parameters such as Young's modulus, relative permittivity, and the thickness, *d* of the elastomer film is correlated according to

$$s = -\frac{\varepsilon_r \varepsilon_0}{Y}\left(\frac{V}{d}\right)^2 \qquad \text{Eq. 1.2}$$

where ε_0 is vacuum permittivity and *V* is the voltage.

For PDMS elastomer, the optimisation is often done with the purpose of increasing the relative permittivity as this elastomer exhibits lower relative permittivity compared to other DEs such as VHB. Therefore, various techniques have been reported in order to increase the relative permittivity of PDMS elastomers, most commonly through the incorporation of permittivity enhancing fillers [15–20]. This compositing technique, however, does increase the Young's modulus of the PDMS elastomer and thereby reduces obtainable actuation strain [20]. In addition to that, the incorporation of filler particles to the PDMS elastomers (compositing) possibly leads to a less controlled elastomer processing as this technique does rely on efficient mixing of filler particles. Therefore, several other techniques have been reported such as chemically grafted organic dipoles to the PDMS elastomer network [21–23], blending in of high-permittivity oils [24], and interpenetrating networks [25–29], which successfully increase relative permittivity of the PDMS elastomers.

In order to remove the dangers associated with high voltage, to enhance commercial viability of DE devices [6] and to increase the breakdown strength [30], decreasing the thickness of the DEs is an excellent approach. This approach, however, is limited

by the thin elastomer film's processing technology availability as the lowest thickness of the available large scale processing of elastomer film at the present time is 40 μm [31].

The actuation performances can also be improved by reducing the Young's modulus of DEs. Several techniques have been developed to decrease the Young's modulus of DEs, such as bimodal networks [32] and solvent techniques [33]. However, these approaches of material optimisation in DEs is not favourable as the DE with low Young's modulus displays poor breakdown strength [34].

Sommer-Larsen and Larsen [35] correlated relative permittivity, Young's modulus, and breakdown strength of elastomers into a single parameter, known as the figure of merit (F_{OM}) to measure the static performances of DEs as actuators. This equation is derived from the equilibrium deformation for an actuator under a constant applied voltage and external load [35]. Therefore, this equation can be applied for the DE actuation only and can be expressed as

$$F_{OM} = \frac{3\varepsilon_r \varepsilon_0 E_{BD}^{\ 2}}{Y} \qquad \text{Eq. 1.3}$$

where E_{BD} is the breakdown strength.

The attempt to increase the breakdown strength of DEs is favourable in DE optimisation. From the F_{OM} equation, of all the elastomer properties, the breakdown strength is the most important, since the output is proportional to the electric field to the second power. Several approaches have been reported in order to improve the breakdown strength of DEs which will be discussed in the next section in detail.

1.7 BREAKDOWN STRENGTH ENHANCING STRATEGIES

There are many strategies that have proven to increase the breakdown strength of DEs such as compositing [19, 20], pre-stretching [14, 30, 36, 37], effective electrode configurations [37] and elastomer processing technique [38]. The breakdown strength enhancement of the DEs, however, is not a trivial pursuit. For instance, the electrode size [37] and sample thickness [30] are the parameters that affect the breakdown strengths of DEs, however, these parameters are not considered in experimental designs of breakdown measurements as well as in reported data in many studies. Therefore, some of the published data may not be comparable resulting to the investigation of the breakdown strength of DEs is scarce. Therefore, standard procedures in breakdown measurements should be developed to prevent

the unstandardized breakdown data. For that reason, Carpi et al. [39] recently reported a set of standards for DE transducers, which highlighted the standard procedures that are recommended to be followed in the breakdown measurements of DEs.

1.7.1 Filler

In 2010, Molberg et al. [19] encapsulated conductive polyaniline (PANI) particles using mini-emulsion polymerization of divinylbenzene. They found that the breakdown strength for the composites showed small deviations to the reference PDMS elastomer breakdown strength, except for the composite containing the highest amount of filler (32 vol.%) and Young's modulus where a deviation of 20% was observed. In 2014, Vudayagiri et al. [20], incorporated permittivity enhancing fillers into liquid PDMS elastomer and room-temperature vulcanisable PDMS elastomer, and several types of fillers were used; an anatase TiO_2, a core–shell TiO_2-SiO_2 and a calcium copper titanate (CCTO), $CaCu_3Ti_4O_{12}$. They obtained a very high breakdown PDMS elastomer composite which contained SiO_2-TiO_2 filler (173 V/μm). They proposed that the high Young's modulus of the PDMS elastomer composite preceded the increase of the breakdown strength of DEs.

1.7.2 Mechanical properties

A study on the effect of Young's modulus on the breakdown strength of DE was performed with focus on different elastomer processing techniques. In 2009, Kollosche et al. [38] studied the effects of elastomers preparation processing steps of tri-block thermoplastic elastomers on the breakdown strength of DEs. The elastomers were prepared by either direct hot-pressing of the formulations, or by dissolving in toluene, centrifuging and drop-casting. They reported that the prepared tri-block thermoplastic elastomers (poly-styrene-ethylene-butadiene-styrene (SEBS)) showed large differences in mechanical properties, and compare them to the commonly used VHB. They found that centrifuged and drop-casted films were seen to be softer than hot-pressed films. They also suggested that the breakdown strength is dependent on the stiffness of the elastomers.

In 2010, Kollosche et al [34] investigated the stiffness dependence of the breakdown strength of soft elastomers (SEBS) without pre-stretching, and they found that the breakdown strength increases in line with the Young's modulus. In 2014, Yu et al [40] also investigated various types of filled PDMS elastomers in the un-stretched state and found that breakdown strength could be approximated proportionally to the Young's modulus.

As high Young's modulus can delay the rapid thinning due to electromechanical instability (EMI) of activated DEs, thus, the DEs with high Young's modulus show high breakdown strengths [8]. However, high Young's modulus of DEs is not favourable for DE actuators as high Young's modulus of DEs exhibit low electromechanical actuation strain.

1.7.3 Electrode configuration

Tröls et al. [37] studied the effect of the electrode configuration on the breakdown strength of acrylic elastomer VHB 4910 and natural rubber ZruElast™ A1040™. Two electrode configurations (**Figure** 1.6) were used for the measurement of the stretch dependence of the breakdown strength of DEs, and the breakdown strengths for compliant and rigid electrodes on the elastomer were compared. They found that breakdown strengths depended on the electrode configuration, being lower when compliant electrodes were used instead of rigid electrodes under clamped conditions. They suggested that the breakdown strength measured with rigid electrodes under clamped conditions revealed the true material limit, while the lower values with compliant electrodes may be caused by the EMI.

Tröls et al. [37] also reported the effects of electrode size on breakdown strength of DEs. They tested the breakdown of VHB and natural rubber and they found that the breakdown strength decreased with increasing area, probably due to material imperfections.

As the electrode size increases, the volume of tested sample also increases as the thickness of the elastomer remains constant. Therefore, it can be postulated that during breakdown measurement, the constant volume of tested samples is recommended in order to obtain comparable data.

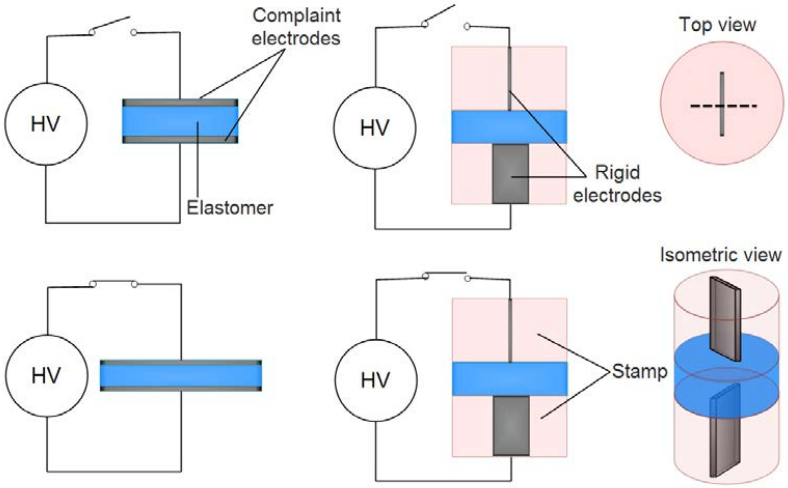

Figure 1.6: Experimental setup designed by Tröls et al. [37] for breakdown measurements with compliant and rigid electrodes. The mechanical clamping between the stamps prevents the elastomer from deforming electromechanically under high voltage.

1.7.4 Pre-stretching

The favourable effect of pre-stretching on breakdown strength has been discussed by severable research groups. Pre-stretching of DEs was firstly introduced by Pelrine et al. [36] as they found that actuated strains up to 117% were achievable with silicone elastomers, and up to 215% with VHB using biaxially and uniaxially pre-stretched films. They also reported that large actuation strains obtained were due to the application of high pre-stretch, which additionally increased the electrical breakdown strength of DEs. Pre-stretched VHB and (Radial pre-stretched (~100% and ~230% biaxial) and un-stretched acrylic elastomers (VHB) with solid metal electrodes have also been tested by Muffoletto et al. [41]. They found that the number of partial discharges steadily increases as the applied voltage increases up to a certain level, where the partial discharges suddenly cease. They suggested, that pre-stretching improves DEs performance as the improved breakdown strength following pre-stretching was caused by the favourable realignment of material imperfections, such as voids and micro-cracks. Huang et al. [30] studied the dependence of the thickness on breakdown strength of VHB. A testing geometry (**Figure** 1.7) that prevents displacements of the electrodes during breakdown measurements was used to determine breakdown strengths for the commonly

investigated VHB. The breakdown strength of DEs was found to depend on both thickness and the biaxial pre-stretching.

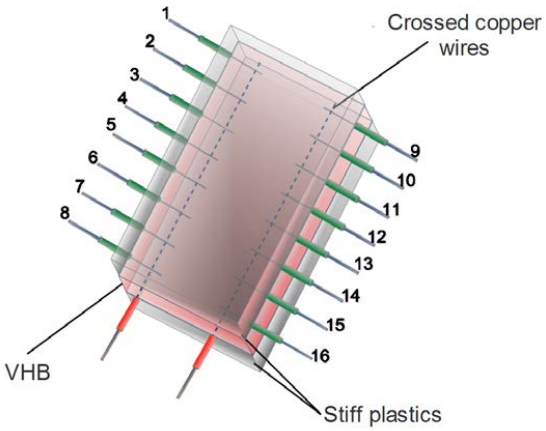

Figure 1.7: Electrical test setup suggested by Huang et al. [30]. This setup consists of a pre-stretched elastomer sheet with an array of crossed cylindrical copper wires as electrodes, which arranged at right angles to one another. Every crossed copper wire resembles a set of breakdown test, for instance, 16 tests can be made in the shown configuration.

Recently, Liu et al. [42] investigated the effects of different ambient temperatures (-10 to 80°C) on the electromechanical deformation of biaxially pre-stretched acrylic VHB polymer. They reported that the effects of the temperature on the VHB based DE actuation were strongly dependent on the pre-stretching strain. They suggested that actuation strain of the DEs that pre-stretched at small strain (s=100%) were more susceptible to temperature change while DEs that were pre-stretched at large strain (s=300%) were relatively insensitive to temperature. During the actuation, the electromechanical deformation was dominated by mechanical stretching, rather than thermal conduction.

From all breakdown strength enhancing techniques which have been discussed in this section, probably pre-stretching is the most practical technique in attempt to increase the breakdown strengths of DEs as this technique was reported to increase the breakdown strengths of the DEs,[14, 30, 36, 37] significantly decrease the thickness of the elastomer (thus requiring lower applied voltage) and can be implemented in many DE based devices. However, pre-stretching has several drawbacks as well. For instance, the elastomers filled with *hard* filler particles experience difficulties to maintain their long-term mechanical reliability as they are susceptible to Mullins effects as the results of pre-stretching [43].

1.8 MECHANICAL AGEING

Mechanical ageing of DEs is an important aspect to be investigated as in many applications, DEs are introduced to harsh mechanical actions such as pre-stretching and multiple deformation cycles. In this thesis, the mechanical ageing of DEs is categorized into two subclasses namely macroscopic and microscopic mechanical ageing.

1.8.1 Macroscopic mechanical ageing

The lifespan/reliability of a DE depends on the type of material used, fabrication techniques, design and operating conditions (such as stretching, frequency and amplitude of applied voltage). Pre-stretching is critical for actuator performance as it helps in preventing EMI of the films under high voltage, thus increasing the breakdown strength of DE [36, 37, 44, 45]. The pre-stretching equipment should be designed in a way so as to impart a uniform pre-stretch to the elastomer film [46]. There is a high tear risk at the corners of the grips used to hold the elastomer film in the pre-stretch equipment. Such tear risks will lead to an early material strength failure [46].

The breakdown strength of an elastomer film can be increased by applying electrodes on the film in a contact-free method to generate a smooth edged electrode layer (**Figure** 1.8) [46]. Sharp electrode edges can be detrimental to the life of the film as the electric charges accumulate over time at such edges, creating field concentration and leading to electrical breakdown, even at low applied voltages [46]. It is advantageous to have a gap between the electrode layer and the edges of the elastomer films where they are attached to the rigid supports, thereby separating the regions of high mechanical stress that susceptible to mechanical ageing from the regions of high electric fields (electrodes) [46]. Having a gap between the electrodes and the rigid support can improve the breakdown strength of DE actuators by 30% [46].

The DEs that experience high mechanical stress such as pre-stretching are susceptible to macroscopic mechanical ageing and could end with the premature mechanical or/and electrical failures. Therefore, it can be argued that, the pre-stretching also leads to mechanical ageing of DE at microscopic level. Therefore, the microscopic mechanical ageing of pre-stretched DEs will be investigated in this thesis and will be discussed in the Section 1.8.2.

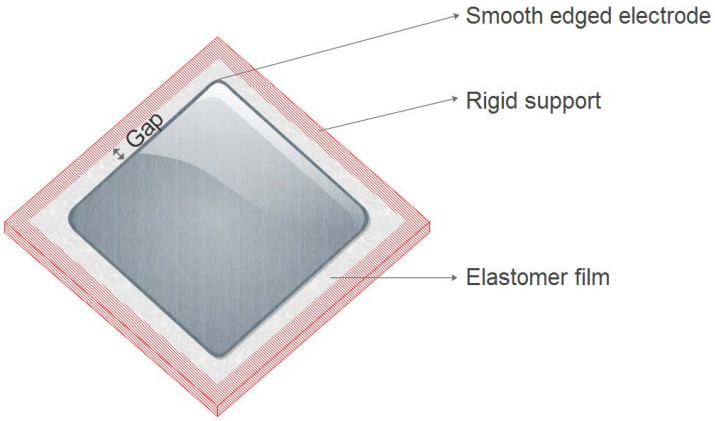

Figure 1.8**:** Gap between the electrode and the rigid support.

1.8.2 Microscopic mechanical ageing

The optimization of the PDMS elastomers mainly to produce high relative permittivity elastomers is manifested through various strategies. However, all modifications so far result in one or several drawbacks such as a reduction in the breakdown strength and an increase in the dielectric loss but also the over-all lifetime of the PDMS elastomer may be significantly altered. In this thesis, the effect of different PDMS elastomer systems, namely compositing, blending in of high-permittivity oils and covalent grafting of high permittivity moieties on the intrinsic mechanical ageing of DEs are emphasised. The investigated PDMS elastomer systems are categorized into two sub-classes, namely *hard* filler (compositing) and *soft* filler (blending in of high-permittivity oils and covalent grafting of high permittivity moieties).

1.8.2.1 Compositing

The incorporation of fillers into elastomers has been proven to be practical and important for relative permittivity enhancement by various techniques, most commonly through the use of filler materials with high dielectric constants. Examples include metal oxide fillers, such as TiO_2 [47–52], Al_2O_3 [53], $BaTiO_3$ [47, 53–56], $CaCuTi_4O_{12}$)[57] and several other types of fillers, such as carbon nanotubes [58–61], expanded graphite[62], and polyaniline (PANI) [19].

This composite approach, however, introduces a negative impact in elastomer processing, as this approach does have an obstacle in achieving uniform composites due to filler agglomeration. Along with the processing issue, this technique does

have certain drawbacks; it increases dielectric losses and substantially raises the Young's modulus of the DEs. Furthermore, rubbers that are incorporated with *hard* filler particles are susceptible to intrinsic mechanical ageing. At small strains, this filled rubber system shows a non-linear viscoelastic behaviour, also known as the Payne effect [63]. On the other hand, at larger deformations, it exhibits a peculiar characteristic stress-strain behaviour after the first deformation which is called the stress-softening phenomenon, also devoted as the Mullins effect [64]. Due to its disruptive nature, this phenomenon has often been considered as an intrinsic mechanical deterioration phenomenon as it does not necessarily lead to material failure [65].

Several physical interpretations have been proposed in order to understand the mechanism of stress-softening, mainly in the filled rubber system as illustrated in **Figure** 1.9. Blanchard and Parkinson [66] proposed the Mullins effect by bond ruptures. In their model, the stretching induces the rupture of the physical bonds at the particle-rubber interface as these interactions are weaker. Houwink [65] proposed that during the first deformation, molecules slip over the filler surfaces and as a result, new bonds are produced along the chains simultaneously. The new bonds may exhibit the same physical nature as the original ones, but shifted at different places along the polymer chains. Kraus et al. [67], however, proposed that the main factor of stress-softening is due to the rupture of the filler structure, which mainly occurs in highly reinforced materials. In addition to that, Hanson et al. [68] proposed another explanation of the Mullins softening. With respect to the extension, they assumed that the entanglements disappeared following the extension direction. Only the entanglement density changes after the first deformation is performed, hence the number of active chains is assumed to remain constant.

The optimisation of DE parameters through compositing technique has great advantages in order to produce the DE with excellent actuation performance, however, this technique also comes with several drawbacks. One of the drawback that potentially downgrade the DE performances over time is the Mullins effects as the DE is associated with pre-stretching and multiple deformations during activation. The effect of these high mechanical stresses experienced by the DEs, therefore, needs to be investigated on the filled PDMS elastomer in order to produce a DE with long-term electromechanical reliability.

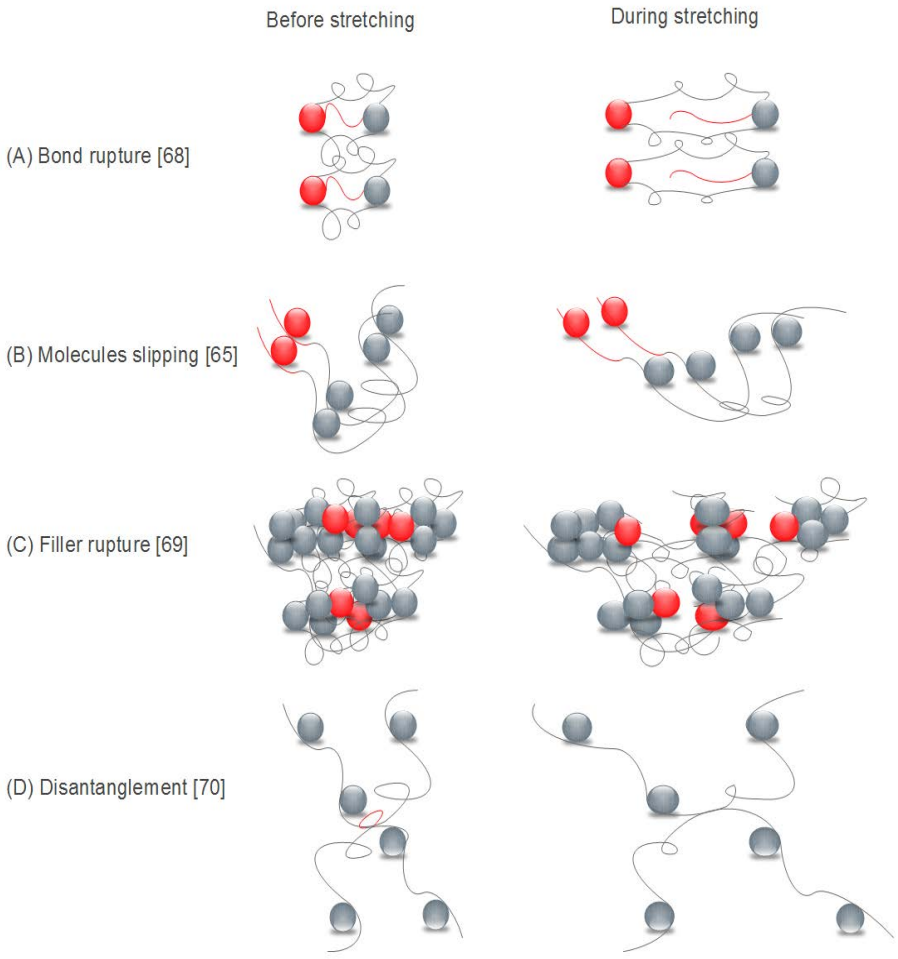

Figure 1.9: Physical explanations of the Mullins effect. The red spheres and red chains show the filler particles and polymer chains, respectively, that are affected by the deformation. The grey spheres and grey chains show the filler particles and polymer chains that are not affected by the deformation.

1.8.2.2 Covalent grafting of organic dipoles to the PDMS network

Another possible approach for relative permittivity enhancement in DEs is chemically grafted organic dipoles to the PDMS elastomer network. This approach could possibly lead to a more controlled elastomer processing, as it does not rely on the effective mixing of particles or blends. Several remarkable systems have been developed in this respect.

Kussmaul et al. [7, 23] and Risse et al. [69] added the dipolar molecule N-allyl-N-methyl-p-nitroaniline and a hydride-functional cross-linker to a PDMS matrix and a commercial PDMS elastomer system, respectively. A two-fold increase in relative permittivity is obtained in this system. Risse et al. [70] blended a cyanoproyl-functional PDMS and a PDMS matrix, where the cyano-functional PDMS acted both as a filler and a plasticiser. Relative permittivity increased significantly, but the increase was accompanied by a substantial decrease of the breakdown strength. Madsen et al. [22] chemically grafted high relative permittivity chemical groups onto the elastomer network. A high relative permittivity of PDMS elastomer was developed through the synthesis of siloxane copolymers, thus allowing the attachment of high relative permittivity molecules through copper-catalysed azide-alkyne 1,3-dipolar cyclo-addition (CuAAC). A high increase in relative permittivity was obtained without compromising other related DE properties such as Young's modulus, dielectric loss and breakdown strength.

One of the advantages of this technique is that the dispersion of the organic dipole in PDMS matrix is homogeneously dispersed and hindered from the formation of particle clusters due to poor mixing efficiency that normally occur in compositing technique. In addition to that, an elastomer grafted with organic dipoles which are strongly bonded with covalent bonds to the PDMS networks most probably exhibit different microscopic mechanical ageing behaviour compared to that elastomer produced by compositing technique.

1.8.2.3 Blending in of high-permittivity oils

Yet another different methodology was implemented by Carpi et al. [24]. The technique consisted of blending PDMS with a highly polarisable conjugated polymer (undoped poly(3-hexylthiophene)). Very low percentages (1–6 wt.%) of poly(3-hexylthiophene) yielded both an increase of the relative permittivity and a reduction of the Young's modulus.

Madsen et al. [71] reported that the blending in of silicone oils to the PDMS based DEs softened the elastomers and that PDMS elastomer which added with high permittivity particles such as TiO_2 (compositing technique) significantly stiffer the PDMS networks. Therefore, it would also be interesting to investigate the effects of pre-stretching on the microscopic mechanical ageing of elastomers that added with *hard* and *soft* fillers.

PART I: Electrical breakdown

2 THE ELECTRICAL BREAKDOWN OF THIN DIELECTRIC ELASTOMERS: THERMAL EFFECTS

The results presented in this chapter have been published in SPIE conference proceeding, Electroactive Polymer Actuators and Devices (EAPAD) California, USA, volume 90562V, page, 1-10 (2013) and is attached as Appendix A.

2.1 INTRODUCTION

In solid dielectrics, electrical breakdown may be thermal which means it is caused by the fact that heat generated within the film cannot be dissipated sufficiently and thereby leads to thermal instability[8]. In thin dielectric films, when the power dissipation increases rapidly with increasing applied voltage, a critical voltage will be reached at a certain point. Whitehead[72] termed this 'the maximum thermal voltage', i.e. the voltage before thermal runway occurs. Analytical and numerical theories to predict thermal runway for thin dielectric films have been developed. For instance, Xiaoguang et al. (2003)[12] studied thermal runway of a thin polypropylene film between two metal electrodes using the finite element method where the temperature rise as function of electric fields for 10 μm thick polypropylene film has been computed and the result showed that the temperature increases slowly prior to the critical voltage (875 V/μm) at which thermal runway occurs.

In this chapter, the thermal effects that may lead to electrical breakdown in thin PDMS film will be modelled. We assume the effect of temperature on electrical breakdown of thin PDMS film is different from polypropylene film as investigated by Xiaoguang et al. [12]. The main difference is that the PDMS elastomer is chemically cross-linked and thus the Young's modulus will not decrease with temperature as for the thermoplastic. Furthermore, recent studies [34] have shown that the breakdown strength increases with increasing Young's modulus.

The modelling will be based on the experimental data of relative permittivity, elasticity and conductivity with varying temperature of PDMS films. Furthermore, thermogravimetric studies will also be performed to evaluate the thermal stability of the materials with no applied electrical field.

2.2 METHODOLOGY

2.2.1 The samples

Five different types of PDMS elastomers with different loadings of reinforcing silica particles as well as a permittivity enhancing filler (titanium dioxide) were studied. Four of the elastomers are commercially available elastomers of either the type LSR (liquid silicone rubber) or RTV (room temperature vulcanizing). In the following, details are given on how the test specimens were manufactured:

Elastosil® LR 3043/30 was obtained from Wacker Chemie AG, Germany and the solvent OS-20 (an ozone-safe volatile methylsiloxane (VMS) fluid) was obtained from Dow Corning®, USA. Elastosil is supplied as a two parts system. The part A contains PDMS and a platinum catalyst, and part B contains PDMS and a cross-linker. The mixing ratio of Elastosil A, B and OS-20 is 5:5:7 by mass, respectively.

POWERSIL® XLR® 630 A/B is an extra-low viscosity LSR and supplied as two parts system. Part A contains PDMS and a platinum catalyst, and part B contains PDMS and a cross-linker. The mixing ratio of parts A and B is 1:1. No solvent is added since the viscosity of the XLR formulations allows for coating without solvent.

POWERSIL® RT® 625 A/B is a *room-temperature vulcanizing (RTV) polymer* supplied as a two parts system. Part A contains PDMS and a cross-linker, and Part B contains PDMS and a platinum catalyst. The mixing ratio of parts A and B is 9:1. No solvent is added since the viscosity of the RT formulations allows for coating without solvent.

Sample V35 is prepared using PDMS chains cross-linked with a 4-functional hydride cross-linker. All the polymers are purchased from Gelest Inc. and the applied molecular weights are supplied by the company. The catalyst platinum, cyclovinylmethyl-siloxane complex (511) is provided by Hanse Chemie. The material is supplied as 2 systems. Part A contains PDMS and cross-linker and Part B contains PDMS and platinum catalyst. The ratio of polymer and cross-linker (r) was set at 1.2. Four ppm catalyst was added to the premixes. The mixing ratio of parts A and B is 1:1 by mass.

The POWERSIL® XLR® 630 A/B with filler is a similar type of material as sample A, except for the addition of a filler. The applied filler is 16% Hombitec® RM130F®, hydrophobic titanium oxide from Sachtleben Chemie, Duisburg, Germany. The average primary particle size is 15 nm. The solvent OS-20 (an ozone-safe volatile methylsiloxane (VMS) fluid) was obtained from Dow Corning®, USA.

The samples were carefully prepared based on the procedures described by Skov et al. [73], as specified below.

A speedmixer DAC 150FVZ (Hauschild Co., Germany) was used to mix part B of the material, the solvent and the filler at 3000 rpm. After 5 min of mixing, part A of the material was added and mixed for another 5 min at 2000 rpm. Glass plates were coated with the premixes, using a thin film 3540 bird applicator (Elcometer, Germany) with a blade gap, in order to acquire consistent thickness for all samples. The samples were then cured in an oven for 5 min at 75 °C and 10 min at 115 °C. The thin films were removed from the glass plates and stored between 50 µm thick ethylene-tetrafluorethylene foils and then kept in a desiccator until use.

2.2.2 Rheology, dielectric characterization and thermogravimetric analysis (TGA)

A TA Instruments ARES G2 Rheometer was used to characterize the rheological properties of the prepared films. The instrument was set to a controlled strain mode at 2% strain, which was ensured to be within the linear viscoelastic regime of the applied elastomers. The sample was inserted between two parallel circular plate geometries of 25 mm with a normal force of approximately 6-8 N. At a frequency of 1.0 Hz, the temperature was varied from 25°C to 450°C.

Dielectric characterization was performed on a TA Instruments ARES G2 Rheometer operating at a frequency of 1.0 Hz, with a normal force of 6-8 N. The sample was inserted between two parallel circular plate geometries of 25 mm and the temperature was varied from 25°C to 450°C.

The thermogravimetric analysis (TGA) was performed with a TA Q500 equipped with autosampler. The samples were heated in an inert atmosphere (nitrogen gas) up to 900°C and the heating rate was 5°C/min.

2.2.3 Resistivity test

Volume resistivity measurements were performed in a three-terminal cell by means of a Keithley 617 electrometer. In order to protect the electrometer from overcurrents, the instrument was connected to the measuring electrode via a series

resistor. The poling DC voltage was supplied to the sample via a gold-plated electrode. The electrode was held in place by a spring system to ensure good contact with the sample. A personal computer equipped with a General Purpose Interface Bus (GPIB) was used for displaying and storing the acquired data. In **Table** 2.1, some specifications of the set-up are given. The current density (J) was obtained by means of Equation 2.2, where *i*(*t*) is the current measured by the electrometer and *A* is the area of the measuring electrode. In order to reach the quasi steady-state regime, the DC field had to be applied for a sufficiently long polarisation time.

$$J(t) = \frac{i(t)}{A} \qquad \text{Eq. 2.1}$$

The quasi steady-state value of the current density, *J*, was used for calculating the conductivity σ of the insulation via Equation 2.3, where *E* is the applied electric field. The volume resistivity is the inverse of the conductivity, σ.

$$\sigma = \frac{J}{E} \qquad \text{Eq. 2.2}$$

Table 2.1: The specifications of the conduction current setup for the resistivity test [18]

Measuring electrode diameter	28 mm
HV electrode diameter	35 mm
Guard electrode diameter	350 mm
Sensitivity	2 x 10^{-11} AM^{-2}
Max temperature	80°C
Max voltage	±30 kV
Series resistor	10 MΩ

2.3 RESULT AND DISCUSSION

2.3.1 Experimental data

In order to evaluate the effect of temperature on the mechanical properties of PDMS film, the storage modulus and tan delta have been measured at elevated temperature and at a frequency of 1.0 Hz. The storage modulus is a measure of the deformation energy stored by the film during the shear process and tan delta, which is also known as the loss factor, is calculated as the ration between the loss modulus and the storage modulus [74].

Figure 2.1 shows the storage modulus and tan delta as a function of PDMS film temperature. The storage modulus for PDMS film increases significantly, from 106 kPa at 190°C to 580 kPa at 450°C. This indicates that the PDMS film is hardened with increasing temperature. In addition, at 320°C the maximum tan delta (0.4) is shown which indicates a strong relaxation process and high energy dissipation in the film.

On the contrary, as mentioned in Tripathi [75], the thermoplastic polypropylene film will show a different behaviour towards elevated temperature compared to the thermoset PDMS elastomer. Therefore, we assumed the difference in rheological properties between PDMS and polypropylene films at high temperature may affect the behaviour of both films with respect to electrothermal breakdown.

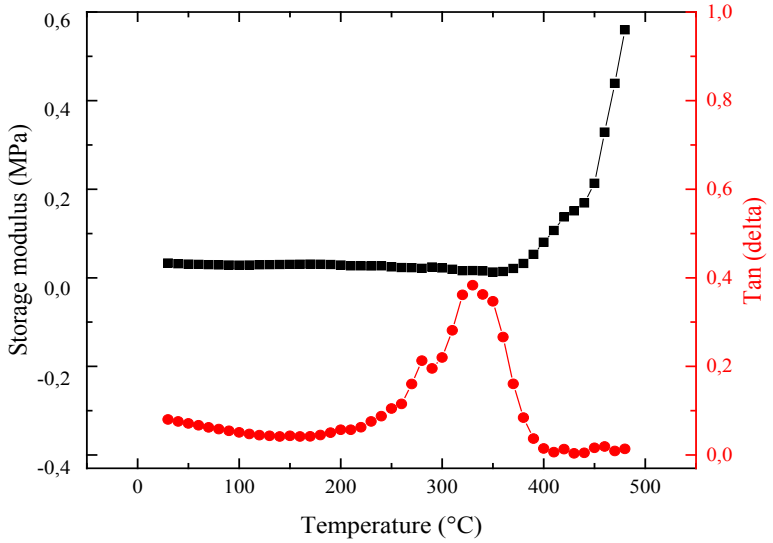

Figure 2.1: Elastosil LR 3043/30 film with 25 mm diameter and 0.8 mm thickness was used for characterization of the thermal dependence of the rheological properties of PDMS. The storage modulus (red curve) and the loss tangent (black curve) are plotted for temperatures between 25°C and 480°C.

Figure 2.2 shows the storage permittivity (ε') and loss permittivity (ε'') as a function of PDMS film temperature for a temperature range from 25°C to 450°C. The storage and loss permittivity are the real and imaginary part of the permittivity, respectively. The relative relative permittivity is given as $\varepsilon_{r=} \varepsilon'/\varepsilon_0$.

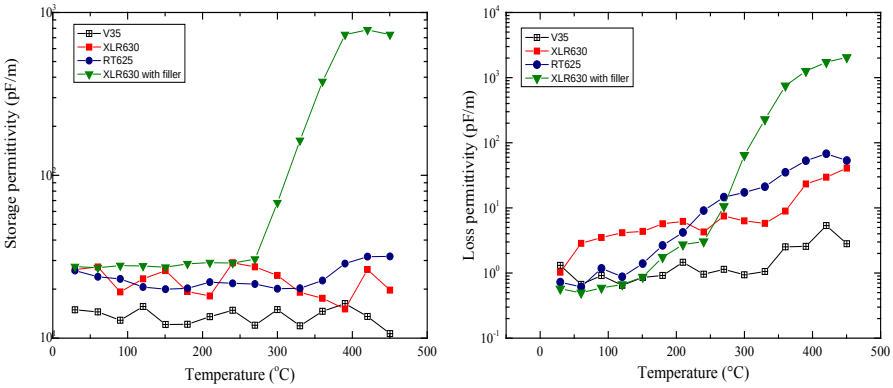

Figure 2.2: The dielectric properties as function of elevated temperatures for several PDMS films: (A) Storage permittivity (B) Loss permittivity.

Figure 2.3 shows the electrical conductivity as a function of temperature. The figures clearly indicate an increase in loss permittivity and electrical conductivity of the titanium dioxide loaded PDMS films upon increase of temperature. This can be attributed to the increased polarisability of the titanium dioxide particles.

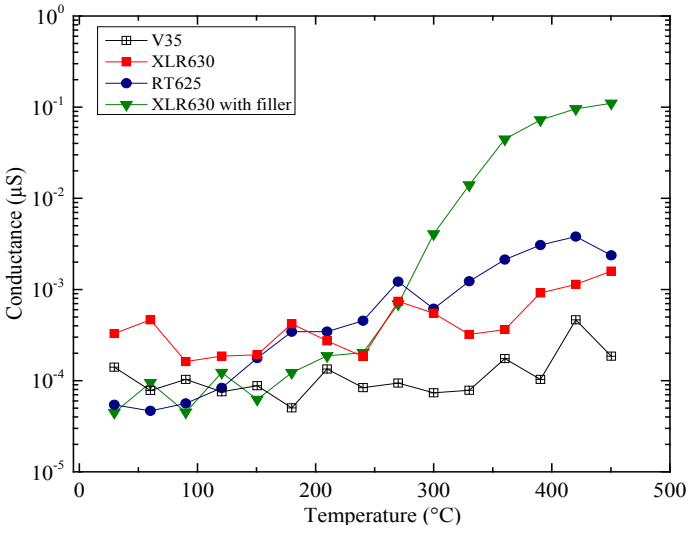

Figure 2.3: The AC electrical conductivity at 1 Hz as function of temperature for several PDMS films.

The increase of the loss permittivity with increasing temperature is attributed to more dissipation of the electrical energy into heat [76]. At the same time, the increase of electrical conductivity at the more elevated temperature causes more heat production since the joule heating is directly proportional to the electrical conductivity [8]. Therefore, these properties are likely to affect the electrothermal breakdown behaviour in PDMS film. Hence, a model that evaluates the effect of temperature and electric field dependence of electrical conductivity on electrothermal breakdown in PDMS film has been applied in this study and will be discussed in the next section.

The purpose of the TGA analysis is to determine the percentages of silica and filler loaded into various PDMS films and also to determine if electrothermal breakdown occurs before film degradation. **Figure** 2.4 illustrates different percentages of weight loss at 900°C for all PDMS films. This behaviour is believed to depend on the percentage of silica and filler inside the films which need higher temperature to degrade.

As shown in **Figures** 2.2 and 2.3, there is a significant increase in the loss permittivity and the electrical conductivity when the temperature of PDMS films is above 150°C.

In **Figure** 2.4 TGA results of the different films are shown. TGA provides useful information on the materials since the mass loss upon heating can be measured. A constant mass at elevated temperature indicates thermal stability. Furthermore the filler content (inorganic components) can be estimated from the solid content at elevated temperature (>800°C). **Figure** 2.4 illustrates that all the investigated PDMS films start to degrade after 300°C and the data in **Table** 2.2 indicates the temperature where 2% of weight of the films has been decomposed. This temperature is deemed relevant since it gives an estimate of the point in time when thermal degradation sets off. Two of the films, namely RT625 and XLR with filler, possess relatively low 2% degradation temperatures (around 300°C) whereas the other two have to be heated above 400°C before significant degradation takes place. Therefore, if the electrothermal breakdown occurs above these characteristic temperatures, it will be a combined – probably accelerated – process of both thermal decomposition as well as electrothermal runaway. The RT625 formulation is most sensitive to degradation at 300-500°C where the degradation occurs more or less constantly.

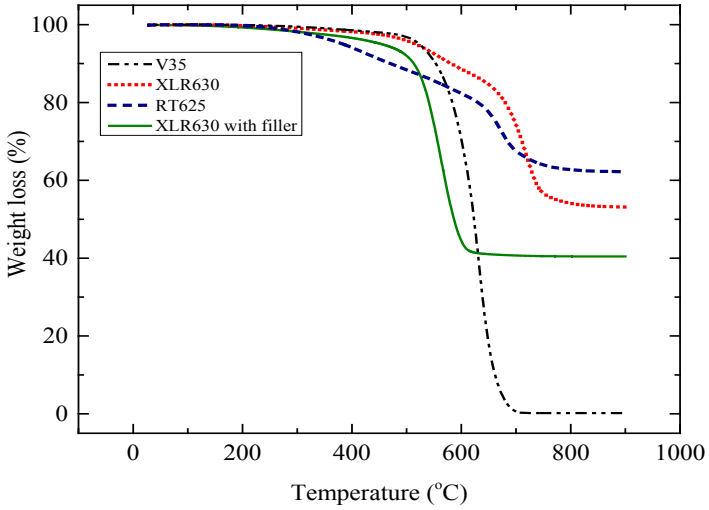

Figure 2.4: TGA thermograms of PDMS films with different percentages of silica and permittivity enhancing filler.

Table 2.2: The temperature where 2% of weight of the films has degraded.

PDMS films	Temperature at 2% of weight loss (°C)
XLR630 with filler	313
XLR630	419
V35	451
RT625	305

2.3.2 Numerical Prediction of Electrothermal Breakdown

For a PDMS film, the volumetric Joule heating from the applied voltage across the film can be calculated as [72]

$$P = \sigma E^2 \qquad \text{Eq. 2.3}$$

where σ is the electrical conductivity and E is the electric field. In this model we assume that voltage across the film is increased in small increments, as well as that thermal steady state is reached at each voltage step. The surface temperatures were fixed and the initial temperature and boundary temperatures were set to room temperature.

In order to model the electrothermal breakdown of thin PDMS based dielectric elastomers, the σ should be expressed as function of temperature (T) and electric field (E). Therefore, a linear interpolation of the σ(T) and the σ(E) was calculated to establish an expression of σ(T,E) from the data in **Figure** 2.5. The interpolation of the electrical dependence is very rough due to the scarcity of experimental data on such systems.

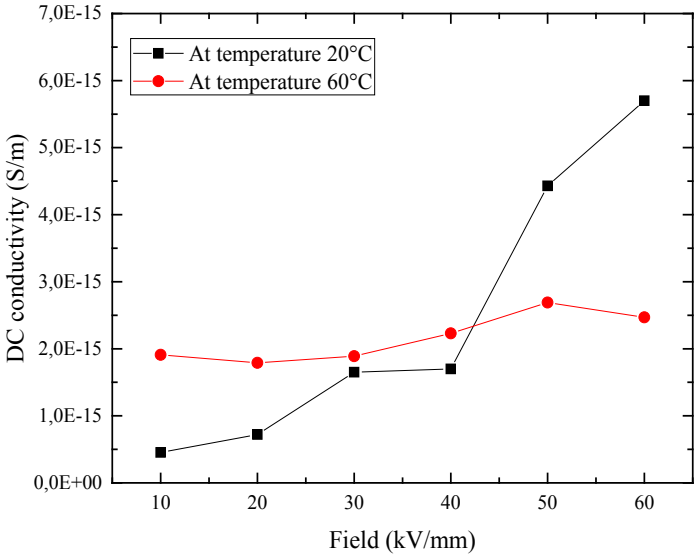

Figure 2.5: The conductivity as function of the electric fields at two different temperatures for RT625 film. There is a big difference between results at room temperature and at 60°C. These data were used to model the correlation of electrical conductivity with temperature and electric fields.

For computational purposes, we assume that thermal conductivity, *K*, of the PDMS film is 0.15 W/mK [77], that the initial temperature is 300 K and that the expression for electrical conductivity is derived from the data in **Figure** 2.5 as illustrated below:

The linear equation for DC conductivity versus electric field

At 20°C: $\sigma(E) = 7.60 \times 10^{-16} E + 1.95 \times 10^{-16}$ Eq. 2.4

and

At 60°C: $\sigma(E) = 1.90 \times 10^{-16} E + 4.88 \times 10^{-17}$ Eq. 2.5

The linear graphs were plotted from the slopes (7.60×10^{-16} and 1.90×10^{-16}) and the y-intercepts (1.95×10^{-16} and 4.88×10^{-16}) from the above equations. Then, the linear equations from the graphs were calculated as shown below

$$\sigma(\mathrm{T}) = -2.32\times10^{-18}T + 1.52\times10^{-16} \quad \text{Eq. 2.6}$$

and

$$\sigma(\mathrm{T}) = 7.20\times10^{-17}T - 2.74\times10^{-15} \quad \text{Eq. 2.7}$$

Lastly the expression of electrical conductivity as function of temperature and electric field is given by

$$\sigma(\mathrm{T},\mathrm{E}) = (-2.32\times10^{-18}T + 1.52\times10^{-16})E + 7.20\times10^{-17}T + 2.74\times10^{-15} \quad \text{Eq. 2.8}$$

As illustrated in **Figure** 2.6, with the electric field applied along the *x* axis, the thickness of the film was given by ***d,*** one boundary of the film is at *x*=0, another boundary at *x*=*d*. The temperature distribution at steady state is then given by[78]

$$dT = \frac{P}{2K}(x(d-x)) \quad \text{Eq. 2.9}$$

where K is the polymer thermal conductivity and P is the averaged volumetric Joule heating. dT is the incremental change in temperature[78]. Then the average film temperature was calculated in order to be applied in computing a new average electrical conductivity (σ).

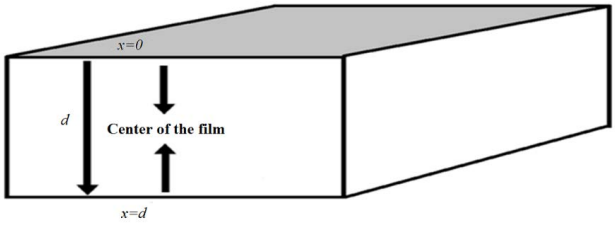

Figure 2.6: The PDMS film where *d* represents the thickness of the film and *x* represents the position where the electrothermal breakdown field is measured. The maximum temperature will be achieved at the centre of the film *X=d/2* as predicted by Xiaoguang et al. [12].

Figure 2.7 shows the general behaviour of temperature versus electric field for PDMS film for which the temperature at the centre of the sample just before thermal runway is only a few degrees above the boundary temperature. With only a few volts increase across the sample, thermal runaway occurs very rapidly. The results of this

work demonstrate that the thermally induced breakdown fields are significantly higher than the breakdown strengths typically reported for PDMS which are in the range from 19 to 133 V/µm [79].

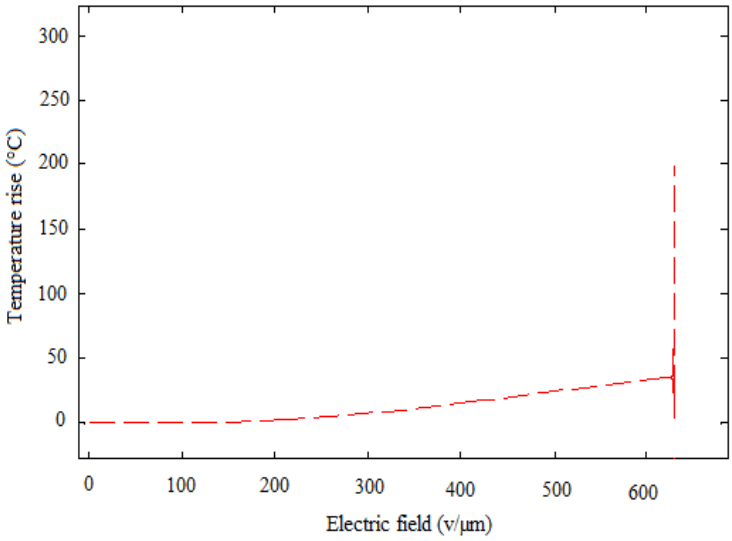

Figure 2.7: The temperature rise (dT) versus electric field for 50 µm thick PDMS film as computed by the quasi-steady state numerical method. The temperature increases slowly prior to the critical field (629 V/µm), at which thermal runaway occurs.

Figure 2.8 shows the breakdown field as function of electrical conductivity for 50 µm thick PDMS film. The plot illustrates that higher electrical conductivity causes a lower breakdown field, as expected. Practically, this has the implication that electrothermal breakdown is relevant at room temperature as well when the electrical conductivity of the material is high.

Figure 2.9(A) shows thermal breakdown strengths measured at different distances from the PDMS film surface. Meanwhile, **Figure** 2.9(B) shows the effect of film thickness on the breakdown field for PDMS film. Both graphs demonstrate similar trends: The breakdown field exhibits a hyperbolic decrease as the position of *x* is closer to the film surface as the result of the heat generated inside the film can be removed rapidly to the surrounding. This characteristic of electrothermal breakdown in thin polymer films agrees well with the predictions reported by Tröls et al. [37].

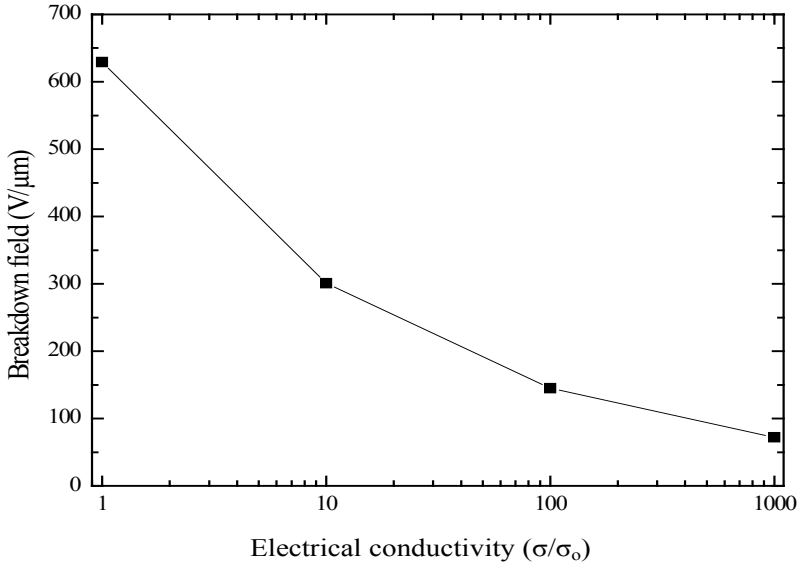

Figure 2.8: Breakdown fields as function of normalized conductivity at room temperature for the 50 μm thick PDMS film as computed by the quasi-steady state numerical method. The initial electrical conductivity, σ_0, of the PDMS film is 2.45×10^{-16} S/m at room temperature.

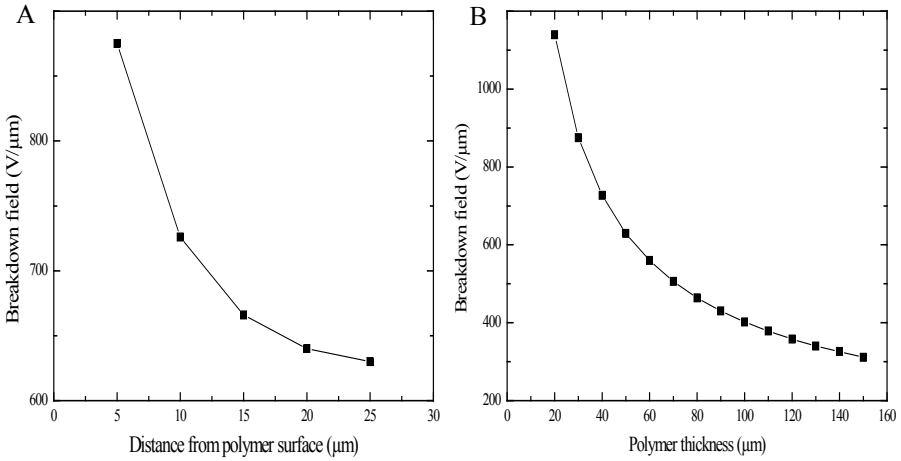

Figure 2.9: (A) Breakdown strengths at given distances *x* from the polymer surface for 50 μm thick PDMS film. (B) The dependence of polymer film thickness on breakdown field computed as described in the text. The value of *x* was fixed as half of the film thickness.

2.4 CONCLUSION

In this chapter, the effect of temperature on dielectric properties of different systems of PDMS dielectric elastomers has been investigated experimentally and a model of electrothermal breakdown in thin PDMS based dielectric elastomers has been applied. From both methods, it can be concluded that electrothermal breakdown of the materials is strongly influenced by the increase in both relative permittivity and conductivity. The electrothermal breakdown may not be a major factor to cause electrical breakdown in thin PDMS based dielectric elastomers since the required electrical field required for thermal runaway is about 5 times larger than the reported breakdown fields of silicones.

3 THE BREAKDOWN STRENGTH OF PRE-STRETCHED ELASTOMERS WITH AND WITHOUT SAMPLE VOLUME CONSERVATION

The results presented in this chapter have been published in Smart Materials and Structures, volume 24, page, issue 055009 (2015) and is attached as Appendix B.

3.1 INTRODUCTION

Electrical breakdown causes the short-circuiting of dielectric elastomers (DEs), resulting in end of life. For that reason, it is important to determine the maximum applied electric field (the breakdown strength) of a given material, such that a safe operational voltage can be defined. This requires reliable and consistent methods for the determination of breakdown strength.

DEs are usually driven by voltages of 1 kV (e.g. AMI haptic device) or higher, resulting in electrical fields of ~50 V/μm and above, depending on the thickness of the film after pre-stretching. Upon biaxially pre-stretching a circular film, the film is radially expanded by a factor of λ, thereby causing a reduction in thickness from H to $h = H/\lambda^2$ due to the general incompressibility of elastomers (**Figure** 3.1). Variations in thickness in response to pre-stretching pose a challenge in relation to how to measure breakdown strength accurately. Tröls et al [37] investigated the effect of different electrode configurations on the breakdown strength of acrylic VHB^{TM} elastomers and pre-stretched up to five times. Stretched elastomer films were sandwiched between compliant carbon grease electrodes or clamped rigidly between two stamp electrodes, in order to take breakdown measurements: breakdown strength increased from 100 to 163 V/μm for rigid electrodes, and from 25 to 143 V/μm for compliant electrodes pre-stretched biaxially five times. It was also found that breakdown strength depends on the surface area of the electrodes.

Normalized thickness was reduced from 1.0 to 0.028 following pre-stretching five times, and thus the sample volumes were not conserved during measurement process.

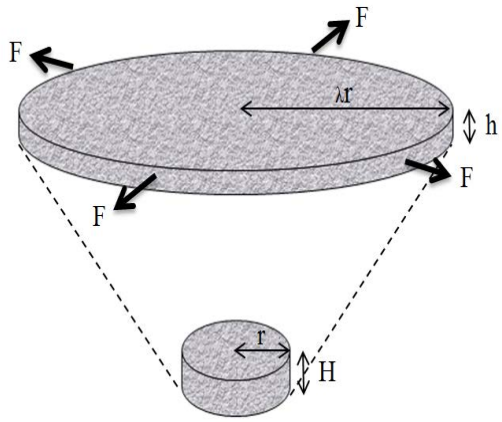

Figure 3.1: A film with thickness H and radius r stretched radially with force F from initial state (bottom) into a deformed film (top), with a reduction in thickness from H to h and an increase in the radius of r to λr.

For these reasons, in this chapter, the effect of volume conservation on breakdown strength was investigated as a function of pre-stretching for four types of polydimethylsiloxane (PDMS) samples. The sample volumes were conserved by enlarging the surface area of the applied electrodes according to the pre-stretch. Subsequently, the results of the breakdown voltage measurements were compared to those obtained from samples without volume conservation. Thereby, reliable and consistent data were produced which could then be used for further interpretation of the favourable effects of pre-stretching.

In many researches, an apparent dependency of breakdown strength on thickness has been reported [8, 30, 80–83], but considerable care has to be exercised in interpreting these results, because often not only does the thickness of the test samples change, but this also happens to other parameters, such as volume under stress, effective electrode area, the morphology of the polymer and the Young's modulus. It is therefore not possible to simply relate a reduction in polymer thickness to increased breakdown strength, and so this can only be done properly when only one single parameter, i.e. thickness, is varied. In the following, the effect of the abovementioned parameters on breakdown strength is discussed based on experimental data for various types of PDMS elastomers.

3.2 THEORY

In the following the effect of different parameters on the breakdown field is discussed.

3.2.1 Sample volume

If the volume of the tested samples changes and all other parameters, for example morphology and Young's modulus, remain unchanged, the effect of volume enlargement on breakdown strength can be calculated. Thus, this approach can only be followed for a constant strain.

A basic statistical treatment of the effect of any change in stress volume on breakdown strength is given in [84]. First, it is assumed that for a single sample of volume V_0 the cumulative probability P_0 of a breakdown in a given electric field E_0 is described by the Weibull function

$$P_0 = 1 - \exp\left(\frac{E_0}{\eta}\right)^{\beta} \qquad \text{Eq. 3.1}$$

where η denotes the Weibull scale parameter and β the Weibull shape parameter.

Then, the sample volume is increased by a factor of n (n elements of volume V_0 each). Now, the breakdown probability P_n of the n times enlarged volume V_n can be calculated if the individual breakdown probabilities $P_{0,i}$ with i between 1 and n are independent and the material being tested is homogeneous. Interface imperfections are ignored. The probability that V_n will break down equals 1 minus the probability that all elements of V_n will not break down

$$P_n = 1 - \prod_{i=1}^{n} (1 - P_{0,i}) \qquad \text{Eq. 3.2}$$

Next, assuming $P_{0,i} = P_0$ (all n elements have the same breakdown probability), we obtain

$$P_n = 1 - (1 - P_0)^n = 1 - \exp\left[n \left(\frac{E_n}{\eta}\right)^{\beta} \right] \qquad \text{Eq. 3.3}$$

For a fixed breakdown probability, E_n is calculated

$$P_0(E_0) = P_n(E_n) \qquad \text{Eq. 3.4}$$

Thus, by equating (**Equation** 3.1) and (**Equation** 3.3)

$$\left(\frac{E_0}{\eta}\right)^{\beta} = n\left(\frac{E_n}{\eta}\right)^{\beta} \qquad \text{Eq. 3.5}$$

and

$$E_n = n^{-\frac{1}{\beta}} E_0 < E_0 \qquad \text{Eq. 3.6}$$

Thus, for a given breakdown probability, the breakdown field of the enlarged sample is reduced. Evidently, the β parameter plays an important role in this reduction, and its value is obtained from step-up voltage tests in which the electric field is raised in constant steps until breakdown. The smaller the scatter in the breakdown field, the larger the shape parameter β and the smaller the effect on the breakdown field of the enlarged volume.

In **Section** 3.4.5, the measured volume effect is compared to the volume effect, which is calculated by following the above steps.

3.2.2 Effective electrode area

The interface between electrode and polymer is a source of potential defects. Thus, it can be argued that—for a given sample volume—the larger the electrode area, the higher the probability of breakdown.

3.2.3 Polymer morphology

If a polymeric sample is stretched, its morphology may change as a result of an alignment of the polymer chains in the plane of stretching [85]. It can therefore be argued that the alignment of the polymer chains perpendicular to the direction of the electric field will lead to an increase in breakdown strength [86], because charge carrier movement has been impeded. The possible effect of polymer alignment can only be studied when all other parameters are constant or have been taken into account properly. Consequently, experimental setups with equal volumes of samples should be stressed, with different stretch applied.

3.3 METHODOLOGY

3.3.1 Materials

Four different types of PDMS elastomers with different silica loadings (in commercial PDMS elastomer) and permittivity-enhancing fillers (titanium dioxide) were studied. The elastomers are commercially available liquid silicone rubber (LSR) or room-temperature vulcanizing (RTV) types.

The pure PDMS elastomers were POWERSIL® XLR® 630 A/B and ELASTOSIL® RT® 625 A/B. POWERSIL® XLR® 630 A/B is an extra-low viscosity LSR and is supplied as a two-part system. Part A contains PDMS and a platinum catalyst, and part B contains PDMS and a cross-linker. The mixing ratio for parts A and B is 1:1. ELASTOSIL® RT® 625 A/B is an RTV polymer also supplied as a two-part system. Part A contains PDMS and a cross-linker, and part B contains PDMS and a platinum catalyst. The mixing ratio for parts A and B is 9:1.

The solvent OS-20 (an ozone-safe volatile methylsiloxane fluid), which was obtained from Dow Corning®, is added to both pure elastomers in order to acquire constant formulation viscosity. The selected elastomers were chosen based on differences in the percentages of reinforcing silica particles in the formulations.

Filled elastomers consist of POWERSIL® XLR® with added fillers. The applied fillers are 16% Hombitec® RM130F® and 35% Sachtleben® R420®, respectively. Both fillers are hydrophobic titanium oxide from Sachtleben Chemie, Duisburg, Germany, and the average primary particle sizes for Hombitec® RM130F® and Sachtleben® R420® are 15 and 250 nm, respectively. The solvent OS-20 is added to both filled elastomers in order to gain consistent formulation viscosity.

3.3.2 Sample preparation

The samples were carefully prepared based on the procedures described in **Section** 2.2.1 (**Chapter** 2).

Silver depositions were performed on a physical vapour deposition chamber (Alcatel) system, which is fitted with a large butterfly valve to control pumping speed and is pumped by an oil diffusion pump with a liquid nitrogen trap. The lid is lifted off the chamber whenever samples or targets need to be changed. The lid wall seal is accomplished by using a large O-ring, and the base vacuum is approximately 2×10^{-5} mbar. The chamber itself is fitted with an evaporation source (for silver), a DC magnetron sputter source and an RF sputter source (for sputtering non-conducting

targets). Silver evaporation was performed on the tungsten boat at the bottom of the chamber. According to instrument calibration, this should result in a sputtering rate of about 1.5 nm s^{-1} and produce a 50–60 nm layer of silver in 30–40 sec. The thin silver electrodes ensure sufficient conductivity. More details on the process can be found in Benslimane et al [87].

3.3.3 Instrumentation

Breakdown measurements were taken on an in-house-built device based on international standards (IEC 60243-1 (1998) and IEC 60243-2 (2001)). The initial thicknesses of the films before stretching were determined with a Leica DMLB microscope with a USB Thorlabs 2.0 digital camera. The stretched film thicknesses were calculated as shown in **Table** 3.1, and the distance between the spherical electrodes was set accordingly with a micrometre stage and gauge.

An indent of less than 5% of sample thickness was added to ensure that the spheres were in contact with the sample. The PDMS film was slid between the two spherical electrodes (radius of 20 mm), and a stepwise increasing voltage was applied (50–100 V/step) at a rate of 0.5–1.0 step/s. Each sample was subjected to ten breakdown measurements, from which an average value was calculated as the breakdown strength of the sample.

Uniaxial tensile quasi-static tests were performed on the set of PDMS films, in order to determine Young's modulus for different strains. The quasi-static measurements were taken on samples shaped as rectangular strips about 6 × 60 mm in size, by applying step-wise increasing loads and by measuring the corresponding elongations from s=0% to s=130%. Young's moduli were determined from the tangent of the stress-strain curves for strains from 0% to 130%.

3.3.4 Sample parameters

3.3.4.1 Sample volume

Two different sets of samples were prepared for the breakdown measurements, i.e. with and without volume conservation. For samples with volume conservation, breakdown measurements were taken on stretched films with circular silver electrodes of varying sizes. The electrodes were applied to the top and to the bottom of the film. The sizes of the electrodes were enlarged from 8 mm^2 to 18 and 32 mm^2 to attain 50 and 100% strains (s), respectively, and the films were stretched before silver deposition. This technique was performed in order to protect the rigid electrodes from damage once the films were stretched. Meanwhile, for samples

without volume conservation, breakdown measurements were taken on stretched films without the electrodes. The films were stretched to 50 and 100%, as shown in **Table** 3.1.

Table 3.1: Parameters for breakdown measurements for samples with volume conservation.

Strain (%)	Radius (mm)	Volume (mm^3)	Thickness (mm)
XLR630			
0	5.0	6.0	0.076
50	7.5	6.0	0.033
100	10.0	6.0	0.019
RT625			
0	5.0	6.5	0.083
50	7.5	6.5	0.037
100	10.0	6.5	0.021
XLR630+16% RM130F			
0	5.0	6.8	0.087
50	7.5	6.8	0.039
100	10.0	6.8	0.022
XLR630+35% R420			
0	5.0	7.2	0.092
50	7.5	7.2	0.041
100	10.0	7.2	0.023

3.3.4.2 Sample thickness

Two different sample preparation methods were applied in the breakdown measurements, in order to study the effect of thickness on the breakdown strength of un-stretched PDMS films, namely a single-layer and a multiple layer technique. For the single layer method, films were prepared by using different blade gap sizes, ranging from 50 to 200 µm, of thin film coater in order to gain different film thicknesses. The real thickness of the film was measured through optical microscopy, and then an average of several measurements was used to represent the true thickness. For the multiple layers method, the films were prepared by using a 50 µm thin film coater blade gap, following which the prepared films were stacked in one to three layers of equal thickness, in order to acquire different overall thicknesses.

3.3.4.3 Effective electrode area

In order to investigate the effect of the electrode area on the breakdown strength of PDMS films, two different sets of samples were prepared, i.e. samples with and without volume conservation. The samples were covered with different sized sputtered silver electrodes on the film surfaces, as described in **Table** 3.2, and the breakdown measurements for both the un-stretched (s= 0%) and stretched (s= 50%) PDMS films of different sample thicknesses were taken on unfilled (XLR630) and filled (XLR630 + 16% RM130F) PDMS films.

Table 3.2: The silver electrode sizes for the different parameters and methods used.

			Electrode radius (mm)	
Material	Strain (%)	Method	Sample thickness = 80 µm	Sample thickness = 40 µm
XLR630	0	With volume conservation	5.0	7.1
		Without volume conservation	5.0	5.0
	50	With volume conservation	7.5	10.7
		Without volume conservation	7.5	5.0
Material	Strain (%)	Method	Sample thickness = 115 µm	Sample thickness = 56 µm
XLR630 + 16% RM130F	0	With volume conservation	5.0	7.2
		Without volume conservation	5.0	5.0
	50	With volume conservation	7.5	10.8
		Without volume conservation	7.5	5.0

3.3.5 Silver deposition and breakdown measurements

A simple method was applied, in order to stretch the elastomers biaxially. A plastic sample container cap was used as a sample holder for the pre-stretched film. The method for measuring the breakdown strength of the pre-stretched films with specially designed caps is shown in **Figures** 3.2-3.4. Biaxial stretching was used in this instance, since it is the most common way to pre-stretch elastomers, and the pre-stretch can also be performed in a very controlled manner.

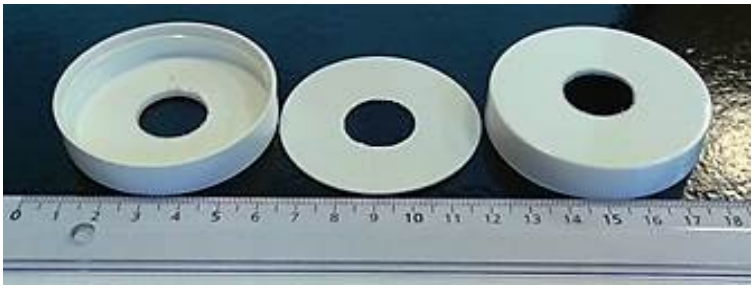

Figure 3.2: Plastic container caps with an inner seal and circular holes in the centre.

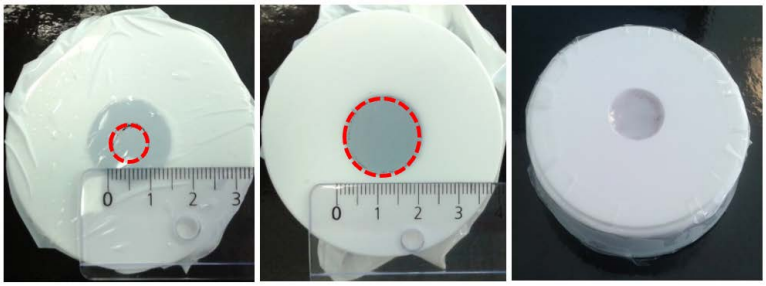

Figure 3.3: (A) A film before stretching. A circle was drawn on the film surfaces as a guideline. (B) The film after biaxially stretching from 5 mm radius (s= 0%) to 10 mm radius (s= 100%). (C) During silver deposition, the stretched films were covered on top by the inner lids with circular shaped holes of the right sizes, thereby allowing for control over the area exposed to sputtering.

Figure 3.4: Stretched film inserted between two hemispherical electrodes for breakdown measurements.

The two experimental techniques employed for measuring breakdown strength as a function of pre-stretching are illustrated in **Figure** 3.5.

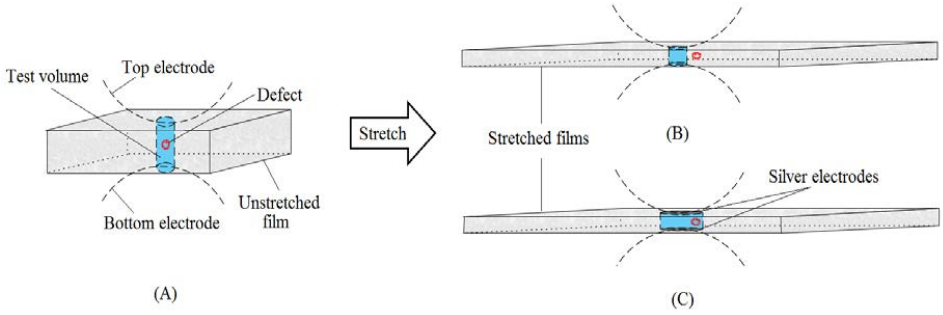

Figure 3.5: Breakdown measurements were performed on films before stretching (A) and after stretching; (B) without volume conservation and (C) with volume conservation.

3.4 RESULTS AND DISCUSSION

Four different PDMS elastomers were investigated, namely an RTV type as well as an LSR type, both with and without permittivity enhancing fillers. The applied LSR was a so-called 'extra-liquid rubber' (XLR) with a relatively low viscosity, thereby allowing for the further addition of particles. The added fillers were two types of TiO_2 shown previously to cause significantly different properties of the resulting elastomer, mainly due to differences in particle sizes [20]. The RM130F filler had been shown previously to reinforce strongly Young's modulus as well as breakdown strength, whereas the R420 does not reinforce to the same extent, and thus higher concentrations are possible [20].

3.4.1 Volume conservation considerations

DEs consisting of various types of silicones with pre-stretching in this study possess no local minimum in their respective voltage–stress curves, and therefore they are not prone to electromechanical instability as defined by Stark and Garton [10]. In **Figure** 3.6, breakdown strengths as a function of the strains for different experimental configurations on several types of PDMS can be seen. Breakdown strengths for four different un-stretched elastomers are in the range 79–103 V/µm, with volume conservation (configuration (C) in **Figure** 3.5), and 100–120 V/µm, without volume conservation (configuration (B) in **Figure** 3.5). For stretched samples (at s= 100%), breakdown strength varies between 227–296 and 247–320 V/µm, with and without volume conservation, respectively. The discrepancies between the two methods in the un-stretched state (s= 0%) are due to different sample volumes as well as variations in the electrodes. The samples with volume conservation are

measured with 5 mm radius electrodes in an un-stretched state, whereas the samples without volume conservation are just contacted by the spherical electrodes and thus the sample volumes are significantly smaller, as shown in **Table** 3.3.

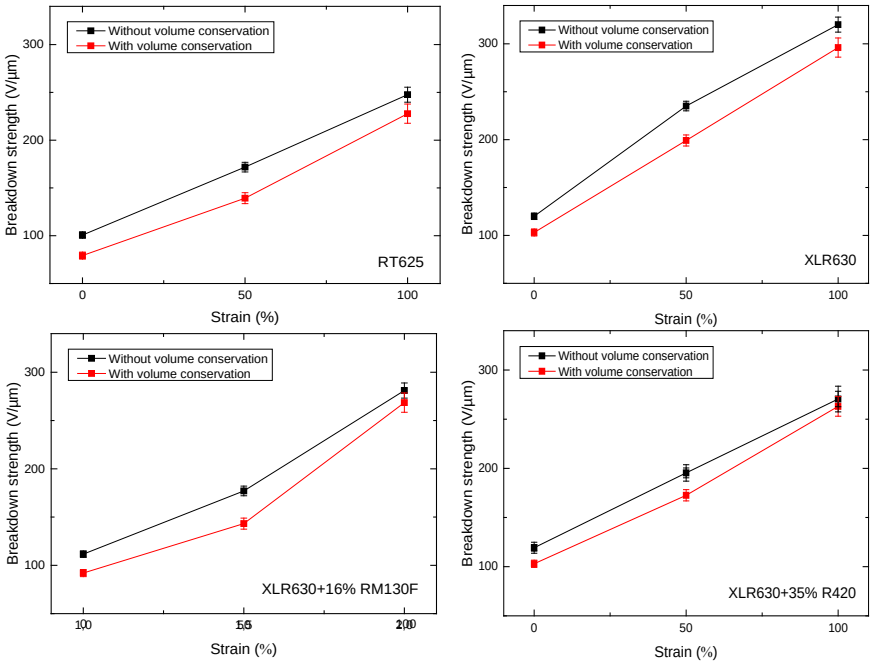

Figure 3.6: Breakdown strength as a function of the strain for several PDMS films.

Table 3.3: Effect of pre-stretch on film thickness for XLR630. Electrode sizes without volume conservation were approximately 0.5 mm. Electrode sizes with volume conservation were enlarged from 8 mm2 (s= 0%) to 18 mm2 and 34 mm2 to obtain s= 50% and s= 100%, respectively. V and v are the sample volumes before and after pre-stretching, respectively.

Strain (%)	Normalized Thickness (h/H)	Normalized sample volume (v/V)		Breakdown strength (V/µm)	
		Without volume conservation	With volume conservation	Without volume conservation	With volume conservation
0	1.00	1.00	1.00	120	113
50	0.43	0.43	1.00	225	171
100	0.25	0.25	1.00	324	286

The strong influence of sample volume on breakdown strength is confirmed further by the consistent deviation between identical samples and identical pre-stretches measured by the two methods. There is an apparent improvement in breakdown

strength of approximately 10 V/µm when the sample volume is not conserved upon pre-stretching.

3.4.2 Young's modulus considerations

In order to evaluate the effect of Young's modulus on breakdown strengths, quasi-static uniaxial tensile tests were performed on the samples. Stress–strain curves for the individual samples can be seen in the supplementary information (SI) for Appendix B. Uniaxial tests were performed because of the ease of such experiments compared to the planar elongation method, such as that performed by Jensen et al [88, 89]. Furthermore, most actuation configurations utilize uniaxial stretching of the elastomer, and as a result Young's modulus is the most common measure of elasticity for DEs. All samples showed a local minimum Young's modulus at s= 50%.

Figure 3.7 shows breakdown strengths as a function of Young's moduli derived from the stress–strain curves of several PDMS films at different strains. It is obvious that there is no simple trend between breakdown strength and Young's modulus, as proposed by Kollosche et al [34] and Vudayagiri et al [20]; however, it is clear that when pre-stretching is applied to the investigated silicones, despite the drop in Young's modulus at moderate pre-strain (s= 50%), breakdown strength still increases. The pre-stretch is therefore very likely to cause the favourable alignment of polymer chains as well as defect realignment, i.e. the favourable effect of pre-stretching is not solely mechanical in character.

3.4.3 Sample thickness considerations

Figure 3.8(A) shows breakdown strength as a function of the thickness of un-stretched PDMS films. It can be seen clearly that breakdown strengths are highest for the thinnest films by almost a factor of two compared to the thickest films. This behaviour is supported by the data shown in **Figure** 3.8 (B), whereby film breakdown strengths decline tremendously, as several layers of the thin films were stacked together. This is due to the fact that the thinner films have a relatively lower sample volume compared to thicker films, which therefore results in less risk of a breakdown. However, when investigating the influence of sample thickness, more than one parameter needs to be considered, since sample volume is not the sole factor—in a breakdown measurement, for instance, the voltage applied across a thin film will generate volumetric Joule heating [8]. As shown in **Chapter** 2, a thinner film with faster excessive heat removal results in higher breakdown strength when accounting for the thermal effect only. Therefore, thicker films will also encounter decreased breakdown strength due to heating and the increased conductivity of the investigated elastomers.

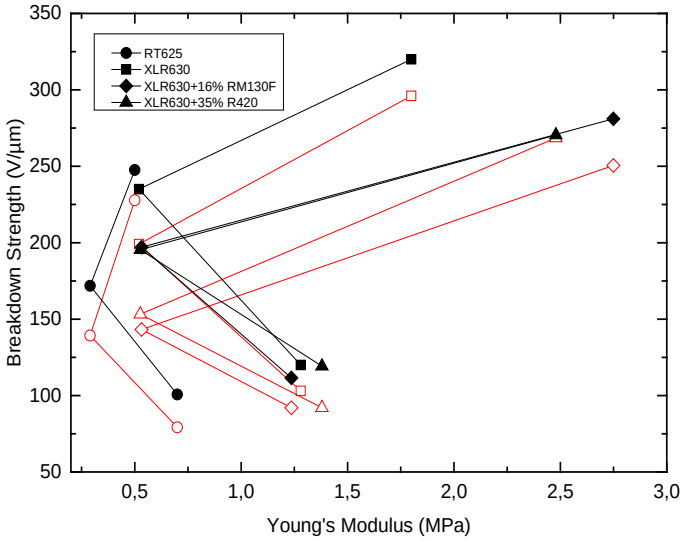

Figure 3.7: Breakdown strength as a function of Young's modulus at different strains (0%, 50% and 100%) for different PDMS materials. The black curves indicate samples without volume conservation and red curves indicate samples with volume conservation.

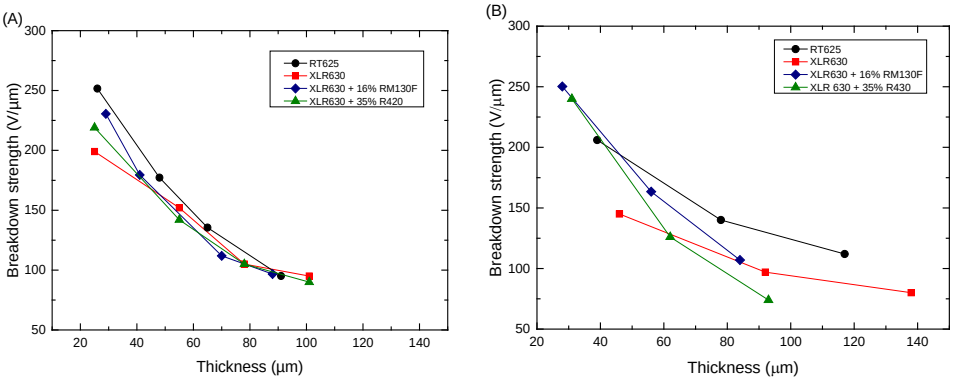

Figure 3.8: Thickness dependence of breakdown strength for different PDMS materials. Breakdown strengths were measured without a sputtered silver electrode in respect to (A) different thicknesses and (B) multiple layers (1–3 layers) of un-stretched films.

3.4.4 Electrode area considerations

In addition, the effective electrode area may influence how breakdown strength is determined, since the interface between the electrode and the polymer can be a source of potential defects. Therefore, this parameter is considered in the following.

The effective electrode area is hard to determine within the experimental setup, and the experimental design was complex due to the dependency of the sample volume on the electrode area in breakdown measurements, i.e. the larger the electrode area, the higher the sample volume. As shown in **Table** 3.4, data for the breakdown measurements without sputtered silver electrode (diamond shape) predicted higher breakdown strengths than the others, due to the absence of electrodes on the film surfaces—and thus relatively small sample volumes. The slight decrease in the breakdown strengths of those samples with volume conservation reflects both the bigger sample volume and the larger effective electrode area compared to the without sample volume conservation method. Therefore, the results possibly demonstrate the effect of volume enlargement rather than effective electrode area. Moreover, the clear influence of the electrode area is not observable.

Table 3.4: Breakdown strengths at different electrode radii and film thicknesses.

Material	Strain (%)	Method	Electrode radius (mm)	Volume (mm^3)	Breakdown strength (V/µm)	Electrode radius (mm)	Volume (mm^3)	Breakdown strength (V/µm)
			Sample thickness = 80 µm			Sample thickness = 40 µm		
XLR630	0	With volume conservation	5.0	6.3	104±2	7.1	6.3	103±2
		Without volume conservation	5.0	6.3	97±1	5.0	3.1	111±7
			Sample thickness = 36 µm			Sample thickness = 18 µm		
	50	With volume conservation	7.5	6.4	141±2	10.7	6.5	188±1
		Without volume conservation	5.0	2.8	140±1	5.0	1.4	195±1
			Sample thickness = 115 µm			Sample thickness = 56 µm		
XLR630 + 16% RM130F	0	With volume conservation	5.0	9.0	82±7	7.2	9.1	123±1
		Without volume conservation	5.0	9.0	78±6	5.0	4.4	130±4
			Sample thickness = 51 µm			Sample thickness = 25 µm		
	50	With volume conservation	7.5	9.0	153±1	10.8	9.2	268±6
		Without volume conservation	5.0	4.0	119±8	5.0	2.0	262±1

3.4.5 Sample size considerations

In order to gain a better insight into the effect of increased sample volume, the effect of sample enlargement on the breakdown strength of PDMS films was investigated, as given by equation (3.6). The breakdown data were analyzed in the Weibull ++

software package, and results in terms of the determination of β (see SI for Appendix B) were used to interpret the experimental data. In the mathematical approach suggested by Hauschild and Mosch [84], some assumptions were included, e.g. that all defects are equally distributed over the volume of the film and that defects produce breakdowns in line with the same field strength.

Figure 3.9 shows how the theory fits with experiments for breakdown strengths as a function of increased sample volume for the two samples. XLR630 has β = 72.4 and XLR + 16% RM130F has β = 39.2, which gives a clear indication of the greater scattering in determining breakdown strengths for the filled elastomer. Samples with a thicknesses of ~40 µm (see **Figure** 3.8) are normalized to 1 (n = 1), and the electrode area is then increased to acquire 100 and 200 times greater volume, respectively. The agreement is striking. However, there is a slight over-prediction from theory compared to the experimental results. This discrepancy can be explained as a result of the Weibull data being used as fitting parameters for the theoretical prediction, based on an experimental setup with less influence from the electrodes, as well as simplifications included in the model described above.

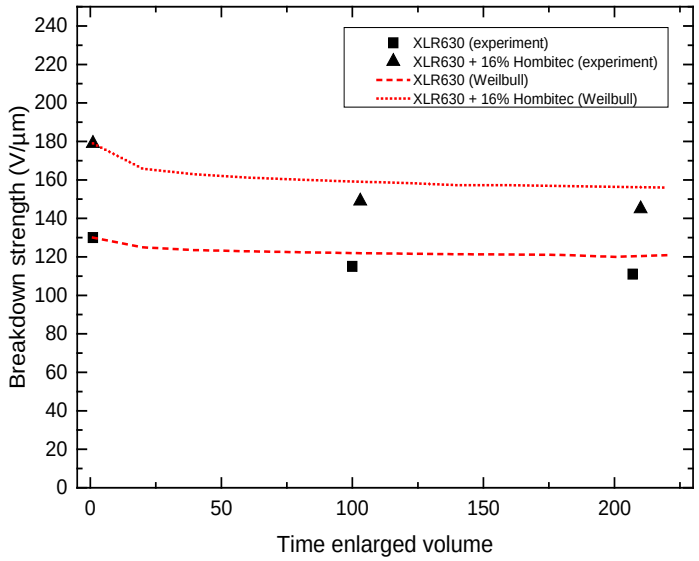

Figure 3.9: The effect of volume enlargement on the breakdown strength of un-stretched PDMS films.

3.5 CONCLUSION

A method for measuring the breakdown strength of pre-stretched films with constant sample volume was presented. The method was compared to a traditional experiment, whereby the sample volume was reduced significantly by pre-stretching. Breakdown strengths of the pre-stretched elastomers were shown to be over-estimated if the reduction in volume following pre-stretching was not taken into consideration. For the materials we tested, it was shown that apparent breakdown strengths taken from traditional breakdown measurements are of the order of 10 V/μm larger than the true breakdown strength of the material measured with a constant sample volume. For reliable determinations of breakdown strength, a careful experimental design is required—as illustrated in the present article. Sample thickness was shown to be a very important factor in determining breakdown strengths, since these breakdown strengths could vary by more than a factor of two when film thicknesses varied from 20 to 120 μm for un-stretched samples.

Pre-stretching of films was shown to have a great impact on the breakdown strength of all tested films, and by pre-stretching films biaxially to four times the original area, it was shown that breakdown strength increased by more than a factor two, even when accounting for the decrease in sample thickness. This clearly indicates that pre-stretching affects the morphology of samples as a result of, for example, chain and defect alignment. It was furthermore shown that breakdown strengths were not coupled in any way whatsoever to Young's moduli of the samples when pre-stretching was applied.

PART II: Mechanical ageing

4 THE INFLUENCE OF STATIC PRE-STRETCHING ON THE MECHANICAL AGEING OF FILLED SILICONE RUBBERS FOR DIELECTRIC ELASTOMER APPLICATIONS

The results presented in this chapter have been published in Material Today Communication, volume 4, page 204-213 (2015) and is attached as Appendix C.

4.1 INTRODUCTION

For PDMS elastomers, mechanical failure is very seldom a failure mode, due to the ultimate extensibility of PDMS elastomers usually exceeding 300%. Common actuation strains introduced in PDMS elastomers are of the order of 20%, so even with pre-stretching the overall strain is far below their maximum extensibility. For PDMS elastomers to make the very most of their potential, i.e. approach actuation strains of the order of their maximum extensibility, greater energy – and thus permittivity – is required.

Incorporating rigid fillers, such as titanium dioxide, into the cross-linked PDMS matrix increases the relative permittivity of the resulting composite elastomer. Mechanical properties are also affected, with results varying according to particle size and surface treatment, from reinforcing to softening [20, 48, 90–92]. On the other hand, a thinly filled elastic film that maintains high strain for a given period of time will, to some extent, suffer mechanical ageing at the microscopic level. The Payne and Mullins effects explain hysteresis in the mechanical properties of filled elastomers. The Payne effect refers to the effect of the strain dependence of the dynamic viscoelastic properties of filled elastomers above their glass transition temperature [63]. Clement et al. [93] investigated the Payne effect in SiO_2-filled PDMS elastomers, and they posited it as the existence of a gradient in elastomeric chain mobility from

the PDMS filler interface to the bulk, leading to a stress-softening effect at low strains upon “initial activation” of the elastomer.

Generally, PDMS elastomers are commercially synthesised through the equilibration polymerisation of cyclic oligomers and end groups in the presence of acid or basic catalysts [94]. One of the disadvantages of this process is the production of by-products as a result of the reaction, consisting of unreacted cyclic oligomers [95]. These residues are mobile within the silicone, and they can also migrate to a device interface. This migration during post-manufacture changes the elastomer surface as well as its mechanical properties such as tensile strength, tear strength, maximum elongation, etc. [96]. As reported by Brook et al. [97], these volatile siloxanes from commercial silicones usually remain within the elastomer when post-curing has been omitted. Post-curing is usually conducted by heating the elastomer far above its curing temperature but below its degradation temperature for some time. Brook et al. [97] showed that the mechanical properties of the elastomer were enhanced (a larger Young’s modulus, greater tensile strength and lower maximum extensibility) upon post-curing. In this case, post-curing was performed by heating a cured elastomer at 200°C for 4 hours subsequent to the traditional curing procedure, where the most common conditions for dielectric PDMS elastomers are curing at ~120°C for 10-30 minutes [98]. To our knowledge the effect of post-curing on, for example, breakdown strength has never been investigated, since the fraction of volatiles is so low (usually cited at 1-2% by the elastomer supplier) that it seems irrelevant.

As reported by Meunier et al. [99], unfilled PDMS lacks the Mullins effect, hysteresis and strain rate dependency. However, for DE applications filled, reinforced silicones are required to obtain acceptable performance. This study was performed in order to understand the intrinsic mechanical behaviour of pre-stretched PDMS elastomers, with and without additional permittivity enhancing fillers, over time. Furthermore, the study aims at elaborating how mechanical ageing affects other parameters relevant to the DE being used, namely the Young’s modulus, breakdown strength and relative permittivity.

4.2 METHODOLOGY

4.2.1 Materials

Four different compositions from two commercial PDMS elastomers, without and with one type of permittivity enhancing filler (TiO_2), were investigated. The elastomers were Elastosil® LR 3043/30 A/B and ELASTOSIL® RT® 625 A/B. POWERSIL® LR® 3043/30 A/B is a high-viscosity LSR and is supplied as a two-part system. The mixing ratio of parts A and B is 1:1. ELASTOSIL® RT® 625 A/B is an RTV elastomer, which is also supplied as a two-part system. The mixing ratio for parts A and B is 9:1. The solvent OS-20 (an ozone-safe, volatile methylsiloxane (VMS) fluid) was obtained from Dow Corning and added in order to get consistent viscosity formulation.

The investigated elastomers are of Elastosil® LR 3043/30 A/B and ELASTOSIL® RT® 625 A/B, respectively, and are denoted as LSR and RTV, respectively. The permittivity-enhancing filler added is alumina-silica-zirconia surface-treated hydrophobic rutile titanium dioxide (TiO_2) Sachtleben® R420® from Sachtleben Chemie, Duisburg, Germany, while the average primary particle size is 250 nm. The filler is added in a weight percentage of the original elastomer (i.e. phr) of 35%. The resulting elastomers are referred to as LSR and RTV composites, respectively. Solvent (OS-20) is also added to both SiO_2/TiO_2-filled elastomers, to reduce the viscosity of the formulations and thereby ease the coating of thin films.

4.2.2 Sample preparation

Thin films were carefully prepared based on the procedures described in **Section** 2.2.1 (**Chapter** 2).

For this study, two sample thicknesses were targeted by using different blade gaps, namely 150 μm (relatively thinner films) and 200 μm (relatively thicker films). Film thicknesses were approximately 34-88 μm and 52-119 μm for the thin and thick samples, respectively. Film details can be seen in **Table** 4.1.

Table 4.1: Details of prepared SiO_2-filled (commercial) and SiO_2-TiO_2-filled (composite) PDMS films.

Sample ID	Material	Thickness	Pre-stretch (%)
A1	RT625	Thin	60
A2	RT625	Thin	120
A3	RT625	Thick	60
A4	RT625	Thick	120
B1	LR304330	Thin	60
B2	LR304330	Thin	120
B3	LR304330	Thick	60
B4	LR304330	Thick	120
C1	RT625+35%R420	Thin	60
C2	RT625+35%R420	Thin	120
C3	RT625+35%R420	Thick	60
C4	RT625+35%R420	Thick	120
D1	LR304330+35%R420	Thin	60
D2	LR304330+35%R420	Thin	120
D3	LR304330+35%R420	Thick	60
D4	LR304330+35%R420	Thick	120

4.2.3 Pre-stretching of the samples

The samples were pre-stretched on an in-house-built frame. The designed frame holds and pre-stretches 150 thin films up to s= 400%. The films were 130 mm in width and 350 mm in length. In order to pre-stretch the films successfully, both ends were rolled with metal rods to prevent slippage. Then the metal rods, together with the stretched films, were attached to the frame, as shown in **Figure** 4.1. The films were then covered by 50 µm-thick ETFE foils to prevent them from contamination. Finally, they were stored for different timespans: one day, one week, one month and three months, before they were released for further characterisation.

Figure 4.1: The device used to pre-stretch the thin filled PDMS elastomer films. The pre-strains were adjusted by changing the position of the metal rods.

4.2.4 Instrumentation

4.2.4.1 Silver deposition

Refer to **Section** 3.3.2

4.2.4.2 Dielectric constant measurement

Dielectric relaxation spectroscopy (DRS) was performed on a Novocontrol Alpha-A high-performance frequency analyser (Novocontrol Technologies GmbH & Co. KG, Germany) operating in the frequency range 10^{-1}–10^{6} Hz at 23°C. Samples were sputtered with silver to provide electrodes 25 mm in diameter, before they were tested for permittivity.

4.2.4.3 Breakdown measurement of un-stretched films

Refer to **Section** 3.3.3

4.2.4.4 Breakdown measurement of stretched films

The breakdown measurements were also performed on the stretched films, which were pre-stretched based on the procedure described in **Section** 3.3.5 (**Chapter** 3) and as shown in **Figure** 4.2. The thickness of the stretched film (refer to SI for Appendix B) was calculated as $t_1 = t_0/\lambda$ where t_0 is initial thickness and λ is the stretch ratio.

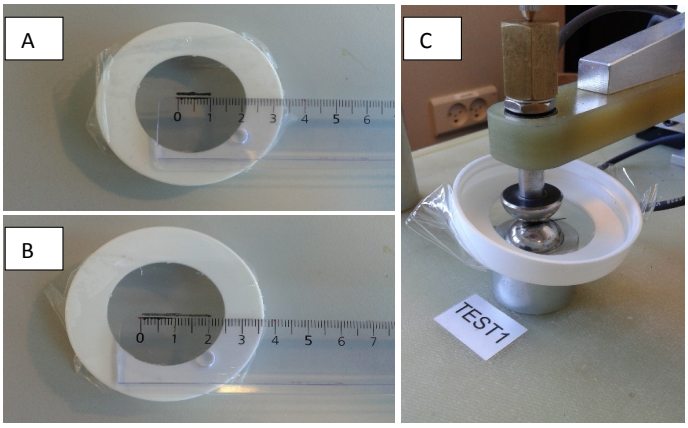

Figure 4.2: The samples were pre-stretched on a cap with a circular hole. A line was drawn (10 mm) on the un-stretched film (a) before the film was extended in the x-direction. (b) The pre-stretched film was slid between 20 mm diameter semi-spherical electrodes (c) for breakdown measurement.

4.2.4.5 Stress-strain measurement

Refer to **Section** 3.3.3

4.3 RESULTS AND DISCUSSION

Understanding the effects of static pre-stretching on PDMS films at different timespans is a prerequisite for making reliable DE transducers based on pre-stretched elastomer films. This understanding will be a step toward more reliable products. The natural subsequent step will be understanding the ongoing electrical ageing [100] and electromechanical ageing phenomena. However, if the developed elastomer cannot survive a static mechanical ageing test, it is very likely to fail prematurely in a coupled electromechanical test. Here we focus on static pre-stretches of 60 and 120%, respectively, and we also investigate how pre-stretching influences other relevant parameters in relation to DE performance. Since the film thickness of PDMS elastomers has been shown previously (**Chapter** 3) to influence strongly breakdown strengths and mechanical properties [101], two thicknesses for each film were investigated, i.e. each elastomer formulation was tested in four configurations at each timespan (thick or thin/60% or 120% pre-stretch), while for the breakdown strength measurements another two configurations were utilised (either non-stretched or stretched to the utilized pre-stretch during the measurement).

4.3.1 Mechanical ageing

All PDMS elastomers tested within this study show a strain-softening effect for strains up to a certain amount (around 60-70%) where after the elastomers strain-harden with increased strains. This characteristic feature leads to a local minimum in the Young's modulus as a function of strain. **Figure** 4.3 (A) shows the Young's modulus ($Y = d\sigma / ds$) as a function of strain for samples subjected to pre-stretching for various timespans. The results shown are for thin samples pre-stretched to 120%, as they were shown to be the most susceptible to mechanical ageing. Data for thin films to 60% pre-stretch, as well as thick samples to both 60% and 120%, are shown in the supplementary information (SI) for Appendix C. In order to ease the comparison of data, normalization was performed in

Figure 4.3 (B). The normalized Young's modulus ($Y_n(s) = Y(s)/Y_0(s)$), where Y(s)= Young's modulus for aged samples at the given strain, and Y_0 is the Young's modulus for the non-aged reference samples at the same strain for the various filled PDMS films at s= 0 to 130%.

For commercial elastomers, RTV (A2) and LSR (B2), i.e. pure commercial elastomers, mechanical ageing is not at first glance significant. However, from the normalized diagrams (**Figure** 4.3 (B)) it is obvious that the dynamics have changed to some extent over time. Initially, it was deemed odd that ageing did not seem to be monotonic. From the results of Brook et al. [97] this discrepancy can be explained by the fact that cyclic silicones from the commercial PDMS elastomer remain within the elastomer, as no harsh post-curing has been performed on our elastomers. For the investigated elastomers, mass losses upon heating up to ~250°C have been investigated previously in **Chapter** 2 by using TGA and were of the order of 1-2%. Therefore, upon pre-stretching, the first process taking place –as expected – is Mullins softening, due to the particulate network being broken down. Then, subsequently, after the surface has been partly broken, the cyclic silicones and residual solvent diffuse out of the elastomer, thus leading to hardening of the elastomers [97]. For both commercial elastomers, the diffusion phenomenon seems to be strongest for the ~1 week timescale, whereas for the composite RTV (C2) elastomer, the effect seems to be delayed significantly, and for the composite LSR (D2), the effect is faster and vanishes between one and three months. For the composite LSR, the elastomer shows such a strong Mullins effect that it never regains its original strength after the first (destructive) 130% strain cycle.

The phenomenon of volatile siloxanes diffusing from the PDMS elastomer can be seen clearly on the RTV (A3) and LSR (B3) commercial elastomer samples, as the mechanical properties of the aged films are higher than the reference after pre-stretching from one day up to three months (refer SI for Appendix C). Meanwhile, for the composites RTV (C3) and LSR (D3), a lesser effect can be seen, as the elastomers show a rather strong Mullins effect (refer SI for Appendix C). Also, when comparing thicknesses, it is evident that the mechanical ageing effect is highly thickness-dependent, since the enhancement of mechanical properties (before the ageing) is significantly slower for thick films.

After the cyclic silicones and residual solvent have evaporated, the commercial RTV elastomer (A) does not demonstrate major changes in mechanical properties. However, the commercial LSR changes its high-strain properties and becomes significantly less strain-hardening over timespans ranging from one to three 3 months. Strain-hardening behaviour is favourable in the context of avoiding electromechanical instability (EMI), so it clearly represents a worsening of mechanical properties.

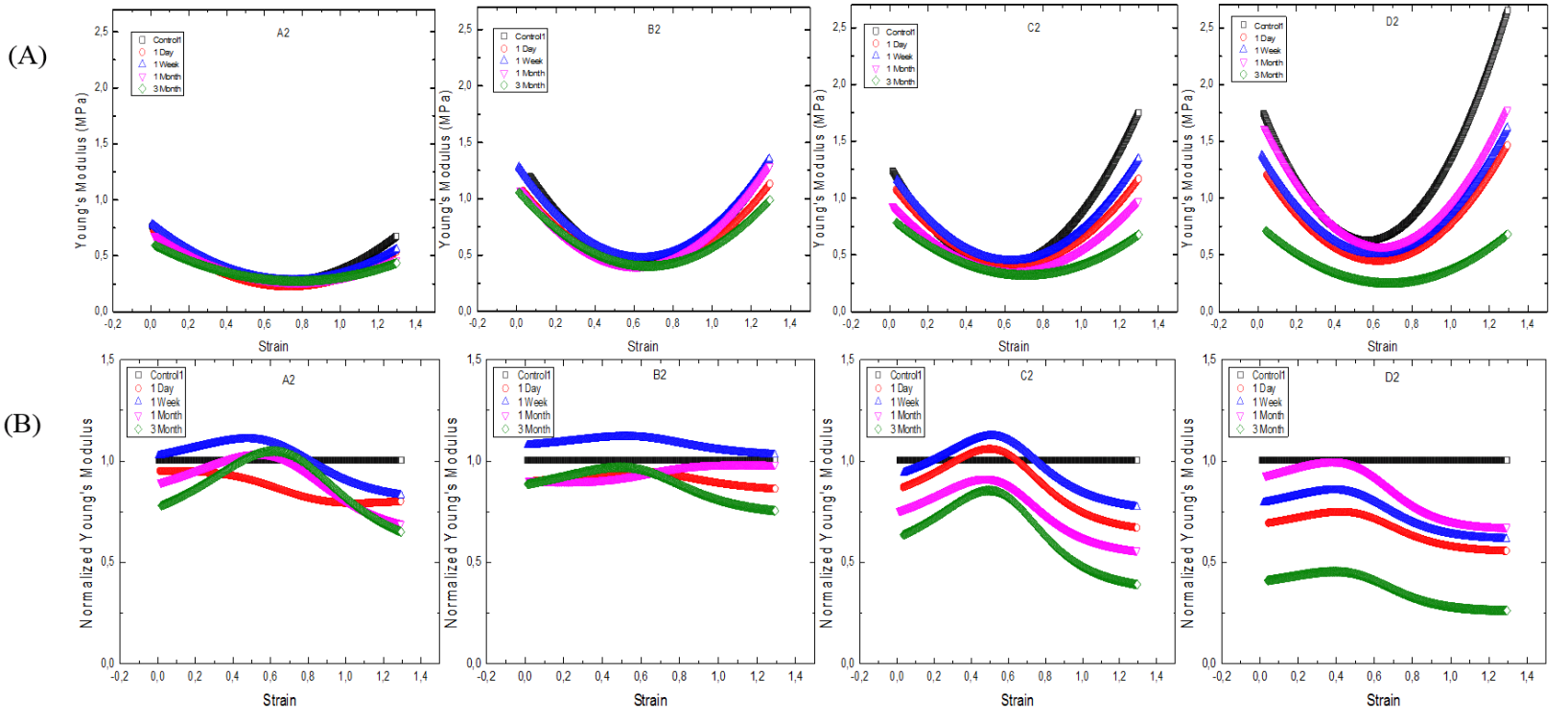

Figure 4.3: Young's moduli (A) and normalized Young's moduli (B) for investigated elastomers as a function of the strains. (A2) and (C2) are commercial and composite RT625 films, respectively, whereas (B2) and (D2) are commercial and composite LR3043/30 films, respectively. Films were pre-stretched at different timespans (black square: control, red circle: 1 day, blue upwards triangle: 1 week, violet downwards triangle: 1 month and diamond green: 3 months). All elastomeric samples had similar conditions; i.e. thin films (coated with 150 µm blade) and s= 120% except for the control samples (s= 0%).

Data on the Young's moduli have been condensed in **Figure** 4.4, in which the Young's moduli at s=120% have been plotted as functions of time for both thin and thick films. The most significant observable mechanical ageing was obtained for composite D2, as the Young's modulus at s= 120% of the non-aged reference sample declines by a factor of approximately four after three months of pre-stretching (2.55 MPa and down to 0.66 MPa). However, only slight changes to the Young's moduli at s=120% were obtained for A2 samples (0.70-0.45 MPa). This indicates a longer term of mechanical reliability for SiO_2-filled elastomers compared to composite elastomers. This is also expected, as commercial elastomers are formulated to high standards. As reported by Dorfmann and Ogden [102], the effect of stress softening is only present to a small extent in unfilled compounds and elastomers with low filler content.

It is clear that the Young's moduli for different PDMS materials and conditions at s= 120% vary significantly over time. The effect of pre-stretching on the mechanical ageing of filled PDMS films can be seen clearly in **Figure** 4.4. The samples that had larger pre-stretches (s= 120%) reveal severe mechanical ageing (red circle and violet downward triangle) compared to the samples that were subjected to smaller pre-stretching (s= 60%) (black square and blue upward triangle), due to stress-softening increasing progressively in line with the increasing strain [64]. Even though the dependency of mechanical ageing on thickness was not clearly noticeable in **Figure** 4.4, nevertheless the coupling of the thin film and a larger strain demonstrates the most severe effect on the mechanical ageing of filled PDMS films. Thick samples will experience delayed ageing, because the constructive evaporation of cyclic silicones and destructive structure changes appear simultaneously at the timescales investigated within this study.

For the two composite formulations, the composite RTV (C2) shows the severest loss of tension on the one month time scale, but it continues to lose tension over time. The composite LSR formulation obviously loses significant tension, with a drop in Young's moduli greater than 50% for all strains investigated following three months of ageing at a pre-stretch of 120%.

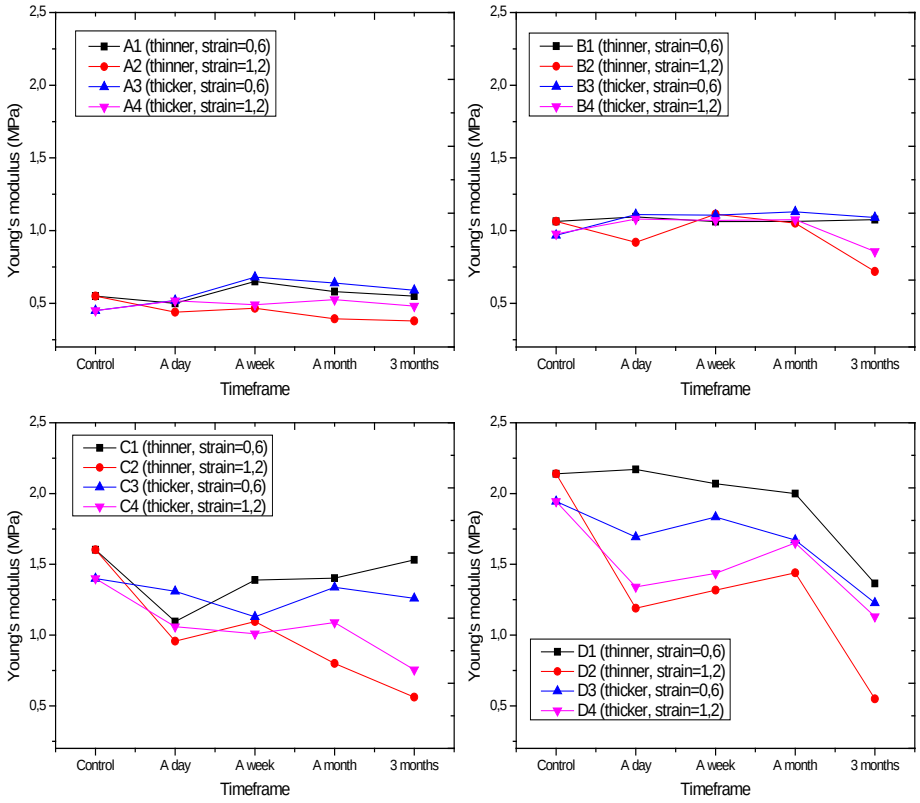

Figure 4.4: Young's moduli of different samples measured at s= 120% after pre-stretching from time=0–control to 3 months. A= RT625, B= RT625+35% TiO_2, C= LR3043/30 and D= LR3043/30+35% TiO_2. Conditions for A1, B1, C1 and D1= the films were coated with a 150 µm blade (thin films) and s= 60%, A2, B2, C2 and D2= the films were coated with a 150 µm blade (thin films) and s= 120%, A3, B3, C3 and D3= the films were coated with a 200 µm blade (thick films) and s= 60% and A4, B4, C4 and D4= the films were coated with a 200 µm blade (thick films) and s= 120%.

To illustrate the loss of tension in the elastomers over time, stress-strain diagrams under cyclic loading conditions are shown in **Figure** 4.5. The cyclic deformation diagrams are shown for two representative samples (lowest (A) and highest (D) total filler content, respectively). Initially before ageing, the control sample strongly exhibits Mullins softening, as the area of hysteresis loop for the first deformation is approximately three times that of the second deformation for both the A2 and D2 samples. After constant pre-stretching, the Mullins effect becomes less pronounced for the aged sample, since the area of the initial hysteresis loop decreases significantly.

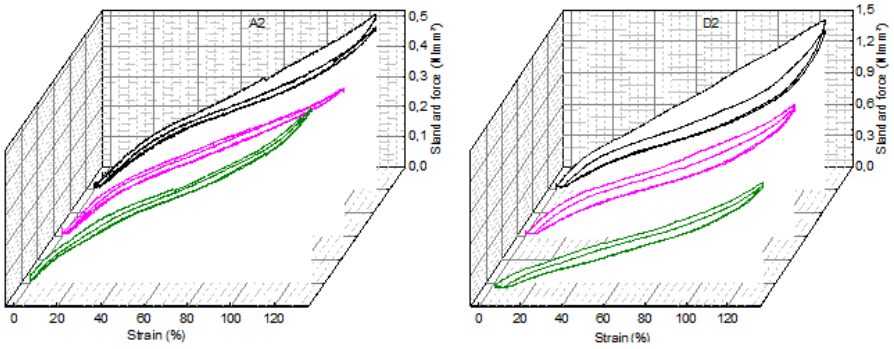

Figure 4.5: Stress-strain diagrams of control (black), 1 month (violet) and 3 months (green) of RTV elastomer (A2) and composite LSR (D2) sample (pre-stretching 120%).

4.3.2 Breakdown strength

Since the mechanical properties of pre-stretched PDMS films change over time, it can be argued that the breakdown strengths of filled PDMS films are also likely to change. **Figure** 4.6 shows the normalized breakdown strengths ($BD_n = BD/BD_0$, where BD= breakdown strength for aged samples and BD_0= breakdown strength for non-aged reference samples) for different filled PDMS films and ageing conditions. The results show breakdown strengths for both un-stretched and stretched (during breakdown test) PDMS samples. The inconsistency of the results is caused mostly by deviations in sample thicknesses (as can be seen in SI for Appendix C), as breakdown strengths were proved previously to be strongly dependent on the thicknesses of elastomeric films as shown previously in **Chapter** 3, i.e. the thicker PDMS films show low breakdown strength compared to the thin films, due to the increased volume – and thus larger number of defects. The thicknesses of the investigated films cannot be controlled precisely due to different PDMS formulation viscosities, and the variation in thicknesses can be seen in SI for Appendix C. Simultaneously, as mechanical properties change, breakdown strengths will also change [34], and as discussed previously the Young's moduli do not change monotonically. This behaviour is also observed within the determinations of breakdown strengths. The commercial elastomer RTV shows – for all samples – a maximum in breakdown strength, which is consistent with the maximum in Y. For the LSR, breakdown strength is enhanced at the end of the ageing study, but at present it remains unclear as to why the mechanical data do not support this behaviour. For the composites there is no clear trend except that, overall, breakdown strength decreases after three months of pre-stretching.

For better comparison –without complications aligned with thickness variations – the breakdown strengths of several samples with minimal thicknesses deviations (±3 μm) in relation to the control samples were compared, as shown in **Table** 4.2. The breakdown results for the one- and three-month samples were chosen, as they show greatest effect of volatile siloxanes diffusion, as shown in SI for Appendix C. The standard deviations were considerably greater for several samples, due to the non-uniformity of film thicknesses and defects contained in the prepared samples, while the major uncertainty of the breakdown data may also indicate bimodal distributions of breakdown strengths for several samples (see in SI for Appendix C). Nonetheless, the data in **Table** 4.2 confirm that the breakdown strengths lower in line with mechanical ageing, due to the decrease in the Young's modulus of the aged samples [34].

4.3.3 Dielectric properties

When the elastomer changes both the mechanical properties and breakdown strength, it is very likely that the dielectric properties will also change over time. The dielectric loss factor does reveal differences in phenomena occurring for the pure elastomers and the composite elastomers. **Figure** 4.7 shows the dielectric loss tangent as a function of frequency for samples A2, B2, C2 and D2 at time=0 and time= 3 months. The results show the dependency of the loss tangent for both composite (C2 and D2) samples in relation to ageing. There is no evidence showing the effect of mechanical ageing on the loss tangent for commercial elastomers (A2 and B2), as there is no significant difference in the permittivities of PDMS and silica. At higher filler loadings, achieving proper dispersion is difficult (despite using a high-speed mixer), and agglomerated particles in the elastomer matrix may occur. Large deformations for a long time interrupt the relatively weak interactions between agglomerated particles (Mullins effect) and thus increase the mobility of the high-permittivity segments in the composite films. Thus, the increase in the loss tangent is assumed to be the result of the mobility of the fillers which separate and thereby increase their effective surface area. This increase can be seen from the loss tangent increasing at low frequencies, due to the predominantly interfacial polarisation.

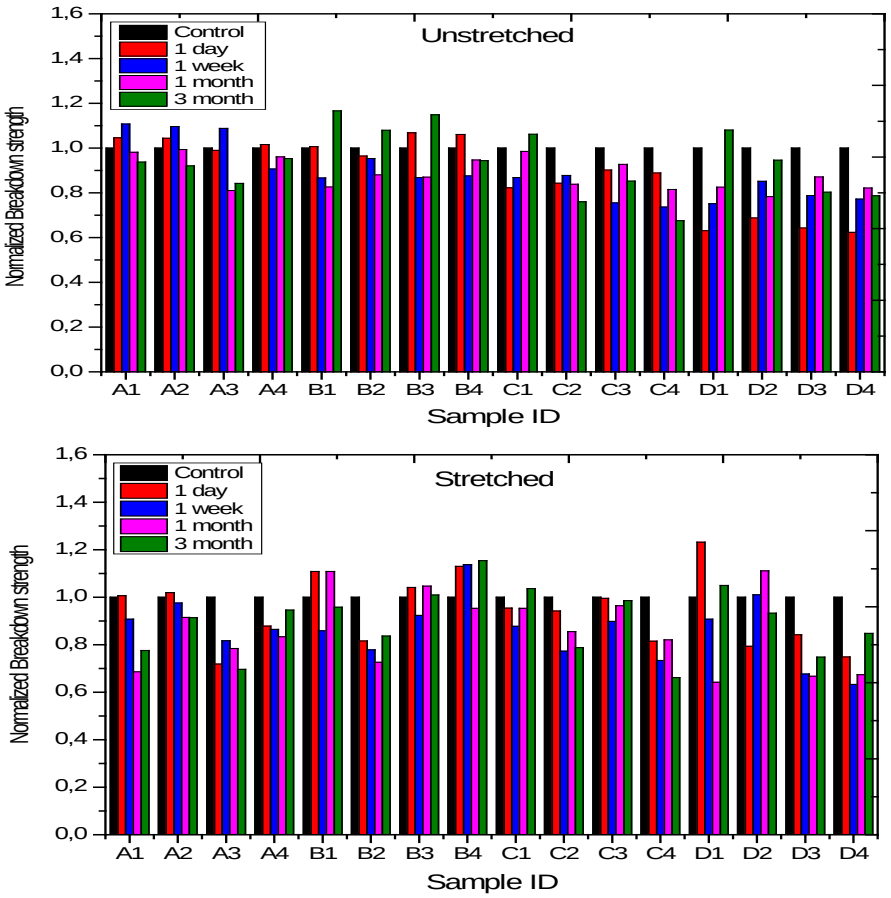

Figure 4.6: Normalized breakdown strength of un-stretched and stretched PDMS films at different timespans. The films were pre-stretched, while breakdown measurements were performed for the stretched samples. A= RT625, B= RT625+35% TiO_2, C= LR3043-30 and D= LR3043-30+35% TiO_2. Conditions for A1, B1, C1 and D1= the films were coated with a 150 µm blade (thin films) and s= 60%, A2, B2, C2 and D2= the films were coated with a 150 µm blade (thin films) and s= 120%, A3, B3, C3 and D3= the films were coated with a 200 µm blade (thick films) and s= 60% and A4, B4, C4 and D4= the films were coated with a 200 µm blade (thick films) and s= 120%.

Table 4.2: Breakdown strengths of several samples that have thickness differences at ±3 µm in relation to the thicknesses of the control films

Sample ID	Control			1 Month			3 Month		
	Sample thickness (µm)	Breakdown strength (V/µm) (Un-stretched)	Breakdown strength (V/µm) (stretched)	Sample thickness (µm)	Breakdown strength (V/µm) (Un-stretched)	Breakdown strength (V/µm) (stretched)	Sample thickness (µm)	Breakdown strength (V/µm) (Un-stretched)	Breakdown strength (V/µm) (stretched)
A3	106	98±4	160±3	108	90±8	125±6			
B4	63	101±5	169±3	66	95±6	161±3			
C1	67	113±3	159±7	67	111±4	151±3			
C2	67	113±3	194±5	64	97±3	166±5			
A2	73	97±4	160±2				76	89±4	146±3
C3	89	114±5	144±4				88	98±8	142±5
C4	89	114±5	190±2				88	77±5	126±4
D2	41	141±4	266±6				41	133±6	249±6

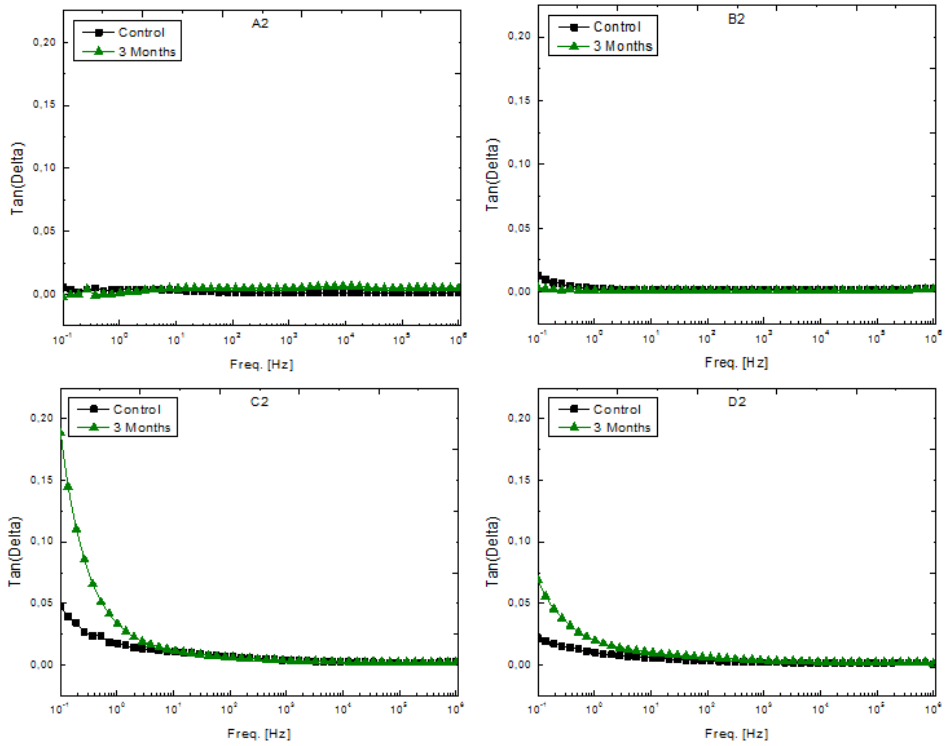

Figure 4.7: Loss tangents for the A2, B2, C2 and D2 samples after pre-stretching from time=0 to 3 months. (A2) and (C2) are commercial and composite RTV elastomers, respectively, whereas (B2) and (D2) are commercial and composite LSR elastomers, respectively. All elastomeric samples had similar conditions, i.e. thin films and s=120%.

4.4 CONCLUSION

DEs with enhanced permittivity are heavily sought after for enhanced actuation, and so many approaches in this respect are being currently developed. The addition of high-permittivity metal oxide fillers to PDMS elastomers is a facile method for such an enhancement, but studies so far have focused solely on how the metal oxides affect instant mechanical behaviour. In this study we show that titanium dioxide cannot be added unlimitedly when pre-stretching the elastomer, since the composites lose their tension very quickly. If such high loadings of fillers are required, it is important to further functionalise the particles for better compatibility and integrity. Another important finding is that even commercial PDMS elastomers require post-curing for electromechanical reliability, which is an overlooked feature for PDMS elastomers utilised in DEs. The two commercial elastomers in this research (RT625 and LR3043/30) both showed improved strength over a time scale of weeks, and thus a decrease in actuation will take place. This phenomenon can be ascribed to the evaporation of volatile cyclic silicones and other residues from elastomers which have had their protective surface broken during pre-stretching. Over a timescale of months, a slight reduction in elasticity takes place due to ageing. In other words, the elastomer will not provide constant actuation over time if it is not ensured beforehand that all volatiles have been removed. The removal of volatiles is additionally favourable, as it increases breakdown strength and thus enhances the reliability of the elastomer.

5 MECHANICAL AND ELECTRICAL AGEING EFFECTS ON THE LONG-TERM STRETCHING OF SILICONE DIELECTRIC ELASTOMERS WITH SOFT FILLERS

The results presented in this chapter have been submitted to Smart Materials and Structures and is attached as Appendix D.

5.1 INTRODUCTION

In order to be commercially viable, DEs should be able to actuate a minimum of 10 million cycles and thereby have a long lifetime. This means that reliable products based on DEs, and thereby also the DE, need to be stable over a long period of time. Additionally, for reliability the DE must be able to maintain important properties over time so that products will not have to be calibrated frequently due to changes, for example, in the Young's modulus – and thus variations in actuation at a given voltage.

Several strategies have been pursued in order to create new elastomers for DE actuators and generators. Soft and high relative permittivity DE actuator materials, for example, were prepared through the chemical modification of elastomer by Kussmaul et al. [23], who added the synthesised dipolar molecule *N*-allyl-*N*-methyl-*p*-nitroaniline, together with compensating amounts of a hydride-functional cross-linker, to a PDMS matrix. Soft PDMS elastomers with high permittivity were also prepared by Racles et al. [103–105], who used cyanopropyl-functional silicones to raise relative permittivity, while Madsen et al. used nitrobenzene- and azonitrobenzene-functional cross-linkers [106] and copolymers[107]. Soft elastomers have also been prepared by making advanced network structures, such as through the use of random or heterogeneous bimodal networks[108] or through the preparation of interpenetrating polymer networks (IPNs) [25, 27, 29, 109, 110].

Also, very recently, Goff et al. [111] presented work on a hetero-bifunctional chain extender which, when condensed, led to infinitely long PDMS chains. This ultimately created a material with superior elasticity and without the waxy consistency of traditional high-molecular weight silicones. Finally, softened DEs have been prepared through the use of permittivity-enhancing blends, where polymers such as poly(3-hexylthiophene) [24], polyethylene glycol [112], a cyanopropyl-functional copolymer[70] and chloropropyl-functional silicone oil [71] have been used.

One of the DE failure mode in DEs is electromechanical instability (EMI), or pull-in instability, which might be the most prevalent failure mode for soft dielectrics such as elastomers [113]. The stress-strain behaviour of an elastomer greatly influences EMI and elastomer must therefore possess strain-hardening behaviour in order to be able to suppress EMI [114]. Investigation of the stress-strain behaviour of elastomers over time is therefore imperative, since some elastomers (e.g. highly filled elastomers) may change characteristics and become strain-softening over time, due to the Mullins effect [39, 115].

In a previous chapter (**Chapter** 4), we investigated the breakdown strength and stress-strain behaviour of commercial filled silicones and composites with hard fillers upon strain-induced ageing. Functional silicones have been another common means of increasing relative permittivity, and therefore, in this study, we investigate ageing effects after static pre-stretching of functional PDMS elastomers. The studied elastomers consist of a strong and relatively stiff commercial elastomer, LR4043/50, ideal for generator applications, which is filled with either functional silicone oil, regular polydimethylsiloxane (PDMS)-based silicone oil or functional co-cross-linkable silicone copolymers, in order to expand the application area of the high breakdown strength elastomer LR3043/50 to actuator applications. These PDMS elastomer modifications may lead to dramatically altered properties over time, and we therefore investigate stress-strain behaviour and breakdown strength after static pre-stretching for different timespans, in order to elucidate the effect on failure modes of the soft additives.

5.2 METHODOLOGY

5.2.1 Materials and sample preparation

Silicone oil, DMS-T22 ($\bar{M}_w$≈ 9,430 g mol^{-1}) and LMS-152 ($\bar{M}_w$≈ 9,000 g mol^{-1}, with chloropropyl-functional groups), and a hydride-functional cross-linker, HMS301 (8-functional (8f), M_w = 1950 g/mol), were acquired from Gelest Inc. Elastosil® LR3043/50 (Wacker Chemie AG) is a two-component silicone comprising a component A and a component B mixed in a 1:1 ratio. Inhibitor Pt88 and the solvent Belsil were also acquired from Wacker Chemie AG. The platinum cyclovinylmethyl siloxane complex catalyst (511) was purchased from Hanse Chemie, while silicon dioxide amorphous hexamethyldisilazane-treated particles (SIS6962.0) were purchased from Fluorochem. Co-1 and Co-2 were synthesised according to previously described procedures.[107] Two types of allyl-terminated chloropropyl-functional copolymers of around 26,000-29,000 g mol^{-1} were prepared: one copolymer contained chloropropyl groups, with 1200 g mol^{-1} dimethylsiloxane spacer units between each group (Co-1), and the other copolymer contained chloropropyl groups, with 580 g mol^{-1} dimethylsiloxane spacers between the functional groups (Co-2). Co-2 thus contains approximately double the amount of chloropropyl groups than Co-1.

5.2.2 General procedure: films with Co-1 or Co-2

Co-1 or Co-2 and an 8-functional cross-linker were mixed with treated silica particles (25 wt%) and an inhibitor (1 wt%, Pt88) and then treated on a FlackTek Inc. DAC 150.1 FVZ-K SpeedMixer™. The platinum catalyst (1.5 ppm) was added thereafter, and the mixture was then speed-mixed once more. The mixture was coated as 150 µm films on a glass substrate and cured at 80°C for 2 hours.

5.2.3 General procedure: elastomer synthesis with soft fillers

An appropriate amount of Co-1, Co-2 or silicone oils was mixed with the first component (A) of the commercial silicone Elastosil® LR3043/50 and solvent (Belsil), as indicated in **Table** 5.1, using a SpeedMixer. The second elastomer component (B) and inhibitor were then added, and the mixture was speed-mixed once more. The mixture was then coated as thin films, using a doctor blade of 150 µm thickness on a glass substrate, and then cured at 115°C for 1 hour. The different sample composition quantities can be found in **Table** 5.1.

Table 5.1: Compositions and quantities of the samples prepared with the soft filler.

No	Composition	SiO_2 (g)	Co-1 (2f, M_w=26000 g mol^{-1}) (g)	Co-2 (2f, M_w= 29000 g mol^{-1}) (g)	HMS301 (8f, M_w=1950 g mol^{-1}) (g) r=2	Inhibitor (0.5%) (g)	LR3043/50 A (g)	LR3043/50 B (g)	Belsil solvent (g)	LMS-152 (chloro-oil) (g)	DMS-T22 (silicone-oil) (g)
#1	LR3043/50	-	-	-	-	-	5	5	5	-	-
#2	Co-1 pure + 25 wt.% SiO_2	3	8.6747	-	0.3253	0.045	-	-	-	-	-
#3	Co-2 pure + 25 wt.% SiO_2	3	-	8.7073	0.2927	0.045	-	-	-	-	-
#4	LR3043/50 + 30 phr Co-1	-	2.8916	-	0.1084	0.015	5	5	3	-	-
#5	LR3043/50 + 30 phr Co-2	-	-	2.9024	0.0976	0.015	5	5	3	-	-
#6	LR3043/50 + 100 phr Co-1	-	5.7832	-	0.2168	0.030	3	3	-	-	-
#7	LR3043/50 + 100 phr Co-2	-	-	5.8048	0.1952	0.030	3	3	-	-	-
#8	LR3043/50 + 30 phr LMS-152 (chloro-oil)	-	-	-	-	-	5	5	3	3	-
#8	LR3043/50 + 100 phr LMS-152 (chloro-oil)	-	-	-	-	-	5	5	-	10	-
#10	LR3043/50 + 30 phr DMS-T22 (silicone-oil)	-	-	-	-	-	5	5	3	-	3
#11	LR3043/50 + 100 phr DMS-T22 (silicone-oil)	-	-	-	-	-	5	5	-	-	10

phr = parts per hundred rubber

5.2.4 Strain-ageing of samples

The samples were strained on an in-house-built frame. The films were 130 mm in width and 350 mm in length. In order to strain the films successfully, both ends of the films were rolled with metal rods to prevent slippage of the stretched films, which were stretched to 60%. The metal rods, together with the stretched films, were then attached to the frame. The films were covered by ETFE foils (50 µm thickness) to prevent contamination. Finally, the stretched films were stored for one month and three months, before they were released for further characterisations.

5.2.5 Instrumentation

5.2.5.1 Breakdown measurement

Refer to **Section** 3.3.3

5.2.5.2 Young's modulus and tensile strength measurements

Uniaxial extensional rheology was performed on the series of elastomer films in order to determine the Young's modulus and tensile strength, as described by Zhang et al.[116] The stress–strain curves of films were tested at RT by ARESG2 rheometer using SER2 geometry. The sample of 20 mm length and 6 mm width was placed between two drums and initially separated by a distance of 12.7 mm. The test specimen was elongated uniaxially at steady Hencky strain rate of 0.01 (s^{-1}) until sample failure at the middle part. Each composition was subjected to four tensile measurements which were then averaged. Young's moduli were obtained from the tangent of the stress-strain curves at 5% strain.

5.3 RESULTS AND DISCUSSION

5.3.1 Properties of different elastomer compositions, before the ageing experiments

The investigated formulations are based on a strong and well-performing [20] PDMS elastomer with high breakdown strength, namely LR3043/50 from Wacker Chemie. Due to its strong and relatively stiff nature this pristine elastomer is suitable for generator applications. In order to broaden its scope, and also to make it applicable for actuator purposes, it can be softened through a range of different approaches. Since it is also desired to increase relative permittivity, functional silicone oils can be used as an alternative to hard fillers such as TiO_2, which has previously been shown

to introduce ageing effects in PDMS elastomers in **Chapter** 4. Functional silicone oils will soften elastomer while at the same time increasing permittivity, and thereby actuator performance will be increased significantly through a synergistic effect [71]. Such additives, however, may induce significant ageing effects due to phase separation and/or migration of the free species. As an alternative to oil, similar softening (functional) copolymers can also be added to the commercial LSR elastomer and reacted into the elastomer structure [117]. This may provide a more stable system over time, since the softening comes from the lubrication effect of chloropropyl groups rather than the solvent effect of oil. Thus, samples with different concentrations of plain silicone oil (PDMS-based), functional silicone oil (chloropropyl-functional) or functional copolymers (with either low or high concentrations of chloropropyl groups, denoted as Co-1 and Co-2, respectively) were prepared. The different sample compositions are shown in **Table** 5.1, whilst their properties before any ageing experiments are shown in **Table** 5.2.

Table 5.2: Initial properties of samples with oils and copolymers.

No	Composition	Breakdown strength [V/µm]	Y @ 5% strain [MPa]	Tensile strength [MPa]	Strain @ break [%]	ε'	F_{om_ref}/ F_{om}
#1	LR3043/50	181±6	2.41	5.23	717	2.7	1.0
#2	Co-1 pure + 25 wt% SiO_2	66±4	0.15	0.65	429	4.7	4.2
#3	Co-2 pure + 25wt% SiO_2	69±5	0.52	1.27	314	5.1	1.4
#4	LR3043/50 + 30 phr Co-1	122±14	1.90	6.51	596	3.1	0.8
#5	LR3043/50 + 30 phr Co-2	113±9	2.00	5.06	314	3.5	0.7
#6	LR3043/50 + 100 phr Co-1	83±5	1.09	1.06	254	3.3	0.6
#7	LR3043/50 + 100 phr Co-2	89±7	1.29	3.71	256	3.6	0.7
#8	LR3043/50 + 30 phr LMS-152 (chloro-oil)	120±10	1.73	3.34	481	4.4	1.1
#9	LR3043/50 + 100 phr LMS-152 (chloro-oil)	62±8	0.60	0.78	269	5.6	1.1
#10	LR3043/50 + 30 phr DMS-T22 (silicone-oil)	98±6	0.87	4.43	658	2.9	1.0
#11	LR3043/50 + 100 phr DMS-T22 (silicone-oil)	61±2	0.27	1.51	493	3.0	1.3

As seen in **Table** 5.2, the addition of copolymers and silicone oils significantly softens the otherwise stiff LR3043/50 (Young's moduli calculated at 5% strain are all considerably lower for samples with additives), due to the softening effect of the additives and the dilution of the heavily filled LR elastomer. Furthermore, all samples with additives have lower strains at breaking than the pure commercial elastomer – as anticipated –, since cross-linking density has been decreased and thus the stress that the elastically active chains can uphold is reduced. All samples, however, have strains at breaking higher than 200%, which is an important requirement for DEs.

Figure 5.1 shows stress-strain curves for samples with copolymers which are covalently bonded to the networks, i.e. in theory there are no free species present in the networks. From **Figure** 5.1 it can be seen that the addition of copolymers to LR3043/50 enables promising generator materials, since 30 phr samples show similar stress-strain responses as pure LR3043/50. The ultimate properties (strain at break), however, are somewhat reduced. It is clear, though, that optimum copolymer loading exists, since the 100 phr samples show significantly reduced mechanical properties (both in terms of stress and strain at breaking). Elastomers based on pure copolymers are soft and quite stretchable, and therefore they are applicable as actuator materials. All samples with copolymers are seen to be strain-hardening, which is a much desired DE property, since this behaviour can suppress electromechanical instability (EMI) [113].

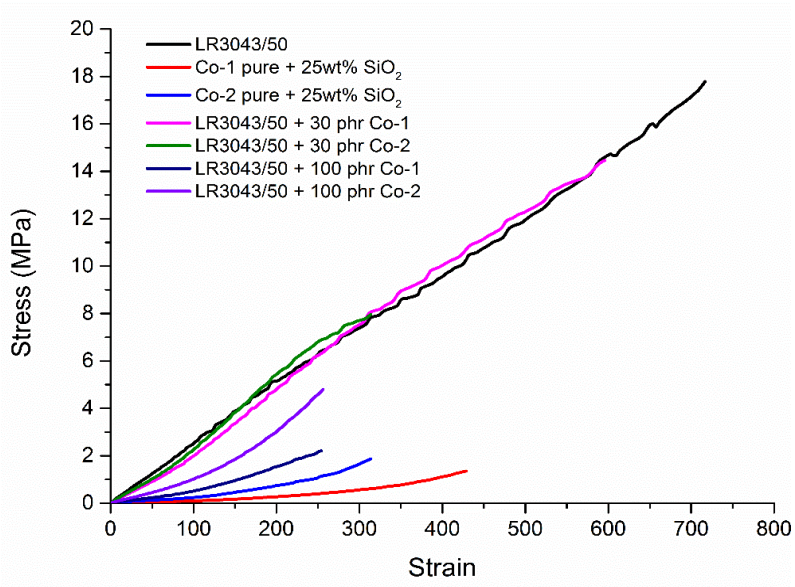

Figure 5.1: Stress-strain curves for samples with copolymers.

Stress-strain curves for samples containing chloropropyl- and PDMS-based silicone oils are shown in **Figure** 5.2. As seen in **Figure** 5.2, both types of silicone oils soften the networks, as expected. At 30 phr the elastomers maintain suitable properties for generator applications, while at 100 phr they are softened to an extent where they would be more suitable as actuator materials. Elastomers with oils do not experience significantly favourable strain-hardening, but on the other hand they do not strain-soften when approaching ultimate properties, and thus their mechanical properties

remain favourable after the addition of oils. Tensile strength decreases in line with increasing oil content, and so the 100 phr samples have low tensile strengths (stress at breaking). Chloropropyl-functional oils induce a lower tensile strength than PDMS-based silicone oil, probably due to slightly lower compatibility between LMS-152 (chloro-oil) and LR3043/50 than the PDMS-based silicone oil has with LR3043/50. Samples with the lowest tensile strength are also seen to have the lowest breakdown strengths (**Table** 5.2).

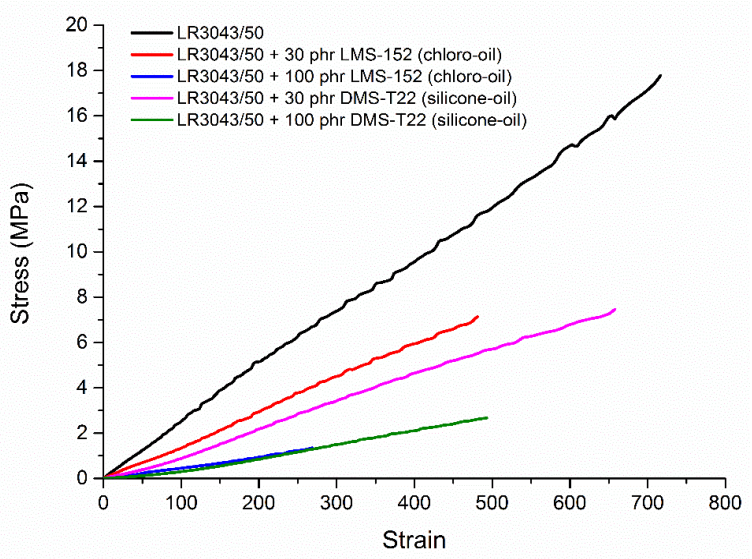

Figure 5.2: Stress-strain curves for samples prepared with chloropropyl-functional and PDMS-based silicone oils.

Pure elastomer LR3043/50 has a very high breakdown strength of 181 V/µm, while elastomers based on pure copolymer (Co-1 or Co-2) have moderate breakdown strengths, due to their softer nature and significantly lower filler content than LR3043/50. Adding silicone oils and copolymers to LR3043/50 decreases the breakdown strength of LR3043/50 significantly, and breakdown decreases in line with increasing content. Breakdown strength is seen to depend strongly on the Young's modulus of the samples, with the softest samples having the lowest breakdown strengths. This is in agreement with previously described results [20, 34, 40], where breakdown strength was found to scale linearly – or even exponentially – with the Young's modulus.

The relative permittivity of pure LR3043/30 is ε' = 2.7 at 100 Hz, while elastomers based on pure chloropropyl-functional copolymer Co-1 and Co-2 have dielectric permittivities of ε' = 4.7 and 5.1, respectively. The addition of chloropropyl-functional copolymers and oils increases the permittivity of LR3043/50 significantly, up to ε' = 5.6 for **sample** 9, which contains 100 phr chloro-oil. Chloropropyl-functional silicone oil increases permittivity to a greater extent than copolymers achieve, which may be due to a higher concentration of chloropropyl groups and greater flexibility of polymer chains which are not covalently bonded to the network, thus leading to greater flexibility and polarisability. The addition of PDMS-based silicone oil does not, as expected, increase the permittivity of LR3043/50, and the result lies within the experimentally expected variance.

A direct comparison, for example based only on relative permittivity, of the elastomers' performance with different compositions is difficult. Therefore, Sommer-Larsen and Larsen [118] defined a universal expression which, through a single parameter, namely the figure of merit, F_{om}, can be used to evaluate the performance of different DE materials. The figure of merit depends on the relative permittivity, breakdown strength (E_B) and Young's modulus according to **Equation** 1.3 in **Section** 1.6 (**Chapter** 1).

In **Table** 5.2, figures of merit for the different compositions are shown relative to the figure of merit for the reference elastomer LR3043/50. Elastomers based on the pure copolymers Co-1 and Co-2 are seen to have the highest increases in the figure of merit compared to LR3043/50. This is due to their high relative permittivity combined with their very soft nature, which in this case contributes significantly more than the moderate breakdown strength values. The addition of a chloropropyl-functional copolymer to LR3043/50, however, does not increase the figure of merit, even though relative permittivity increases while the Young's modulus decreases. This means that the breakdown strength reduction is greater than the permittivity and moduli contributions. The addition of chloropropyl-functional silicone oil increases the figure of merit and thereby DE performance by 10%. A larger concentration of oil (100 phr), interestingly, does not increase performance more than the lower concentration (30 phr), because the 100 phr sample has significantly lower breakdown strength. PDMS-based silicone oil increases the figure of merit by 10 and 30%, respectively, for concentrations of 30 and 100 phr, respectively. In this case 100 phr oil increases F_{om} more than the lower concentration, due to the significant softening effect of PDMS-based silicone oil. It can therefore be deduced that PDMS-based silicone oil softens the elastomer to a greater extent than the chloropropyl-functional silicone oil, without compromising breakdown strength as much, due to greater compatibility.

5.3.2 Properties after ageing experiments: mechanical properties

Ageing experiments were carried out on an in-house-built frame, where 150 µm thin samples remained stretched to 60% for one to three months, before they were released from the frames for characterisation. It has previously been shown in **Chapter** 4 that relative permittivity does not change drastically over time during such strain ageing experiments. In **Figure** 5.3 strains at breaking, before and after the ageing experiments, are shown. The results are summarised further in **Table** 5.4. The strain at breaking for the pure commercial elastomer LR3043/50 (**sample** 1) is seen to decrease after ageing, although this phenomenon is not seen for all samples; **sample** 6 (LR3043/50 + 100 phr Co-1), for example, experiences a significant increase in strain at breaking, from 269% to 661%. **Sample**s 7 (LR3043/50 + 100 phr Co-2) and 9 (LR3043/50 + 100 phr chloro-oil) also exhibit this behaviour, perhaps due to the reduction of cross-linking density while maintaining significant cross-linked polymer chain strength (i.e. the chloropropyl-functional polymer chains may uphold stress while their mobility is strongly decreased).

Most importantly, however, all investigated compositions fulfilled the requirements of more than 200% strain at any given time during the ageing experiments. This property is important in relation to a product's reliability and its lifetime, in order to make sure that DE products do not experience mechanical failure as a first failure mode.

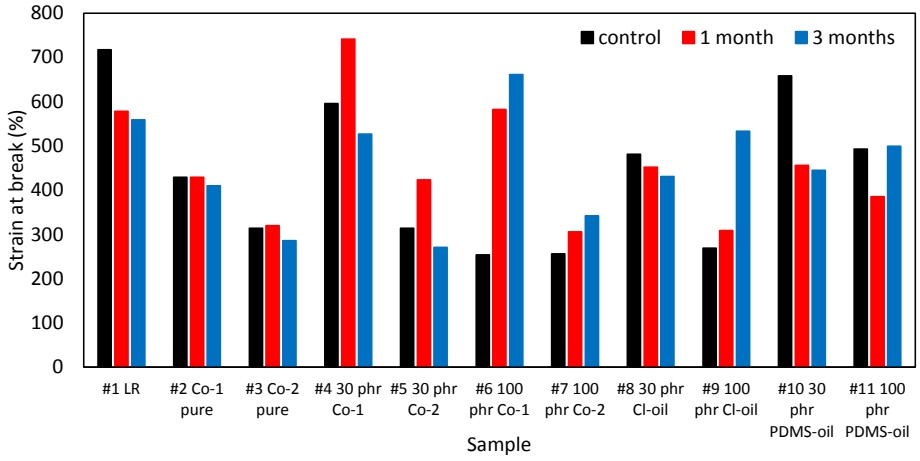

Figure 5.3: Strain at breaking before and after ageing for one and three months.

Tensile strengths, before and after ageing, for one and three months are shown in **Figure** 5.4, and the results are summarised further in **Table** 5.4.

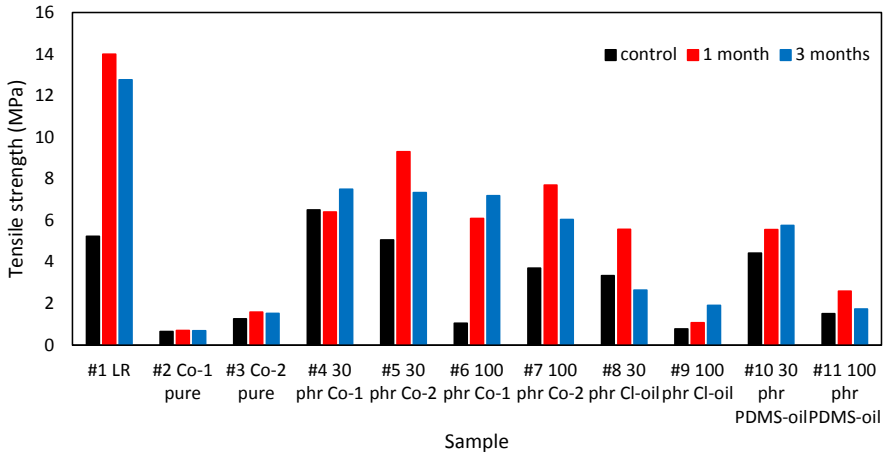

Figure 5.4: Tensile strengths from the ageing experiments.

There is no clear pattern between tensile strength and ageing, although most samples seem to experience increased tensile strength after one month of strain ageing, after which tensile strength decreases at further ageing for three months. This may be due to two phenomena occurring simultaneously. The first phenomenon is most likely small siloxanes and residual solvent leaving the elastomers [119]. This has previously been shown to significantly increase the Young's modulus and tensile strength of stretched elastomers with hard filler particles in **Chapter** 4. When the surface of an elastomer is broken upon pre-stretching, small molecules, consisting mainly of cyclic siloxanes, which are bi-products from the initial polymer synthesis, and residual solvent are able to diffuse out of the elastomer. The migration and evaporation of volatiles significantly hardens the elastomers, which can also be seen in **Figure** 5.5, where Young's moduli as a function of the strain timeframe are shown. The phenomenon is particularly evident for **sample** 1 (pure commercial elastomers LR3043/50), **sample** 5 (LR3043/50 + 30 phr Co-2), **sample** 6 (LR3043/50 + 100 phr Co-1), **sample** 7 (LR3043/50 + 100 phr Co-2) and **sample** 8 (LR3043/50 + 30 phr chloro-oil), all of which show significant increases in tensile strength and Young's moduli after one month of pre-stretching. After three months, tensile strength as well as Young's moduli dropped for most of the samples that showed increased values after one month. This is due to ageing effects, whereby properties deteriorate after long-term pre-stretching. **Sample** 6 (LR3043/50 + 100 phr Co-1), however, does not show any ageing effects after three months, and all samples with oils show a

decreased Young's modulus after three months of strain. It is clear that samples containing oils exhibit similar behaviours, namely initial stiffening, due to the evaporation of small molecules, followed by ageing, which deteriorates mechanical properties. Most samples with copolymers also follow this trend, albeit not to the same extent.

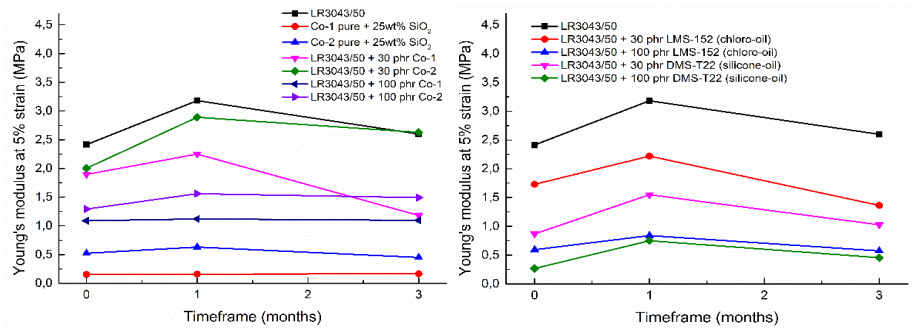

Figure 5.5: Young's modulus at 5% strain after ageing for one and three months for left: Samples with copolymers and right: samples with oils.

Furthermore, the effect of oil concentration on mechanical properties upon ageing can be seen in **Figure** 5.6, where stress-strain curves for pure LR3043/50 and LR3043/50 containing 30 and 100 phr oil are shown. Overall, the commercial elastomer LR3043/50 maintains its mechanical properties. After one month of ageing, hardening is seen in the fact that the volatiles, which act as plasticisers, have left the elastomer and the ultimate strain has reduced. After three months, there is no further significant ageing beyond what happened at one month. It is clear that **sample** 11, which contains 100 phr PDMS-based silicone oil, behaves differently upon ageing than pure LR3043/50 and the low-oil concentration (30 phr) sample. The high concentration sample clearly ages more than the low concentration sample, where only minor differences in stress-strain behaviour are observed compared to the reference sample LR3043/50. The 30 phr sample, however, slightly hardens continuously throughout the three months, though the maximum extension of >650% is lost within the first month. The chloropropyl-functional oil-containing samples behave somewhat differently to the PDMS-based silicone oil-containing samples. Contrary to its PDMS-based silicone oil counterpart, the 10 phr chloropropyl-functional silicone softens after ageing, and a degree of extension is lost. The 100 phr chloropropyl-functional oil sample behaves differently to all of the other oil samples after three months of ageing. As the only sample, both its tensile strength and maximum strain increase after ageing. Chloropropyl-functional and PDMS-based silicone oil thus behave differently in the PDMS matrix upon long-term

pre-stretching, which might be due to the chloropropyl-functional silicone oil not having the same affinity for reinforcing silica particles in the elastomer as the PDMS-based silicone oil does. Therefore, silica particles in the chloropropyl-functional oil-containing samples are not affected by silicone oil and are plasticised to the same extent as the PDMS-based oil samples. Thus, silica particles are able to reinforce the network even better after age straining, since the chloropropyl-functional oil has had time to diffuse away from the silica particles (and probably phase-separate, to some extent) during the ageing experiment. Overall, it is clear that oil content plays a role in the ageing of PDMS elastomers, and it is evident that high concentrations of silicone oils should be avoided for DEs with a desired long lifetime, due to significantly reduced mechanical properties and the tendency toward strain-softening behaviour over time – as observed most obviously for the 100 phr chloropropyl-functional silicone oil sample.

For samples containing copolymers, the trend in stress-strain-related ageing is not so obvious (all results can be found in the supplementary information (SI) for Appendix D), since elastomers based on pure Co-1 or Co-2 do not age significantly upon pre-stretching for one or three months. This may be due to these samples' inherent softness and lower filler content. LR3043/50 samples with copolymers all age to some extent, whereby some age strongly and others only slightly. One of the samples with the most interesting behaviour is **sample** 4 (LR3043/50 + 30 phr Co-1), which fails completely after ageing (both one and three months), as seen in **Figure** 5.7, since it starts to show strain-softening behaviour and significantly reduced tensile strength.

Sample 6, which contains 100 phr Co-1, also dramatically changes properties over time, albeit in a positive way this time, since its tensile strength and maximum strain increase significantly. This may again be due to the chloropropyl-functional nature, which acts in a similar way to the 100 phr chloropropyl-functional silicone oil sample. **Sample** 7, which contains 100 phr Co-2, also gains in both tensile strength and maximum strain after ageing, but it loses its strain-hardening behaviour after three months of ageing, and its Young's modulus is constant up to its breaking point at a strain of approximately 325%.

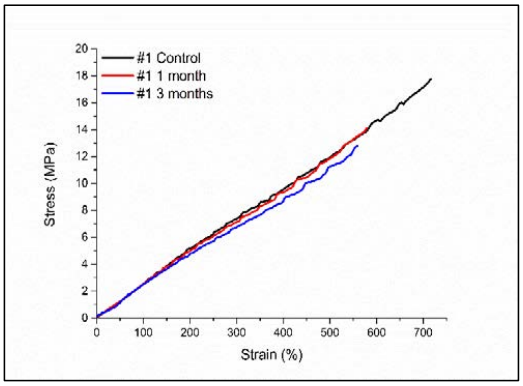

Stress-strain curve for #1, LR3043/50

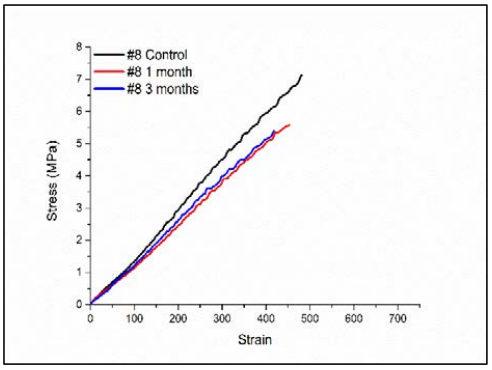

Stress-strain curve for #8, LR3043/50+ 30 phr chloropropyl-functional silicone oil

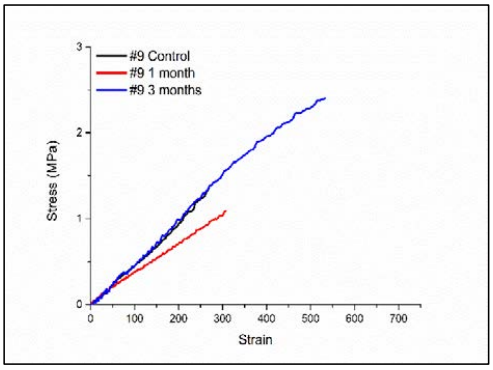

Stress-strain curve for #9 LR3043/50+ 100 phr chloropropyl-functional silicone oil

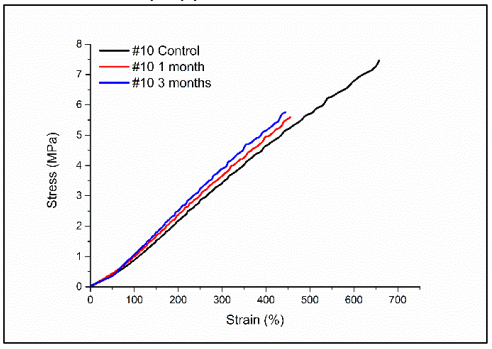

Stress-strain curve for #10 LR3043/50+ 30 phr PDMS-based silicone oil

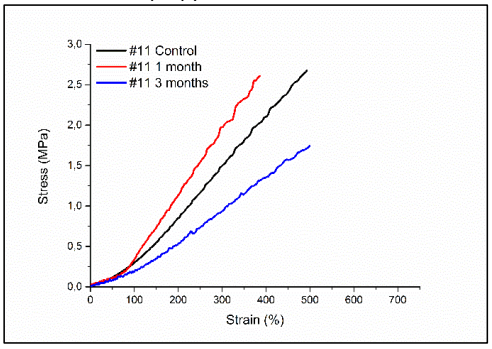

Stress-strain curve for #11 LR3043/50+ 100 phr PDMS-based silicone oil

Figure 5.6: Stress strain curves, before and after ageing of samples with oils.

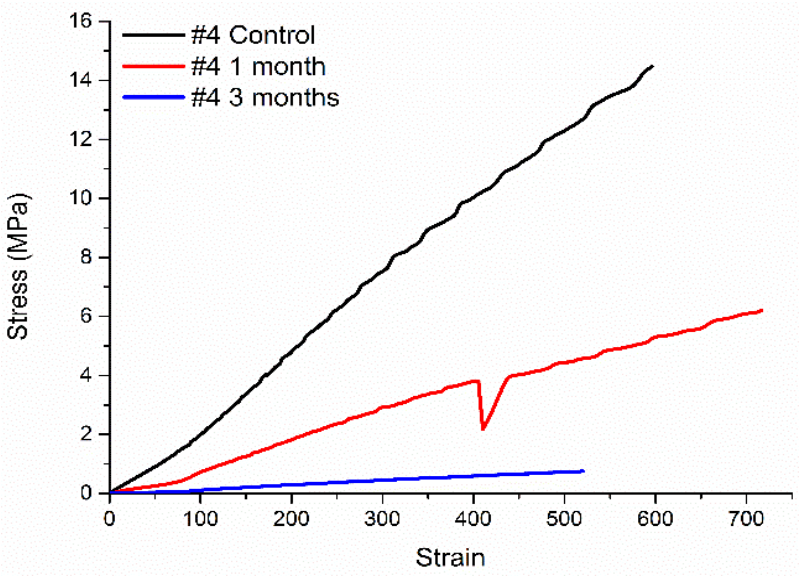

Figure 5.7: Stress-strain curves, before and after ageing, for sample #4 ((LR3043/50 + 30 phr Co-1).

5.3.3 Properties after ageing experiments: breakdown properties

Since the mechanical properties of samples containing copolymers and oils were all affected in one way or another by the strain-ageing experiments, it is also expected that the breakdown strength of the samples will be affected. The average breakdown strength from eight breakdown tests on each sample is shown in **Figure** 5.8 and summarised further in **Table** 5.4.

Within the bounds of experimental uncertainty, all samples roughly maintain their breakdown strength after ageing. There is, however, a trend for decreasing breakdown strengths after three months of ageing, expect for **samples** 6 (100 phr Co-1) and 7 (100 phr Co-2). These decreasing and increasing trends closely follow the detected changes in Young's moduli upon ageing.

In order to investigate the effect of ageing experiments on breakdown distribution, Weibull analyses were performed. Weibull is one of the most used methods for lifetime analysis and can furthermore provide information about the homogeneity and electrical reliability of an elastomer.

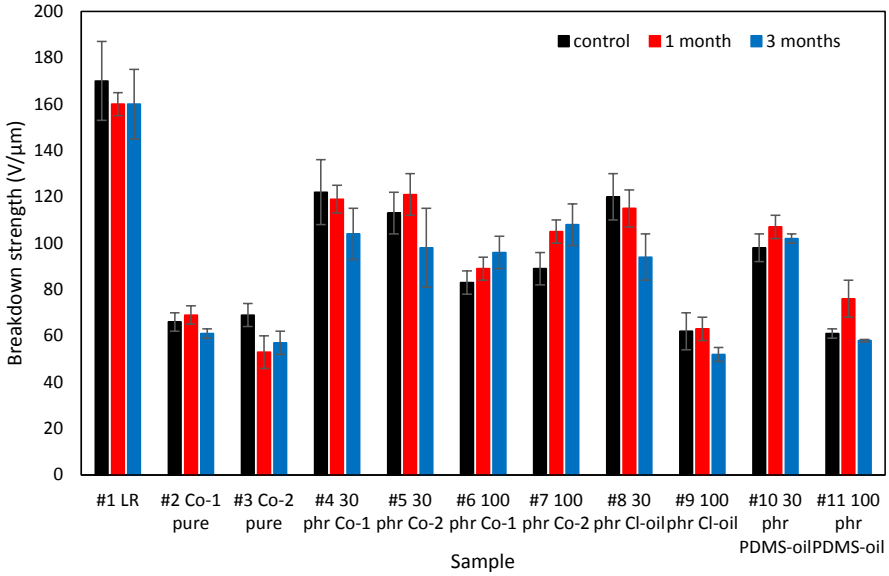

Figure 5.8: reakdown strengths, before and after the ageing experiments.

The breakdown data points (E_B) are therefore fitted to the Weibull cumulative distribution function, $F(E_B)$

$$F(E_B) = 1 - exp\left(-\frac{E_B}{\eta}\right)^{\beta} \qquad \text{Eq. 5.1}$$

The Weibull distribution function then can be linearised to give

$$ln[-ln(1 - F(E_B))] = \beta \cdot \ln(E_B) - \beta \cdot \ln(\eta) \qquad \text{Eq. 5.2}$$

The shape parameter, β, is then equal to the slope of the regressed line. It is desirable to have as large a β-value as possible, since this means that the breakdown values fall within a narrow range of voltages. A high β-value also gives an indication about homogeneity at the microscale, as the breakdown strength measurement is very sensitive to imperfections. η should also be as high as possible and is determined from the distribution at which 63% of the samples have broken down. The Weibull distribution results with β, η and a linear regression value (r^2) are shown in **Table** 5.3, whereas the Weibull probability plots from which the parameters have been determined can be found in the SI of Appendix D. The probability plot for LR3043/50 after three months of ageing shows two distributions, whereas the control sample and the sample after one month of ageing only show one distribution.

This indicates that three months of ageing destroys locally the properties of the LR3043/50 network and reduces local breakdown strength. Many of the samples containing chloropropyl functionality show peculiar breakdown behaviour in the Weibull probability plots, with two clearly separated distributions signifying two breakdown processes. As an example of this behaviour, the Weibull plot for **sample** 5 (LR3043/50 + 30 phr Co-2), after one month of ageing, is shown in **Figure** 5.9. This indicates that breakdown in these samples occurs specifically as a result of the presence of the chloropropyl groups and less because of actual defects. Chloropropyl groups may act as local 'defects' in the samples, perhaps owing to the agglomeration of the polar chloropropyl groups.

Table 5.3: Weibull parameters and r^2, before and after the ageing experiments. Red numbers indicate decreasing values compared to the control, and green numbers indicate increasing values in this regard.

		Scale (η) (V/μm)			Shape (β)			r^2		
No	Composition	control	one month	three months	control	one month	three months	control	one month	three months
#1	LR3043/50	183	158	167	11	53	11	0.76	0.95	0.89
#2	Co-1 pure + 25 wt% SiO_2	68	66	62	20	14	41	0.95	0.87	0.66
#3	Co-2 pure + 25wt% SiO_2	71	56	59	16	9	12	0.79	0.84	0.91
#4	LR3043/50 + 30 phr Co-1	127	119	109	11	19	11	0.75	0.95	0.75
#5	LR3043/50 + 30 phr Co-2	117	118	106	15	20	6	0.76	0.85	0.95
#6	LR3043/50 + 100 phr Co-1	85	82	100	19	25	13	0.82	0.88	0.98
#7	LR3043/50 + 100 phr Co-2	92	104	112	15	41	13	0.81	0.86	0.89
#8	LR3043/50 + 30 phr LMS-152 (chloro-oil)	124	114	99	13	31	9	0.97	0.87	0.97
#9	LR3043/50 + 100 phr LMS-152 (chloro-oil)	65	61	53	8	26	23	0.88	0.88	0.82
#10	LR3043/50 + 30 phr DMS-T22 (silicone-oil)	101	108	103	16	63	51	0.97	0.91	0.92
#11	LR3043/50 + 100 phr DMS-T22 (silicone-oil)	62	73	58	26	27	123	0.97	0.63	0.78

The Weibull distribution parameters show that strain-ageing experiments affect the reliability of the tested samples negatively as the scale parameter for most samples decreases. On the other hand, it can be seen from the shape parameters that most samples benefit from one month of ageing, since this leads to increases in β. This is probably due to the aforementioned removal of volatiles, which leads to more

homogenous elastomers and higher Young's moduli. After three months of ageing, only four samples maintain this positive effect of volatile removal, and true ageing effects have therefore set in. Furthermore, r^2, the linear regression goodness-of-fit value, decreases after three months of ageing for approximately half of the samples with no clear trend.

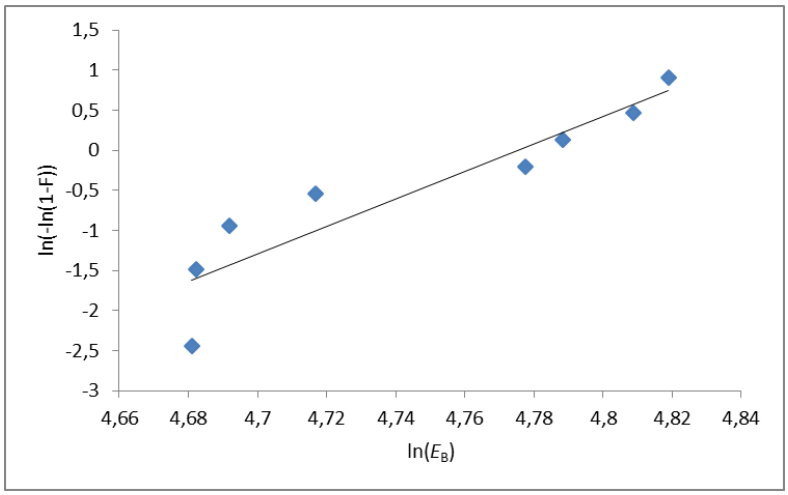

Figure 5.9: Weibull probability plot for #5 LR3043/50 + 30 phr Co-2 after one month of ageing.

5.3.4 Properties after the ageing experiments: figure of merit

The figures of merit, normalized to the reference elastomer LR3043/50 before and after the ageing experiments, are shown in **Table** 5.4. It is evident that the predicted performance of most elastomers improves after one month of aging, since normalized figure of merit values increase due to the small siloxanes and or solvent that have evaporated away from the elastomers and have thus increased breakdown strength. After three months of ageing, samples with high concentrations of oils (**sample** 9 and 11) show decreased predicted performance as a result of true ageing effects. Again, high concentrations of free species in the elastomers are shown to decrease overall DE properties significantly over time. The other samples' figures of merit after three months do not seem to follow any specific trend.

Table 5.4: Summary of properties, before and after the ageing experiments. Red numbers indicate decreasing values compared to the control, and green numbers indicate increasing values in this regard.

No	Composition	Thickness (µm)			Breakdown (V/µm)			Y @ 5% strain (MPa)			Tensile strength (MPa)			Strain @ break (%)			Normalized figure of merit		
		control	one month	three months	control	one month	three months	control	one month	three months	control	one month	three months	control	one month	three months	control	one month	three months
#1	LR3043/50	49	52	52	181±6	160±5	160±15	2.41	3.18	2.60	5.23	14.0	12.8	717	578	559	1	1	1
#2	Co-1 pure + 25 wt% SiO_2	80	76	82	66±4	69±4	61±2	0.54	0.16	0.17	0.65	0.70	0.70	429	429	410	3.7	6.4	4.0
#3	Co-2 pure + 25wt% SiO_2	113	153	140	69±5	53±7	57±5	0.52	0.63	0.45	1.27	1.59	1.52	314	320	286	1.3	1.0	1.4
#4	LR3043/50 + 30 phr Co-1	75	83	80	122±14	119±6	104±11	1.90	2.25	1.18	6.51	6.40	7.50	596	741	527	0.7	0.9	1.1
#5	LR3043/50 + 30 phr Co-2	106	86	106	113±9	121±9	98±17	2.00	2.89	2.63	5.06	9.30	7.34	314	423	271	0.7	0.8	0.5
#6	LR3043/50 + 100 phr Co-1	80	77	73	83±5	89±5	96±7	1.09	1.12	1.10	1.06	6.10	7.19	254	582	661	0.6	1.1	1.0
#7	LR3043/50 + 100 phr Co-2	129	111	87	89±7	105±5	108±9	1.29	1.56	1.49	3.71	7.70	6.04	256	306	342	0.6	1.2	1.1
#8	LR3043/50 + 30 phr LMS-152 (chloro-oil)	78	77	82	120±10	115±8	94±10	1.73	2.22	1.36	3.34	5.57	2.65	481	452	431	1.0	1.2	1.1
#9	LR3043/50 + 100 phr LMS-152 (chloro-oil)	96	101	101	62±8	63±5	52±3	0.60	0.84	0.57	0.78	1.08	1.91	269	309	533	1.0	1.2	1.0
#10	LR3043/50 + 30 phr DMS-T22 (silicone-oil)	99	75	71	98±6	107±5	102±2	0.87	1.55	1.03	4.43	5.56	5.76	658	456	445	0.9	1.0	1.1
#11	LR3043/50 + 100 phr DMS-T22 (silicone-oil)	94	71	85	61±2	76±8	58±0.5	0.27	0.75	0.46	1.51	2.60	1.74	493	385	499	1.1	1.1	0.8

5.4 CONCLUSION

Soft PDMS elastomers were prepared by using a strong commercial elastomer, LR3043/50, mixed with a choice of cross-linkable chloropropyl-functional copolymers, chloropropyl-functional silicone oil or PDMS-based silicone oil. Elastomer samples with different concentrations of soft fillers were subjected to static pre-stretching of 60% for up to three months, and characteristic dielectric elastomer properties, such as Young's modulus, strain at breaking and breakdown strength, were analyzed before and after the strain ageing experiments. The results showed that adding soft functional fillers to the LR3043/50 elastomer influenced its properties after ageing. One month of strain seemed to benefit most compositions, since small volatiles were allowed to escape from the elastomers during pre-stretching. This phenomenon enhanced the Young's moduli, tensile strength and strain at breaking, as well as breakdown strength, for the majority of the samples. After three months of pre-stretching, true ageing effects were seen for most of the samples, although some samples, such as those containing chloropropyl groups, seemed to benefit from three months of strain treatment, with significantly increased Young's moduli, strain at breaking and breakdown strengths as a consequence. This might be due to the migration of chloropropyl groups away from silica particles which are then able to reinforce the elastomers significantly. High concentrations of oils, whether chloropropyl-functional or PDMS-based, should be avoided, since this induces significantly reduced breakdown strengths and electromechanical reliability, both before and after strain ageing.

6 POST-CURING AS AN EFFECTIVE MEANS OF ENSURING THE LONG-TERM RELIABILITY OF PDMS THIN FILMS FOR DIELECTRIC ELASTOMER APPLICATIONS

The results presented in this chapter have been submitted to Macromolecular Materials and Engineering and is attached as Appendix E.

6.1 INTRODUCTION

Polydimethylsiloxane (PDMS) elastomers are synthesised through the equilibration polymerisation of low molecular weight linear and cyclic siloxanes in the presence of acid or base catalysts. One disadvantage of this process is the formation of undesired by-products caused by a premature chain termination reaction and unreacted cyclic oligomers [95]. These residues are mobile within the resulting PDMS elastomers, and under certain conditions they outgas to the elastomer's surface or any device interface, thus leading to contamination. Siloxane oligomers from the polymerisation process are a main contributor to silicone outgassing [119]; nonetheless, they are compatible with the PDMS elastomer matrix and may have very low vapour pressures, so the outgassing process is often very slow indeed. The performance of many PDMS elastomer-based devices is often reduced by outgassing [120], which changes the mechanical properties of elastomers, such as their tear strength and maximum elongation, due to the loss of a plasticising effect from the oligomers [119]. If the PDMS elastomer is intended for use in human-contact products such as medical applications, post-curing is mandatory in order to exclude outgassing in the final product. Post-curing, however, is tedious and therefore generally avoided. In post-curing, the volatiles from the cross-linked PDMS are normally removed by diffusion and evaporation at a higher temperature than the curing temperature. The rate at which this development proceeds depends on the physical and chemical properties of the utilised PDMS as well as on the geometry

and the design of devices (for example the thickness and total surface area) [119]. Rothka et al. [121] investigated the effect of post-curing on the outgassing of PDMS elastomers, which were initially post-cured for 4 hours at 204°C, resulting in a 2.7% mass loss. Subsequently, the post-cured PDMS elastomers were treated at 177°C for 20 hours, and the observed mass loss was then less than 0.5%. In comparison, with no post-curing the mass loss at 177°C for 24 hours was in the order of 4% (about eight times greater). It is thus evident that post-curing is a key parameter in respect to outgassing.

Several methods to produce PDMS elastomers with improved electromechanical properties have been developed, with the addition of fillers, such as metal oxides, being the most commonly investigated due to the ease of elastomer formulation. Incorporating rigid fillers into PDMS elastomers, though, changes intrinsic mechanical behaviour such as the Mullins effect, as discussed earlier. In a previous study (Chapter 4) we showed that non-post-cured elastomers with significant amounts of filler showed significant loss of tension over time upon pre-stretching to 120% for 3 months.

Brook et al.[119] reported that post-curing increases the Young's moduli of PDMS elastomers. Since the breakdown strength of PDMS elastomers is strongly dependent on the Young's modulus, breakdown strength is also very likely affected by post-curing [34]. Long-term mechanical and electrical reliability should be achievable if PDMS elastomers are post-cured before they are used in DE applications. Therefore, this study focuses on two types of PDMS elastomers commonly utilised as DE materials, namely commercial PDMS elastomers, one with and one without an additional 35 phr permittivity-enhancing filler (TiO_2), in order to investigate the effect of post-curing on the mechanical and electrical stability of DEs. The study was carried out by heating the cured PDMS elastomers at 200°C for 0, 5, 30, 60, 120 and 240 minutes subsequent to the initial curing procedure. Most commonly used curing conditions for addition-cure PDMS elastomers are ~120°C for 10-30 minutes. The resulting mechanical and electrical properties of the various samples were then measured. To our knowledge the effect of post-curing on, for example, breakdown strength has not been investigated previously, since the fraction of volatiles is so low (usually stated to be 1-2% by the elastomer supplier) that it has – so far – seemed irrelevant.

6.2 EXPERIMENTAL SECTION

6.2.1 Materials

Four different compositions of commercial PDMS, with and without permittivity-enhancing filler, were investigated. The pristine elastomers were Elastosil RT625 A/B and Elastosil LR3040/30 A/B from Wacker Chemie AG. Elastosil RT625 A/B is a room-temperature vulcanising *(*RTV) elastomer, supplied as a two-part system. The utilised mixing ratio of parts A and B is 9:1. Elastosil LR3040/30 A/B is a high-viscosity liquid silicone rubber (LSR) which is also supplied as a two-part system. The utilised mixing ratio of parts A and B was 1:1, as recommended by the supplier. Both commercial elastomers are naturally filled with SiO_2. The solvent OS-20 (an ozone-safe, volatile methylsiloxane fluid) was obtained from Dow Corning and was added in order to achieve a suitable viscosity for film coating. The OS-20 was added to the silicone formulation, as it also facilitates filler dispersion and thus produces more homogenous elastomer films.

The composites consist of the abovementioned elastomers compounded with hydrophobic titanium dioxide (TiO_2) R420 from Sachtleben Chemie, with an average primary particle size of 250 nm. The particles were added in quantities of 35 parts per hundred rubber (phr), equating to a mass fraction of 26% in the final composite. The OS-20 was added to both silicone formulations with TiO_2. For clarity, the commercial PDMS films will be referred to as *pristine* PDMS films, and composites containing additional 35 phr TiO_2 will be referred to as *filled* PDMS elastomers.

6.2.2 Sample preparation

Thin films were carefully prepared based on the procedures described in **Section** 2.2.1 (**Chapter** 2).

The prepared films were removed from the glass plates before post-curing was carried out in a ventilated oven at 200°C for 0 (control), 5, 30, 60, 120 and 240 minutes. The thicknesses of the prepared films were around 52-105 µm. Finally, the films were stored between 50 µm-thick ethylene-tetrafluorethylene (ETFE) foils, and kept in a desiccator until use.

6.2.3 Methods

6.2.3.1 The volatile content

The volatile content measurements were performed on 150 x 50 mm PDMS films with thicknesses of 52-105 µm. The weights of the PDMS films before and after 240 minutes of post-curing were taken, and the weight loss percentages of the volatiles were then calculated.

6.2.3.2 The differential scanning calorimetry (DSC)

The differential scanning calorimetry (DSC) analysis was performed with a TA Discovery DSC in an air atmosphere ranging from -90 to 100°C and at a heating rate of 10°C/min.

6.2.3.3 The thermogravimetric analysis (TGA)

The thermogravimetric analysis (TGA) was performed with a TA Discovery TGA. The films were heated in an air atmosphere up to 700°C and the heating rate was 10 °C/min.

6.2.3.4 Uniaxial extensional rheology

Uniaxial extensional rheology was performed to determine the Young's modulus at different strains. Rectangular strips of approximately 6 mm x 20 mm and 52-105 µm in thickness were prepared for the measurements, which were carried out by using an ARES-G2 with Sentmanat extensional rheology 2 (SER2) geometry. The SER2 has rotary clamps which are basically two cylinders winding up the sample, thus a step-wise increasing load can be applied and the corresponding elongations can be measured. The test specimen was elongated uniaxially at a steady Hencky strain rate of 0.001 (s^{-1}). Young's moduli were obtained from the tangent of the stress-strain curves from 0 to 130% strains.

6.2.3.5 Breakdown measurements

Refer to **Section** 3.3.3.

6.2.3.6 Linear viscoelasticity

Linear viscoelasticity for all samples was measured using an ARES-G2 rheometer (TA Instruments) set to a controlled strain mode, at 0.5% strain and with frequency sweeps from 100 Hz to 0.01 Hz at ambient temperature, using a parallel-plate

geometry of 25 mm in diameter. The elastomer samples for LVE measurements were 25 mm in diameter and 0.5-1.3 mm thick. Frequency sweeps of the samples were measured at different post-cure times (0, 5, 30, 60, 120 and 240 minutes). Time sweeps were performed on samples, A, B, C and D at 0 and 240 minutes of post-curing at a temperature of 200°C for 480 minutes at a constant strain (0.5%) and frequency (1 Hz). Temperature sweeps were likewise performed on these samples, using a temperature ramp mode within a temperature range of 20-200°C at a constant strain (0.5%) and frequency (1 Hz).

6.3 RESULTS AND DISCUSSION

Four different PDMS elastomer compositions were tested in post-cure experiments, namely the two commercial elastomers RT625 and LR3040/30 as well as RT625 with 35 phr TiO_2 and LR3040/30 filled with 35 phr TiO_2. The TiO_2 particles were mixed into the elastomer premixes (using a SpeedMixer) before curing together with solvent, in order to facilitate proper mixing and film-casting. After the initial cure, which was carried out at 75^{o}C for 5 minutes and subsequently at 115^{o}C for 10 minutes, the prepared films were removed from the glass plates, following which post-curing was carried out at 200°C for 0 (control), 5, 30, 60, 120 and 240 minutes.

The content of volatiles in the samples was measured by examining the weight of the samples before and after the post-curing treatment at 200°C for 5, 30, 60, 120 and 240 minutes. The results were calculated in terms of actual loss as a percentage as well as loss relative to the pure elastomer matrix for samples containing TiO_2. The results are also shown in **Table** 6.1 and **Figure** 6.1.

Table 6.1: Weight loss of PDMS elastomer films after post-curing for 5, 30, 60, 120 and 240 minutes. The weight loss of samples with TiO_2 is furthermore calculated relative to the commercial elastomer (by excluding the TiO_2 mass) for easy comparison with pure commercial elastomers.

Sample ID	Materials	5 min.		30 min.		60 min.		120 min.		240 min.	
		Loss (%)	Loss relative to elastomer matrix (excluding filler) (%)	Loss (%)	Loss relative to elastomer matrix (excluding filler) (%)	Loss (%)	Loss relative to elastomer matrix (excluding filler) (%)	Loss (%)	Loss relative to elastomer matrix (excluding filler) (%)	Loss (%)	Loss relative to elastomer matrix (excluding filler) (%)
A	RT625	0.4	0.4	0.7	0.7	1.0	1.0	1.1	1.1	1.2	1.2
B	LR3040/30	0.2	0.2	0.7	0.7	1.3	1.3	1.4	1.4	1.7	1.7
C	RT625 + 35 phr TiO_2	1.4	1.9	2.6	3.6	3.2	4.4	3.7	4.9	3.9	5.3
D	LR3040/30 + 35 phr TiO_2	1.8	2.4	2.4	3.2	2.7	3.7	3.2	4.3	3.5	4.7

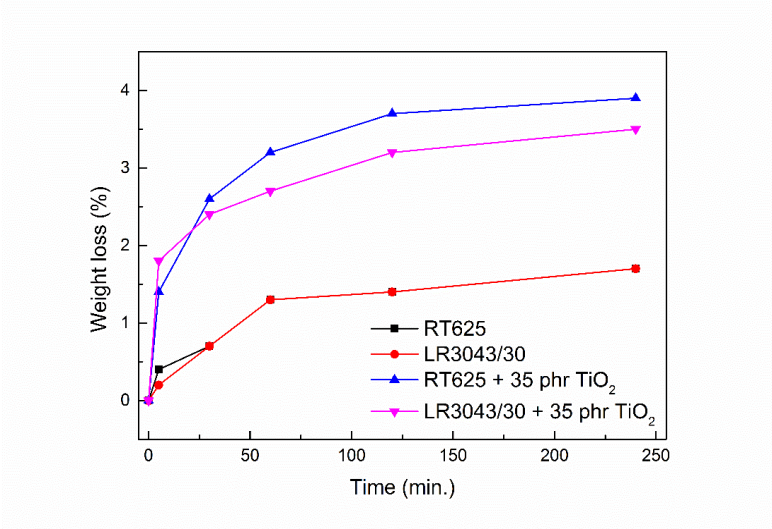

Figure 6.1: Weight loss as a function of post-cure time.

From the results in **Table** 6.1 **and Figure** 6.1, it is clear that post-curing filled elastomers results in a higher mass loss of volatiles compared to the two pristine PDMS elastomers. During film preparation, solvent and other volatiles may be adsorbed by the TiO_2 particles, and thus these strongly influence the diffusion of volatiles during the initial cure. In principle the solvent utilised for the filled samples should have been completely removed during curing, but from the results in **Table** 6.1 it is clear that the cured samples with TiO_2 contain a higher fraction of volatiles.

This again illustrates the importance of post-curing especially for PDMS elastomers with high filler content. It is also clear that outgassing depends not only on sample geometry, but also, to a large extent, on sample composition. It can also be seen from **Figure** 6.1 that most of the outgassing occurs after approximately 60 minutes, and thereafter only minor outgassing is taking place.

A determination of the content of volatiles in the films before and after post-curing was undertaken using thermogravimetric analysis (TGA). **Figure** 6.2 shows TGA thermograms of the four elastomers after 0 and 240 minutes of post-curing, respectively.

A time of 240 minutes was chosen as the maximum post-curing time, as this is a commonly required treatment for thick PDMS elastomers.[119] Samples without post-curing show significant weight loss from room temperature to the first degradation process (around 350^{o}C) in the order of 3-5%. In comparison, samples which have been extensively post-cured show significantly smaller weight loss over the same temperature range, as the volatiles inside the elastomer films have been effectively removed during the post-curing process. The TGA thermograms for all samples post-cured at the different timespans can be found as supplementary information (SI) for Appendix E.

The effect of post-curing on thermal transition behaviour in elastomers was examined by differential scanning calorimetry (DSC). All thermograms for samples post-cured at different timespans can be found as SI for Appendix E. An exothermic peak is observed for both the post-cured and the non-post-cured PDMS films during cooling, which corresponds to crystallisation processes taking place in the films. During heating, an endothermic peak is observed, which corresponds to the crystallites melting. The temperatures for which crystallisation and melting occur are denoted by T_c and T_m, respectively. The DSC results indicate that post-curing causes only a marginal effect on T_m. The results also indicate that the pristine PDMS films (*A* and *B*) exhibit lower T_c upon post-curing. Inversely, upon post-curing, the TiO_2-filled PDMS films have higher than or similar T_c to their non-post-cured counterparts. The high filler content in the filled samples thus greatly influences the thermal behaviour of the PDMS films. The glass transition temperatures, T_g, do not change significantly after post-curing.

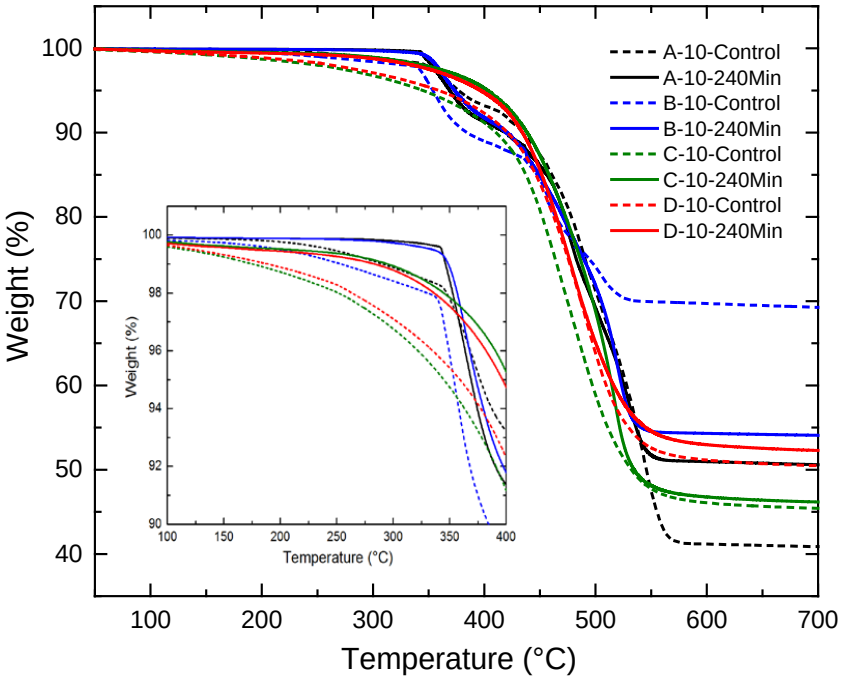

Figure 6.2: TGA curves for the investigated pristine and filled PDMS elastomer films with and without post-curing treatment. Heating rate of 10 °C/min in air atmosphere. (A = RT625, B = LR3040/30, C = RT625 + 35 phr TiO_2, D = LR3040/30 + 35 phr TiO_2).

From the obtained results – so far – it is obvious that outgassing is to be expected if post-curing is omitted during film fabrication. Thus, changes in the mechanical properties of the elastomer films over time are expected. In order to investigate these changes in mechanical properties with post-curing time, the Young's modulus as a function of strain for the different samples was measured before and after post-curing for different timespans. **Figure** 6.3 shows the Young's modulus at 5% strain as a function of post-curing time. The Young's moduli at 5% strain are furthermore summarised in **Table** 6.2 together with their percentage-wise increase induced by the post-cure. As seen in **Figure** 6.3 and **Table** 6.2, the Young's moduli of the control samples of the two pristine elastomers are in the same order of magnitude. After post-curing, the Young's moduli, however, have increased to different extents. RT625 experienced a maximum increase of 68% following 120 minutes of post-curing, while LR3040/30 experienced a maximum increase in the Young's modulus of 108% after 240 minutes of post-curing. LR3040/30 thus becomes significantly

stiffer than RT625 over time despite it containing a lower percentage of volatiles. This also means that LR3040/30 will change more over time than RT625 if the post-curing of samples is not performed prior to use as DEs. As seen in **Figure** 6.3 and **Table** 6.2, elastomers with TiO_2 experience a dramatic increase in the Young's modulus compared to the pristine elastomers. This is expected when adding hard fillers to a PDMS elastomer. Nevertheless, the samples do not experience similar increases despite having similar initial Young's moduli, possibly due to a difference in the composition of the two elastomers RT625 and LR3040/30. Upon post-curing, the two elastomers with TiO_2 also show different behaviour. The modulus of RT625 + 35 phr TiO_2 increases by more than 200% after post-curing, which thus has a dramatic effect upon the mechanical properties of the filled RT625. LR3040/30 + 35 phr TiO_2 show a modulus increase of 100%, which is comparable to what was experienced by its pristine counterpart. Furthermore, it applies to all samples that increase in Young's modulus levels after 120 minutes of post-curing.

Table 6.2: Breakdown strength data and Young's moduli at 5% strain for different post-cure times. (A = RT625, B = LR3040/30, C = RT625 + 35 phr TiO_2, D = LR3040/30 + 35 phr TiO_2).

Sample ID	Post-cure time (min)	Breakdown strength (V/μm)	Increase in breakdown strength compared to control (%)	Thickness (μm)	Breakdown voltage (V)	Y at 5% strain (MPa)	Increase in Young's modulus compared to control (%)
A-Control	0	98±4	-	69	6791	0.56	-
A-5Min	5	107±3	9.2	69	7419	0.72	28.6
A-30Min	30	112±5	14.3	68	7683	0.77	37.5
A-60Min	60	109±4	11.2	67	7368	0.88	57.1
A-120Min	120	115±3	17.3	67	7718	0.94	67.9
A-240Min	240	114±4	16.3	66	7545	0.86	53.6
B-Control	0	108±5	-	70	7566	0.53	-
B-5Min	5	106±3	-1.9	69	7353	0.56	5.7
B-30Min	30	117±3	8.3	68	8018	0.96	81.1
B-60Min	60	119±3	10.2	68	8126	0.89	67.9
B-120Min	120	122±3	13.0	67	8195	1.03	94.3
B-240Min	240	126±4	16.7	67	8421	1.10	107.5
C-Control	0	133±6	-	53	7031	1.04	-
C-5Min	5	140±4	5.3	53	7460	1.65	58.7
C-30Min	30	152±5	14.3	53	8083	2.18	109.6
C-60Min	60	155±5	16.5	52	8098	2.31	121.2
C-120Min	120	165±4	24.1	52	8591	3.06	194.2
C-240Min	240	179±6	34.6	52	9305	3.23	210.6
D-Control	0	138±4	-	65	8911	2.71	-
D-5Min	5	141±4	2.2	65	9205	3.64	34.3
D-30Min	30	147±3	6.5	65	9586	3.77	39.1
D-60Min	60	158±3	14.5	63	9967	4.73	74.5
D-120Min	120	168±3	21.7	63	10593	5.42	100
D-240Min	240	184±3	33.3	63	11790	5.42	100

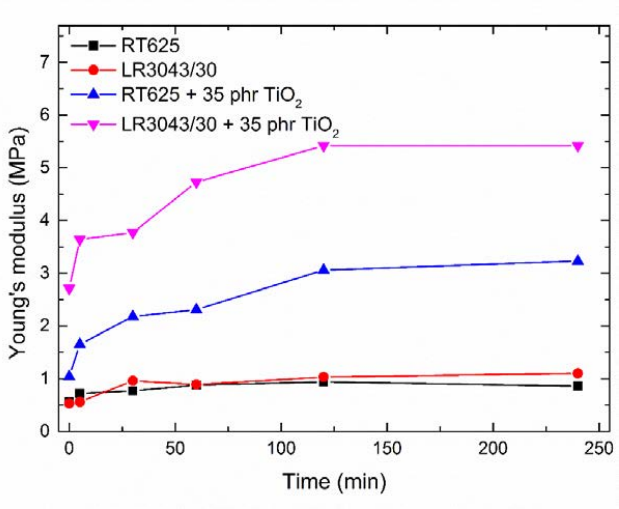

Figure 6.3: Young's modulus at 5% strain as a function of post-cure time.

Figure 6.4 illustrates stress-strain behaviour up to 130% strain of elastomers before and after post-curing for 240 minutes. The stress-strain curves clearly illustrate the stiffening effect of post-curing, which is especially pronounced for elastomers with TiO_2 fillers.

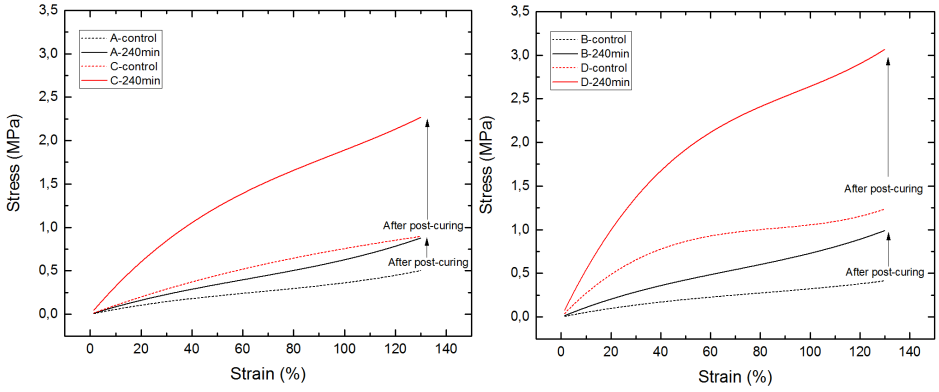

Figure 6.4: Illustrates stress-strain behaviour up to 130% strain of elastomers before and after post-curing for 240 minutes. The stress-strain curves clearly illustrate the stiffening effect of post-curing, which is especially pronounced for elastomers with TiO_2 fillers.

Figure 6.5 shows the Young's moduli and normalized Young's moduli as a function of strain after different post-curing timespans for the pristine PDMS films RT625 and LR3040/30. Normalized Young's moduli ($Y_n(s)$) are calculated from $Y_n(s) = \frac{Y(s)}{Y_0(s)}$,

where *Y(s)* is the Young's modulus for post-cured elastomer films at a given strain, and Y_0 is the corresponding Young's modulus for the non-post-cured samples at the same strain. The effect of post-curing on the pristine elastomers is illustrated in **Figure** 6.5. Both investigated pristine elastomers show identical behaviour with increased Young's moduli during increased post-curing periods. The pristine elastomers both exhibit significant strain-softening up to approximately 70% strain, following which strain-hardening effects sets in. This characteristic property of PDMS elastomers leads to a local minimum in the Young's modulus as a function of strain. Strain-hardening is particularly favourable in the context of avoiding the electromechanical instability (EMI) phenomenon which occurs when local Maxwell pressure exceeds the compressive stress of the elastomer [10, 122, 123]. The normalized Young's modulus plots (**Figure** 6.5 (b)) show that LR3040/30 benefits on this occasion from post-curing, since the curves become more strain-hardening. The effect is less pronounced for RT625.

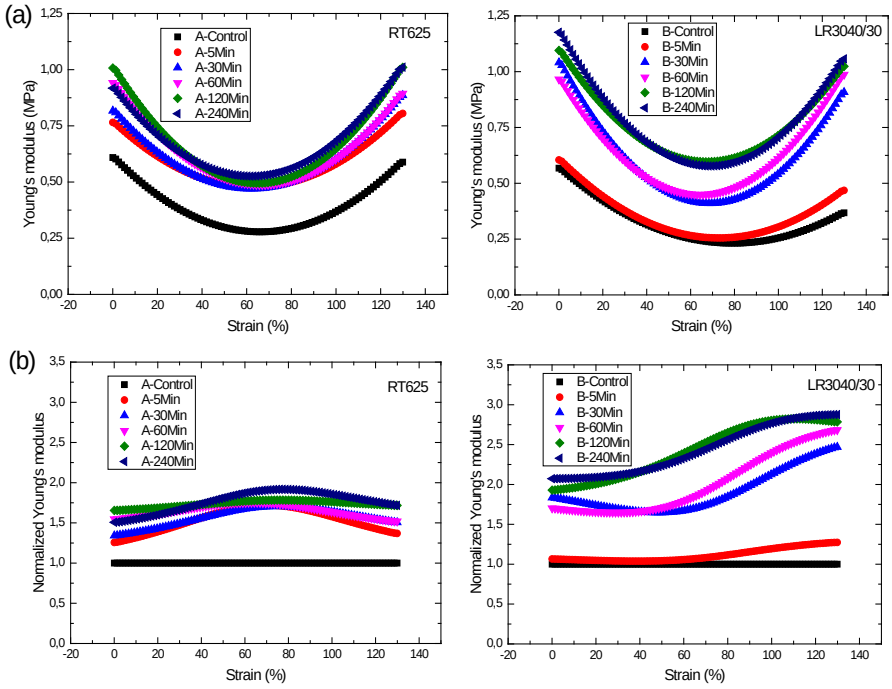

Figure 6.5: Young's modulus (a) and normalized Young's modulus (b) as function of strain at different post-curing period for the pristine PDMS films. (A = RT625 and B = LR3040/30)

Young's moduli and normalized Young's moduli as functions of strain for RT625 and LR3040/30 with 35 phr TiO_2 are shown in **Figure** 6.6. The two different TiO_2-filled elastomers show very different responses in the Young's modulus as a function of strain. Filled LR3040/30 shows significantly more strain-hardening and softening behaviour than filled RT625, while the normalized Young's moduli plots as functions of strain (**Figure** 6.6 (b)) also illustrate the different behaviours between the two elastomers. After post-curing the filled RT625 exhibits more strain-dependent effects than the non-post-cured control sample. LR3040/30, on the other hand, experiences very different effects. After post-curing for longer than 5 minutes, the curves change shapes from concave to convex, with a peak maximum at approximately 85% strain. This phenomenon is only seen for the filled LR3040/30 elastomer and can be attributed to the high filler content within the elastomer. Up to a certain strain the elastomer exhibits stress-hardening behaviour where after stress-softening sets in due to the high filler content, which in turn induces significant Mullins effects such as the rupture of filler clusters and the separation of weak polymer chains from the fillers [102]. The strain-hardening that is experienced after post-curing up to approximately 80% strain is, as mentioned previously, beneficial in the context of avoiding EMI. Post-curing therefore improves this failure mode of filled DEs.

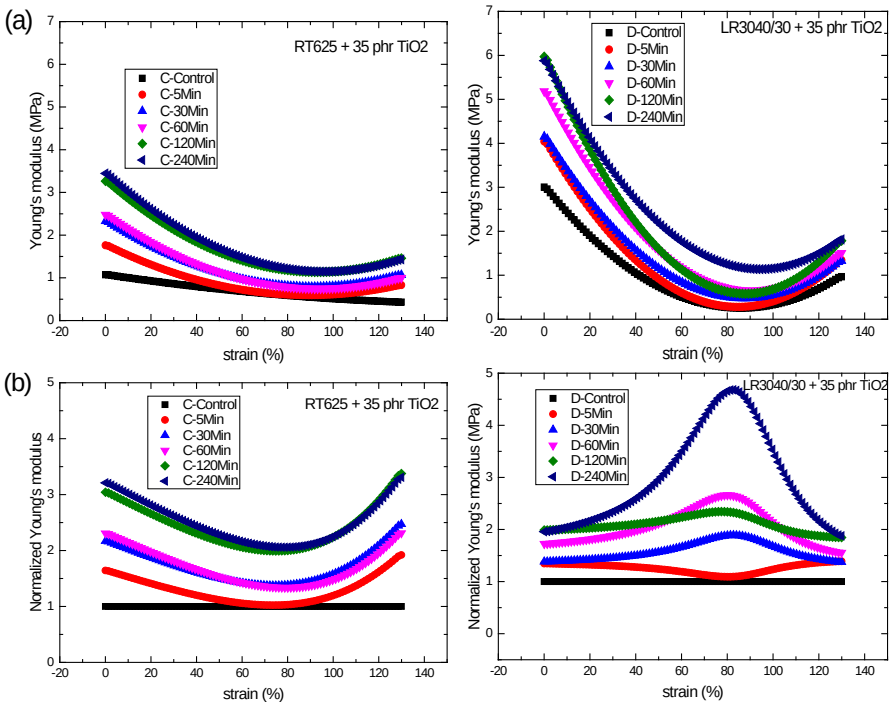

Figure 6.6: Young's modulus (a) and normalized Young's modulus (b) as function of strain at different post-curing period for the filled PDMS films. (C = RT625 + 35 phr TiO_2 and D = LR3040/30 + 35 phr TiO_2).

Figure 6.7 shows the storage modulus and loss (tan δ) as a function of temperature at a constant strain and frequency. It can be seen that all samples experience the same behaviour, to a greater or lesser extent. After post-curing, all materials have become significantly stiffer, as illustrated by the increase in storage modulus. Before post-curing, all samples experience a temperature-independent storage modulus, whereas thereafter the storage modulus drops as a function of temperature. Since the modulus drop is more pronounced for samples with high filler content, it may be ascribed to polymer-filler interactions such as the relaxation of polymer chains surrounding the fillers. Thus, for these samples polymer-filler interactions are more pronounced than entropic elasticity, which would have led to storage modulus increases in line with increasing temperatures [124]. The losses are seen to decrease when the temperature increases, meaning that the samples become less dissipative at increasing temperatures. In the SI for Appendix E, time and frequency sweeps for different post-cure timespans can be found for all samples. These results confirm that samples become stiffer after post-curing and that no 'actual' post-curing (further cross-linking) takes place during the process, since the loss factor does not decrease thereafter.

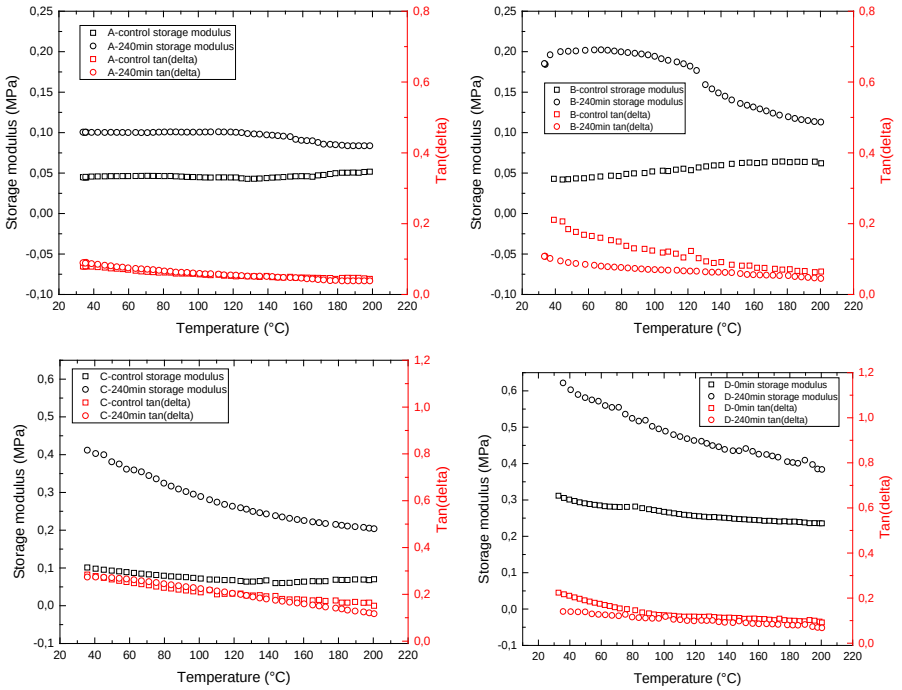

Figure 6.7: Storage modulus and loss (tan δ) as a function of temperature before and after 240 minutes of post-curing for (A = RT625, B = LR3040/30, C = RT625 + 35 phr TiO_2 and D = LR3040/30 + 35 phr TiO_2).

Since post-curing changes the Young's moduli of elastomers, breakdown strength may also be affected, as the breakdown strength of DE films has been found previously to scale linearly – or even exponentially – with the Young's modulus[20, 34]. **Table** 6.2 shows breakdown strength and Young's moduli at 5% strain at different post-cure times. Breakdown strength as a function of Young's moduli at 5% strain is furthermore shown in **Figure** 6.8. As expected, the breakdown strengths of elastomer samples increase as the Young's moduli increase. For both types of pristine elastomers a maximum increase of 16-17% is obtained following post-curing, which means that post-curing effectively increases the breakdown strength of commercial DE films. Furthermore, the results show that the breakdown strength of heavily filled PDMS elastomers increases to a greater extent than for the pristine elastomers. The filled elastomers both experience an increase in breakdown strength of 33-34%, which is almost two-fold higher than for the pristine elastomers.

This means that heavily filled elastomers benefit to a very great extent from post-curing.

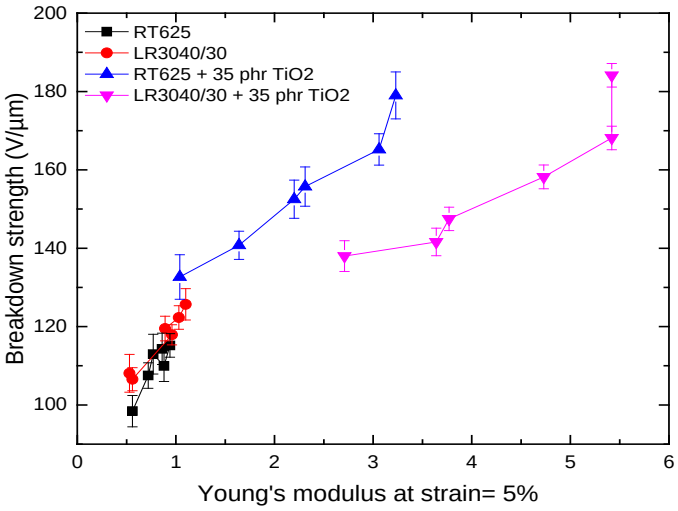

Figure 6.8: Breakdown strength as function of Young's modulus for the PDMS films. The Young's moduli for all tested samples are presented according to elevated post-curing periods at 0-control, 5 min, 30 min, 60 min, 120 min and 240 min.

An analysis was performed in order to investigate the effect of post-curing elastomer films on breakdown strength distribution. The Weibull distribution is one of the most commonly used methods in lifetime analysis and can provide insights into the electrical reliability of an elastomer. The breakdown data points (E_B) are therefore fitted to the Weibull cumulative distribution function, $F(E_B)$ (**Equation** 5.1 (**Chapter** 5)) which can be linearised to give **Equation** 5.2 (**Chapter** 5).

The Weibull shape parameter, β, is equal to the slope of the regressed line. Different β values lead to noticeable effects on lifetime distribution, and β is also required to be as large as possible, such that the measured breakdown strengths all fall within a narrow range of voltages. This is furthermore an indication of homogeneity on the microscale. The Weibull scale parameter, η, which is determined from the distribution at which 63% of the films have broken down electrically, should be as high as possible and locate distribution along the scale. **Table** 6.3 shows the Weibull distribution results with β, η and linear regression (r^2) in a probability plot for control samples and 240 min of post-cured films. The results show that post-curing significantly increases the reliability of the tested elastomer films as the scale and

the shape parameters increase. This improvement is, amongst other things, attributed to the increase in the Young's modulus of the PDMS films upon post-curing.[34] Post-curing also extensively removes the volatiles that contribute to modulus inhomogeneities and defects which are introduced during film preparation.[119] Furthermore, since r^2, the linear regression goodness-of-fit values become closer to 1, and the breakdown data thus become better fitted to the Weibull distribution after post-curing. This again indicates that elastomers become more homogenous after post-curing, since small-molecule inhomogeneities have been removed.

Table 6.3: Weibull parameters and r^2 for the control and 240-minute post-cured films.

Parameter	scale (η) (V/μm)		shape (β)		r^2	
	Before post-cure	After post-cure 240 min	Before post-cure	After post-cure 240 min	Before post-cure	After post-cure 240 min
A(RT625)	99	114	27	33	0.95	0.97
B(LR3040/30)	110	127	26	34	0.85	0.94
C(RT625 + 35 phr TiO_2)	135	182	28	34	0.88	0.96
D(LR3040/30 + 35 phr TiO_2)	140	186	42	71	0.92	0.93

Figure 6.9 and **Figure** 6.10 show the cumulative probability of failure, from which shape and scale parameters as well as r^2 have been determined. It is clear from **Figure** 6.9 that sample B, before post-curing, experiences breakdown behaviour, with two clearly separated distributions signifying two breakdown processes. The first part of the data points is most likely due to small defects and filler agglomeration in the highly filled LR3040/30, whereas the second part of the data point distribution represents 'true' breakdown processes. This behaviour is significantly smaller after post-curing, thereby indicating that post-curing eliminates some of the causes of early breakdown phenomena, which can also be seen from the shape and scale parameters as well as the r^2 values. The same behaviour can be seen for the TiO_2-filled samples in **Figure** 6.10, where both elastomers experience two breakdown distributions before post-curing, and where the behaviour is significantly reduced thereafter.

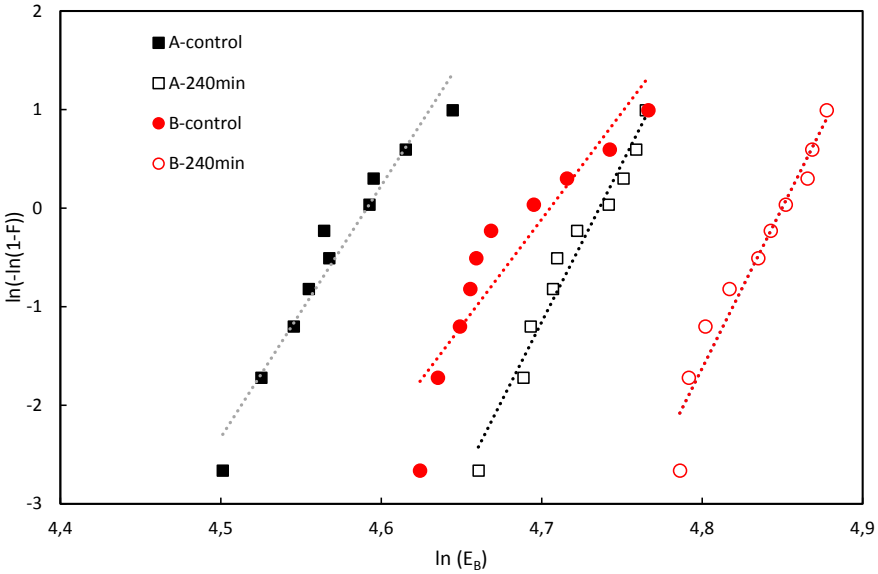

Figure 6.9: Cumulative probability of failure of the pristine PDMS films before and after post-curing. (A=RT625 and B=LR3040/30)

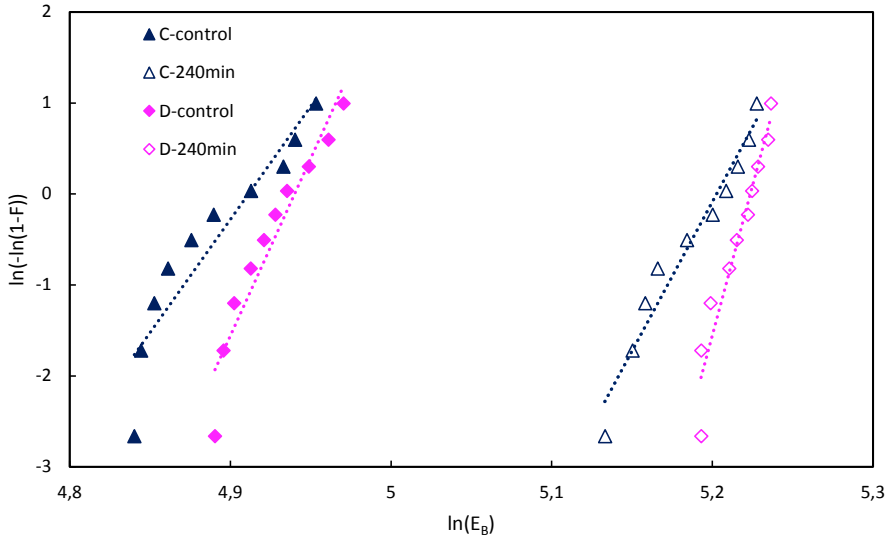

Figure 6.10: Cumulative probability of failure of the filled PDMS films before and after post-curing. (A= RT625 + 35 phr TiO_2 and B= LR3040/30 + 35 phr TiO_2)

6.4 CONCLUSION

Four samples with different compositions were prepared, namely a commercial RTV elastomer, RT625, a commercial LSR elastomer, LR3040/30, and the two mentioned elastomers with additional 35 phr added TiO_2. Important properties in relation to dielectric elastomers were measured before and after post-cure treatment at 200°C for up to 240 minutes. This included the effect of post-curing on thermal properties, elastic/mechanical properties and breakdown strength. This study shows that even commercial PDMS elastomers require post-curing for electromechanical reliability. This is an overlooked feature of PDMS elastomers utilised in dielectric elastomers. The two commercial elastomers (RTV and LSR) both show improved strength over the post-curing period. This phenomenon can be ascribed to the evaporation of volatiles and other residues from the PDMS films at high temperatures. In other words, the elastomer will not provide constant actuation over time if it is not ensured that all volatiles have been removed beforehand. The removal of volatiles is furthermore favourable, as it increases breakdown strength and thus enhances the reliability of the elastomer.

7 CONCLUSION AND FUTURE WORK

The summary of the research and some suggestions for future work are discussed in this chapter.

7.1 CONCLUSION

In this thesis, two research strategies are presented in order to produce a dielectric elastomer (DE) which not only possesses excellent electrical performance but also with electromechanical reliable. The first strategy is to understand the mechanism behind the electrical breakdown of DEs. The effect of temperature on dielectric properties of polydimethylsiloxane (PDMS) elastomers was investigated experimentally and subsequently the electrothermal breakdown in PDMS elastomers was modelled from the obtained data. From this study, it can be concluded that electrothermal breakdown of the PDMS elastomers was strongly affected by the increase in both relative permittivity and conductivity. Furthermore, since the electrical field required for thermal runaway was predicted about 5 times larger than the reported breakdown fields of PDMS elastomers, therefore, the electrothermal breakdown may not be a major factor to cause electrical breakdown in PDMS based DEs.

Several parameters related to breakdown measurements of pre-stretched PDMS elastomers, namely sample volume, sample thickness, sample strain and electrode configuration were also characterized. From the obtained results, it can be concluded that breakdown strengths of the pre-stretched PDMS elastomers were shown to be over-estimated if the decrease in volume following pre-stretching was not taken into consideration. Therefore, in order to get reliable determinations of breakdown strength a careful experimental design is required. In addition to that, pre-stretching of PDMS elastomer films was also shown to have a great influence on

the breakdown strength of PDMS elastomers. It means that the morphology of samples was affected by pre-stretching as a result of, for instance, chain and defect alignment.

The second strategy of the thesis is to investigate the long-term electromechanical reliability of DEs. Therefore, long-term electromechanical reliability of pre-stretched PDMS elastomers with *hard* and *soft* fillers was investigated. From this study, the PDMS elastomers with *hard* filler particles were found to lose their tension very quickly upon pre-stretching of the elastomer. Therefore, it is recommended to further functionalise the filler particles when high loadings of fillers are required in elastomer formulations for better compatibility and mechanical integrity. Interestingly, the commercial elastomers (RT625 and LR3043/30) showed increased Young's modulus over a time scale of weeks, and thus a decrease in actuation took place. This phenomenon can be ascribed to the evaporation of solvents and other volatiles from elastomers which have had their protective surface broken during pre-stretching. Meanwhile, for over a timescale of months, a small reduction in elasticity took place due to mechanical ageing.

The effect of pre-stretching of PDMS elastomers with *soft* filler on electromechanical reliability was also investigated. The results showed that the pre-stretched PDMS elastomer that adding soft functional fillers also affected its properties after pre-stretching up to 3 months. Interestingly, the PDMS elastomers filled with *soft* fillers showed similar strain ageing behaviour with pre-stretched PDMS elastomers filled with *hard* filler. The first stage of strain ageing (one month of pre-stretching) showed to benefit most samples, since small volatiles were allowed to escape from the elastomers during pre-stretching. This phenomenon increased the Young's moduli, tensile strength and strain at break, as well as breakdown strength, for the majority of the samples. Then, the second stage of stain ageing (after three months of pre-stretching), true ageing effects were seen for most of the samples. However, PDMS elastomers with covalently grafted chloropropyl groups seemed to benefit from three months of strain treatment, with significantly increased Young's moduli, strain at break and breakdown strengths as a consequence. This might be due to the migration of chloropropyl groups away from silica particles which are then able to reinforce the elastomers significantly. High concentrations of oils, whether chloropropyl-functional or PDMS-based, are not recommended, since the oils lead to significantly reduced breakdown strengths and mechanical reliability, both before and after strain ageing.

Lastly, the effect of post-curing on the electromechanical reliability of PDMS elastomers was investigated. This study showed that even commercial PDMS films require post-curing for electromechanical reliability. The commercial elastomers (RTV and LSR) showed improved elasticity over the post-curing period. This phenomenon can be ascribed to the evaporation of volatiles and other residues from

the PDMS films at high temperature. In other words, the elastomer will not provide constant actuation over time if it is not ensured that all volatiles have been removed beforehand.

7.2 FUTURE WORK

Considerations and proposals for future work derived from the project are discussed in the following:

7.2.1 Electrical breakdown

Electrothermal breakdown can also be investigated experimentally by measuring the breakdown strength of PDMS elastomers at different temperatures. A device capable of measuring the breakdown strength of PDMS elastomers at different temperatures could be developed and attached to the breakdown instrument. The data obtained together with the data from this thesis then could be used to model the electrothermal breakdown of DEs. Another breakdown mechanism that normally occurs in DEs is electromechanical instability (EMI). EMI occurs on activated DEs and causes the elastomer to thin drastically, often leading to electrical breakdown due to the resulting high field. Therefore in the future, EMI phenomenon in DEs could be modelled. The results of this proposed study would be even more valuable if the synergy effects of both mechanisms, i.e. electrothermal breakdown and EMI, were taken into consideration in investigation the electrical breakdown mechanisms in the DEs.

7.2.2 Mechanical ageing

It would also be interesting to study the effect of dynamic stretching on the mechanical ageing of PDMS elastomers, which are expected to show significantly different behaviour compared to static pre-stretching. In addition, a mechanical ageing study of DEs also could be done on the dynamic stretched PDMS elastomers with a constant voltage applied over the elastomer. Thus, mechanical and electrical ageing effects of DEs could be investigated.

7.2.3 Post-curing

A further study could also be done on post-curing the PDMS elastomers filled with soft fillers, such as investigating the effects of heat treatment on theirs long-term electromechanical reliability.

REFERENCES

1. Kornbluh R, Eckerle J, Andeen G (1991) Artificial muscle: the next generation of robotic actuators. The 4th World Conference of Robotics Research SME Paper MS91–331:1–8
2. Pelrine R, Eckerle J, Chiba S (1992) Review of artificial muscle approaches, invited paper. Proceedings of the 3rd International Symposium on Micro Machine and Human Science: 1–19
3. Kornbluh R, Pelrine R, Joseph J (1995) Elastomeric dielectric artificial muscle actuators for small robots. Proceedings of the 3rd IASTED International Conference on Robotics and Manufacturing: 1–6
4. Pelrine R, Kornbluh RD, Eckerle J, Jeuck P, Oh S, Pei Q, Stanford S (2001) Dielectric elastomers: generator mode fundamentals and applications. Proceeding of SPIE 4329:148–156
5. Carpi F, De Rossi D, Kornbluh R, Pelrine R, Sommer-Larsen P (2008) Dielectric Elastomers as Electromechanical Transducers: Fundamentals, Materials, Devices, Models and Applications of an Emerging Electroactive Polymer Technology. Elsevier Ltd, Oxford UK
6. Brochu P, Pei Q (2010) Advances in dielectric elastomers for actuators and artificial muscles. Macromolecular rapid communications 31:10–36
7. Kussmaul B, Risse S, Wegener M, Kofod G, Krüger H (2012) Matrix stiffness dependent electro-mechanical response of dipole grafted silicones. Smart Materials and Structures 21:64005
8. Fothergill JC, Dissado LA (1992) Electrical degradation and breakdown in polymers. IET, UK
9. Anonymous (2012) Danfoss PolyPower A/S – White Paper: PolyPower® DEAP actuator elements. Danfoss A/S, Nordborg, Denmark
10. Stark KH, Garton CG (1955) Electric strength of irradiated polythene. Nature 176:1225
11. Blok J, LeGrand DG (1969) Dielectric breakdown of polymer films. Journal of Applied Physics 40:288–293
12. Xiaoguang Q, Zhong Z, Boggs S (2003) Computation of electro-thermal breakdown of polymer films. Conference on Electrical Insulation and Dielectric Phenomena: 337–340
13. Kulik VM, Boiko AV, Bardakhanov SP, Park H, Chun HH, Lee I (2011) Viscoelastic properties of silicone rubber with admixture of SiO2 nanoparticles. Materials Science and Engineering: A 528:5729–5732

14. Pelrine BR, Kornbluh R, Kofod G (2000) High Strain Actuator Materials Based on dielectric elastomers. Advanced Materials 94025:1–6

15. Stoyanov H, Mc Carthy D, Kollosche M, Kofod G (2009) Dielectric properties and electric breakdown strength of a subpercolative composite of carbon black in thermoplastic copolymer. Applied Physics Letters 94:232903–232905

16. Fuqiang T, Qingquan L, Xuan W, Yi W (2012) Investigation of electrical properties of LDPE/ZnO nanocomposite dielectrics. IEEE Transactions on Dielectrics and Electrical Insulation 19:763–769

17. Mendes SF, Costa CM, Caparros C, Sencadas V, Lanceros-Méndez S (2012) Effect of filler size and concentration on the structure and properties of poly(vinylidene fluoride)/BaTiO3 nanocomposites. Journal of Materials Science 47:1378–1388

18. Andritsch T, Kochetov R, Gebrekiros YT, Lafont U, Morshuis PHF, Smit JJ (2009) Synthesis and dielectric properties of epoxy based nanocomposites. IEEE Conference on Electrical Insulation and Dielectric Phenomena, CEIDP '09: 523–526

19. Molberg M, Crespy D, Rupper P, Nüesch F, Månson J-AE, Löwe C, Opris DM, Nuesch F, Manson JAE, Lowe C (2010) High Breakdown Field Dielectric Elastomer Actuators Using Encapsulated Polyaniline as High Dielectric Constant Filler. Advanced Functional Materials 20:3280–3291

20. Vudayagiri S, Zakaria S, Yu L, Hassouneh SS, Benslimane M, Skov AL (2014) High breakdown-strength composites from liquid silicone rubbers. Smart Materials and Structures 23:105017

21. Dünki SJ, Ko YS, Nüesch FA, Opris DM (2015) Self-Repairable, High Permittivity Dielectric Elastomers with Large Actuation Strains at Low Electric Fields. Advanced Functional Materials 25:2467–2475

22. Madsen FB, Yu L, Daugaard AE, Hvilsted S, Skov AL (2014) Silicone elastomers with high dielectric permittivity and high dielectric breakdown strength based on dipolar copolymers. Polymer 55:6212–6219

23. Kussmaul B, Risse S, Kofod G, Waché R, Wegener M, McCarthy DN, Krüger H, Gerhard R (2011) Enhancement Of Dielectric Permittivity And Electromechanical Response In Silicone Elastomers: Molecular Grafting Of Organic Dipoles To The Macromolecular Network. Advanced Functional Materials 21:4589–4594

24. Carpi F, Gallone G, Galantini F, De Rossi D (2008) Silicone–Poly(hexylthiophene) Blends as Elastomers with Enhanced Electromechanical Transduction Properties. Advanced Functional Materials 18:235–241

25. Yu L, Madsen FB, Hvilsted S, Skov AL (2015) Dielectric elastomers, with very high dielectric permittivity, based on silicone and ionic interpenetrating networks. RSC Advances 5:49739–49747

26. Tugui C, Stiubianu GT, Iacob M, Ursu C, Bele A, Vlad S, Cazacu M (2015) Bimodal silicone interpenetrating networks sequentially built as electroactive dielectric elastomers. Journal Material Chemistry C 3:8963–8969

27. Ha SM, Yuan W, Pei Q, Pelrine R, Stanford S (2007) Interpenetrating networks of elastomers exhibiting 300% electrically-induced area strain. Smart Materials and Structures 16:S280–S287

28. Ha SM, Wissler M, Pelrine R, Stanford S, Kovacs G, Pei Q (2007) Characterization of electroelastomers based on interpenetrating polymer networks. Proceeding of SPIE 6524:652408–1–652408–10

29. Brochu P, Stoyanov H, Niu X, Pei Q (2013) All-silicone prestrain-locked interpenetrating polymer network elastomers: free-standing silicone artificial muscles with improved performance and robustness. Smart Materials and Structures 22:055022

30. Huang J, Shian S, Diebold RM, Suo Z, Clarke DR (2012) The thickness and stretch dependence of the electrical breakdown strength of an acrylic dielectric elastomer. Applied Physics Letters 101:122905

31. Vudayagiri S, Junker M, Skov A (2013) Factors affecting the surface and release properties of thin polydimethylsiloxane films. Polymer journal 45:871–878

32. Larsen AL, Sommer-Larsen P, Hassager O (2004) How to tune rubber elasticity. Proceeding of SPIE 5385:108–117

33. Balakrisnan B, Smela E (2010) Challenges in the microfabrication of dielectric elastomer actuators. Proceeding of SPIE 7642:76420K–1–76420K–10

34. Kollosche M, Stoyanov H, Ragusch H, Risse S, Becker A, Kofod G (2010) Electrical breakdown in soft elastomers: Stiffness dependence in un-pre-stretched elastomers. Proceedings of the IEEE International Conference on Solid Dielectrics, ICSD: 1–4

35. Sommer-Larsen P, Larsen A (2004) Materials for dielectric elastomer actuators. Proceeding of SPIE 5385:68–77

36. Pelrine R, Kornbluh R, Pei Q, Joseph J (2000) High-speed electrically actuated elastomers with strain greater than 100%. Science 287:836–839

37. Tröls A, Kogler A, Baumgartner R, Kaltseis R, Keplinger C, Schwödiauer R, Graz I, Bauer S (2013) Stretch dependence of the electrical breakdown strength and dielectric constant of dielectric elastomers. Smart Materials and Structures 22:104012

38. Kollosche M, Melzer M, Becker A, Stoyanov H, McCarthy DN, Ragusch H, Kofod G (2009) The influence of mechanical properties in the electrical breakdown in poly-styrene-ethylene-butadiene-styrene thermoplastic elastomer. Proceeding of SPIE 7287:728729–1–728729–8

39. Carpi F, Anderson I, Bauer S, et al (2015) Standards for dielectric elastomer transducers. Smart Materials and Structures 24:105025

40. Yu L, Vudayagiri S, Zakaria S, Benslimane MY, Skov AL (2014) Filled liquid silicone rubbers: possibilities and challenges. Proceeding of SPIE 9056:90560S–1–90560S–9

41. Muffoletto DP, Burke KM, Zirnhel JL (2012) Partial Discharge Analysis of Prestretched and Unstretched Acrylic Elastomers for Dielectric Elastomer Actuators (DEA). Proceeding of SPIE 8340:834021–1–834021–8

42. Liu L, Chen H, Li B, Sheng J, Zhang J, Zhang C, Wang Y, Li D (2015) Experimental investigation on electromechanical deformation of dielectric elastomers under different temperatures. Theoretical and Applied Mechanics Letters 5:155–159

43. Clément F, Bokobza L, Monnerie L (2001) On the Mullins Effect in Silica-Filled Polydimethylsiloxane Networks. Rubber Chemistry and Technology 74:847–870

44. Li B, Chen H, Qiang J, Hu S, Zhu Z, Wang Y (2011) Effect of mechanical pre-stretch on the stabilization of dielectric elastomer actuation. Journal of Physics D: Applied Physics 44:155301

45. Koh SJA, Li T, Zhou J, Zhao X, Hong W, Zhu J, Suo Z (2011) Mechanisms of large actuation strain in dielectric elastomers. Journal of Polymer Science, Part B: Polymer Physics 49:504–515

46. Bigue JL, Chouinard P, Proulx S, Miron G, Plante J (2009) Preliminary assessment of manufacturing impacts on dielectric elastomer actuators reliability. Smart Materials and structures, Cansmart Workshop: 303–314

47. Gallone G, Galantini F, Carpi F (2010) Perspectives for new dielectric elastomers with improved electromechanical actuation performance: composites versus blends. Polymer International 59:400–406

48. Carpi F, De Rossi D (2005) Improvement of electromechanical actuating performances of a silicone dielectric elastomer by dispersion of titanium dioxide powder. IEEE Transactions on Dielectrics and Electrical Insulation 12:835–843

49. Ouyang GM, Wang KY, Chen XY (2011) Enhanced electro-mechanical performance of TiO2 nano-particle modified polydimethylsiloxane (PDMS) as electroactive polymers. 2011 16th International Solid-State Sensors, Actuators and Microsystems Conference: 614–617

50. Zhao H, Wang D-R, Zha J-W, Zhao J, Dang Z-M (2013) Increased electroaction through a molecular flexibility tuning process in TiO2–polydimethylsilicone nanocomposites. Journal of Materials Chemistry A 1:3140–3145

51. Liu H, Zhang L, Yang D, Yu Y, Yao L, Tian M (2013) Mechanical, Dielectric, and Actuated Strain of Silicone Elastomer Filled with Various Types of TiO2. Soft Materials 11:363–370

52. Stoyanov H, Brochu P, Niu X, Della Gaspera E, Pei Q (2012) Dielectric elastomer transducers with enhanced force output and work density. Applied Physics Letters 100:262902

53. Szabo JP, Hiltz JA, Cameron CG, Underhill RS, Massey J, White B, Leidner J (2003) Elastomeric composites with high dielectric constant for use in Maxwell stress actuators. Proceedings of SPIE 5051:180–190

54. Lotz P, Matysek M, Lechner P, Hamann M, Schlaak HF (2008) Dielectric elastomer actuators using improved thin film processing and nanosized particles. Polymer 7976:692723–692723–10

55. Zhang Z, Liu L, Fan J, Yu K, Liu Y, Shi L, Leng J (2008) New silicone dielectric elastomer with a high dielectric constant. Proceedings of SPIE 6926:692610–1–692610–8

56. Liu Y, Liu L, Zhang Z, Leng J (2009) Dielectric elastomer film actuators: characterization, experiment and analysis. Smart Materials and Structures 18:095024

57. Romasanta LJ, Leret P, Casaban L, Hernández M, de la Rubia M a., Fernández JF, Kenny JM, Lopez-Manchado M a., Verdejo R (2012) Towards materials with enhanced electro-mechanical response: CaCu3Ti4O12–polydimethylsiloxane composites. Journal of Materials Chemistry 22:24705–24712

58. Chen LZ, Liu CH, Hu CH, Fan SS (2008) Electrothermal actuation based on carbon nanotube network in silicone elastomer Electrothermal actuation based on carbon nanotube network in silicone elastomer. Applied Physics Letters 26:263104

59. Chen L, Liu C, Liu K, Meng C, Hu C, Wang J, Fan S (2011) High-performance, low-voltage, and easy-operable bending actuator based on aligned carbon nanotube/polymer composites. ACS Nano 5:1588–1593

60. Park IS, Kim KJ, Nam JD (2007) Mechanical, dielectric, and magnetic properties of the silicone elastomer with multi-walled carbon nanotubes as a nanofiller. Polymer Engineering & Science 47:1396–1405

61. Yadav SK, Kim IJ, Kim HJ, Kim J, Hong SM, Koo CM (2013) PDMS/MWCNT nanocomposite actuators using silicone functionalized multiwalled carbon nanotubes via nitrene chemistry. Journal of Materials Chemistry C 1:5463–5470

62. Daugaard AE, Hassouneh SS, Kostrzewska M, Bejenariu AG, Skov AL (2013) High-dielectric permittivity elastomers from well-dispersed expanded graphite in low concentrations. Proceedings of SPIE 8687:868729–1–868729–8

63. Payne AR, Kraus G (1965) Reinforcement of elastomers. Interscience, New York 69:69–123

64. Diani J, Fayolle B, Gilormini P (2009) A review on the Mullins effect. European Polymer Journal 45:601–612

65. Rey T, Chagnon G, Le Cam JB, Favier D (2013) Influence of the temperature on the mechanical behaviour of filled and unfilled silicone rubbers. Polymer Testing 32:492–501

66. Blanchard AF, Parkinson D (1952) Breakage of Carbon-Rubber Networks by Applied Stress. Industrial & Engineering Chemistry 44:799–812

67. Kraus G, Childers CW, Rollmann KW (1966) Stress softening in carbon black-reinforced vulcanizates. Strain rate and temperature effects. Journal of Applied Polymer Science 10:229–244

68. Hanson DE, Hawley M, Houlton R, Chitanvis K, Rae P, Orler EB, Wrobleski DA (2005) Stress softening experiments in silica-filled polydimethylsiloxane provide insight into a mechanism for the Mullins effect. Polymer 46:10989–10995

69. Risse S, Kussmaul B, Kruger H, Kofod G (2012) A versatile method for enhancement of electromechanical sensitivity of silicone elastomers. RSC Advances 2:9029–9035

70. Risse S, Kussmaul B, Krüger H, Kofod G (2012) Synergistic Improvement of Actuation Properties with Compatibilized High Permittivity Filler. Advanced Functional Materials 22:3958–3962

71. Madsen FB, Yu L, Hvilsted S, Skov AL (2015) Super soft silicone elastomers with high dielectric permittivity. Proceeding of SPIE 9430:94301D–1–94301D–14

72. Whitehead S (1951) Dielectric breakdown of solids. Clarendon Press Oxford

73. Skov AL, Vudayagiri S, Benslimane M (2013) Novel silicone elastomer formulations for DEAPs. Proceeding of SPIE: 86871 86871I–86871I–8

74. Mezger TG (2006) The rheology handbook: for users of rotational and oscillatory rheometers. Vincentz Network GmbH & Co KG

75. Tripathi D (2002) Practical guide to polypropylene [electronic resource]. iSmithers Rapra Publishing

76. Von Hippel AR, Hippel AR (1954) Dielectrics and waves. Artech House

77. Wu J, Cao W, Wen W, Chang DC, Sheng P (2009) Polydimethylsiloxane microfluidic chip with integrated microheater and thermal sensor. Biomicrofluidics 3:12005

78. Carslaw HS, Jaeger JC (1959) Conduction of Heat in Solids, 2nd ed. Oxford University Press

79. Gerratt AP, Bergbreiter S (2013) Dielectric breakdown of PDMS thin films. Journal of Micromechanics and Microengineering 23:67001

80. Chen G, Zhao J, Li S, Zhong L (2012) Origin of thickness dependent dc electrical breakdown in dielectrics. Applied Physics Letters 100:222904

81. Park J-J (2013) Electrical Insulation Breakdown Strength in Epoxy/Spherical Alumina Composites for HV Insulation. Transactions on Electrical and Electronic Materials 14:105–109

82. McPherson JW, Jinyoung K, Shanware A, Mogul H, Rodriguez J (2003) Trends in the ultimate breakdown strength of high dielectric-constant materials. IEEE Transactions on Electron Devices 50:1771–1778

83. Kim HK, Shi FG (2001) Thickness dependent dielectric strength of a low-permittivity dielectric film. IEEE Transactions on Dielectrics and Electrical Insulation 8:248–252

84. Hauschild W, Mosch W (1992) Statistical Techniques for High-Voltage Engineering. Peter Peregrinus Ltd., london, UK

85. Prisacariu C (2011) Polyurethane Elastomers: From Morphology to Mechanical Aspects. Springer-Verlag, Vienna

86. Reiser A, Lock M, Knight J (1969) Migration and trapping of extrinsic charge carriers in polymer films. Transactions of the Faraday Society 65:2168–2185

87. Benslimane M, Kiil HE, Tryson MJ (2010) Electromechanical properties of novel large strain PolyPower film and laminate components for DEAP actuator and sensor applications. Proceeding of SPIE 7642:764231–764231–11

88. Jensen MK, Hassager O, Rasmussen HK, Skov AL, Bach A, Koldbech H (2009) Planar elongation of soft polymeric networks. Rheologica Acta 49:1–13

89. Jensen MK, Rasmussen HK, Skov AL, Hassager O (2011) Reversed planar elongation of soft polymeric networks. Rheologica Acta 50:729–740

90. Yu L, Skov AL (2015) Silicone rubbers with improved dielectrical and mechanical properties as a result of substituting silica with titanium dioxide. International Journal of Smart and Nano Materials 1:1–22

91. Baker D, Charlesby A, Morris J (1968) Reinforcement of silicone elastomer by fine particles. Polymer 9:437–448

92. Clément F, Lapra A, Bokobza L, Monnerie L, Ménez P (2001) Atomic force microscopy investigation of filled elastomers and comparison with transmission electron microscopy — application to silica-filled silicone elastomers. Polymer 42:6259–6270

93. Clément F, Bokobza L, Monnerie L (2005) Investigation of the Payne Effect and its Temperature Dependence on Silica-Filled Polydimethylsiloxane Networks. Part II: Test of Quantitative Models. Rubber Chemistry and Technology 78:232–244

94. Chojnowski J (1993) Polymerization in Siloxane Polymers. PTR Prentice Hall, Englewood Cliffs, New Jersey

95. Noll W (1968) Chemistry and Technology of Silicones. Academic, New York

96. Ghosh A, Rajeev RS, Bhattacharya AK, Bhowmick AK, De SK (2003) Recycling of silicone rubber waste: Effect of ground silicone rubber vulcanizate powder on the properties of silicone rubber. Polymer Engineering & Science 43:279–296

97. Brook MA, Saier H-U, Schnabel J, Town K, Maloney M (2007) Pretreatment of Liquid Silicone Rubbers to Remove Volatile Siloxanes. Industrial & Engineering Chemistry Research 46:8796–8805

98. Vudayagiri S, Skov AL (2014) Methods to ease the release of thin polydimethylsiloxane films from difficult substrates. Polymers for Advanced Technologies 25:249–257

99. Meunier L, Chagnon G, Favier D, Orgéas L, Vacher P (2008) Mechanical experimental characterisation and numerical modelling of an unfilled silicone rubber. Polymer Testing 27:765–777

100. Kochetov R, Tsekmes I a, Morshuis PHF (2015) Electrical conductivity, dielectric response and space charge dynamics of an electroactive polymer with and without nanofiller reinforcement. Smart Materials and Structures 24:075019

101. Liu M, Sun J, Sun Y, Bock C, Chen Q (2009) Thickness-dependent mechanical properties of polydimethylsiloxane membranes. Journal of Micromechanics and Microengineering 19:035028

102. Dorfmann A, Ogden RW (2004) A constitutive model for the Mullins effect with permanent set in particle-reinforced rubber. International Journal of Solids and Structures 41:1855–1878

103. Racles C, Cazacu M, Fischer B, Opris DM (2013) Synthesis and characterization of silicones containing cyanopropyl groups and their use in dielectric elastomer actuators. Smart Materials and Structures 22:104004

104. Racles C, Alexandru M, Bele A, Musteata VE, Cazacu M, Opris DM (2014) Chemical modification of polysiloxanes with polar pendant groups by co-hydrosilylation. RSC Advances 4:37620

105. Racles C, Bele A, Dascalu M, Musteata VE, Varganici CD, Ionita D, Vlad S, Cazacu M, Dünki SJ, Opris DM (2015) Polar–nonpolar interconnected elastic networks with increased permittivity and high breakdown fields for dielectric elastomer transducers. RSC Adv 5:58428–58438

106. Madsen FB, Daugaard AE, Hvilsted S, Benslimane MY, Skov AL (2013) Dipolar cross-linkers for PDMS networks with enhanced dielectric permittivity and low dielectric loss. Smart Materials and Structures 22:104002

107. Madsen FB, Javakhishvili I, Jensen RE, Daugaard AE, Hvilsted S, Skov AL (2014) Synthesis of telechelic vinyl/allyl functional siloxane copolymers with structural control. Polym Chem 5:7054–7061

108. Madsen FB, Daugaard AE, Fleury C, Hvilsted S, Skov AL (2014) Visualisation and characterisation of heterogeneous bimodal PDMS networks. RSC Advances 4:6939–6945

109. Ha SM, Yuan W, Pei Q, Pelrine R, Stanford S (2006) Interpenetrating Polymer Networks for High-Performance Electroelastomer Artificial Muscles. Advanced Materials 18:887–891

110. Yu L, Madsen FB, Hvilsted S, Skov AL (2015) High energy density interpenetrating networks from ionic networks and silicone. Proceedings of SPIE 9430:94300T–1–94300T–11

111. Goff J, Sulaiman S, Arkles B (2015) High elongation silicone elastomers derived from dual functional siloxane macromonomers. ACS Boston 2015

112. Liu H, Zhang L, Yang D, Ning N, Yu Y, Yao L, Yan B, Tian M (2012) A new kind of electro-active polymer composite composed of silicone elastomer and polyethylene glycol. Journal of Physics D: Applied Physics 45:485303

113. Suo Z (2010) Theory of dielectric elastomers. Acta Mechanica Solida Sinica 23:549–578

114. Zhao X, Hong W, Suo Z (2007) Electromechanical hysteresis and coexistent states in dielectric elastomers. Physical Review B - Condensed Matter and Materials Physics 76:134113–1–134113–9

115. Rosset S, Maffli L, Houis S, Shea HR (2014) An instrument to obtain the correct biaxial hyperelastic parameters of silicones for accurate DEA modelling. Proceeding of SPIE. doi: 10.1117/12.2044777

116. Zhang X-M, Li H, Chen W-X, Feng L-F (2012) Rheological properties and morphological evolutions of polypropylene/ethylene-butene copolymer blends. Polymer Engineering & Science 52:1740–1748

117. Madsen FB, Yu L, Daugaard AE, Hvilsted S, Skov AL (2015) A new soft dielectric silicone elastomer matrix with high mechanical integrity and low losses. RSC Advances 5:10254–10259

118. Sommer-Larsen P, Larsen AL (2004) Materials for dielectric elastomer actuators. Proceedings of SPIE 5385:68–77

119. Brook MA, Saier HU, Schnabel J, Town K, Maloney M (2007) Pretreatment of liquid silicone rubbers to remove volatile siloxanes. Industrial and Engineering Chemistry Research 46:8796–8805

120. Villahermosa RM, Ostrowski AD (2008) Chemical analysis of silicone outgassing. Proc SPIE 7069, Optical System Contamination: Effects, Measurements, and Control 706906–706906–10

121. Rothka J, Studd R, Tate K, Timpe D (2000) Outgassing of Silicone Elastomers. ArlonSilicone Technology Division, ISC.

122. Zhao X, Suo Z (2010) Theory of Dielectric Elastomers Capable of Giant Deformation of Actuation. Physical Review Letters 104:178302

123. Gatti D, Haus H, Matysek M, Frohnapfel B, Tropea C, Schlaak HF (2014) The dielectric breakdown limit of silicone dielectric elastomer actuators. Applied Physics Letters 104:052905

124. Stricher AM, Rinaldi RG, Barrès C, Ganachaud F, Chazeau L (2015) How I met your elastomers: from network topology to mechanical behaviours of conventional silicone materials. RSC Adv 5:53713–53725

SYMBOLS AND ABBREVIATIONS

d	Thickness
DE	Dielectric elastomer
DPP	Danfoss Polypower A/S
DRS	Dielectric relaxation spectroscopy
DSC	Differential scanning calorimetry
ε'	Storage permittivity
ε''	Loss permittivity
ε_o	Permittivity of free space
ε_r	Relative permittivity
ω	Frequency
F_{om}	Figure of merit
G	Shear modulus
G'	Storage modulus
G''	Loss modulus
IPN	Interpenetrating network
LSR	Liquid silicone rubber
LVE	Linear viscoelastic
PDMS	Polydimethylsiloxane
phr	Parts per hundred rubber
rpm	Rotations per minute
RTV	Room temperature vulcanisable
tan δ	G''/G'
TGA	Thermogravimetric analysis
TiO_2	Titanium dioxide
V	Voltage
Wt. %	Weight percent
Y	Young's modulus
μ	Micron
σ	Conductivity
A	Area
p	Compressive stress
S_d	Thickness strain
λ	Stretch ratio
υ	Poisson ratio

LIST OF TABLES

LIST OF FIGURES

APPENDIX A:

The electrical breakdown of thin dielectric elastomers: thermal effects

Zakaria S, Morshuis PHF, Benslimane MY, Gernaey KV and Skov AL

Proceeding of SPIE, Electroactive Polymer Actuators and Devices (EAPAD) California, USA

2014

The Electrical Breakdown of Thin Dielectric Elastomers: Thermal Effects

Zakaria Shamsul[a], Peter H. F. Morshuis[b], Benslimane Mohamed Yahia[c], Krist V. Gernaey[d], Anne Ladegaard Skov[*a]

a: Danish Polymer Center, Department of Chemical and Biochemical Engineering, Technical University of Denmark, Søltofts Plads, Building 229, 2800 Kgs. Lyngby.

b: Faculty of Electrical Engineering, Mathematics and Computer Science, Technology University of Delft, Mekelweg 4, 2628 CD Delft, The Netherland.

c: Danfoss Polypower A/S, Nordborgvej 81 DK-6430 Nordborg.

d: Center for Process Engineering and Technology, Department of Chemical and Biochemical Engineering, Technical University of Denmark, Søltofts Plads, Building 229, 2800 Kgs. Lyngby.

ABSTRACT

Dielectric elastomers are being developed for use in actuators, sensors and generators to be used in various applications, such as artificial eye lids, pressure sensors and human motion energy generators. In order to obtain maximum efficiency, the devices are operated at high electrical fields. This increases the likelihood for electrical breakdown significantly. Hence, for many applications the performance of the dielectric elastomers is limited by this risk of failure, which is triggered by several factors. Amongst others thermal effects may strongly influence the electrical breakdown strength.

In this study, we model the electrothermal breakdown in thin PDMS based dielectric elastomers in order to evaluate the thermal mechanisms behind the electrical failures. The objective is to predict the operation range of PDMS based dielectric elastomers with respect to the temperature at given electric field. We performed numerical analysis with a quasi-steady state approximation to predict thermal runaway of dielectric elastomer films. We also studied experimentally the effect of temperature on dielectric properties of different PDMS dielectric elastomers. Different films with different percentages of silica and permittivity enhancing filler were selected for the measurements. From the modeling based on the fitting of experimental data, it is found that the electrothermal breakdown of the materials is strongly influenced by the increase in both dielectric permittivity and conductivity.

Keywords: DEAP, PDMS, electrothermal breakdown, numerical method

1. INTRODUCTION

The advantages of the dielectric electroactive polymer (DEAP) technology such as flexibility, lightweight and relatively low cost[1] make them outperforming pneumatics and electromagnetics in many ways[2]. Even with the DEAP technology being at a maturing level, it is believed to possess huge potential for inclusion into mainstream products[3].

For electrical insulation systems in high-voltage applications such as power cables, the mechanisms of the electrical breakdown in these solid insulators have been discussed for several decades. Several factors that might lead to electrical breakdown such as intrinsic breakdown, thermal breakdown, electromechanical breakdown and partial discharge breakdown have been studied extensively[4]. Even though power cable and DEAP are operated at high electrical fields, the differences in functionalities, applications and properties make them distinct from each other. Thus, current studies of the mechanisms of electrical breakdown in DEAP are important and in line with the development of DEAP technology and certainly this information can give numerous benefits especially for the manufacturers. For instance, in the early 1960s,

* al@kt.dtu.dk; phone +45 4525 2825

Electroactive Polymer Actuators and Devices (EAPAD) 2014, edited by Yoseph Bar-Cohen, Proc. of SPIE
Vol. 9056, 90562V · © 2014 SPIE · CCC code: 0277-786X/14/$18 · doi: 10.1117/12.2037292

polyethylene was chosen as an insulator for power cables[5]. This hydrophobic material[6] was assumed to be a perfect insulator at that time. However, after a few years in service the cables started to break down[5]. Therefore, the investigations were performed to elucidate the mechanisms behind this failure. The investigations showed that the cable encountered water degradation which now is well-known as 'water treeing'. Consequently, many solutions for avoiding water treeing were introduced such as lead shields, swelling powders and triple extrusion in order to prevent moisture inside the cable and thereby reduce the water treeing problem considerably[4].

In solid dielectrics, electrical breakdown may be thermal which means it is caused by the fact that heat generated within the film cannot be dissipated sufficiently and thereby leads to thermal instability[4]. The heat balance equation is given by[7]

$$C\frac{dT}{dt} = \sigma(E,T)E^2 + \nabla(K(T)\nabla T) \quad (1)$$

where C is volumetric heat capacity, T is temperature, t is time, E is electrical field, ∇ is the Laplace operator, K(T) is the temperature dependent thermal conductivity, and σ(E,T) is field and temperature dependent electrical conductivity.

In thin dielectric films, when the power dissipation increases rapidly with increasing applied voltage, a critical voltage will be reached at a certain point. Whitehead[8] termed this 'the maximum thermal voltage', i.e. the voltage before thermal runway occurs. Analytical and numerical theories to predict thermal runway for thin dielectric films have been developed. For instance, Xiaoguang et al. (2003)[7] studied thermal runway of a thin polypropylene film between two metal electrodes using the finite element method (FEM) where the temperature rise as function of electric fields for 10 μm thick polypropylene film has been computed and the result showed that the temperature increases slowly prior to the critical voltage (875 V/μm) at which thermal runway occurs.

In this study, the thermal effects that may lead to electrical breakdown in thin PDMS film will be modeled. We assume the effect of temperature on electrical breakdown of thin PDMS film is different from polypropylene film as investigated by Xiaoguang et al. (2003)[7]. The main difference is that the PDMS elastomer is chemically crosslinked and thus the Young's modulus will not decrease with temperature as for the thermoplastic. Furthermore, recent studies (Kollosche et al. 2011)[9] have shown that the breakdown strength increases with increasing Young's modulus.

The modeling will be based on the experimental data of dielectric permittivity, elasticity and conductivity with varying temperature of PDMS films. Furthermore, thermogravimetric studies will also be performed to evaluate the thermal stability of the materials with no applied electrical field.

2. METHODOLOGY

2.1 The samples

Five different types of silicone elastomers with different loadings of reinforcing silica particles as well as a permittivity enhancing filler (titanium dioxide) were studied. Four of the elastomers are commercially available elastomers of either the type LSR (liquid silicone rubber) or RTV (room temperature vulcanizing). In the following, details are given on how the test specimens were manufactured:

A. Elastosil® LR 3043/30 was obtained from Wacker Chemie AG, Germany and the solvent OS-20 (an ozone-safe volatile methylsiloxane (VMS) fluid) was obtained from Dow Corning®, USA. Elastosil is supplied as a two parts system. The part A contains PDMS and a platinum catalyst, and part B contains PDMS and a cross-linker. The mixing ratio of Elastosil A, B and OS-20 is 5:5:7 by mass, respectively.

B. POWERSIL® XLR® 630 A/B is an extra-low viscosity LSR and supplied as two parts system. Part A contains PDMS and a platinum catalyst, and part B contains PDMS and a cross-linker. The mixing ratio of parts A and B is 1:1. No solvent is added since the viscosity of the XLR formulations allows for coating without solvent.

C. POWERSIL® RT® 625 A/B is a *room-temperature vulcanizing (RTV)* polymer supplied as a two parts system. Part A contains PDMS and a cross-linker, and Part B contains PDMS and a platinum catalyst. The mixing ratio of parts A and B is 9:1. No solvent is added since the viscosity of the RT formulations allows for coating without solvent.

D. Sample V35 is prepared using PDMS chains cross-linked with a 4-functional hydride cross-linker. All the polymers are purchased from Gelest Inc. and the applied molecular weights are supplied by the company. The catalyst platinum, cyclovinylmethyl-siloxane complex (511) is provided by Hanse Chemie. The material is supplied as 2 systems. Part A contains PDMS and cross-linker and Part B contains PDMS and platinum catalyst. The ratio of polymer and crosslinker (r) was set at 1.2. Four ppm catalyst was added to the premixes. The mixing ratio of parts A and B is 1:1 by mass.

E. The POWERSIL® XLR® 630 A/B with filler is a similar type of material as sample A, except for the addition of a filler. The applied filler is 16% Hombitec® RM130F®, hydrophobic titanium oxide from Sachtleben Chemie, Duisburg, Germany. The average primary particle size is 15 nm. The solvent OS-20 (an ozone-safe volatile methylsiloxane (VMS) fluid) was obtained from Dow Corning®, USA.

All samples were prepared based on the procedures described by Skov et al. (2013)[10] as specified below:

A speedmixer DAC 150FVZ (Hauschild Co., Germany) is used to mix premixes for 5 minutes. Glass plates are coated with the different materials using a thin film 3540 bird applicator (Elcometer, Germany). Then, the sample is cured in the oven for 10 minutes at 80°C. The final networks prepared as thin films are removed from the glass plates and stored between 50 μm thickness ethylene-tetrafluorethylen (ETFE) foils, and kept in a dry place until use.

2.2 Rheological and dielectric characterization and thermogravimetric analysis (TGA)

A TA Instruments ARES G2 Rheometer was used to characterize the rheological properties of the prepared films. The instrument was set to a controlled strain mode at 2% strain, which was ensured to be within the linear viscoelastic regime of the applied elastomers. The sample was inserted between two parallel circular plate geometries of 25 mm with a normal force of approximately 3 N. At a frequency of 1.0 Hz, the temperature was varied from 25°C to 450°C. Dielectric characterization was performed on a TA Instruments ARES G2 Rheometer operating at a frequency of 1.0 Hz, with a normal force of 3 N. The sample was inserted between two parallel circular plate geometries of 25 mm and the temperature was varied from 25°C to 450°C. Additionally, the thermogravimetric analysis (TGA) was performed with a TA Q500 equipped with autosampler. The samples were heated in an inert atmosphere (nitrogen gas) up to 900°C and the heating rate was 5°C/min.

2.3 Resistivity test

Volume resistivity measurements were performed in a three-terminal cell by means of a Keithley 617 electrometer. In order to protect the electrometer from overcurrents, the instrument was connected to the measuring electrode via a series resistor. The poling DC voltage was supplied to the sample via a gold-plated electrode. The electrode was held in place by a spring system to ensure good contact with the sample. A personal computer equipped with a General Purpose Interface Bus (GPIB) was used for displaying and storing the acquired data. In table 1, some specifications of the set-up are given. The current density was obtained by means of equation (2), where $i(t)$ is the current measured by the electrometer and A is the area of the measuring electrode. In order to reach the quasi steady-state regime, the DC field had to be applied for a sufficiently long polarization time.

$$j(t) = \frac{i(t)}{A} \tag{2}$$

The quasi steady-state value of the current density, J, was used for calculating the conductivity σ of the insulation via equation (3), where E is the applied electric field. The volume resistivity is the inverse of the conductivity, σ.

$$\sigma = \frac{J}{E} \tag{3}$$

Table 1. The specifications of the conduction current setup for the resistivity test[11]

Measuring electrode diameter	28 mm
HV electrode diameter	35 mm
Guard electrode diameter	350 mm
Sensitivity	$2 \times 10^{-11} AM^{-2}$
Max temperature	80°C
Max voltage	±30 kV
Series resistor	10 MΩ

3.0 RESULT AND DISCUSSION

3.1 Experimental data

In order to evaluate the effect of temperature on the mechanical properties of PDMS film, the storage modulus and tan delta have been measured at elevated temperature and at a frequency of 1.0 Hz. The storage modulus is a measure of the deformation energy stored by the film during the shear process and tan delta, which is also known as the loss factor, is calculated as the ration between the loss modulus and the storage modulus[12].

Figure 1 shows the storage modulus and tan delta as a function of PDMS film temperature. The storage modulus for PDMS film increases significantly, from 106 kPa at 190°C to 580 kPa at 450°C. This indicates that the PDMS film is hardened with increasing temperature. In addition, at 320°C the maximum tan delta (0.4) is shown which indicates a strong relaxation process and high energy dissipation in the film.

On the contrary, as mentioned in Tripathi (2002)[13], the thermoplastic polypropylene film will show a different behavior towards elevated temperature compared to the thermoset silicone elastomer. Therefore, we assumed the difference in rheological properties between PDMS and polypropylene films at high temperature may affect the behavior of both films with respect to electrothermal breakdown.

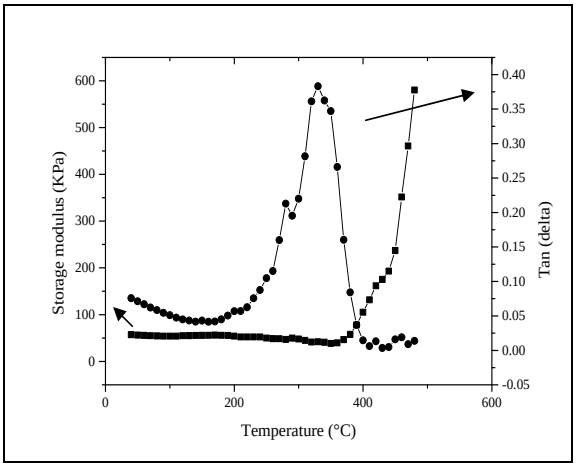

Figure 1. Elastosil LR 3043/30 film with 25 mm diameter and 0.8 mm thickness was used for characterization of the thermal dependence of the rheological properties of PDMS. The storage modulus and the loss tangent are plotted for temperatures between 25°C and 480°C.

Figure 2 shows the storage permittivity (ε') and loss permittivity (ε'') as a function of PDMS film temperature for a temperature range from 25°C to 450°C. The storage and loss permittivity are the real and imaginary part of the permittivity, respectively. The relative dielectric permittivity is given as $\varepsilon_r=\varepsilon'/\varepsilon_o$.

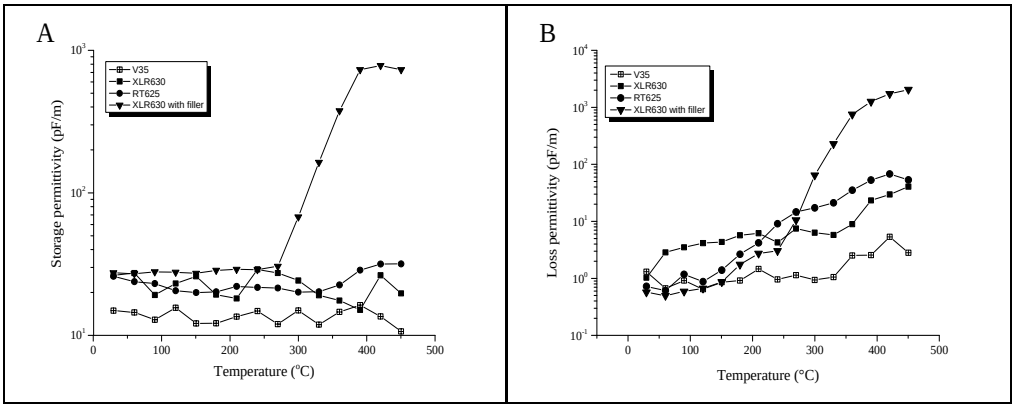

Figure 2. The dielectric properties as function of elevated temperatures for several PDMS films: (A) Storage permittivity (B) Loss permittivity.

Figure 3 shows the electrical conductivity as a function of temperature. The figures clearly indicate an increase in loss permittivity and electrical conductivity of the titanium dioxide loaded PDMS films upon increase of temperature. This can be attributed to the increased polarizability of the titanium dioxide particles.

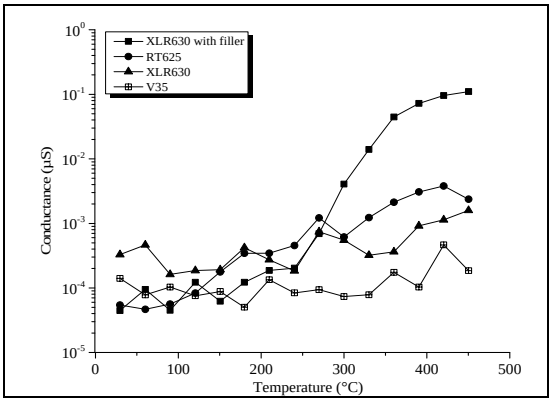

Figure 3. The AC electrical conductivity at 1 Hz as function of temperature for several PDMS films.

The increase of the loss permittivity with increasing temperature is attributed to more dissipation of the electrical energy into heat[14]. At the same time, the increase of electrical conductivity at the more elevated temperature causes more heat production since the joule heating is directly proportional to the electrical conductivity[4]. Therefore, these properties are likely to affect the electrothermal breakdown behavior in PDMS film. Hence, a model that evaluates the effect of temperature and electric field dependence of electrical conductivity on electrothermal breakdown in PDMS film has been applied in this study and will be discussed in the next section.

The purpose of the TGA analysis is to determine the percentages of silica and filler loaded into various PDMS films and also to determine if electrothermal breakdown occurs before film degradation. Figure 4 illustrates different percentages of weight loss at 900°C for all PDMS films. This behavior is believed to depend on the percentage of silica and filler inside the films which need higher temperature to degrade.

As shown in figures 2 and 3, there is a significant increase in the loss permittivity and the electrical conductivity when the temperature of PDMS films is above 150°C.

In figure 4 TGA results of the different films are shown. TGA provides useful information on the materials since the mass loss upon heating can be measured. A constant mass at elevated temperature indicates thermal stability. Furthermore the filler content (inorganic components) can be estimated from the solid content at elevated temperature (>800°C). Figure 4 illustrates that all the investigated PDMS films start to degrade after 300°C and the data in table 2 indicates the temperature where 2% of weight of the films has been decomposed. This temperature is deemed relevant since it gives an estimate of the point in time when thermal degradation sets off. Two of the films, namely RT625 and XLR with filler, possess relatively low 2% degradation temperatures (around 300°C) whereas the other two have to be heated above 400°C before significant degradation takes place. Therefore, if the electrothermal breakdown occurs above these characteristic temperatures, it will be a combined – probably accelerated – process of both thermal decomposition as well as electrothermal runaway. The RT625 formulation is most sensitive to degradation at 300-500°C where the degradation occurs more or less constantly.

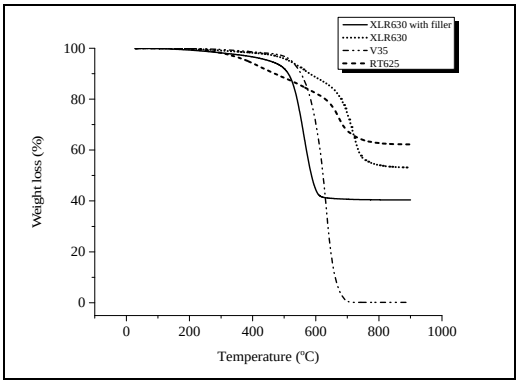

Figure 4. TGA thermograms of PDMS films with different percentages of silica and permittivity enhancing filler.

Table 2. The temperature where 2% of weight of the films has degraded.

PDMS films	Temperature at 2% of weight loss (°C)
XLR630 with filler	313
XLR630	419
V35	451
RT625	305

3.2 Numerical Prediction of Electrothermal Breakdown

For a PDMS film, the volumetric Joule heating from the applied voltage across the film can be calculated as[8]

$$P = \sigma E^2 \tag{4}$$

where σ is the electrical conductivity and E is the electric field. In this model we assume that voltage across the film is increased in small increments, as well as that thermal steady state is reached at each voltage step. The surface temperatures were fixed and the initial temperature and boundary temperatures were set to room temperature.

In order to model the electrothermal breakdown of thin PDMS based dielectric elastomers, the σ should be expressed as function of temperature (T) and electric field (E). Therefore, a linear interpolation of the σ(T) and the σ(E) was calculated to establish an expression of σ(T,E) from the data in figure 5. The interpolation of the electrical dependence is very rough due to the scarcity of experimental data on such systems.

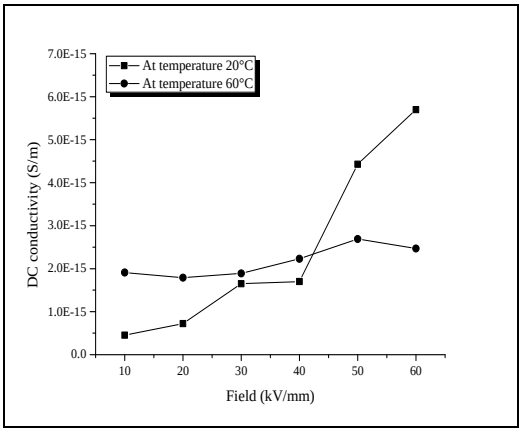

Figure 5. The conductivity as function of the electric fields at two different temperatures for RT625 film. There is a big difference between results at room temperature and at 60°C. These data were used to model the correlation of electrical conductivity with temperature and electric fields.

For computational purposes, we assume that thermal conductivity, *K*, of the PDMS film is 0.15 W/mK[15], that the initial temperature is 300 K and that the expression for electrical conductivity is derived from the data in figure 5 as illustrated below:

The linear equation for DC conductivity versus electric field

$$\text{at } 20°\text{C} : \sigma(\text{E}) = 7.60 \times 10^{-16}\text{E} + 1.95 \times 10^{-16} \quad (5)$$

and

$$\text{at } 60°\text{C} : \sigma(\text{E}) = 1.90 \times 10^{-16}\text{E} + 4.88 \times 10^{-17} \quad (6)$$

The linear graphs were plotted from the slopes (7.60×10^{-16} and 1.90×10^{-16}) and the y-intercepts (1.95×10^{-16} and 4.88×10^{-16}) from the above equations. Then, the linear equations from the graphs were calculated as shown below

$$\sigma(\text{T}) = -2.32 \times 10^{-18}\text{T} + 1.52 \times 10^{-16} \quad (7)$$

and

$$\sigma(\text{T}) = 7.20 \times 10^{-17}\text{T} - 2.74 \times 10^{-15} \quad (8)$$

Lastly the expression of electrical conductivity as function of temperature and electric field is given by

$$\sigma(\mathrm{T},\mathrm{E}) = (-2.32\times10^{-18}\mathrm{T} + 1.52\times10^{-16})\mathrm{E} + 7.20\times10^{-17}\mathrm{T} - 2.74\times10^{-15} \quad (9)$$

As illustrated in figure 6, with the electric field applied along the *x* axis, the thickness of the film was given by *l*, one boundary of the film is at *x*=0, another boundary at *x*=*l*. The temperature distribution at steady state is then given by[16]

$$dT = \frac{P}{2K}\left(x(l-x)\right) \quad (10)$$

where K is the polymer thermal conductivity and P is the averaged volumetric Joule heating. dT is the incremental change in temperature[16]. Then the average film temperature was calculated in order to be applied in computing a new average electrical conductivity (σ).

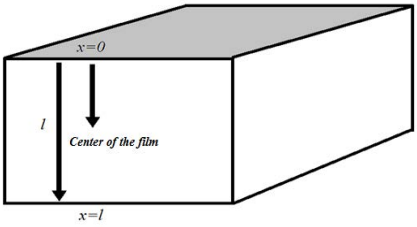

Figure 6: The PDMS film where *l* represents the thickness of the film and *x* represents the position where the electrothermal breakdown field is measured. The maximum temperature will be achieved at the center of the film ($x=\frac{l}{2}$) as predicted by Xiaoguang et al.(2003)[7].

Figure 7 shows the general behavior of temperature versus electric field for PDMS film for which the temperature at the center of the sample just before thermal runway is only a few degrees above the boundary temperature. With only a few volts increase across the sample, thermal runaway occurs very rapidly. The results of this work demonstrate that the thermally induced breakdown fields are significantly higher than the electrical breakdown strengths typically reported for PDMS which are in the range from 19 to 133 V/μm[17].

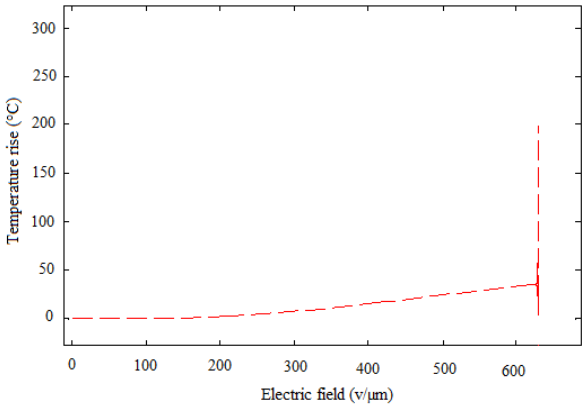

Figure 7. The temperature rise (dT) versus electric field for 50 μm thick PDMS film as computed by the quasi-steady state numerical method. The temperature increases slowly prior to the critical field (629V/μm), at which thermal runaway occurs.

Figure 8 shows the breakdown field as function of electrical conductivity for 50 μm thick PDMS film. The plot illustrates that higher electrical conductivity causes a lower breakdown field, as expected. Practically, this has the implication that electrothermal breakdown is relevant at room temperature as well when the electrical conductivity of the material is high.

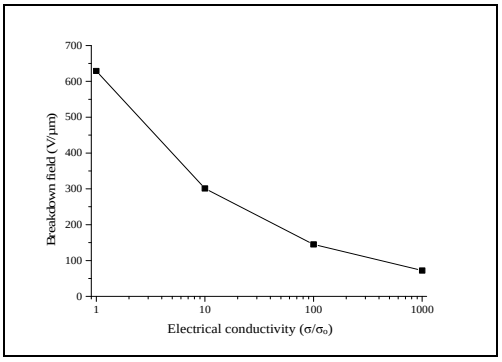

Figure 8. Breakdown fields as function of normalized conductivity at room temperature for the 50 μm thick PDMS film as computed by the quasi-steady state numerical method. The initial electrical conductivity, σ_0, of the PDMS film is 2.45×10^{-16} S/m at room temperature.

Figure 9(A) shows thermal breakdown strengths measured at different distances from the PDMS film surface. Meanwhile, figure 9(B) shows the effect of film thickness on the breakdown field for PDMS film. Both graphs demonstrate similar trends: The breakdown field exhibits a hyperbolic decrease as the position of *x* is closer to the film surface as the result of the heat generated inside the film can be removed rapidly to the surrounding. This characteristic of electrothermal breakdown in thin polymer films agrees well with the predictions reported by Tröls et al. (2013)[18].

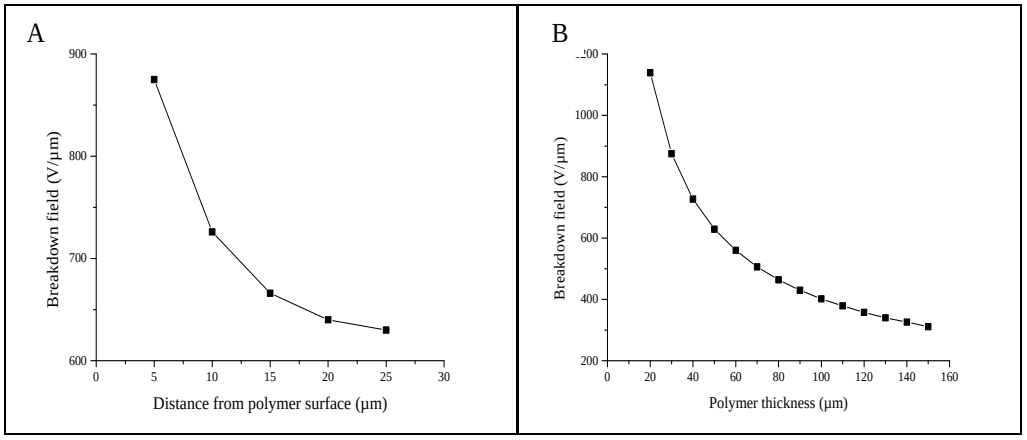

Figure 9. (A) Breakdown strengths at given distances (*x*) from the polymer surface for 50 µm thick PDMS film. (B) The dependence of polymer film thickness on breakdown field computed as described in the text. The value of *x* was fixed as half of the film thickness.

5.0 CONCLUSION

In this study, the effect of temperature on dielectric properties of different systems of PDMS dielectric elastomers has been studied experimentally and a model of electrothermal breakdown in thin PDMS based dielectric elastomers has been applied. From both methods, it can be concluded that electrothermal breakdown of the materials is strongly influenced by the increase in both dielectric permittivity and conductivity. The electrothermal breakdown may not be a major factor to cause electrical breakdown in thin PDMS based dielectric elastomers since the required electrical field required for thermal runaway is about 5 times larger than the reported breakdown fields of silicones.

ACKNOWLEDGEMENT

The authors gratefully acknowledge the financial support from the Ministry of Education of Malaysia and Universiti Malaysia Pahang. Danfoss PolyPower A/S is also acknowledged for financial support to Z. Shamsul.

REFERENCES

[1] R. Shankar, T. K. Ghosh, and R. J. Spontak, "Dielectric elastomers as next-generation polymeric actuators," Soft Matter **3**(9), 1116 (2007).

[2] J. E. Huber, N. A. Fleck, and M. F. Ashby, "The selection of mechanical actuators based on performance indices," Proc. R. Soc. London. Ser. A Math. Phys. Eng. Sci. **453**(1965), 2185–2205 (1997).

[3] Anonymous, [Danfoss PolyPower A/S – White Paper: PolyPower® DEAP actuator elements], Danfoss A/S, Nordborg, Denmark (2012).

[4] J. C. Fothergill and L. A. Dissado, [Electrical degradation and breakdown in polymers], IET (1992).

[5] W. Thue, Electrical power cable engineering, 3rd ed., CRC Press (2012).

[6] M. Ashraf Khan and R. Hackam, "Loss of hydrophobicity of high density polyethylene," in Electr. Insul. Dielectr. Phenomena, 1997. IEEE 1997 Annu. Report., Conf. **2**, pp. 378–381 vol.2 (1997).

[7] Q. Xiaoguang, Z. Zhong, and S. Boggs, "Computation of electro-thermal breakdown of polymer films," in Electr. Insul. Dielectr. Phenomena, 2003. Annu. Report. Conf., pp. 337–340 (2003).

[8] S. Whitehead, [Dielectric breakdown of solids], Clarendon Press Oxford (1951).

[9] M. Kollosche, H. Stoyanov, H. Ragusch, S. Risse, A. Becker, and G. Kofod, “Electrical breakdown in soft elastomers: stiffness dependence in un-pre-stretched elastomers,” in 2010 10th IEEE Int. Conf. Solid Dielectr., pp. 1–4 (2010).
[10] A. L. Skov, S. Vudayagiri, and M. Benslimane, “Novel silicone elastomer formulations for DEAPs,” in SPIE Smart Struct. Mater. Nondestruct. Eval. Heal. Monit., pp. 86871I–86871I–8, International Society for Optics and Photonics (2013).
[11] T. Andritsch, R. Kochetov, Y. T. Gebrekiros, U. Lafont, P. H. F. Morshuis, and J. J. Smit, “Synthesis and dielectric properties of epoxy based nanocomposites,” in Electr. Insul. Dielectr. Phenomena, 2009. CEIDP ’09. IEEE Conf., pp. 523–526 (2009).
[12] T. G. Mezger, [The rheology handbook: for users of rotational and oscillatory rheometers], Vincentz Network GmbH & Co KG (2006).
[13] D. Tripathi, [Practical guide to polypropylene [electronic resource]], iSmithers Rapra Publishing (2002).
[14] A. R. Von Hippel and A. R. Hippel, [Dielectrics and waves], Artech House (1954).
[15] J. Wu, W. Cao, W. Wen, D. C. Chang, and P. Sheng, “Polydimethylsiloxane microfluidic chip with integrated microheater and thermal sensor,” Biomicrofluidics **3**, 12005 (2009).
[16] H. S. Carslaw and J. C. Jaeger, [Conduction of Heat in Solids], 2nd ed., Oxford University Press (1959).
[17] A. P. Gerratt and S. Bergbreiter, “Dielectric breakdown of PDMS thin films,” J. Micromechanics Microengineering **23**(6), 67001 (2013).
[18] A. Tröls, A. Kogler, R. Baumgartner, R. Kaltseis, C. Keplinger, R. Schwödiauer, I. Graz, and S. Bauer, “Stretch dependence of the electrical breakdown strength and dielectric constant of dielectric elastomers,” Smart Mater. Struct. **22**(10), 104012 (2013).

Supplementary Information (SI) for Appendix A

The Electrical Breakdown of Thin Dielectric Elastomers: Thermal Effects

Thermal breakdown script (Matlab R2014b)

```
clear all
clc
close all
fid=fopen('change_temp.dat','w');

Cv=4.53e-22;
for E=1:10:30290;

    d=50;%thickness
    k=0.15;%thermal conductivity
    x=25;%position of breakdown
    T=20;%initial temperature


    P=Power(Cv,E,Ar,d);
    Pow=P;
    dT=Change_temp(d,k,x,Pow);
    Change=dT;
    T1=Local_temp(T,Change);
    Local=T1;
    Cv1=New_cond(Local,E);
    New=Cv1;
    Cv=New;

    fprintf(fid,'%2i %9.6f %80.12f %28.8f\n',E,Cv,dT,T1);
    if dT<50;
        disp('OK');
        EB=E
    else dT>50;
        disp('breakdown occurs');
        EB=E
    end
end

A=importdata('change_temp.dat');
Ea=A(:,1);
%c=A(:,2);
dt=A(:,3);
%t1=A(:,4);

figure
plot(Ea,dt,'r--')
grid
xlabel('Electric field [v/μm]')
ylabel('Temperature rise (oC)')
title('Temperature rise vs electric field')
…
```

```
function P=Power(Cv,E,Ar,d)

P=Cv*E.^2;%Heat production rate-volumetric, E= electric field

end
…

function dT=Change_temp(d,k,x,Pow)

dT=((Pow)/(2*k))*(x*(d-x)); % Steady state temperature

end
…

function T1=Local_temp(T,Change)

T1=T+Change; %initial local temperature

end
…

function Cv=New_cond(Local,E)

Cv=((((-2.26e-23*Local)+1.52e-21)*E)+((7.2e-22*Local)-2.74e-20));% new
conductivity

end
```

APPENDIX B:

The breakdown strength of pre-stretched elastomers, with and without sample volume conservation

Zakaria S, Morshuis PHF, Benslimane MY, Yu L and Skov AL

Smart Materials and Structures

2015

IOP Publishing Smart Materials and Structures
Smart Mater. Struct. 24 (2015) 055009 (10pp) doi:10.1088/0964-1726/24/5/055009

The electrical breakdown strength of pre-stretched elastomers, with and without sample volume conservation

Shamsul Zakaria[1,4], Peter H F Morshuis[2], Mohamed Yahia Benslimane[3], Liyun Yu[1] and Anne Ladegaard Skov[1]

[1] Danish Polymer Center, Department of Chemical and Biochemical Engineering, Technical University of Denmark, Søltofts Plads, Building 229, DK 2800 Kgs. Lyngby, Denmark
[2] Faculty of Electrical Engineering, Mathematics and Computer Science, Technology University of Delft, Mekelweg 4, 2628 CD Delft, The Netherlands
[3] Danfoss Polypower A/S, Nordborgvej 81, DK 6430 Nordborg, Denmark
[4] Faculty of Industrial Science and Technology, Universiti Malaysia Pahang, Lebuhraya Tun Razak 26300 Gambang, Pahang, Malaysia

E-mail: al@kt.dtu.dk

Received 28 November 2014, revised 3 February 2015
Accepted for publication 3 March 2015
Published 9 April 2015

Abstract

In practice, the electrical breakdown strength of dielectric electroactive polymers (DEAPs) determines the upper limit for transduction. During DEAP actuation, the thickness of the elastomer decreases, and thus the electrical field increases and the breakdown process is determined by a coupled electro-mechanical failure mechanism. A thorough understanding of the mechanisms behind the electro-mechanical breakdown process is required for developing reliable transducers. In this study, two experimental configurations were used to determine the stretch dependence of the electrical breakdown strength of polydimethylsiloxane (PDMS) elastomers. Breakdown strength was determined for samples with and without volume conservation and was found to depend strongly on the stretch ratio and the thickness of the samples. PDMS elastomers are shown to increase breakdown strength by a factor of ~3 when sample thickness decreases from 120 to 30 μm, while the biaxial pre-stretching ($\lambda = 2$) of samples leads similarly to an increase in breakdown strength by a factor of ~2.5.

S Online supplementary data available from stacks.iop.org/SMS/24/055009/mmedia

Keywords: dielectric elastomer, silicone, dielectric breakdown strength, volume dependent breakdown, pre-stretch

(Some figures may appear in colour only in the online journal)

1. Introduction

Electrical breakdown causes the short-circuiting of dielectric electroactive polymers (DEAPs), resulting in end of life. For that reason, it is important to determine the maximum applied electric field (the breakdown strength) of a given material, such that a safe operational voltage can be defined. This requires reliable and consistent methods for the determination of breakdown strength.

Generally, when an electric field is applied, DEAPs undergo dielectric thinning due to a factor known as 'Maxwell pressure', as identified by Stark and Garton [1]. The degree of thinning depends on the mechanical properties of the elastomer [2–4]. Simultaneously, this thinning behaviour leads to an increase in the electric field and thus to further thinning. If no stable operating point is found, this combined positive feedback process may continue until breakdown strength is reached, resulting in electrical failure. However,

0964-1726/15/055009+10$33.00

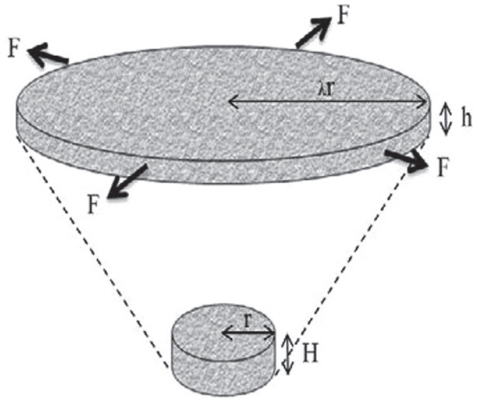

Figure 1. A film with thickness H and radius r stretched radially with force F from an initial state (bottom) in to a deformed film (top), with a reduction in thickness from H to h and an increase in the radius of r to λr.

the internal pressure of the elastomer usually exceeds Maxwell pressure, since stretching usually stiffens the elastomer in the upper operational limits of DEAP. This knowledge is utilized in the pre-stretch approach, whereby it is commonly applied to suppress electromechanical instability [5].

The effects of pre-stretching on the breakdown strength of DEAPs have been studied previously [6–9]. For instance, one of the most commonly studied dielectric elastomers, namely the electrical breakdown strength of the acrylic elastomer VHB, produced by the 3M Corporation, has been reported to increase from 18 to 218 V μm^{-1} when pre-stretched biaxially six times [8]. However, the mechanisms by which pre-stretching improves the electrical breakdown strength of DEAPs are still not understood fully.

DEAPs are usually driven by voltages of 1 kV (e.g. AMI haptic device) or higher, resulting in electrical fields of ~50 V μm^{-1} and above, depending on the thickness of the film after pre-stretching. Upon biaxially pre-stretching a circular film, the film is radially expanded by a factor of λ, thereby causing a reduction in thickness from H to $h = H/\lambda^2$ due to the general incompressibility of elastomers (figure 1). Variations in thickness in response to pre-stretching pose a challenge in relation to how to measure electrical breakdown strength accurately. Tröls *et al* [9] investigated the effect of different electrode configurations on the breakdown strength of acrylic VHB elastomers supplied by 3M and pre-stretched up to five times. Stretched elastomer films were sandwiched between compliant carbon grease electrodes or clamped rigidly between two stamp electrodes, in order to take breakdown measurements: breakdown strength increased from 100 to 163 V μm^{-1} for rigid electrodes, and from 25 to 143 V μm^{-1} for compliant electrodes pre-stretched biaxially five times. It was also found that breakdown strength depends on the surface area of the electrodes. Normalized thickness (h/H) was reduced from 1.0 to 0.028 following pre-stretching five times, and thus the sample volumes were not conserved during measurement process.

The favourable effect of pre-stretching on breakdown strength has been discussed by severable research groups. Muffoletto *et al* [10], for instance, argued that improved breakdown strength following pre-stretching was caused by the favourable realignment of material imperfections, such as voids and micro-cracks. Huang *et al* [11], in the meantime, showed that breakdown strength depends on the thickness of the samples tested. Furthermore, improved breakdown strength as a result of pre-stretching may be due to rapid heat dissipation into the environment for thinner films [12, 13], while the effect of the Young's modulus on breakdown strength of elastomers has also been investigated by several groups. Yu *et al* [14] investigated various types of filled silicone elastomers in an un-stretched state and found that breakdown strength could be approximated proportionally to the Young's modulus. Kollosche *et al* [15] investigated the stiffness dependence of the electrical breakdown strength of soft elastomers without pre-stretching, and they found that the breakdown field increases in line with the Young's modulus.

For these reasons, in the present study, the effect of volume conservation on breakdown strength was investigated as a function of pre-stretching for four types of polydimethylsiloxane (PDMS) samples. The sample volumes were conserved by enlarging the surface area of the applied electrodes according to the pre-stretch. Subsequently, the results of the breakdown voltage measurements were compared to those obtained from samples without volume conservation. Thereby, reliable and consistent data were produced which could then be used for further interpretation of the favourable effects of pre-stretching.

In many papers, an apparent dependency of electrical breakdown strength on thickness has been reported [11, 13, 16–19], but considerable care has to be exercised in interpreting these results, because often not only does the thickness of the test samples change, but this also happens to other parameters, such as volume under stress, effective electrode area, the morphology of the polymer and the Young's modulus. It is therefore not possible to simply relate a reduction in polymer thickness to increased electrical breakdown strength, and so this can only be done properly when only one single parameter, i.e. thickness, is varied. In the following, the effect of the abovementioned parameters on electrical breakdown strength is discussed based on experimental data for various types of silicone elastomers.

2. Theory

In the following the effect of different parameters on the breakdown field is discussed.

2.1. Sample volume

If the volume of the tested samples changes and all other parameters, for example morphology and Young's modulus, remain unchanged, the effect of volume enlargement on breakdown strength can be calculated. Thus, this approach can only be followed for a constant stretch ratio.

A basic statistical treatment of the effect of any change in stress volume on electrical breakdown strength is given in [20].

First, it is assumed that for a single sample of volume V_0 the cumulative probability P_0 of a breakdown in a given electric field E_0 is described by the Weibull function:

$$P_0 = 1 - \exp\left(\frac{E_0}{\eta}\right)^{\beta}, \tag{1}$$

where η denotes the Weibull scale parameter and β the Weibull shape parameter.

Then, the sample volume is increased by a factor of n (n elements of volume V_0 each). Now, the breakdown probability P_n of the n times enlarged volume V_n can be calculated if the individual breakdown probabilities $P_{0,i}$ with i between 1 and n are independent and the material being tested is homogeneous. Interface imperfections are ignored. The probability that V_n will break down equals 1 minus the probability that all elements of V_n will not break down:

$$P_n = 1 - \prod_{i=1}^{n}\left(1 - P_{0,i}\right). \tag{2}$$

Next, assuming $P_{0,i} = P_0$ (all n elements have the same breakdown probability), we obtain:

$$P_n = 1 - \left(1 - P_0\right)^n = 1 - \exp\left[n\left(\frac{E_n}{\eta}\right)^{\beta}\right]. \tag{3}$$

For a fixed breakdown probability, E_n is calculated:

$$P_0\left(E_0\right) = P_n\left(E_n\right). \tag{4}$$

Thus, by equating (1) and (3):

$$\left(\frac{E_0}{\eta}\right)^{\beta} = n\left(\frac{E_n}{\eta}\right)^{\beta} \tag{5}$$

and:

$$E_n = n^{-\frac{1}{\beta}}E_0 < E_0. \tag{6}$$

Thus, for a given breakdown probability, the breakdown field of the enlarged sample is reduced. Evidently, the β parameter plays an important role in this reduction, and its value is obtained from step-up voltage tests in which the electric field is raised in constant steps until breakdown. The smaller the scatter in the breakdown field, the larger the shape parameter β and the smaller the effect on the breakdown field of the enlarged volume.

In section 4.5, the measured volume effect is compared to the volume effect, which is calculated by following the above steps.

2.2. Effective electrode area

The interface between electrode and polymer is a source of potential defects. Thus, it can be argued that—for a given sample volume—the larger the electrode area, the higher the probability of breakdown.

2.3. Polymer morphology

If a polymeric sample is stretched, its morphology may change as a result of an alignment of the polymer chains in the plane of stretching [21]. It can therefore be argued that the alignment of the polymer chains perpendicular to the direction of the electric field will lead to an increase in breakdown strength [22], because charge carrier movement has been impeded. The possible effect of polymer alignment can only be studied when all other parameters are constant or have been taken into account properly. Consequently, experimental setups with equal volumes of samples should be stressed, with different stretch applied.

3. Methodology

3.1. Materials

Four different types of silicone elastomers with different silica loadings (in commercial silicone elastomer) and permittivity-enhancing fillers (titanium dioxide) were studied. The elastomers are commercially available liquid silicone rubber (LSR) or room-temperature vulcanizing (RTV) types.

The pure PDMS elastomers were POWERSIL® XLR® 630 A/B and ELASTOSIL® RT® 625 A/B. POWERSIL® XLR® 630 A/B is an extra-low viscosity LSR and is supplied as a two-part system. Part A contains PDMS and a platinum catalyst, and part B contains PDMS and a cross-linker. The mixing ratio for parts A and B is 1:1. ELASTOSIL® RT® 625 A/B is an RTV polymer also supplied as a two-part system. Part A contains PDMS and a cross-linker, and part B contains PDMS and a platinum catalyst. The mixing ratio for parts A and B is 9:1.

The solvent OS-20 (an ozone-safe volatile methylsiloxane fluid), which was obtained from Dow Corning®, is added to both pure elastomers in order to acquire constant formulation viscosity. The selected elastomers were chosen based on differences in the percentages of reinforcing silica particles in the formulations.

Filled elastomers consist of POWERSIL® XLR® 630 A/B with added fillers. The applied fillers are 16% Hombitec® RM130F® and 35% Sachtleben® R420®, respectively. Both fillers are hydrophobic titanium oxide from Sachtleben Chemie, Duisburg, Germany, and the average primary particle sizes for Hombitec® RM130F® and Sachtleben® R420® are 15 and 250 nm, respectively. The solvent OS-20 is added to both filled elastomers in order to gain consistent formulation viscosity.

3.2. Sample preparation

The samples were carefully prepared based on the procedures described by Skov *et al* [23], as specified below.

A speedmixer DAC 150FVZ (Hauschild Co., Germany) was used to mix part B of the material, the solvent and the filler at 3000 rpm. After 5 min of mixing, part A of the material was added and mixed for another 5 min at 2000 rpm. Glass plates were coated with the premixes, using a thin film 3540 bird applicator (Elcometer, Germany) with a blade gap,

Table 1. Parameters for breakdown measurements for samples with volume conservation.

Stretch ratios (λ)	Radius (mm)	Volume (mm^3)	Thickness (mm)
XLR630			
1.0	5.0	6.0	0.076
1.5	7.5	6.0	0.033
2.0	10.0	6.0	0.019
RT625			
1.0	5.0	6.5	0.083
1.5	7.5	6.5	0.037
2.0	10.0	6.5	0.021
XLR630 + 16% Hombitec® RM130F®			
1.0	5.0	6.8	0.087
1.5	7.5	6.8	0.039
2.0	10.0	6.8	0.022
XLR630 + 35% Sachtleben® R420®			
1.0	5.0	7.2	0.092
1.5	7.5	7.2	0.041
2.0	10.0	7.2	0.023

in order to acquire consistent thickness for all samples. The samples were then cured in an oven for 5 min at 75 °C and 10 min at 115 °C. The thin films were removed from the glass plates and stored between 50 μm thick ethylene-tetrafluorethylen foils and then kept in a desiccator until use.

Silver depositions were performed on a physical vapour deposition chamber (Alcatel) system, which is fitted with a large butterfly valve to control pumping speed and is pumped by an oil diffusion pump with a liquid nitrogen trap. The lid is lifted off the chamber whenever samples or targets need to be changed. The lid wall seal is accomplished by using a large O-ring, and the base vacuum is approximately 2×10^{-5} mbar. The chamber itself is fitted with an evaporation source (for silver), a dc magnetron sputter source and an RF sputter source (for sputtering non-conducting targets). Silver evaporation was performed on the tungsten boat at the bottom of the chamber. According to instrument calibration, this should result in a sputtering rate of about 1.5 nm s^{-1} and produce a 50–60 nm layer of silver in 30–40 sec. The thin silver electrodes ensure sufficient conductivity. More details on the process can be found in Benslimane *et al* [24].

3.3. Instrumentation

Breakdown measurements were taken on an in-house-built device based on international standards (IEC 60243-1 (1998) and IEC 60243-2 (2001)). The initial thicknesses of the films before stretching were determined with a Leica DMLB microscope with a USB Thorlabs 2.0 digital camera. The stretched film thicknesses were calculated as shown in table 1, and the distance between the spherical electrodes was set accordingly with a micrometre stage and gauge.

An indent of less than 5% of sample thickness was added to ensure that the spheres were in contact with the sample. The PDMS film was slid between the two spherical electrodes (radius of 20 mm), and a stepwise increasing voltage was applied (50–100 V/step) at a rate of 0.5–1.0 step/s. Each sample was subjected to ten breakdown measurements, from which an average value was calculated as the breakdown strength of the sample.

Uniaxial tensile quasi-static tests were performed on the set of PDMS films, in order to determine Young's modulus for different stretch ratios. The quasi-static measurements were taken on samples shaped as rectangular strips about 6×60 mm in size, by applying step-wise increasing loads and by measuring the corresponding elongations. Each elongation measurement was taken after three minutes from each application of a new stress value. Young's modulus was obtained from the tangent of the stress–strain curve at stretch ratios of 1.0, 1.5 and 2.0.

3.4. Sample parameters

3.4.1. Sample volume. Two different sets of samples were prepared for the breakdown measurements, i.e. with and without volume conservation. For samples with volume conservation, breakdown measurements were taken on stretched films with circular silver electrodes of varying sizes. The electrodes were applied to the top and to the bottom of the film. The sizes of the electrodes were enlarged from 8 mm^2 ($\lambda = 1.0$) to 18 and 32 mm^2 to attain 1.5 and 2.0 stretch ratios, respectively, and the films were stretched before silver deposition. This technique was performed in order to protect the rigid electrodes from damage once the films were stretched. Meanwhile, for samples without volume conservation, breakdown measurements were taken on stretched films without the electrodes. The films were stretched to 1.5 and 2.0, as shown in table 1.

3.4.2. Sample thickness. Two different sample preparation methods were applied in the breakdown measurements, in order to study the effect of thickness on the breakdown strength of un-stretched PDMS films, namely a single-layer and a multiple layer technique. For the single layer method, films were prepared by using different blade gap sizes, ranging from 50 to 200 μm, of thin film coater in order to gain different film thicknesses. The real thickness of the film was measured through optical microscopy, and then an average of several measurements was used to represent the true thickness. For the multiple layers method, the films were prepared by using a 50 μm thin film coater blade gap, following which the prepared films were stacked in one to three layers of equal thickness, in order to acquire different overall thicknesses.

3.4.3. Effective electrode area. In order to investigate the effect of the electrode area on the breakdown strength of PDMS films, two different sets of samples were prepared, i.e. samples with and without volume conservation. The samples were covered with different sized sputtered silver electrodes on the film surfaces, as described in table 2, and the

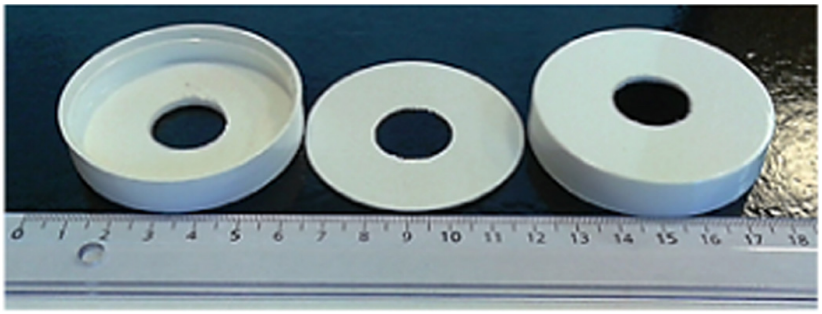

Figure 2. Plastic container caps with an inner seal and circular holes in the centre.

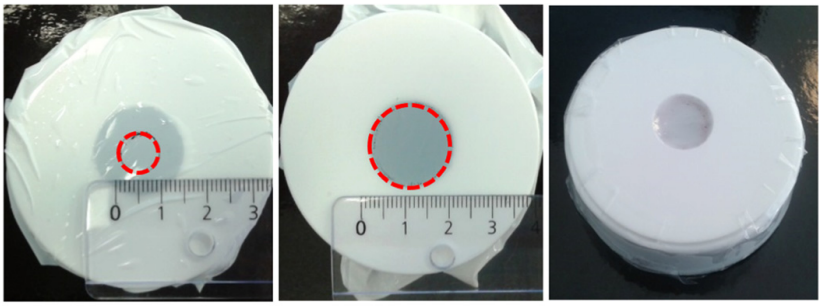

Figure 3. (A) A film before stretching. A circle was drawn on the film surfaces as a guideline. (B) The film after biaxially stretching from 5 mm radius ($\lambda = 1$) to 10 mm radius ($\lambda = 2$). (C) During silver deposition, the stretched films were covered on top by the inner lids with circular shaped holes of the right sizes, thereby allowing for control over the area exposed to sputtering.

Table 2. The silver electrode sizes for the different parameters and methods used.

			Electrode radius (mm)	
Material	Stretch ratio (λ)	Method	Sample thickness = 80 μm	Sample thickness = 40 μm
XLR630	1.0	With volume conservation	5.0	7.1
		Without volume conservation	5.0	5.0
	1.5	With volume conservation	7.5	10.7
		Without volume conservation	5.0	5.0
Material	Stretch ratio (λ)	Method	Sample thickness = 115 μm	Sample thickness = 56 μm
XLR630 + 16% Hombitec	1.0	With volume conservation	5.0	7.2
		Without volume conservation	5.0	5.0
	1.5	With volume conservation	7.5	10.8
		Without volume conservation	5.0	5.0

breakdown measurements for both the un-stretched ($\lambda = 1.0$) and stretched ($\lambda = 1.5$) PDMS films of different sample thicknesses were taken on unfilled (XLR630) and filled (XLR630 + 16% Hombitec) PDMS films.

3.5. Silver deposition and breakdown measurements

A simple method was applied, in order to stretch the elastomers biaxially. A plastic sample container cap was used as a sample holder for the pre-stretched film. The method for measuring the electrical breakdown strength of the pre-stretched films with specially designed caps is shown in figures 2–4. Biaxial stretching was used in this instance, since it is the most common way to pre-stretch elastomers, and the pre-stretch can also be performed in a very controlled manner.

The two experimental techniques employed for measuring breakdown strength as a function of pre-stretching are illustrated in figure 5.

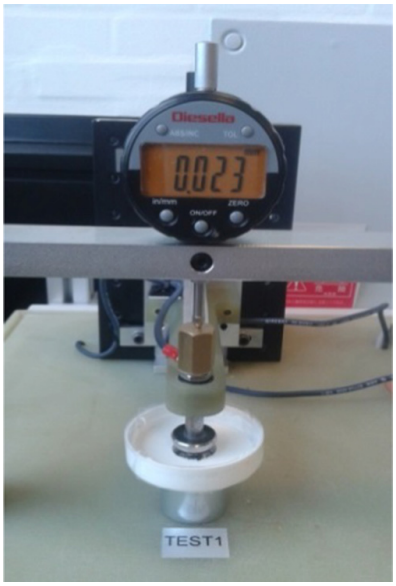

Figure 4. Stretched film inserted between two semispherical electrodes for breakdown measurements.

4. Results and discussion

Four different silicone elastomers were investigated, namely an RTV type as well as an LSR type, both with and without permittivity enhancing fillers. The applied LSR was a so-called 'extra-liquid rubber' (XLR) with a relatively low viscosity, thereby allowing for the further addition of particles. The added fillers were two types of TiO_2 shown previously to cause significantly different properties of the resulting elastomer, mainly due to differences in particle sizes [25]. The Hombitec filler had been shown previously to reinforce strongly Young's modulus as well as electrical breakdown strength, whereas the R420 does not reinforce to the same extent, and thus higher concentrations are possible [25].

4.1. Volume conservation considerations

DEAPs consisting of various types of silicones with corrugated electrodes utilized in this study possess no local minimum in their respective voltage–stress curves, and therefore they are not prone to snap-through instability as defined by Zhao and Suo [2]. In figure 6, breakdown strengths as a function of the stretch ratio for different experimental configurations on several types of PDMS can be seen. Breakdown strengths for four different un-stretched elastomers are in the range 79–103 V μm^{-1}, with volume conservation (configuration (C) in figure 5), and 100–120 V μm^{-1}, without volume conservation (configuration (B) in figure 5). For stretched samples (at $\lambda = 2$), breakdown strength varies between 227–296 and 247–320 V μm^{-1}, with and without volume conservation, respectively. The discrepancies between the two methods in the un-stretched state ($\lambda = 1$) are due to different sample volumes as well as variations in the electrodes. The samples with volume conservation are measured with 5 mm radius electrodes in an un-stretched state, whereas the samples without volume conservation are just contacted by the spherical electrodes and thus the sample volumes are significantly smaller, as shown in table 3.

The strong influence of sample volume on breakdown strength is confirmed further by the consistent deviation between identical samples and identical pre-stretches measured by the two methods. There is an apparent improvement in breakdown strength of approximately 10 V μm^{-1} when the sample volume is not conserved upon pre-stretching.

4.2. Young's modulus considerations

In order to evaluate the effect of Young's modulus on breakdown strengths, quasi-static uniaxial tensile tests were performed on the samples. Stress–strain curves for the individual samples can be seen in the supplementary information (SI). Uniaxial tests were performed because of the ease of such experiments compared to the planar elongation method, such as that performed by Jensen *et al* [26, 27]. Furthermore, most actuation configurations utilize uniaxial stretching of the elastomer, and as a result Young's modulus is the most

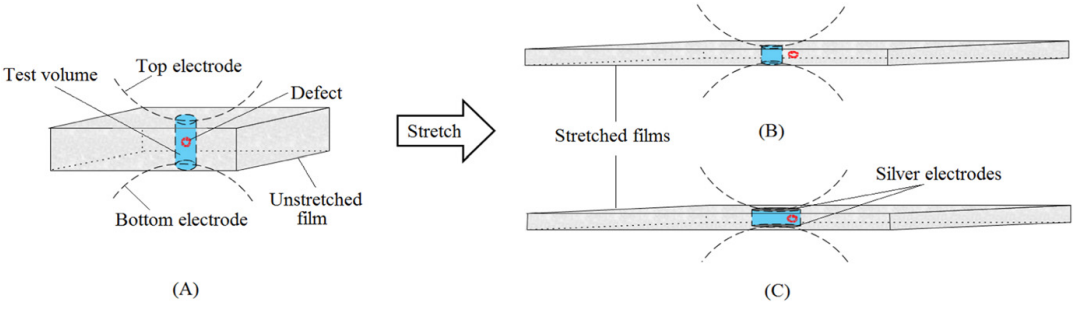

Figure 5. Breakdown measurements were performed on films before stretching (A) and after stretching; (B) without volume conservation and (C) with volume conservation.

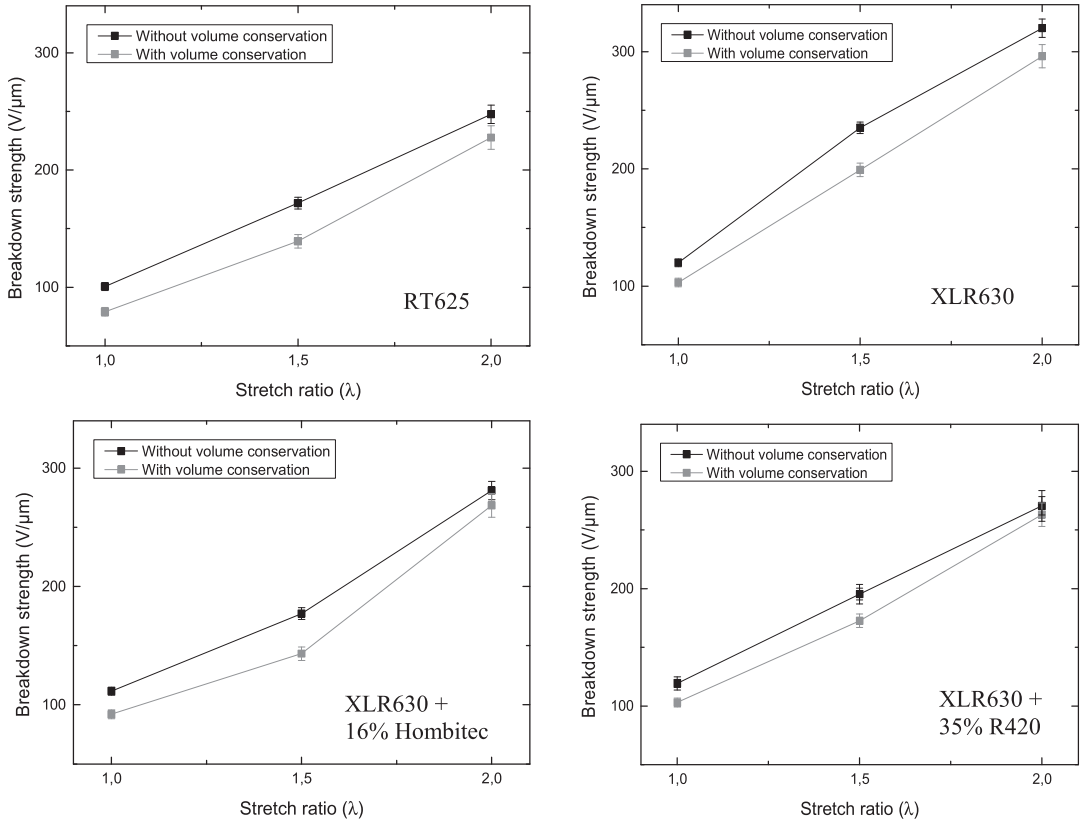

Figure 6. Breakdown strength as a function of the stretch ratio for several PDMS films.

Table 3. Effect of pre-stretch on film thickness for XLR630. Electrode sizes without volume conservation were approximately 0.5 mm. Electrode sizes with volume conservation were enlarged from 8 mm^2 ($\lambda = 1.0$) to 18 mm^2 and 34 mm^2 to obtain $\lambda = 1.5$ and $\lambda = 2.0$, respectively. V and v are the sample volumes before and after pre-stretching, respectively.

		Normalized sample volume (v/V)		Breakdown strength (V/μm)	
Stretch ratio	Normalized thickness (h/H)	Without volume conservation	With volume conservation	Without volume conservation	With volume conservation
1.0	1.00	1.00	1.00	120	113
1.5	0.43	0.43	1.00	225	171
2.0	0.25	0.25	1.00	324	286

common measure of elasticity for DEAPs. All samples showed a local minimum Young's modulus at $\lambda = 1.5$.

Figure 7 shows breakdown strengths as a function of Young's moduli derived from the stress–strain curves of several PDMS films at different stretch ratios. It is obvious that there is no simple trend between breakdown strength and Young's modulus, as proposed by Kollosche *et al* [15] and Vudayagiri *et al* [25]; however, it is clear that when pre-stretching is applied to the investigated silicones, despite the drop in Young's modulus at moderate pre-strain ($\lambda = 1.5$), breakdown strength still increases. The pre-stretch is therefore very likely to cause the favourable alignment of polymer chains as well as defect realignment, i.e. the favourable effect of pre-stretching is not solely mechanical in character.

4.3. Sample thickness considerations

Figure 8(A) shows breakdown strength as a function of the thickness of un-stretched PDMS films. It can be seen clearly that breakdown strengths are highest for the thinnest films by almost a factor of two compared to the thickest films.

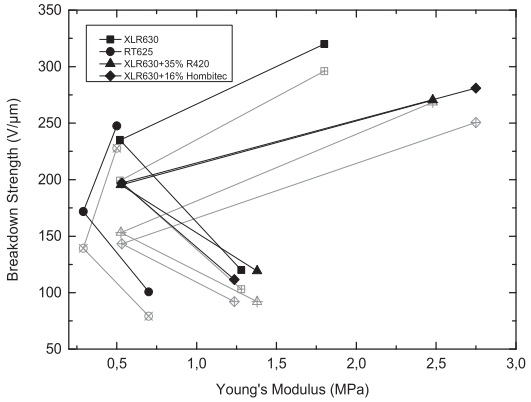

Figure 7. Breakdown strength as a function of Young's modulus at different stretch ratios ($\lambda = 1.0$, $\lambda = 1.5$ and $\lambda = 2.0$) for different PDMS materials. The black curves indicate samples without volume conservation and grey curves indicate samples with volume conservation.

This behaviour is supported by the data shown in figure 8(B), whereby film breakdown strengths decline tremendously, as several layers of the thin films were stacked together. This is due to the fact that the thinner films have a relatively lower sample volume compared to thicker films, which therefore results in less risk of a breakdown. However, when investigating the influence of sample thickness, more than one parameter needs to be considered, since sample volume is not the sole factor—in a breakdown measurement, for instance, the voltage applied across a thin film will generate volumetric Joule heating [13]. As shown by Zakaria *et al* [12], a thinner film with faster excessive heat removal results in higher breakdown strength when accounting for the thermal effect only. Therefore, thicker films will also encounter decreased breakdown strength due to heating and the increased conductivity of the investigated elastomers.

4.4. Electrode area considerations

In addition, the effective electrode area may influence how breakdown strength is determined, since the interface between the electrode and the polymer can be a source of potential defects. Therefore, this parameter is considered in the following. The effective electrode area is hard to determine within the experimental setup, and the experimental design was complex due to the dependency of the sample volume on the electrode area in breakdown measurements, i.e. the larger the electrode area, the higher the sample volume. As shown in figure 9, data for the breakdown measurements without sputtered silver electrode (diamond shape) predicted higher breakdown strengths than the others, due to the absence of electrodes on the film surfaces—and thus relatively small sample volumes. The slight decrease in the breakdown strengths of those samples with volume conservation reflects both the bigger sample volume and the larger effective electrode area compared to the without sample volume conservation method. Therefore, the results possibly demonstrate the effect of volume enlargement rather than effective electrode area. Moreover, the clear influence of the electrode area is not observable.

4.5. Sample size considerations

In order to gain a better insight into the effect of increased sample volume, the effect of sample enlargement on the breakdown strength of PDMS films was investigated, as given by equation (6). The breakdown data were analyzed in the Weibull++ software package, and results in terms of the determination of β (see SI) were used to interpret the experimental data. In the mathematical approach suggested by Hauschild and Mosch [20], some assumptions were included, e.g. that all defects are equally distributed over the volume of the film and that defects produce breakdowns in line with the same field strength.

Figure 10 shows how the theory fits with experiments for breakdown strengths as a function of increased sample volume for the two samples. XLR630 has $\beta = 72.4$ and

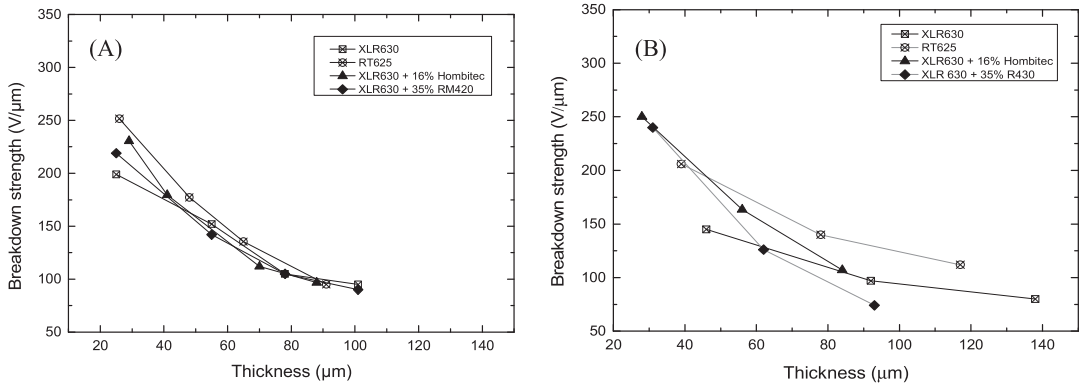

Figure 8. Thickness dependence of breakdown strength for different PDMS materials. Breakdown strengths were measured without a sputtered silver electrode in respect to (A) different thicknesses and (B) multiple layers (1–3 layers) of un-stretched films.

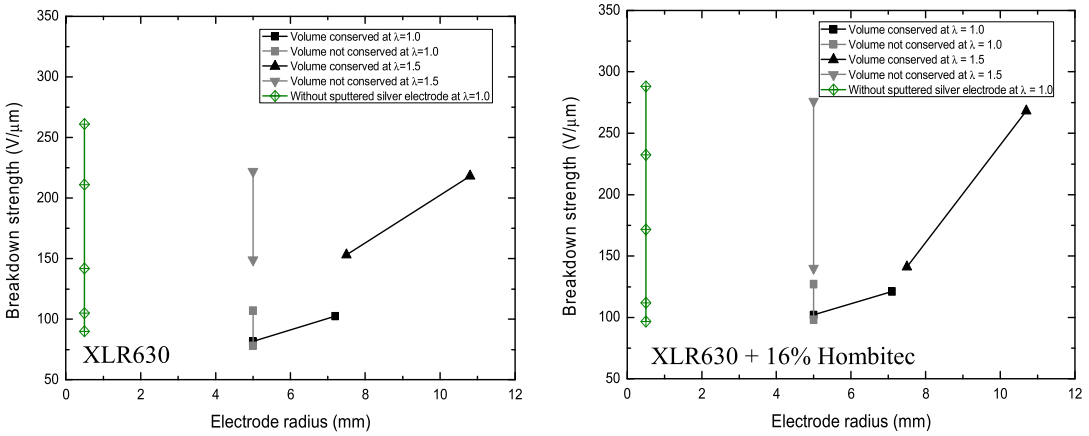

Figure 9. Breakdown strengths as a function of electrode radius for different film thicknesses. For XLR 630 at $\lambda = 1$, the film thicknesses are 80 and 40 μm, respectively, and at $\lambda = 1.5$, the film thicknesses are 36 and 18 μm, respectively. For XLR630 + 16% filler at $\lambda = 1$, the film thicknesses are 115 and 56 μm, respectively, and at $\lambda = 1.5$, the film thicknesses are 51 and 25 μm.

XLR + 16% Hombitec has $\beta = 39.2$, which gives a clear indication of the greater scattering in determining breakdown strengths for the filled elastomer. Samples with a thicknesses of ~40 μm (see figure 8) are normalized to 1 ($n = 1$), and the electrode area is then increased to acquire 100 and 200 times greater volume, respectively. The agreement is striking. However, there is a slight over-prediction from theory compared to the experimental results. This discrepancy can be explained as a result of the Weibull data being used as fitting parameters for the theoretical prediction, based on an experimental setup with less influence from the electrodes, as well as simplifications included in the model described above.

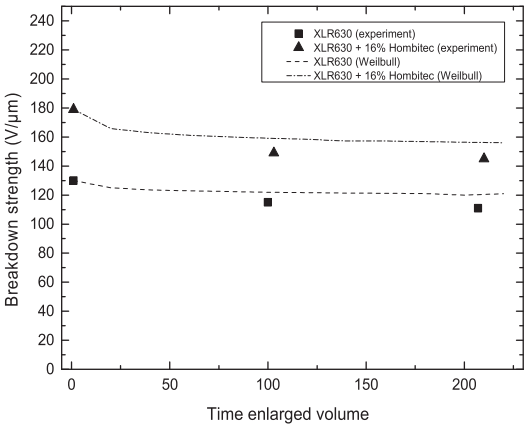

Figure 10. The effect of volume enlargement on the breakdown strength of un-stretched PDMS films.

5. Conclusion

A method for measuring the breakdown strength of pre-stretched films with constant sample volume was presented. The method was compared to a traditional experiment, whereby the sample volume was reduced significantly by pre-stretching. Breakdown strengths of the pre-stretched elastomers were shown to be over-estimated if the reduction in volume following pre-stretching was not taken into consideration. For the materials we tested, it was shown that apparent breakdown strengths taken from traditional breakdown measurements are of the order of 10 V μm^{-1} larger than the true breakdown strength of the material measured with a constant sample volume. For reliable determinations of breakdown strength, a careful experimental design is required —as illustrated in the present article. Sample thickness was shown to be a very important factor in determining electrical breakdown strengths, since these breakdown strengths could vary by more than a factor of two when film thicknesses varied from 20 to 120 μm for un-stretched samples.

Pre-stretching of films was shown to have a great impact on the breakdown strength of all tested films, and by pre-stretching films biaxially to four times the original area, it was shown that breakdown strength increased by more than a factor two, even when accounting for the decrease in sample thickness. This clearly indicates that pre-stretching affects the morphology of samples as a result of, for example, chain and defect alignment. It was furthermore shown that breakdown strengths were not coupled in any way whatsoever to Young's moduli of the samples when pre-stretching was applied.

Acknowledgments

The authors gratefully acknowledge the financial support of the Ministry of Education of Malaysia and Universiti Malaysia Pahang as well as Innovationsfonden Danmark.

References

[1] Stark K H and Garton C G 1955 Electric strength of irradiated polythene *Nature* **176** 1225–6

[2] Zhao X and Suo Z 2010 Theory of dielectric elastomers capable of giant deformation of actuation *Phys. Rev. Lett.* **104** 178302

[3] Pelrine R E, Kornbluh R D and Joseph J P 1998 Electrostriction of polymer dielectrics with compliant electrodes as a means of actuation *Sensors Actuators* A **64** 77–85

[4] Gatti D, Haus H, Matysek M, Frohnapfel B, Tropea C and Schlaak H F 2014 The dielectric breakdown limit of silicone dielectric elastomer actuators *Appl. Phys. Lett.* **104** 052905

[5] Pelrine R 2000 High-speed electrically actuated elastomers with strain greater than 100% *Science* **287** 836–9

[6] Plante J-S and Dubowsky S 2006 Large-scale failure modes of dielectric elastomer actuators *Int. J. Solids Struct.* **43** 7727–51

[7] Jordi C, Schmidt A, Kovacs G, Michel S and Ermanni P 2011 Performance evaluation of cutting-edge dielectric elastomers for large-scale actuator applications *Smart Mater. Struct.* **20** 075003

[8] Kofod G, Sommer-Larsen P, Kornbluh R and Pelrine R 2003 Actuation response of polyacrylate dielectric elastomers *J. Intell. Mater. Syst. Struct.* **14** 787–93

[9] Tröls A, Kogler A, Baumgartner R, Kaltseis R, Keplinger C, Schwödiauer R, Graz I and Bauer S 2013 Stretch dependence of the electrical breakdown strength and dielectric constant of dielectric elastomers *Smart Mater. Struct.* **22** 104012

[10] Muffoletto D P, Burke K M and Zirnheld J L 2012 Partial discharge analysis of pre-stretched and un-stretched acrylic elastomers for dielectric elastomer actuators (DEA) *Proc. SPIE* **8340** 834021

[11] Huang J, Shian S, Diebold R M, Suo Z and Clarke D R 2012 The thickness and stretch dependence of the electrical breakdown strength of an acrylic dielectric elastomer *Appl. Phys. Lett.* **101** 122904

[12] Zakaria S, Morshuis P H F, Benslimane M Y, Gernaey K V and Skov A L 2014 The electrical breakdown of thin dielectric elastomers: thermal effects *Proc. SPIE* **9056** 90562V

[13] Fothergill J C and Dissado L A 1992 *Electrical Degradation and Breakdown in Polymers* (UK: IET)

[14] Yu L, Vudayagiri S, Zakaria S, Benslimane M Y and Skov A L 2014 Filled liquid silicone rubbers: possibilities and challenges *Proc. SPIE* **9056** 90560S

[15] Kollosche M, Stoyanov H, Ragusch H, Risse S, Becker A and Kofod G 2010 Electrical breakdown in soft elastomers: stiffness dependence in un-pre-stretched elastomers *ICSD: 10th IEEE Int. Conf. on Solid Dielectrics* pp 1–4

[16] Chen G, Zhao J, Li S and Zhong L 2012 Origin of thickness dependent dc electrical breakdown in dielectrics *Appl. Phys. Lett.* **100** 222904

[17] Park J-J 2013 Electrical insulation breakdown strength in epoxy/spherical alumina composites for HV insulation *Trans. Electr. Electron. Mater.* **14** 105–9

[18] McPherson J W, Jinyoung K, Shanware A, Mogul H and Rodriguez J 2003 Trends in the ultimate breakdown strength of high dielectric-constant materials *IEEE Trans. Electron Devices* **50** 1771–8

[19] Kim H K and Shi F G 2001 Thickness dependent dielectric strength of a low-permittivity dielectric film *IEEE Trans. Dielectr. Electr. Insul.* **8** 248–52

[20] Hauschild W and Mosch W 1992 *Statistical Techniques for High-Voltage Engineering* (London: Peter Peregrinus Ltd)

[21] Prisacariu C 2011 *Polyurethane Elastomers: From Morphology to Mechanical Aspects* (Vienna: Springer)

[22] Reiser A, Lock M W B and Knight J 1969 Migration and trapping of extrinsic charge carriers in polymer films *Trans. Faraday Soc.* **65** 2168–85

[23] Skov A L, Vudayagiri S and Benslimane M 2013 Novel silicone elastomer formulations for DEAPs *Proc. SPIE* **8687** 86871I

[24] Benslimane M, Kiil H E and Tryson M J 2010 Electromechanical properties of novel large strain polypower film and laminate components for DEAP actuator and sensor applications *Proc. SPIE* **7642** 764231

[25] Vudayagiri S, Zakaria S, Yu L, Hassouneh S S, Benslimane M and Skov A L 2014 High breakdown-strength composites from liquid silicone rubbers *Smart Mater. Struct.* **23** 105017

[26] Jensen M K, Hassager O, Rasmussen H K, Skov A L, Bach A and Koldbech H 2009 Planar elongation of soft polymeric networks *Rheol. Acta* **49** 1–13

[27] Jensen M K, Rasmussen H K, Skov A L and Hassager O 2011 Reversed planar elongation of soft polymeric networks *Rheol. Acta* **50** 729–40

Supplementary Information (SI) for Appendix B

The breakdown strength of pre-stretched elastomers with and without sample volume conservation

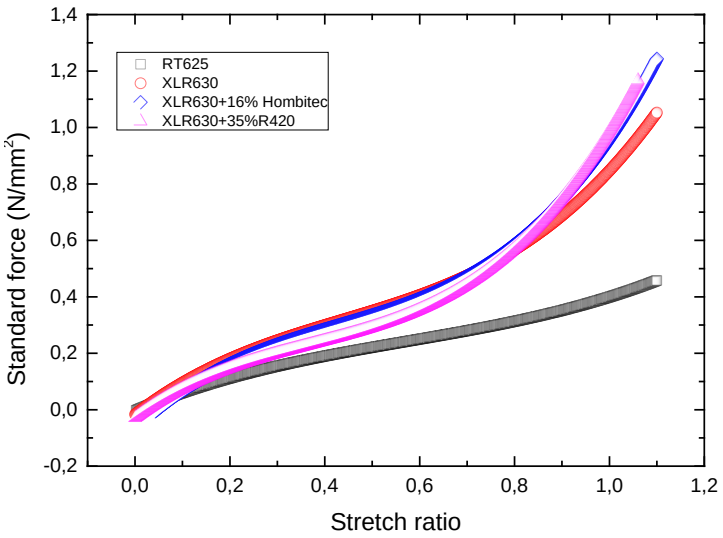

Figure S1: The stress-strain curves for the investigated PDMS films at room temperature.

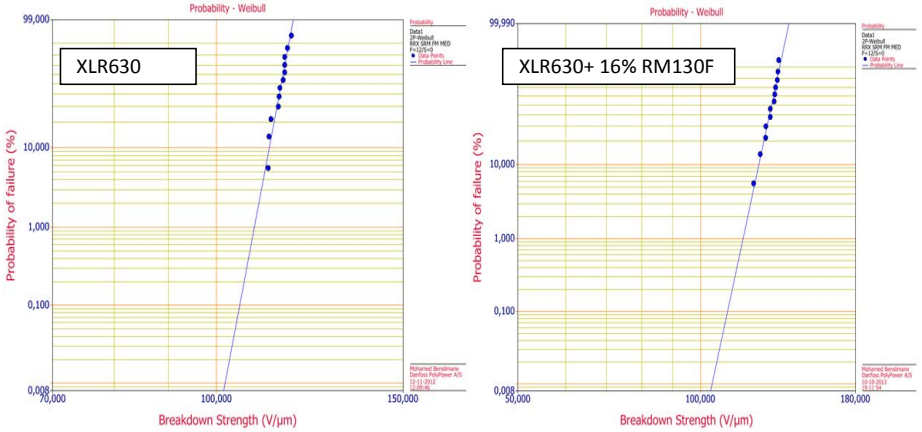

Figure S2: Weibull distribution diagrams (β value for XLR630= 72.4 and XLR630 + 16% RM130F= 39.2).

APPENDIX C:

The influence of static pre-stretching on the mechanical ageing of filled silicone rubbers for dielectric elastomer applications

Zakaria S, Yu L, Guggi Kofod and Skov AL

Material Today Communication

2015

Materials Today Communications 4 (2015) 204–213

Contents lists available at ScienceDirect

Materials Today Communications

journal homepage: www.elsevier.com/locate/mtcomm

The influence of static pre-stretching on the mechanical ageing of filled silicone rubbers for dielectric elastomer applications

Shamsul Zakaria[a,b], Liyun Yu[a], Guggi Kofod[c], Anne Ladegaard Skov[a,*]

[a] Danish Polymer Center, Department of Chemical and Biochemical Engineering, Technical University of Denmark, Søltofts Plads, Building 229, 2800 Kgs. Lyngby, Denmark
[b] Faculty of Industrial Science and Technology, Universiti Malaysia Pahang, Lebuhraya Tun Razak, 26300 Gambang, Pahang, Malaysia
[c] InMold A/S, Diplomvej 381, 2800 Lyngby, Denmark

ARTICLE INFO

Article history:
Received 28 July 2015
Accepted 9 August 2015
Available online 20 August 2015

Keywords:
Pre-stretching
Mechanical ageing
Silicone composite
PDMS
Dielectric elastomer

ABSTRACT

Dielectric elastomer (DE) pre-stretching is a key aspect of attaining better actuation performance, as it helps prevent electromechanical instability (EMI) and usually lowers the Young's modulus, thus leading to easier deformation. The pre-stretched DE is not only susceptible to a high risk of tearing and the formation of mechanical defects, but films with sustained and substantial strain may also experience mechanical degradation. In this study a long-term mechanical reliability study of DE is performed. Young's moduli, dielectric breakdown strengths and dielectric permittivities of commercial silica-reinforced silicone elastomers, with and without an additional 35% (35 phr) of titanium dioxide (TiO_2), were investigated after being subjected to pre-stretching for various timespans at pre-stretches to strains of 60 and 120%, respectively. The study shows that mechanical stability when pre-stretching is difficult to achieve with highly filled elastomers. However, despite the negative outlook for metal oxide-filled silicone elastomers, the study paves the way for reliable dielectric elastomers by indicating that simply post-curing silicone elastomers before use may increase reliability.

1. Introduction

The reliability of dielectric elastomer (DE) transducers depends on the types of material used, as well as fabrication techniques and design and transducer operating conditions (such as maximum stretching, applied frequency and amplitude of the applied voltage). The acrylic double-adhesive VHB 4910, produced by 3 M, is one of the best-performing elastomers with respect to actuation strain (s) at a given applied field, and it chiefly outperforms silicone-based elastomers over short time scales. Silicone elastomers, however, possess a faster actuation response as well as reliability over time, since performance remains more or less unaltered up to about 10 million cycles when pre-stretching is avoided [1]. Pre-stretching is well-known to be a prerequisite for the actuation of acrylic-based elastomers, since it simultaneously reduces thickness, decreases the Young's modulus and suppresses electromechanical instability (EMI). [2–4] The effect of the first two parameters can be seen from the equation of actuation derived by Pelrine et al. [3]:

$$s = -\epsilon_r \epsilon_0 \frac{(V/d)^2}{Y} \quad (1)$$

where s is actuation strain, V is applied voltage, d is the thickness of the film and Y is the Young's modulus.

Pre-stretching has also been shown to cause the alignment of elastomer chains in the plane of stretching [5]. This alignment, which is perpendicular to the direction of the electric field, leads to an increase in breakdown strength, because charge carrier movement is impeded. [6]. For acrylics, pre-stretching is also favourable due to strain-softening, whereas for silicone elastomers the elastomer usually does not show the same tendency and in many cases strain-hardening behaviour actually sets in. However, pre-stretching remains very favourable for silicone elastomers, as largely improved actuation strains can be obtained through the avoidance of EMI.

The most common failure modes of DE transducers are pull-in instability, dielectrical breakdown and material strength failure [7,8]. Electromechanical pull-in instability, also known as electromechanical instability (EMI), was identified by Stark and Garton [9] and occurs when Maxwell pressure locally exceeds the com-

* Corresponding author.
E-mail address: al@kt.dtu.dk (A.L. Skov).

http://dx.doi.org/10.1016/j.mtcomm.2015.08.002
2352-4928/

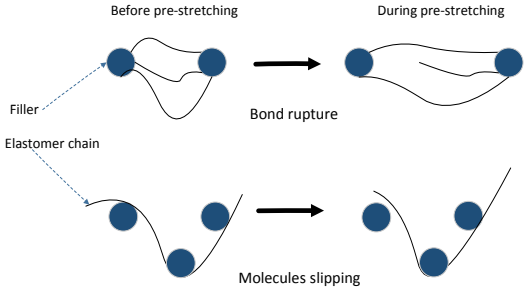

Fig. 1. Physical explanations of the Mullins effect.

pressive stress of the elastomer [4–10]. For silicone elastomers, mechanical strength failure is very seldom a failure mode, due to the ultimate extensibility of silicone elastomers usually exceeding 300%. Common actuation strains introduced in silicone elastomers are of the order of 20%, so even with pre-stretching the overall strain is far below their maximum extensibility. For silicone elastomers to make the very most of their potential, i.e. approach actuation strains of the order of their maximum extensibility, greater energy – and thus permittivity – is required.

The major disadvantage of silicone elastomers over acrylics is their low dielectric permittivity. Several approaches have been developed to enhance dielectric permittivity, with the addition of metal oxides being the most frequently investigated due the ease of elastomer formulation. TiO_2–silicone composites have by far been the most commonly investigated elastomer system due to the availability of nanosized TiO_2 particles with various surface functionalizations. More complex approaches exist such as the covalent grafting of dipoles [11–13] and the creation of heterogeneous elastomers with hard and soft domains from controlled network formation [14–17]. Incorporating rigid fillers, such as titanium dioxide, into the cross-linked PDMS matrix increases the dielectric permittivity of the resulting composite elastomer. Mechanical properties are also affected, with results varying according to particle size and surface treatment, from reinforcing to softening [18–22]. On the other hand, a thinly filled elastic film that maintains high strain for a given period of time will, to some extent, suffer mechanical ageing at the microscopic level. The Payne and Mullins effects explain hysteresis in the mechanical properties of filled elastomers. The Payne effect refers to the effect of the strain dependence of the dynamic viscoelastic properties of filled elastomers above their glass transition temperature [23]. Clement et al. [24] investigated the Payne effect in SiO_2-filled PDMS elastomers, and they posited it as the existence of a gradient in elastomeric chain mobility from the PDMS filler interface to the bulk, leading to a stress-softening effect at low strains upon "initial activation" of the elastomer. Clement et al. [25] also investigated the Mullins effect, i.e. the stress-softening phenomenon that occurs in elastomers during the first deformation of a given strain [26]. They attributed Mullins softening to bond ruptures or elastomer chain slippage (as illustrated in Fig. 1). Additionally, they observed the dependency of the Mullins effect on the degree of filler dispersion. They found that non-homogeneity in the spatial distribution of SiO_2 inside the elastomer matrix exhibits a greater Mullins effect due to the fact that larger local strains were acquired in regions with high concentrations of SiO_2. Due to its disruptive nature, stress softening has often been considered as damaging, but it does not necessarily lead to failure [27]; in general, it just leads to strain-history-dependent mechanical properties, though this dependency can be avoided by stretching the elastomer to more than its maximum actuation strain before applying it in products. Irradiation ageing has previously been studied by Stevenson et al. [28], but during such experiments crosslinking density changed, whereas in this study crosslink density remains constant.

Generally, silicone elastomers are commercially synthesised through the equilibration polymerisation of cyclic oligomers and end groups in the presence of acid or basic catalysts [29]. One of the disadvantages of this process is the production of by-products as a result of the reaction, consisting of unreacted cyclic oligomers [30]. These residues are mobile within the silicone, and they can also migrate to a device interface. This migration during post-manufacture changes the elastomer surface as well as its mechanical properties such as tensile strength, tear strength, maximum elongation, etc [31]. As reported by Brook et al. [32], these volatile siloxanes from commercial silicones usually remain within the elastomer when post-curing has been omitted. Post-curing is usually conducted by heating the elastomer far above its curing temperature but below its degradation temperature for some time. Brook et al. [32] showed that the mechanical properties of the elastomer were enhanced (a larger Young's modulus, greater tensile strength and lower maximum extensibility) upon post-curing. In this case, post-curing was performed by heating a cured elastomer at 200 °C for 4 h subsequent to the traditional curing procedure, where the most common conditions for dielectric silicone elastomers are curing at ~120 °C for 10–30 min [33]. To our knowledge the effect of post-curing on, for example, dielectric breakdown strength has never been investigated, since the fraction of volatiles is so low (usually cited at 1–2% by the elastomer supplier) that it seems irrelevant.

In order to introduce reliable DE-based products, the pre-stretching frame should be designed in such a way as to impart uniform pre-stretching to the elastomer film over a large area, regardless of whether it is a symmetrical or non-symmetrical pre-stretch [7]. There is a high risk of tearing at the corners of the grips used to hold the thin polymeric film in the pre-stretch equipment, which would lead to premature material strength failure, as the thin films are prone to tearing [7]. With respect to the elastomers, precautions are also required. Micro-voids, deviations in film thickness, surface roughness, inhomogeneous mechanical stiffness, dust particles, contaminants and scratches are the most common defects in thin elastomer films. For acrylics it was shown that during mechanical tests, additional groove-like defects rapidly appear at the film edges attached to rigid supports, and they expand gradually as the test continues [7]. The propagation of such cracks/grooves at stress gradients will age the material faster, thereby leading ultimately to mechanical failure.

As reported by Meunier et al. [34], unfilled PDMS lacks the Mullins effect, hysteresis and strain rate dependency. However, for DE applications filled, reinforced silicones are required to obtain acceptable performance. This study was performed in order to understand the intrinsic mechanical behaviour of pre-stretched PDMS elastomers, with and without additional permittivity enhancing fillers, over time. Furthermore, the study aims at elaborating how mechanical ageing affects other parameters relevant to the DE being used, namely the Young's modulus, electrical breakdown strength and dielectric permittivity.

2. Methodology

2.1. Materials

Four different compositions from two commercial silicone elastomers, without and with one type of permittivity enhancing filler (TiO_2), were investigated. The elastomers were Elastosil® LR 3043/30 A/B and ELASTOSIL® RT® 625 A/B. POWERSIL® LR® 3043/30 A/B is a high-viscosity LSR and is supplied as a two-part system. The mixing ratio of parts A and B is 1:1. ELASTOSIL® RT®

Table 1
Details of prepared SiO_2-filled (commercial) and SiO_2-TiO_2-filled (composite) PDMS films.

Sample ID	Material	Thickness	Pre-stretch (%)
A1	RT625	Thin	60
A2	RT625	Thin	120
A3	RT625	Thick	60
A4	RT625	Thick	120
B1	LR304330	Thin	60
B2	LR304330	Thin	120
B3	LR304330	Thick	60
B4	LR304330	Thick	120
C1	RT625 + 35%R420	Thin	60
C2	RT625 + 35%R420	Thin	120
C3	RT625 + 35%R420	Thick	60
C4	RT625 + 35%R420	Thick	120
D1	LR304330 + 35%R420	Thin	60
D2	LR304330 + 35%R420	Thin	120
D3	LR304330 + 35%R420	Thick	60
D4	LR304330 + 35%R420	Thick	120

625 A/B is an RTV elastomer, which is also supplied as a two-part system. The mixing ratio for parts A and B is 9:1. The solvent OS-20 (an ozone-safe, volatile methylsiloxane (VMS) fluid) was obtained from Dow Corning and added in order to get consistent viscosity formulation.

The investigated elastomers are of Elastosil® LR 3043/30 A/B and ELASTOSIL® RT® 625 A/B, respectively, and are denoted as LSR and RTV, respectively. The permittivity-enhancing filler added is alumina-silica-zirconia surface-treated hydrophobic rutile titanium dioxide (TiO_2) Sachtleben® R420® from Sachtleben Chemie, Duisburg, Germany, while the average primary particle size is 250 nm. The filler is added in a weight percentage of the original elastomer (i.e. phr) of 35%. The resulting elastomers are referred to as LSR and RTV composites, respectively. Solvent (OS-20) is also added to both SiO_2/TiO_2-filled elastomers, to reduce the viscosity of the formulations and thereby ease the coating of thin films.

2.2. Sample preparation

Thin films were carefully prepared based on the procedures described in Zakaria et al. [35]—as summarised below.

Part B of the elastomer, the solvent and the filler were mixed with a DAC 150FVZ (Hauschild Co., Germany) speed mixer at 3000 rpm. After 5 min of mixing, part A of the material was added and mixed for another 5 min at 2000 rpm. Glass plates were coated with the premixes using a thin 3540 bird applicator film (Elcometer, Germany). The samples were cured in an oven for 5 min at 75 °C and subsequently for 10 min at 115 °C. The thin films were removed from the glass plates, stored between 50 μm-thick ethylene-tetrafluorethylene (ETFE) foils and then kept in a desiccator until use. For this study, two sample thicknesses were targeted by using different blade gaps, namely 150 μm (relatively thinner films) and 200 μm (relatively thicker films). Film thicknesses were approximately 34–88 μm and 52–119 μm for the thin and thick samples, respectively. Film details can be seen in Table 1.

2.2.1. Pre-stretching of the samples

The samples were pre-stretched on an in-house-built frame. The designed frame holds and pre-stretches 150 thin films up to $\lambda = 400\%$. The films were 130 mm in width and 350 mm in length. In order to pre-stretch the films successfully, both ends were rolled with metal rods to prevent slippage. Then the metal rods, together with the stretched films, were attached to the frame, as shown in Fig. 2. The films were then covered by 50 μm-thick ETFE foils to prevent them from contamination. Finally, they were stored for different timespans: one day, one week, one month and three months, before they were released for further characterisation.

Fig. 2. The device used to pre-stretch the thin filled PDMS elastomer films. The pre-strains were adjusted by changing the position of the metal rods.

2.3. Instrumentation

2.3.1. Silver deposition

Silver depositions were performed on a physical vapor deposition (PVD) chamber system for reliable dielectric measurements. The chamber is fitted with a large butterfly valve to control pumping speed, and it is pumped by an oil diffusion pump (ODP) with a liquid nitrogen trap. The lid is lifted off the chamber whenever samples or targets need to be changed, and the lid wall seal is accomplished by the addition of a large ring. The base vacuum is approximately 2×10^{-5} mbar. The chamber is fitted with an evaporation source (for silver), a DC magnetron sputter source and an RF sputter source (for sputtering non-conducting targets). Silver evaporation was performed on the tungsten boat at the bottom of the chamber. According to the instrument calibration this should result in a sputtering rate of about 1.5 nm/s and produce a monolayer thickness of silver about 50–60 nm thick within 30–40 s. Thin silver electrodes ensure sufficient conductivity. More details on the process can be found in Benslimane et al. [36].

2.3.2. Dielectric constant measurement

Dielectric relaxation spectroscopy (DRS) was performed on a Novocontrol Alpha-A high-performance frequency analyser (Novocontrol Technologies GmbH & Co. KG, Germany) operating in the frequency range 10^{-1}–10^{6} Hz at 23 °C. Samples were sputtered with silver to provide electrodes 25 mm in diameter, before they were tested for permittivity.

2.3.3 Breakdown measurement

Breakdown measurements were performed on an in-house-built device based on international standards (IEC 60243-1 (1998) and IEC 60243-2 (2001)). The initial thicknesses of the films before pre-stretching was determined with a Leica DMLB microscope along with a USB Thorlabs 2.0 digital camera. The thickness of the stretched film (refer to SI) was calculated as $t_1 = t_0/\lambda$, where t_0 is initial thickness and λ is the stretch ratio. The distance between the two spherical electrodes (ø=20 mm) was set according to sample thickness with a micrometer stage and gauge. An indent of less than 3% of sample thickness was added to ensure that the spheres were in contact with the sample. A step-wise increasing voltage was applied (50–100 V/step) at a rate of 0.5–1.0 step/s, and each sample was subjected to 10 breakdown measurements and an average of the values indicated as the breakdown strength of the sample.

The breakdown measurements were also performed on the stretched films, which were pre-stretched based on the procedure described in Zakaria et al. [37]. and as shown in Fig. 3.

2.3.4. Stress–strain measurement

Uniaxial tensile quasi-static tests were performed to determine Young's moduli at different strains. The quasi-static measurements were carried out on specimens shaped as rectangular strips of about 6 mm × 60 mm in size, by applying a step-wise increasing load and measuring the corresponding elongations from $s = 0\%$ to $s = 130\%$. Young's moduli were determined from the tangent of the stress–strain curves for strains from 0% to 130%.

3. Results and discussion

Understanding the effects of static pre-stretching on PDMS films at different timespans is a prerequisite for making reliable DE transducers based on pre-stretched elastomer films. This understanding will be a step toward more reliable products. The natural subsequent step will be understanding the ongoing electrical ageing [38] and electro-mechanical ageing phenomena. However, if the developed elastomer cannot survive a static mechanical ageing test, it is very likely to fail prematurely in a coupled electro-mechanical test. Here we focus on static pre-stretches of 60 and 120%, respectively, and we also investigate how pre-stretching influences other relevant parameters in relation to DE performance. Since the film thickness of silicone elastomers has been shown to influence strongly electrical breakdown strengths [37] and mechanical properties [39], two thicknesses for each film were investigated, i.e. each elastomer formulation was tested in four configurations at each timespan (thick or thin/60% or 120% pre-stretch), while for the breakdown strength measurements another two configurations were utilised (either non-stretched or stretched to the utilized pre-stretch during the measurement).

3.1. Mechanical ageing

All silicone elastomers tested within this study show a strain-softening effect for strains up to a certain amount (around 60–70%) where after the elastomers strain–harden with increased strains. This characteristic feature leads to a local minimum in the Young's modulus as a function of strain. Fig. 4(A) shows the Young's modulus ($Y = \partial\sigma/\partial s$) as a function of strain for samples subjected to pre-stretching for various timespans. The results shown are for thin samples pre-stretched to 120%, as they were shown to be the most susceptible to mechanical ageing. Data for thin films to 60% pre-stretch, as well as thick samples to both 60% and 120%, are shown in the SI. In order to ease the comparison of data, normalisation was performed in Fig. 4(b). The normalised Young's modulus $Y_n(s) = Y(s)/Y_0(s)$, where $Y(s)$ = Young's modulus for aged samples at the given strain, and Y_0 is the Young's modulus for the non-aged reference samples at the same strain for the various filled PDMS films at $s = 0$ to 130%.

For commercial elastomers, RTV (A2) and LSR (B2), i.e. pure commercial elastomers, mechanical ageing is not at first glance significant. However, from the normalised diagrams (Fig. 4(B)) it is obvious that the dynamics have changed to some extent over time. Initially, it was deemed odd that ageing did not seem to be monotonic. From the results of Brook et al. [32] this discrepancy can be explained by the fact that cyclic silicones from the commercial silicone elastomer remain within the elastomer, as no harsh post-curing has been performed on our elastomers. For the investigated elastomers, mass losses upon heating up to ~250 °C have been investigated previously by using TGA and were of the order of 1–2%.[40] Therefore, upon pre-stretching, the first process taking place –as expected – is Mullins softening, due to the particulate network being broken down. Then, subsequently, after the surface has been partly broken, the cyclic silicones and residual solvent diffuse out of the elastomer, thus leading to hardening of the elastomers [32]. For both commercial elastomers, the diffusion phenomenon seems to be strongest for the ~1 week timescale, whereas for the composite RTV (C2) elastomer, the effect seems to be delayed significantly, and for the composite LSR (D2), the effect is faster and vanishes between one and three months. For the composite LSR, the elastomer shows such a strong Mullins effect that it never regains its original strength after the first (destructive) 130% strain cycle.

The phenomenon of volatile siloxanes diffusing from the PDMS elastomer can be seen clearly on the RTV (A3) and LSR (B3) commercial elastomer samples, as the mechanical properties of the aged films are higher than the reference after pre-stretching from one day up to three months (refer to Fig. 2 in SI). Meanwhile, for the composites RTV (C3) and LSR (D3), a lesser effect can be seen, as the elastomers show a rather strong Mullins effect (refer to Fig. 2 in SI). Also, when comparing thicknesses, it is evident that the mechanical ageing effect is highly thickness-dependent, since the enhancement of mechanical properties (before the degradation) is significantly slower for thick films.

After the cyclic silicones and residual solvent have evaporated, the commercial RTV elastomer (A) does not demonstrate major changes in mechanical properties. However, the commercial LSR changes its high-strain properties and becomes significantly less strain-hardening over timespans ranging from one to three 3 months. Strain-hardening behaviour is favourable in the context of avoiding electro-mechanical instability (EMI), so it clearly represents a worsening of mechanical properties.

Data on the Young's moduli have been condensed in Fig. 5, in which the Young's moduli at $s = 120\%$ have been plotted as functions of time for both thin and thick films. The most significant observable mechanical degradation was obtained for composite D2, as the Young's modulus at $s = 120\%$ of the non-aged reference sample declines by a factor of approximately four after three months of pre-stretching (2.55 MPa and down to 0.66 MPa). However, only slight changes to the Young's moduli at $s = 120\%$ were obtained for A2 samples (0.70–0.45 MPa). This indicates a longer term of mechanical reliability for SiO_2-filled elastomers compared to composite elastomers. This is also expected, as commercial elastomers are formulated to high standards. As reported by Dorfmann and Ogden [41], the effect of stress softening is only present to a small extent in unfilled compounds and elastomers with low filler content.

It is clear that the Young's moduli for different PDMS materials and conditions at $s = 120\%$ vary significantly over time. The effect of pre-stretching on the mechanical degradation of filled PDMS films can be seen clearly in Fig. 5. The samples that had larger pre-stretches ($\lambda = 120\%$) reveal severe mechanical ageing (red circle and violet downward triangle) compared to the samples that were subjected to smaller pre-stretching ($\lambda = 60\%$) (black square and blue upward triangle), due to stress-softening increasing pro-

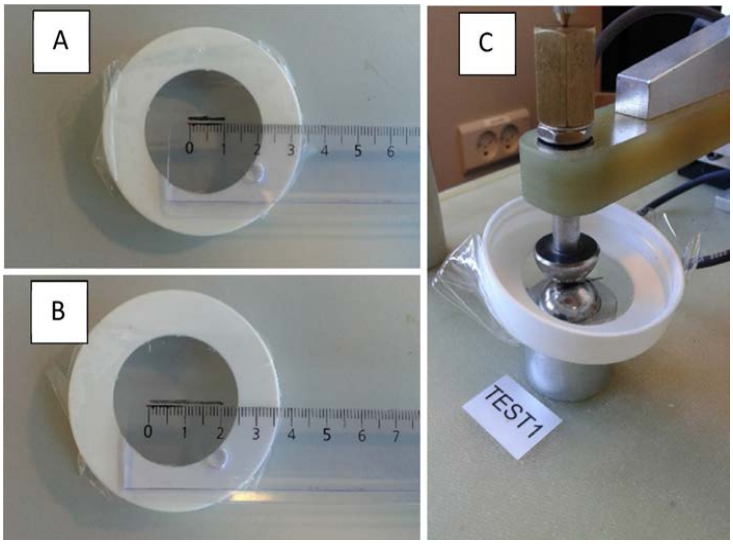

Fig. 3. The samples were pre-stretched on a cap with a circular hole. A line was drawn (10 mm) on the unstretched film (a) before the film was extended in the *x*-direction. (b) The pre-stretched film was slid between 20 mm diameter semi-spherical electrodes (c) for breakdown measurement.

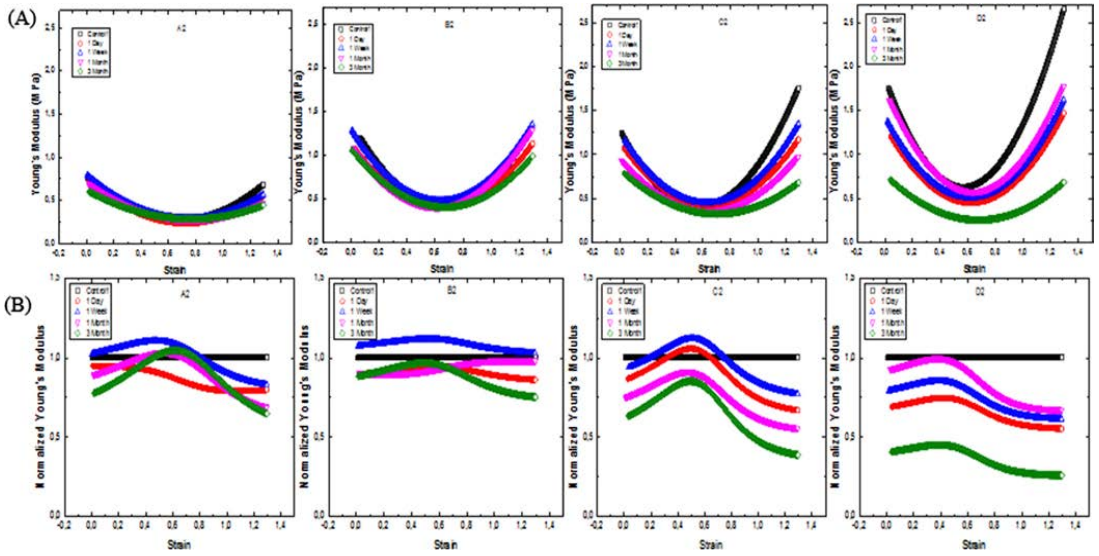

Fig. 4. Young's moduli (a) and normalised Young's moduli (b) for investigated elastomers as a function of the strains. (A2) and (C2) are commercial and composite RT625 films, respectively, whereas (B2) and (D2) are commercial and composite LR3043/30 films, respectively. Films were pre-stretched at different timespans (black square: control, red circle: 1 day, blue upwards triangle: 1 week, violet downwards triangle: 1 month and diamond green: 3 months). All elastomeric samples had similar conditions; i.e. thin films (coated with 150 μm blade) and $\lambda = 120\%$ except for the control samples ($\lambda = 0\%$). (For interpretation of the references to colour in this figure legend, the reader is referred to the web version of this article.)

gressively in line with the increasing strain [42]. Even though the dependency of mechanical ageing on thickness was not clearly noticeable in Fig. 5, nevertheless the coupling of the thin film and a larger strain demonstrates the most severe effect on the mechanical ageing of filled PDMS films. Thick samples will experience delayed ageing, because the constructive evaporation of cyclic silicones and destructive structure changes appear simultaneously at the timescales investigated within this study.

For the two composite formulations, the composite RTV (C2) shows the severest loss of tension on the one month time scale, but it continues to lose tension over time. The composite LSR formulation obviously loses significant tension, with a drop in Young's moduli greater than 50% for all strains investigated following three months of ageing at a pre-stretch of 120%.

To illustrate the loss of tension in the elastomers over time, stress–strain diagrams under cyclic loading conditions are shown in Fig. 6. The cyclic deformation diagrams are shown for two representative samples (lowest (A) and highest (D) total filler content, respectively). Initially before ageing, the control sample strongly exhibits Mullins softening, as the area of hysteresis loop for the

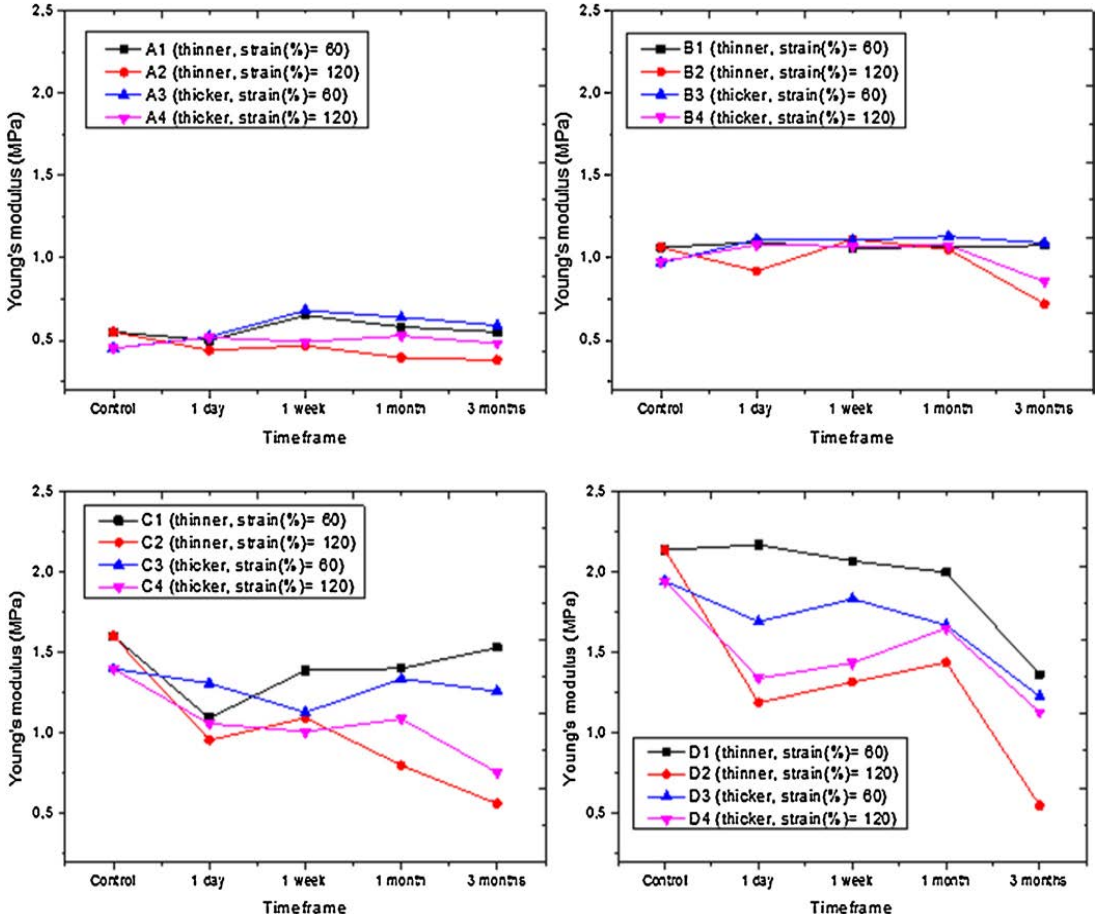

Fig. 5. Young's moduli of different samples measured at s = 120% after pre-stretching from time = 0–control to 3 months. A = RT625, B = RT625 + 35% TiO_2, C = LR3043/30 and D = LR3043/30 + 35% TiO_2. Conditions for A1, B1, C1 and D1 = the films were coated with a 150 μm blade (thin films) and λ = 60%, A2, B2, C2 and D2 = the films were coated with a 150 μm blade (thin films) and λ = 120%, A3, B3, C3 and D3 = the films were coated with a 200 μm blade (thick films) and λ = 60% and A4, B4, C4 and D4 = the films were coated with a 200 μm blade (thick films) and λ = 120%.

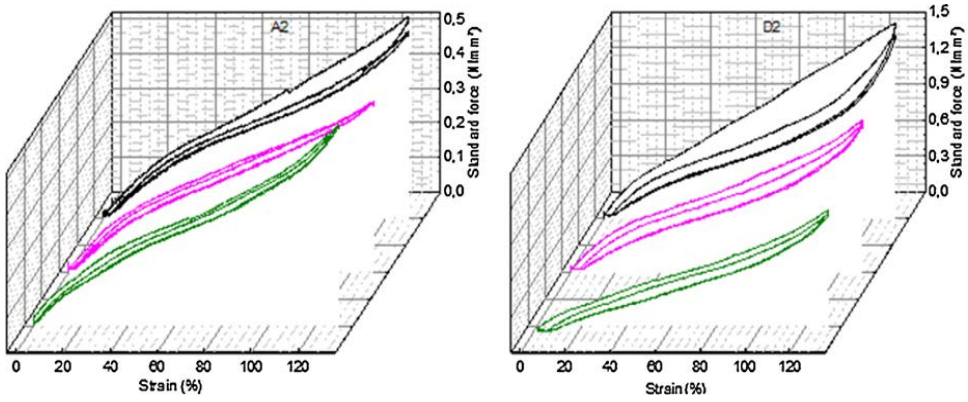

Fig. 6. Stress–strain diagrams of control (black), 1 month (violet) and 3 months (green) of RTV elastomer (A2) and composite LSR (D2) sample (pre-stretching 120%). (For interpretation of the references to colour in this figure legend, the reader is referred to the web version of this article.)

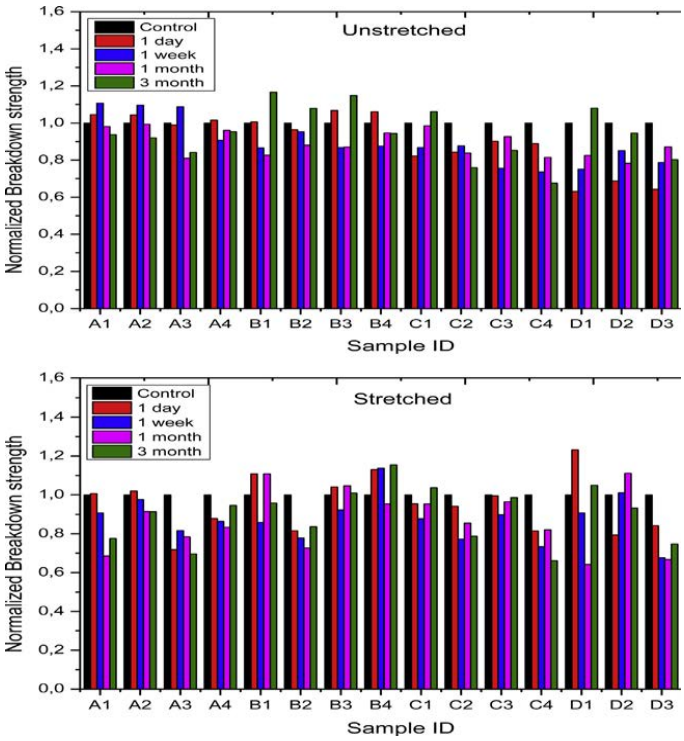

Fig. 7. Normalised breakdown strength of unstretched and stretched PDMS films at different timespans. The films were pre-stretched, while breakdown measurements were performed for the stretched samples. A = RT625, B = RT625 + 35% TiO_2, C = LR3043-30 and D = LR3043-30 + 35% TiO_2. Conditions for A1, B1, C1 and D1 = the films were coated with a 150 μm blade (thin films) and λ = 60%, A2, B2, C2 and D2 = the films were coated with a 150 μm blade (thin films) and λ = 120%, A3, B3, C3 and D3 = the films were coated with a 200 μm blade (thick films) and λ = 60% and A4, B4, C4 and D4 = the films were coated with a 200 μm blade (thick films) and λ = 120%.

first deformation is approximately three times that of the second deformation for both the A2 and D2 samples. After constant pre-stretching, the Mullins effect becomes less pronounced for the aged sample, since the area of the initial hysteresis loop decreases significantly.

3.2. Breakdown strength

Since the mechanical properties of pre-stretched PDMS films change over time, it can be argued that the breakdown strengths of filled PDMS films are also likely to change. Fig.7 shows the normalised breakdown strengths ($BD_n = BD/BD_0$, where BD = breakdown strength for aged samples and BD_0 = breakdown strength for non-aged reference samples) for different filled PDMS films and ageing conditions. The results show breakdown strengths for both unstretched and stretched (during breakdown test) PDMS samples. The inconsistency of the results is caused mostly by deviations in sample thicknesses (as can be seen in Table 1 in SI), as breakdown strengths were proved previously to be strongly dependent on the thicknesses of elastomeric films [37], i.e. the thicker PDMS films show low breakdown strength compared to the thin films, due to the increased volume—and thus larger number of defects. The thicknesses of the investigated films cannot be controlled precisely due to different PDMS formulation viscosities, and the variation in thicknesses can be seen in Table 1 in SI. Simultaneously, as mechanical properties change, breakdown strengths will also change [43], and as discussed previously the Young's moduli do not change monotonically. This behaviour is also observed within the determinations of breakdown strengths. The commercial elastomer RTV shows – for all samples – a maximum in breakdown strength, which is consistent with the maximum in Y. For the LSR, breakdown strength is enhanced at the end of the ageing study, but at present it remains unclear as to why the mechanical data do not support this behaviour. For the composites there is no clear trend except that, overall, breakdown strength decreases after three months of pre-stretching.

For better comparison – without complications aligned with thickness variations – the breakdown strengths of several samples with minimal thicknesses deviations (±3 μm) in relation to the control samples were compared, as shown in Table 2. The breakdown results for the one- and three-month samples were chosen, as they show greatest effect of volatile siloxanes diffusion, as shown in SI. The standard deviations were considerably greater for several samples, due to the non-uniformity of film thicknesses and defects contained in the prepared samples, while the major uncertainty of the breakdown data may also indicate bimodal distributions of breakdown strengths for several samples (see Fig. 4 in SI). Nonetheless, the data in Table 2 confirm that the breakdown strengths lower in line with mechanical ageing, due to the decrease in the Young's modulus of the aged samples [43].

3.3. Dielectric properties

When the elastomer changes both the mechanical properties and electrical breakdown strength, it is very likely that the dielectric properties will also change over time. Fig. 8 shows normalised storage permittivity where ϵ' = storage permittivity for aged samples and ϵ'_0 = storage permittivity for non-aged reference samples)

Table 2
Breakdown strengths of several samples that have thickness differences at ±3 μm in relation to the thicknesses of the control films.

Sample ID	Control			1 Month			3 Month		
	Sample thickness (μm)	Breakdown strength (V/μm) (unstretched)	Breakdown strength (V/μm) (stretched)	Sample thickness (μm)	Breakdown strength (V/μm) (unstretched)	Breakdown strength (V/μm) (stretched)	Sample thickness (μm)	Breakdown strength (V/μm) (unstretched)	Breakdown strength (V/μm) (stretched)
A3	106	98 ± 4	160 ± 3	108	90 ± 8	125 ± 6			
B4	63	101 ± 5	169 ± 3	66	95 ± 6	161 ± 3			
C1	67	113 ± 3	159 ± 7	67	111 ± 4	151 ± 3			
C2	67	113 ± 3	194 ± 5	64	97 ± 3	166 ± 5			
A2	73	97 ± 4	160 ± 2				76	89 ± 4	146 ± 3
C3	89	114 ± 5	144 ± 4				88	98 ± 8	142 ± 5
C4	89	114 ± 5	190 ± 2				88	77 ± 5	126 ± 4
D2	41	141 ± 4	266 ± 6				41	133 ± 6	249 ± 6

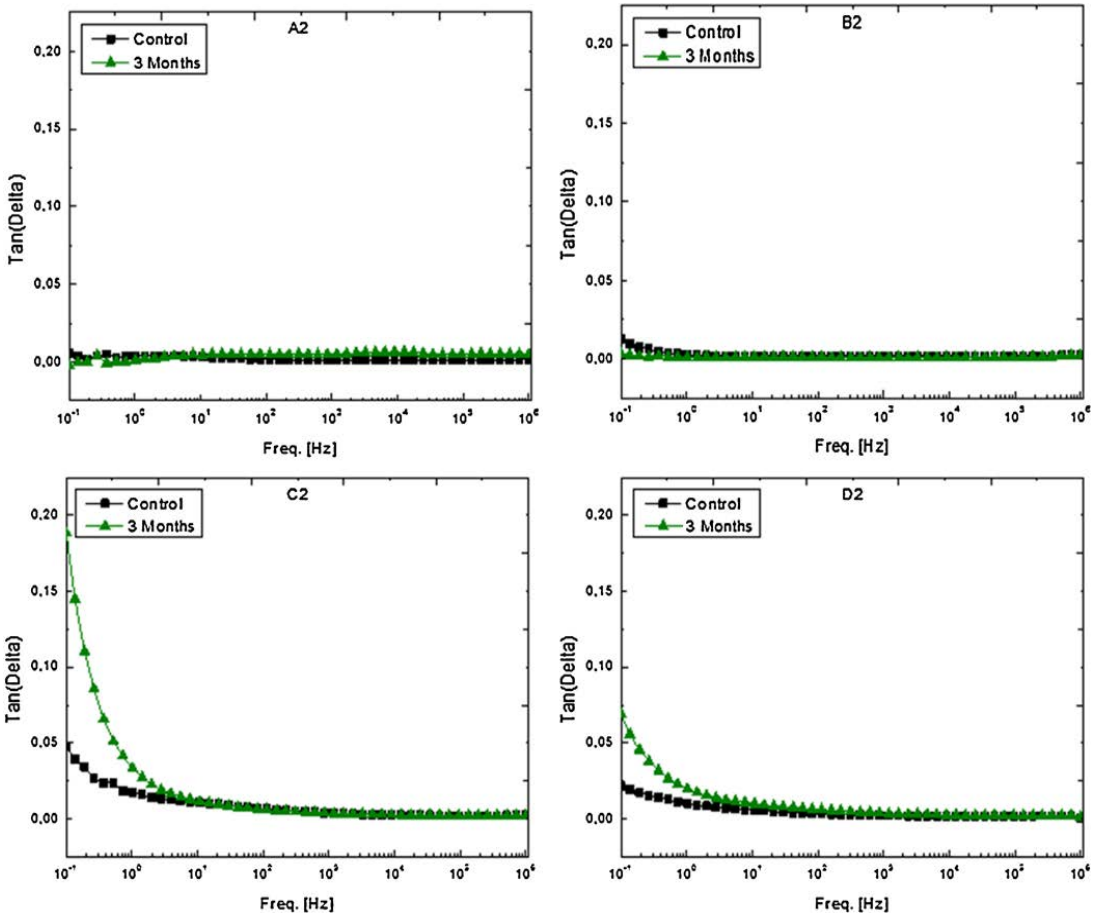

Fig. 8. Loss tangents for the A2, B2, C2 and D2 samples after pre-stretching from time = 0 to 3 months. (A2) and (C2) are commercial and composite RTV elastomers, respectively, whereas (B2) and (D2) are commercial and composite LSR elastomers, respectively. All elastomeric samples had similar conditions, i.e. thin films and $\lambda = 120\%$.

for filled PDMS films at a frequency of 10^{-1} and 10^{6} Hz, respectively. Despite the unfavourable effect of mechanical ageing on breakdown strength, the dielectric constants of the filled PDMS films improve at both low and high frequencies (10^{-1} Hz and 10^{6} Hz) after pre-stretching at given timespans where all aged samples show higher storage permittivity in comparison to the control. This is a clear indication of the complex network structure within the composites (consisting of polymeric network as well as polymer–particle and particle–particle interactions) being altered. This is most likely due to a decrease in particle–particle interactions, i.e. the agglomerates are broken and facilitating smaller particles—and thus increased permittivity. However, the data is so scattered that temperature scans would have been required to perform any general conclusion. The dielectric loss factor does, however, reveal differences in phenomena occurring for the pure elastomers and the composite elastomers. Fig. 8 shows the dielectric loss tangent as a function of frequency for samples A2, B2, C2 and D2 at time = 0 and time = 3 months. The results show the dependency of the loss tangent for both composite (C2 and D2) samples in relation to ageing. There is no evidence showing the effect of mechanical ageing on the loss tangent for commercial elastomers (A2 and B2), as there is no significant difference in the permittivities of PDMS and silica. At higher filler loadings, achieving proper dispersion is difficult (despite using a high-speed mixer), and agglomerated particles in the elastomer matrix may occur. Large deformations for a long time interrupt the relatively weak interactions between agglomerated particles (Mullins effect) and thus increase the mobility of the high-permittivity segments in the composite films, as discussed above. Thus, the increase in the loss tangent is assumed to be the result of the mobility of the fillers which separate and thereby increase their effective surface area. This increase can be seen from the loss tangent increasing at low frequencies, due to the predominantly interfacial polarisation.

4. Conclusion

Dielectric elastomers with enhanced permittivity are heavily sought after for enhanced actuation, and so many approaches in this respect are being currently developed. The addition of high-permittivity metal oxide fillers to silicone elastomers is a facile method for such an enhancement, but studies so far have focused solely on how the metal oxides affect instant mechanical behaviour. In this study we show that titanium dioxide cannot be added unlimitedly when pre-stretching the elastomer, since the composites lose their tension very quickly. If such high loadings of fillers are required, it is important to further functionalise the particles for better compatibility and integrity. Another important finding is that even commercial silicone elastomers require post-curing for

mechanical stability, which is an overlooked feature for silicone elastomers utilised in dielectric elastomers. The two commercial elastomers in this research (RT625 and LR3043/30) both showed improved strength over a time scale of weeks, and thus a decrease in actuation will take place. This phenomenon can be ascribed to the evaporation of volatile cyclic silicones and other residues from elastomers which have had their protective surface broken during pre-stretching. Over a timescale of months, a slight reduction in elasticity takes place due to ageing. In other words, the elastomer will not provide constant actuation over time if it is not ensured beforehand that all volatiles have been removed. The removal of volatiles is additionally favourable, as it increases electrical breakdown strength and thus enhances the reliability of the elastomer.

Acknowledgements

The authors gratefully acknowledge financial support from the Ministry of Education of Malaysia and Universiti Malaysia Pahang. Danfoss PolyPower A/S and Innovationsfonden Danmark are acknowledged for additional funding.

Appendix A. Supplementary data

Supplementary data associated with this article can be found, in the online version, at http://dx.doi.org/10.1016/j.mtcomm.2015.08.002.

References

[1] F. Carpi, D. De Rossi, R. Kornbluh, R. Pelrine, P. Sommer-Larsen, Fundamentals, materials, devices, models and applications of an emerging electroactive polymer technology, in: Dielectric Elastomers as Electromechanical Transducers, Elsevier Ltd., Oxford UK, 2008.
[2] R. Palakodeti, M.R. Kessler, Influence of frequency and prestrain on the mechanical efficiency of dielectric electroactive polymer actuators, Mater. Lett. 60 (2006) 3437–3440.
[3] R. Pelrine, R. Kornbluh, Q. Pei, J. Joseph, High-speed electrically actuated elastomers with strain greater than 100%, Science 287 (2000) 836–839.
[4] X. Zhao, Z. Suo, Theory of dielectric elastomers capable of giant deformation of actuation, Phys. Rev. Lett. 104 (2010) 178302.
[5] C. Prisacariu, Polyurethane Elastomers: From Morphology to Mechanical Aspects, Springer Vienna, Vienna, 2011.
[6] A. Reiser, M. Lock, J. Knight, Migration and trapping of extrinsic charge carriers in polymer films, Trans. Faraday Soc. 65 (1969) 2168–2185.
[7] J.L. Bigue, P. Chouinard, S. Proulx, G. Miron, J. Plante, Preliminary assessment of manufacturing impacts on dielectric elastomer actuators reliability, Smart Materials and Structures, Cansmart Workshop (2009) 303–314.
[8] J. Plante, S. Dubowsky, On the properties of dielectric elastomer actuators and their design implications, Smart Mater. Struct. 16 (2007) 227–236.
[9] K.H. Stark, C.G. Garton, Electric strength of irradiated polythene, Nature 176 (1955) 1225–1226.
[10] D. Gatti, H. Haus, M. Matysek, B. Frohnapfel, C. Tropea, H.F. Schlaak, The dielectric breakdown limit of silicone dielectric elastomer actuators, Appl. Phys. Lett. 104 (2014) 052905.
[11] B. Kussmaul, S. Risse, G. Kofod, R. Waché, M. Wegener, D.N. McCarthy, H. Krüger, R. Gerhard, Enhancement of dielectric permittivity and electromechanical response in silicone elastomers: molecular grafting of organic dipoles to the macromolecular network, Adv. Funct. Mater. 21 (2011) 4589–4594.
[12] F.B. Madsen, L. Yu, A.E. Daugaard, S. Hvilsted, A.L. Skov, A new soft dielectric silicone elastomer matrix with high mechanical integrity and low losses, RSC Adv. 5 (2015) 10254–10259.
[13] F.B. Madsen, L. Yu, A.E. Daugaard, S. Hvilsted, A.L. Skov, Silicone elastomers with high dielectric permittivity and high dielectric breakdown strength based on dipolar copolymers, Polymer 55 (2014) 6212–6219.
[14] F.B. Madsen, A.E. Daugaard, C. Fleury, S. Hvilsted, A.L. Skov, Visualisation and characterisation of heterogeneous bimodal PDMS networks, RSC Adv. 4 (2014) 6939–6945.
[15] J.A. Crowe-Willoughby, K.L. Weiger, A.E. Özçam, J. Genzer, Formation of silicone elastomer networks films with gradients in modulus, Polymer 51 (2010) 763–773.
[16] C. Huang, Q.-M. Zhang, Fully functionalized high-dielectric-constant nanophase polymers with high electromechanical response, Adv. Mater. 17 (2005) 1153–1158.
[17] K. Goswami, A.E. Daugaard, A.L. Skov, Dielectric properties of ultraviolet cured poly(dimethyl siloxane) sub-percolative composites containing percolative amounts of multi-walled carbon nanotubes, RSC Adv. 5 (2015) 12792–12799.
[18] S. Vudayagiri, S. Zakaria, L. Yu, S.S. Hassouneh, M. Benslimane, A.L. Skov, High breakdown-strength composites from liquid silicone rubbers, Smart Mater. Struct. 23 (2014) 105017.
[19] F.B. Madsen, L. Yu, S. Hvilsted, A.L. Skov, Dielectric elastomers, with very high dielectric permittivity, based on silicone and ionic interpenetrating networks, RSC Adv. 5 (2015) 49739–49747.
[20] F. Carpi, D. De Rossi, Improvement of electromechanical actuating performances of a silicone dielectric elastomer by dispersion of titanium dioxide powder, IEEE Trans. Dielectr. Electr. Insul. 12 (2005) 835–843.
[21] D. Baker, A. Charlesby, J. Morris, Reinforcement of silicone elastomer by fine particles, Polymer 9 (1968) 437–448.
[22] F. Clément, A. Lapra, L. Bokobza, L. Monnerie, P. Ménez, Atomic force microscopy investigation of filled elastomers and comparison with transmission electron microscopy—application to silica-filled silicone elastomers, Polymer 42 (2001) 6259–6270.
[23] A.R. Payne, G. Kraus, Reinforcement of Elastomers, vol. 69, Interscience, New York, 1965, pp. 69–123.
[24] F. Clément, L. Bokobza, L. Monnerie, Investigation of the payne effect and its temperature dependence on silica-filled polydimethylsiloxane networks. Part II: Test of quantitative models, Rubber Chem. Technol. 78 (2005) 232–244.
[25] F. Clément, L. Bokobza, L. Monnerie, On the Mullins effect in silica-filled polydimethylsiloxane networks, Rubber Chem. Technol. 74 (2001) 847–870.
[26] L. Mullins, Softening of rubber by deformation, Rubber Chem. Technol. 42 (1969) 339–362.
[27] T. Rey, G. Chagnon, J.B. Le Cam, D. Favier, Influence of the temperature on the mechanical behaviour of filled and unfilled silicone rubbers, Polym. Test. 32 (2013) 492–501.
[28] I. Stevenson, L. David, C. Gauthier, L. Arambourg, J. Davenas, G. Vigier, Influence of SiO_2 fillers on the irradiation ageing of silicone rubbers, Polymer 42 (2001) 9287–9292.
[29] J. Chojnowski, Polymerization in Siloxane Polymers, PTR Prentice Hall, Englewood Cliffs, New Jersey, 1993.
[30] W. Noll, Chemistry and Technology of Silicones, Academic, New York, 1968.
[31] A. Ghosh, R.S. Rajeev, A.K. Bhattacharya, A.K. Bhowmick, S.K. De, Recycling of silicone rubber waste: effect of ground silicone rubber vulcanizate powder on the properties of silicone rubber, Polym. Eng. Sci. 43 (2003) 279–296.
[32] M.A. Brook, H.-U. Saier, J. Schnabel, K. Town, M. Maloney, Pretreatment of liquid silicone rubbers to remove volatile siloxanes, Ind. Eng. Chem. Res. 46 (2007) 8796–8805.
[33] S. Vudayagiri, A.L. Skov, Methods to ease the release of thin polydimethylsiloxane films from difficult substrates, Polym. Adv. Technol. 25 (2014) 249–257.
[34] L. Meunier, G. Chagnon, D. Favier, L. Orgéas, P. Vacher, Mechanical experimental characterisation and numerical modelling of an unfilled silicone rubber, Polym. Test. 27 (2008) 765–777.
[35] A.L. Skov, S. Vudayagiri, M. Benslimane, Novel silicone elastomer formulations for DEAPs, in: Proceeding of SPIE, Electroactive Polymer Actuators and Devices (EAPAD): 86871, San Diego, California, USA, 2013, 86,871I–86871I–8.
[36] M. Benslimane, H.E. Kiil, M.J. Tryson, Electromechanical properties of novel large strain PolyPower film and laminate components for DEAP actuator and sensor applications, in: Proceeding of SPIE, Electroactive Polymer Actuators and Devices (EAPAD): 7642, San Diego, California, USA, 2010, 64,231–764231–11.
[37] S. Zakaria, P.H.F. Morshuis, M.Y. Benslimane, L. Yu, A.L. Skov, The electrical breakdown strength of pre-stretched elastomers, with and without sample volume conservation, Smart Mater. Struct. 24 (2015) 055009.
[38] Kochetov Roman, I.A. Tsekmes, P.H.F. Morshuis, Electrical conductivity, dielectric response and space charge dynamics of electroactive polymer with and without nanofiller reinforcement, Smart Mater. Struct. (2015), Provisiona.
[39] M. Liu, J. Sun, Y. Sun, C. Bock, Q. Chen, Thickness-dependent mechanical properties of polydimethylsiloxane membranes, J. Micromech. Microeng. 19 (2009), 035028.
[40] S. Zakaria, P.H.F. Morshuis, M.Y. Benslimane, K.V. Gernaey, A.L. Skov, The electrical breakdown of thin dielectric elastomers: thermal effects, in: Proceeding of SPIE, Electroactive Polymer Actuators and Devices (EAPAD): 9056, San Diego, California, USA, 2014, 90562V.
[41] A. Dorfmann, R.W. Ogden, A constitutive model for the Mullins effect with permanent set in particle-reinforced rubber, Int. J. Solids Struct. 41 (2004) 1855–1878.
[42] J. Diani, B. Fayolle, P. Gilormini, A review on the Mullins effect, Eur. Polym. J. 45 (2009) 601–612.
[43] M. Kollosche, H. Stoyanov, H. Ragusch, S. Risse, A. Becker, G. Kofod, Electrical breakdown in soft elastomers: Stiffness dependence in un-pre-stretched elastomers, Proceedings of the IEEE International Conference on Solid Dielectrics, ICSD (2010) 1–4.

Supplementary Information (SI) for Appendix C

The influence of static pre-stretching on the mechanical ageing of filled silicone rubbers for dielectric elastomer applications

Table S1: The thicknesses of stretched and un-stretched films.

Sample ID	Material	Thickness (μm)									
		Control		1 Day		1 Week		1 Month		3 Month	
		Un-stretched	Stretched	Un-stretched	Stretched	Un-stretched	Stretched	Un-stretched	Stretched	Un-stretched	Stretched
						s= 60%					
A1	RT625	73	46	66	41	47	29	92	41	95	43
A3	RT625	106	66	119	74	72	45	108	67	112	70
B1	LR304330	51	32	56	35	67	41	61	38	64	40
B3	LR304330	63	39	78	48	106	66	73	45	71	44
C1	RT625+35%R420	67	30	41	18	60	27	67	30	61	27
C3	RT625+35%R420	89	40	58	26	117	53	94	42	88	40
D1	LR304330+35%R420	41	18	76	34	59	26	36	16	35	15
D3	LR304330+35%R420	52	23	95	43	92	41	70	31	64	29
						s= 120%					
A2	RT625	73	46	66	41	47	29	82	51	76	47
A4	RT625	106	66	119	74	73	45	118	73	106	66
B2	LR304330	51	32	76	47	70	43	76	47	67	41
B4	LR304330	63	39	82	51	107	66	66	41	76	47
C2	RT625+35%R420	67	30	53	24	72	32	64	29	73	33
C4	RT625+35%R420	89	40	64	29	68	30	73	33	88	40
D2	LR304330+35%R420	41	18	75	34	59	26	34	15	41	18
D4	LR304330+35%R420	52	23	98	44	78	35	56	25	59	26

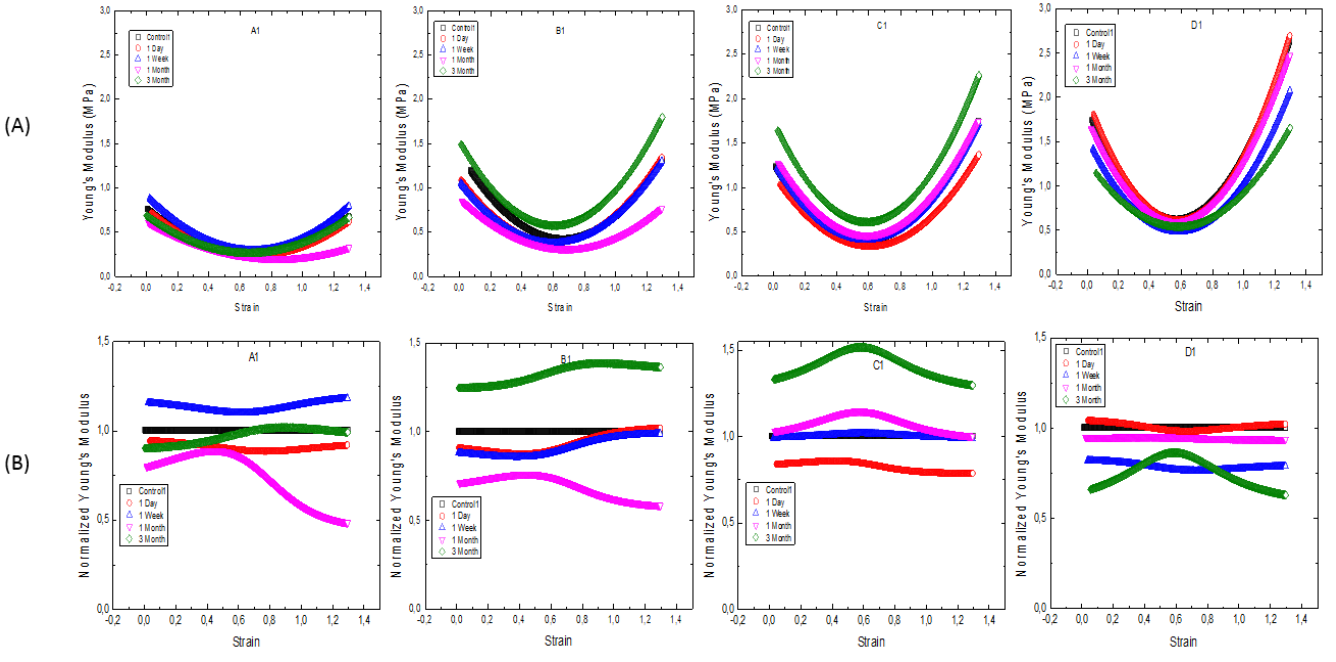

Figure S1: Young's moduli (A) and normalized Young's moduli (B) for different filled PDMS films as function of the strains. (A1) and (C1) were SiO_2-filled and SiO_2/TiO_2-filled RT625 films, respectively, meanwhile (B1) and (D1) were SiO_2-filled and SiO_2/TiO_2-filled LR3043/30 films, respectively were pre-stretched at different timeframes (black square: control, red circle: 1 day, blue upwards triangle: 1 week, violet downwards triangle: 1 month and diamond green: 3 months). All elastomeric samples had similar conditions; i.e. thin films (coated with 150 µm blade) and s= 60% except for the control samples (s= 0%).

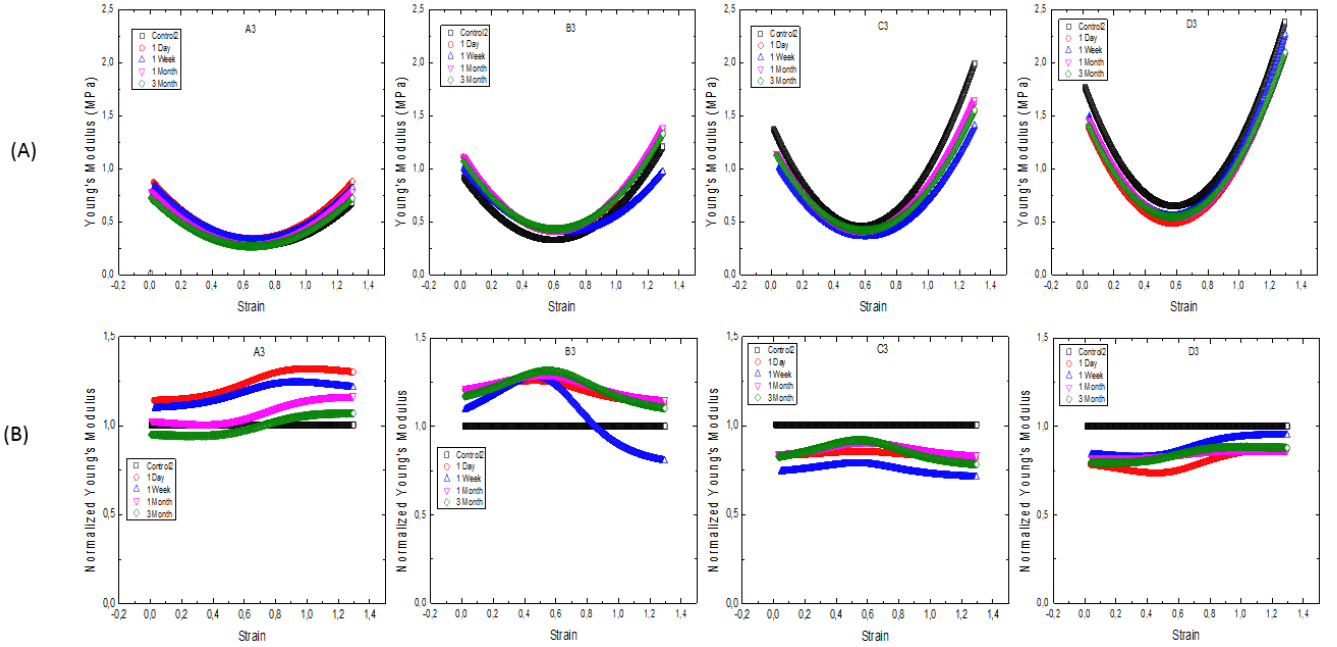

Figure S2: Young's moduli (A) and normalized Young's moduli (B) for different filled PDMS films as function of the strains. (A3) and (C3) were SiO_2-filled and SiO_2/TiO_2-filled RT625 films, respectively, meanwhile (B3) and (D3) were SiO_2-filled and SiO_2/TiO_2-filled LR3043/30 films, respectively were pre-stretched at different timeframes (black square: control, red circle: 1 day, blue upwards triangle: 1 week, violet downwards triangle: 1 month and diamond green: 3 months). All elastomeric samples had similar conditions; i.e. thick films (coated with 200 µm blade) and s= 60% except for the control samples (s= 0%).

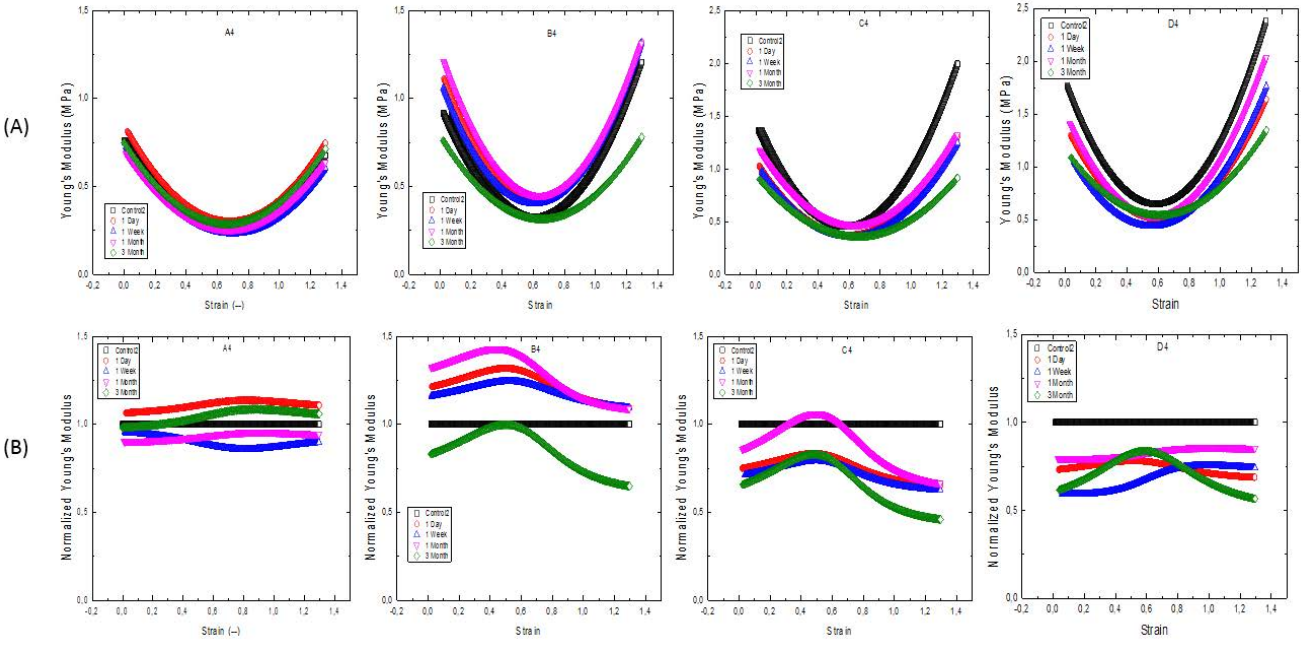

Figure S3: Young's moduli (A) and normalized Young's moduli (B) for different filled PDMS films as function of the strains. (A4) and (C4) were SiO_2-filled and SiO_2/TiO_2-filled RT625 films, respectively, meanwhile (B4) and (D4) were SiO_2-filled and SiO_2/TiO_2-filled LR3043/30 films, respectively were pre-stretched at different timeframes (black square: control, red circle: 1 day, blue upwards triangle: 1 week, violet downwards triangle: 1 month and diamond green: 3 months). All elastomeric samples had similar conditions; i.e. thick films (coated with 200 µm blade) and s= 120% except for the control samples (s= 0%).

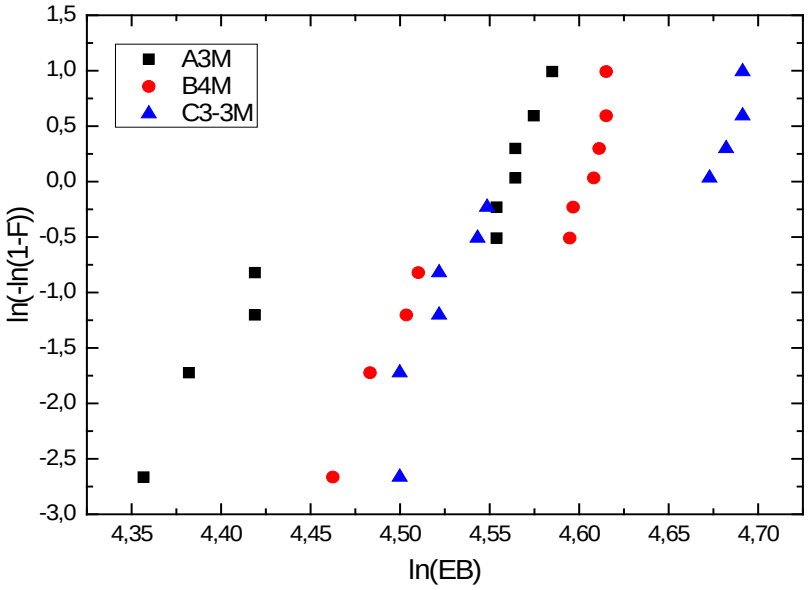

Figure S4: Weibull distributions for several samples that showing bimodal breakdown distributions, where F= Weibull cumulative distribution function and EB= breakdown strength. A3M is RT625 with condition: thin films and pre-stretched (ʎ= 60%) for 1 month, B4M is LR3043/30 with condition: thick films and pre-stretched (s= 60%) for 1 month, C3-3M is LR3043/30+35% TiO_2 with condition: thick films and pre-stretched (s= 120%) for 3 month.

APPENDIX D:

Mechanical and electrical ageing effects on the long-term stretching of silicone dielectric elastomers with soft fillers

Madsen FB, Zakaria S, Yu L and Skov AL

Smart Materials and Structures

2015

Mechanical and electrical ageing effects on the long-term stretching of silicone dielectric elastomers with soft fillers

F. B. Madsen[a], S. Zakaria[a,b], L. Yu[a] and A. L. Skov[a]*
[a]Danish Polymer Centre, Department of Chemical and Biochemical Engineering, Technical University of Denmark, DTU, Søltofts Plads, building 227, 2800 Kgs. Lyngby, Denmark
[b]Faculty of Industrial Science and Technology, Universiti Malaysia Pahang, Lebuhraya Tun Razak 26300 Gambang, Pahang, Malaysia.

*E-mail: al@kt.dtu.dk

Abstract. For dielectric elastomers (DEs) to be fully implementable in commercial products a leap in material technology is required, and in particular the lifetime of elastomer materials needs further investigation. In addition, different application areas require different material properties, and elastomers are usually utilised in various configurations. Actuator elastomer materials, for example, need to be soft and stretchable while possessing high dielectric permittivity for enhanced actuation responses at a given voltage. Soft silicone elastomers can be obtained through the use of silicone oils, while enhanced permittivity can be obtained through the use of dipolar groups on the polymer backbone. Such elastomers were prepared by adding soft fillers to a strong and relatively stiff elastomer, LR3043/50, with fillers consisting of a choice of cross-linkable chloropropyl-functional copolymers, chloropropyl-functional silicone oil or PDMS-based silicone oil. The long-term stability of the materials was tested by straining the elastomers 60% statically for up to three months. The properties typically characterising DEs, namely Young's modulus, maximum strain and dielectric breakdown strength, were thereafter measured, and the results showed that soft fillers significantly influence the long-term stability of silicone elastomers, with breakdown strength being the most influenced. Especially high concentrations of mobile silicone oils should be avoided if long-term mechanically stable DEs are desired, as they fail mechanically and thus will not stand a chance in electromechanical testing.

1. Introduction

Dielectric elastomers (DEs), which consist of thin elastomer films sandwiched between compliant electrodes, constitute a promising area of soft transducers.[1] What sets DEs apart from other transducer technologies is their flexibility and ability to produce high extensions. For the full implementation of DEs into commercial products, however, a significant leap in material technology is still required. In particular, the lifetime of elastomer materials needs further investigation, understanding and optimisation, and there is also a great need for a holistic view on elastomer properties – as discussed in a current review on dielectric elastomer materials.[2]

Principally, the focus needs to be aimed at different applications for which different material requirements exist. For sensors, for instance, many different elastomers can be used without a problem, which is why sensors have found more widespread commercial use up to this point. Conversely, for actuators, soft and very extensible elastomers are needed, whereas for generators stiffer and more durable elastomers are required. Therefore, attention should focus on elastomer material. In particular, improving the properties of elastomers could lead to better DE performance by, for instance, reducing driving voltage, which is now typically in the lower kV range. Scientifically, this has been achieved through increases in the elastomer's dielectric permittivity (ε'), since the Maxwell stress is proportional to permittivity. Furthermore, elastomers with high dielectric breakdown strength (E_B) are required, so that the DE does not fail prematurely. Increasing the breakdown strength of DEs has proven a difficult challenge and is usually only achieved through an increase in the Young's modulus (Y).[3] This, however, significantly decreases obtainable actuation strain and might therefore only be an option for DE

generators. In Table 1 the material requirements for the three main DE application types are shown. These requirements were stated by the company Danfoss Polypower as targets for their materials to be commercially viable in different applications. The figure of merit, F_{om}, is a universal expression which can be used to compare and evaluate different DE materials (at a constant potential).[4] In Table 1, figures of merit for the requirements have been calculated relative to a commercial benchmark silicone elastomer, namely Elastosil RT625, the properties of which are regarded as follows: $\varepsilon' = 3$, $Y = 1$ MPa and $E_B = 80$ V/µm.[5] Additionally – not explicit from the figure of merit – elastomers should possess maximum elongations above 200% in order to be processable and survive large degrees of straining.

Table 1. Minimum requirements for realising the potential of dielectric elastomers, as stated by Danfoss PolyPower.

Type of transducer	Y [MPa]	ε'	E_B [V/µm]	$F_{om} = (\varepsilon'/Y*E_B^2)_{norm}$ with respect to Elastosil RT 625
Sensor	~1	3	~50	1
Actuator	<1	10	100	13
Generator	~2 (1-10 MPa)	10	100	7

It can be seen from Table 1 that elastomer material requirements for sensors are easily achieved through the use of commercial silicone elastomers, such as Elastosil RT625, as well as most other commercially available silicone elastomers. On the other hand commercial elastomers do not meet material specifications for actuators and generators. Therefore, there is a need for specifically designed elastomers, in order to meet the requirements of these two types of applications. Designing such elastomers, however, is not an easy task. The combination of a high dielectric permittivity of $\varepsilon' = 10$ and a high breakdown strength of $E_B = 100$ V/µm have proven a difficult challenge, since increases in permittivity have often led to decreases in breakdown strength.[2] A breakdown strength of 80 V/µm, however, may be acceptable for many applications.[2] Furthermore, in order to be commercially viable, DEs should be able to actuate a minimum of 10 million cycles and thereby have a long lifetime. This means that reliable products based on DEs, and thereby also the DE, need to be stable over a long period of time. Additionally, for reliability the DE must be able to maintain important properties over time so that products will not have to be calibrated frequently due to changes, for example, in the Young's modulus – and thus variations in actuation at a given voltage.

Several strategies have been pursued in order to create new elastomers for DE actuators and generators. Soft and high dielectric permittivity DE actuator materials, for example, were prepared through the chemical modification of elastomer by Kussmaul et al.[6], who added the synthesised dipolar molecule *N*-allyl-*N*-methyl-*p*-nitroaniline, together with compensating amounts of a hydride-functional cross-linker, to a silicone matrix. Soft silicone elastomers with high permittivity were also prepared by Racles et al.[7–9], who used cyanopropyl-functional silicones to raise dielectric permittivity, while Madsen et al. used nitrobenzene- and azonitrobenzene-functional cross-linkers[10] and copolymers[11]. Soft elastomers have also been prepared by making advanced network structures, such as through the use of random or heterogeneous bimodal networks[12] or through the preparation of interpenetrating polymer networks (IPNs)[13–17]. Also, very recently, Goff et al.[18] presented work on a

hetero-bifunctional chain extender which, when condensed, led to infinitely long silicone chains. This ultimately created a material with superior elasticity and without the waxy consistency of traditional high-molecular weight silicones. Finally, softened DEs have been prepared through the use of permittivity-enhancing blends, where polymers such as poly(3-hexylthiophene)[19], polyethylene glycol[20], a cyanopropyl-functional copolymer[21] and chloropropyl-functional silicone oil[22] have been used.

Silicone materials for DE generators may in general be stiffer and less extensible, and so elastomers with rigid permittivity-enhancing fillers such as TiO_2 can be excellent candidates[23,24]. Composite materials with high stiffness and moderately high permittivity furthermore include elastomers with expanded graphite[25], Ag/SiO_2 core shell particles[26,27] and encapsulated polyaniline particles.[28] Other materials that have proven ideal for generator applications include interpenetrating ionic networks that have shown predicted high performance at low frequencies.[17]

For both actuators and generators a full characterisation of elastomer material is required. Several studies have focused on the dielectric breakdown performance of DEs in relation to the Young's modulus,[3] applied pre-strain[29–32] and elastomer thickness.[30,32] Electrical breakdown strength can be analysed statistically through a Weibull distribution analysis, from which the probability of breakdown can be determined. The Weibull cumulative distribution function ($F(E_B)$) is:

$$F(E_B) = 1 - exp\left(-\frac{E_B}{\eta}\right)^{\beta} \quad (1)$$

where E_B is the measured dielectric breakdown strength, β is the Weibull shape parameter and η is the Weibull scale parameter.

Another DE failure mode is electromechanical instability (EMI), or pull-in instability, which might be the most prevalent failure mode for soft dielectrics such as elastomers.[33] The stress-strain behaviour of an elastomer greatly influences EMI and elastomer must therefore possess strain-hardening behaviour in order to be able to suppress EMI.[34] Investigation of the stress-strain behaviour of elastomers over time is therefore imperative, since some elastomers (e.g. highly filled elastomers) may change characteristics and become strain-softening over time, due to the Mullins effect.[35–37]

In a previous study by Zakaria et al.[37], we investigated the breakdown strength and stress-strain behaviour of commercial filled silicones and composites with hard fillers upon strain-induced ageing. Functional silicones have been another common means of increasing dielectric permittivity, and therefore, in this study, we investigate ageing effects after static straining of functional silicone elastomers. The studied elastomers consist of a strong and relatively stiff commercial elastomer, LR4043/50, ideal for generator applications, which is filled with either functional silicone oil, regular polydimethylsiloxane (PDMS)-based silicone oil or functional co-cross-linkable silicone copolymers, in order to expand the application area of the high dielectric breakdown strength elastomer LR3043/50 to actuator applications. These silicone elastomer modifications may lead to dramatically altered properties over time, and we therefore investigate stress-strain behaviour and dielectric breakdown strength after static straining for different timespans, in order to elucidate the effect on failure modes of the soft additives.

2. Experimental

2.1 Materials and sample preparation

Silicone oil, DMS-T22 ($\bar{M}_w \approx$ 9,430 g mol^{-1}) and LMS-152 ($\bar{M}_w \approx$ 9,000 g mol^{-1}, with chloropropyl-functional groups), and a hydride-functional cross-linker, HMS301 (8-functional (8f), M_w = 1950 g/mol), were acquired from Gelest Inc. Elastosil® LR3043/50 (Wacker Chemie AG) is a two-component silicone comprising a component A and a component B mixed in a 1:1 ratio. Inhibitor Pt88 and the solvent Belsil were also acquired from Wacker Chemie AG. The platinum cyclovinylmethyl siloxane complex catalyst (511) was purchased from Hanse Chemie, while silicon dioxide amorphous hexamethyldisilazane-treated particles (SIS6962.0) were purchased from Fluorochem. Co-1 and Co-2 were synthesised according to previously described procedures.[11] Two types of allyl-terminated chloropropyl-functional copolymers of around 26,000-29,000 g mol^{-1} were prepared: one copolymer contained chloropropyl groups, with 1200 g mol^{-1} dimethylsiloxane spacer units between each group (Co-1), and the other copolymer contained chloropropyl groups, with 580 g mol^{-1} dimethylsiloxane spacers between the functional groups (Co-2). Co-2 thus contains approximately double the amount of chloropropyl groups than Co-1.

2.1.1 General procedure: films with Co-1 or Co-2

Co-1 or Co-2 and an 8-functional cross-linker were mixed with treated silica particles (25 wt%) and an inhibitor (1 wt%, Pt88) and then treated on a FlackTek Inc. DAC 150.1 FVZ-K SpeedMixer™. The platinum catalyst (1.5 ppm) was added thereafter, and the mixture was then speed-mixed once more. The mixture was coated as 150 µm films on a glass substrate and cured at 80°C for 2 hours.

2.1.2 General procedure: elastomer synthesis with soft fillers

An appropriate amount of Co-1, Co-2 or silicone oils was mixed with the first component (A) of the commercial silicone Elastosil® LR3043/50 and solvent (Belsil), as indicated in Table 2, using a SpeedMixer. The second elastomer component (B) and inhibitor were then added, and the mixture was speed-mixed once more. The mixture was then coated as thin films, using a doctor blade of 150 µm thickness on a glass substrate, and then cured at 115°C for 1 hour. The different sample composition quantities can be found in Table 2.

Table 2. Compositions and quantities of the samples prepared with the soft filler.

No	Composition	SiO_2 (g)	Co-1 (2f, M_w=26000 g mol^{-1}) (g)	Co-2 (2f, M_w= 29000 g mol^{-1}) (g)	HMS301 (8f, M_w=1950 g mol^{-1}) (g) r=2	Inhibitor (0.5%) (g)	LR3043/50A (g)	LR3043/50B (g)	Belsil solvent (g)	LMS-152 (chloro-oil) (g)	DMS-T22 (silicone-oil) (g)
#1	LR3043/50	-	-	-	-	-	5	5	5	-	-
#2	Co-1 pure + 25 wt% SiO_2	3	8.6747	-	0.3253	0.045	-	-	-	-	-
#3	Co-2 pure + 25 wt% SiO_2	3	-	8.7073	0.2927	0.045	-	-	-	-	-
#4	LR3043/50 + 30 phr Co-1	-	2.8916	-	0.1084	0.015	5	5	3	-	-
#5	LR3043/50 + 30 phr Co-2	-	-	2.9024	0.0976	0.015	5	5	3	-	-
#6	LR3043/50 + 100 phr Co-1	-	5.7832	-	0.2168	0.030	3	3	-	-	-
#7	LR3043/50 + 100 phr Co-2	-	-	5.8048	0.1952	0.030	3	3	-	-	-
#8	LR3043/50 + 30 phr LMS-152 (chloro-oil)	-	-	-	-	-	5	5	3	3	-
#8	LR3043/50 + 100 phr LMS-152 (chloro-oil)	-	-	-	-	-	5	5	-	10	-
#10	LR3043/50 + 30 phr DMS-T22 (silicone-oil)	-	-	-	-	-	5	5	3	-	3
#11	LR3043/50 + 100 phr DMS-T22 (silicone-oil)	-	-	-	-	-	5	5	-	-	10

phr = parts per hundred rubber

2.2 Strain-ageing of samples

The samples were strained on an in-house-built frame. The films were 130 mm in width and 350 mm in length. In order to strain the films successfully, both ends of the films were rolled with metal rods to prevent slippage of the stretched films, which were stretched to 60%. The metal rods, together with the stretched films, were then attached to the frame. The films were covered by ETFE foils (50 μm thickness) to prevent contamination. Finally, the stretched films were stored for one month and three months, before they were released for further characterisations.

2.3 Instrumentation

2.3.1 Breakdown measurement

Electrical breakdown measurements were performed on an in-house-built device based on international standards (IEC 60243-1 (1998) and IEC 60243-2 (2001)). The initial thicknesses of the films before straining were determined with a Leica DMLB microscope with a USB Thorlabs 2.0 digital camera, and with multiple determinations along the cross-section. The thickness of the stretched film (which can be seen in the supporting information) was calculated as $t_1 = \frac{t_0}{\lambda}$, where t_0 is the initial thickness and λ is the stretch ratio. The distance between the two spherical electrodes (ø = 20 mm) was set, according to sample thickness, with a micrometre stage and gauge. An indent of less than 3% of sample thickness was added to ensure that the spheres were in contact with the sample. A step-wise increasing voltage was applied (50-100 V/step) at a rate of 0.5-1.0 step/s. Each sample was subjected to eight breakdown measurements, and an average of the values was indicated as the breakdown strength of the sample. Data were then fitted to Weibull distribution and plotted.

2.3.2 Young's modulus and tensile strength measurements

Uniaxial extensional rheology was performed on the series of elastomer films in order to determine the Young's modulus and tensile strength, as described by Zhang et al.[38] The stress–strain curves of films were tested at RT by ARESG2 rheometer using SER2 geometry. The sample of 20 mm length and 6 mm width was placed between two drums and initially separated by a distance of 12.7 mm. The test specimen was elongated uniaxially at steady Hencky strain rate of 0.01 (s^{-1}) until sample failure at the middle part. Each composition was subjected to four tensile measurements which were then averaged. Young's moduli were obtained from the tangent of the stress-strain curves at 5% strain.

3. Results and discussion

3.1 Properties of different elastomer compositions, before the ageing experiments

The investigated formulations are based on a strong and well-performing[23] silicone elastomer with high breakdown strength, namely LR3043/50 from Wacker Chemie. Due to its strong and relatively stiff nature this pristine elastomer is suitable for generator applications. In order to broaden its scope, and also to make it applicable for actuator purposes, it can be softened through a range of different approaches. Since it is also desired to increase dielectric permittivity, functional silicone oils can be used as an alternative to hard fillers such as TiO_2, which has previously been shown to introduce ageing effects in silicone elastomers[37]. Functional silicone oils will soften elastomer while at the same time increasing permittivity, and thereby actuator performance will be increased significantly through a synergistic effect.[22] Such additives, however, may induce significant ageing effects due to phase separation and/or migration of the free species. As an

alternative to oil, similar softening (functional) copolymers can also be added to the commercial LSR elastomer and reacted into the elastomer structure.[39] This may provide a more stable system over time, since the softening comes from the lubrication effect of chloropropyl groups rather than the solvent effect of oil. Thus, samples with different concentrations of plain silicone oil (PDMS-based), functional silicone oil (chloropropyl-functional) or functional copolymers (with either low or high concentrations of chloropropyl groups, denoted as Co-1 and Co-2, respectively) were prepared. The different sample compositions are shown in Table 2, whilst their properties before any ageing experiments are shown in Table 3.

Table 3. Initial properties of samples with oils and copolymers.

No	Composition	Breakdown strength [V/µm]	Y @ 5% strain [MPa]	Tensile strength [MPa]	Strain @ break [%]	ε'	F_{om_ref} / F_{om}
#1	LR3043/50	181±6	2.41	5.23	717	2.7	1.0
#2	Co-1 pure + 25 wt% SiO_2	66±4	0.15	0.65	429	4.7	4.2
#3	Co-2 pure + 25wt% SiO_2	69±5	0.52	1.27	314	5.1	1.4
#4	LR3043/50 + 30 phr Co-1	122±14	1.90	6.51	596	3.1	0.8
#5	LR3043/50 + 30 phr Co-2	113±9	2.00	5.06	314	3.5	0.7
#6	LR3043/50 + 100 phr Co-1	83±5	1.09	1.06	254	3.3	0.6
#7	LR3043/50 + 100 phr Co-2	89±7	1.29	3.71	256	3.6	0.7
#8	LR3043/50 + 30 phr LMS-152 (chloro-oil)	120±10	1.73	3.34	481	4.4	1.1
#9	LR3043/50 + 100 phr LMS-152 (chloro-oil)	62±8	0.60	0.78	269	5.6	1.1
#10	LR3043/50 + 30 phr DMS-T22 (silicone-oil)	98±6	0.87	4.43	658	2.9	1.0
#11	LR3043/50 + 100 phr DMS-T22 (silicone-oil)	61±2	0.27	1.51	493	3.0	1.3

As seen in Table 3, the addition of copolymers and silicone oils significantly softens the otherwise stiff LR3043/50 (Young's moduli calculated at 5% strain are all considerably lower for samples with additives), due to the softening effect of the additives and the dilution of the heavily filled LR elastomer. Furthermore, all samples with additives have lower strains at breaking than the pure commercial elastomer – as anticipated –, since cross-linking density has been decreased and thus the stress that the elastically active chains can uphold is reduced. All samples, however, have strains at breaking higher than 200%, which is an important requirement for DEs.

Figure **1** shows stress-strain curves for samples with copolymers which are covalently bonded to the networks, i.e. in theory there are no free species present in the networks.

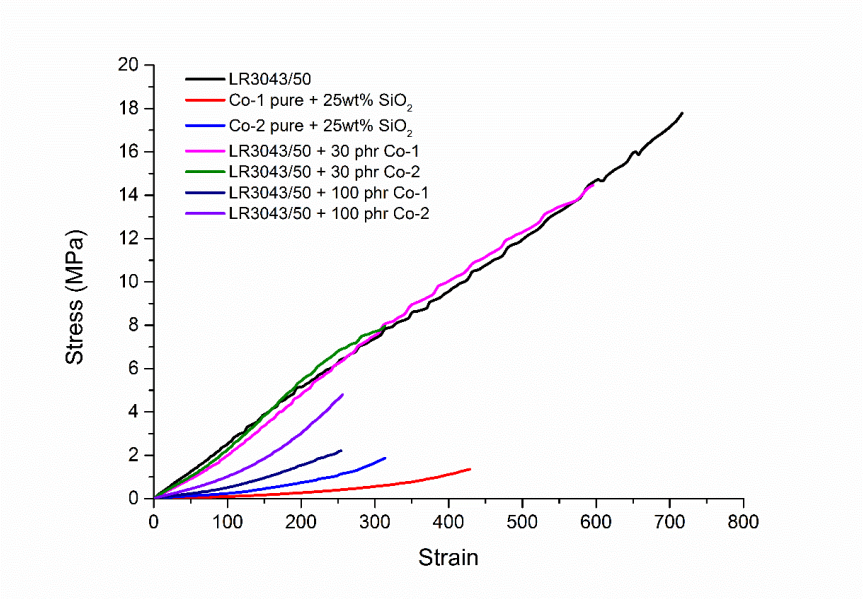

Figure 1. Stress-strain curves for samples with copolymers.

From Figure 1 it can be seen that the addition of copolymers to LR3043/50 enables promising generator materials, since 30 phr samples show similar stress-strain responses as pure LR3043/50. The ultimate properties (strain at break), however, are somewhat reduced. It is clear, though, that optimum copolymer loading exists, since the 100 phr samples show significantly reduced mechanical properties (both in terms of stress and strain at breaking). Elastomers based on pure copolymers are soft and quite stretchable, and therefore they are applicable as actuator materials. All samples with copolymers are seen to be strain-hardening, which is a much desired DE property, since this behaviour can suppress electromechanical instability (EMI).[33]

Stress-strain curves for samples containing chloropropyl- and PDMS-based silicone oils are shown in Figure 2.

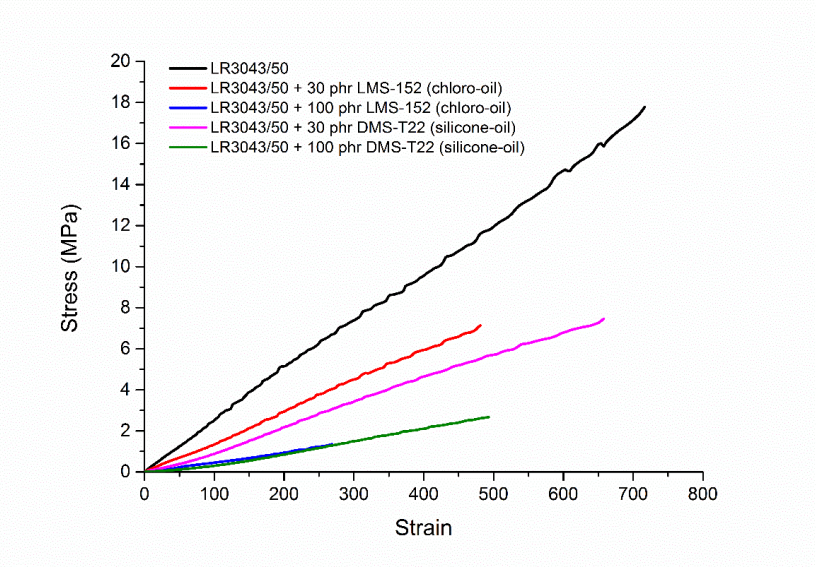

Figure 2. Stress-strain curves for samples prepared with chloropropyl-functional and PDMS-based silicone oils.

As seen in Figure 2, both types of silicone oils soften the networks, as expected. At 30 phr the elastomers maintain suitable properties for generator applications, while at 100 phr they are softened to an extent where they would be more suitable as actuator materials. Elastomers with oils do not experience significantly favourable strain-hardening, but on the other hand they do not strain-soften when approaching ultimate properties, and thus their mechanical properties remain favourable after the addition of oils. Tensile strength decreases in line with increasing oil content, and so the 100 phr samples have low tensile strengths (stress at breaking). Chloropropyl-functional oils induce a lower tensile strength than PDMS-based silicone oil, probably due to slightly lower compatibility between LMS-152 (chloro-oil) and LR3043/50 than the PDMS-based silicone oil has with LR3043/50. Samples with the lowest tensile strength are also seen to have the lowest dielectric breakdown strengths (Table 3).

Pure elastomer LR3043/50 has a very high dielectric breakdown strength of 181 V/μm, while elastomers based on pure copolymer (Co-1 or Co-2) have moderate breakdown strengths, due to their softer nature and significantly lower filler content than LR3043/50. Adding silicone oils and copolymers to LR3043/50 decreases the breakdown strength of LR3043/50 significantly, and breakdown decreases in line with increasing content. Breakdown strength is seen to depend strongly on the Young's modulus of the samples, with the softest samples having the lowest breakdown strengths. This is in agreement with previously described results[3,23,40], where breakdown strength was found to scale linearly – or even exponentially – with the Young's modulus.

The dielectric permittivity of pure LR3043/30 is ε' = 2.7 at 100 Hz, while elastomers based on pure chloropropyl-functional copolymer Co-1 and Co-2 have dielectric permittivities of ε' = 4.7 and 5.1, respectively. The addition of chloropropyl-functional copolymers and oils increases the permittivity of LR3043/50 significantly, up to ε' = 5.6 for sample 9, which contains 100 phr chloro-oil. Chloropropyl-functional silicone oil increases permittivity to a greater extent than copolymers achieve, which may be due to

a higher concentration of chloropropyl groups and greater flexibility of polymer chains which are not covalently bonded to the network, thus leading to greater flexibility and polarisability. The addition of PDMS-based silicone oil does not, as expected, increase the permittivity of LR3043/50, and the result lies within the experimentally expected variance.

A direct comparison, for example based only on dielectric permittivity, of the elastomers' performance with different compositions is difficult. Therefore, Sommer-Larsen and Larsen[4] defined a universal expression which, through a single parameter, namely the *figure of merit*, F_{om}, can be used to evaluate the performance of different DE materials. The figure of merit depends on the dielectric permittivity, dielectric breakdown strength (E_B) and Young's modulus according to:

$$F_{\mathrm{om}} = \frac{3\varepsilon_r {E_B}^2}{\mathrm{Y}} \qquad (2)$$

In Table 3, figures of merit for the different compositions are shown relative to the figure of merit for the reference elastomer LR3043/50. Elastomers based on the pure copolymers Co-1 and Co-2 are seen to have the highest increases in the figure of merit compared to LR3043/50. This is due to their high dielectric permittivity combined with their very soft nature, which in this case contributes significantly more than the moderate dielectric breakdown strength values. The addition of a chloropropyl-functional copolymer to LR3043/50, however, does not increase the figure of merit, even though dielectric permittivity increases while the Young's modulus decreases. This means that the breakdown strength reduction is greater than the permittivity and moduli contributions. The addition of chloropropyl-functional silicone oil increases the figure of merit and thereby DE performance by 10%. A larger concentration of oil (100 phr), interestingly, does not increase performance more than the lower concentration (30 phr), because the 100 phr sample has significantly lower dielectric breakdown strength. PDMS-based silicone oil increases the figure of merit by 10 and 30%, respectively, for concentrations of 30 and 100 phr, respectively. In this case 100 phr oil increases F_{om} more than the lower concentration, due to the significant softening effect of PDMS-based silicone oil. It can therefore be deduced that PDMS-based silicone oil softens the elastomer to a greater extent than the chloropropyl-functional silicone oil, without compromising dielectric breakdown strength as much, due to greater compatibility.

3.2 Properties after ageing experiments: mechanical properties

Ageing experiments were carried out on an in-house-built frame, where 150 μm thin samples remained stretched to 60% for one to two months, before they were released from the frames for characterisation. It has previously been shown that dielectric permittivity does not change drastically over time during such strain ageing experiments.[37] In Figure 3 strains at breaking, before and after the ageing experiments, are shown. The results are summarised further in Table 5. The strain at breaking for the pure commercial elastomer LR3043/50 (sample 1) is seen to decrease after ageing, although this phenomenon is not seen for all samples; sample 6 (LR3043/50 + 100 phr Co-1), for example, experiences a significant increase in strain at breaking, from 269% to 661%. Samples 7 (LR3043/50 + 100 phr Co-2) and 9 (LR3043/50 + 100 phr chloro-oil) also exhibit this behaviour, perhaps due to the reduction of cross-linking density while maintaining significant cross-linked polymer chain strength (i.e. the chloropropyl-functional polymer chains may uphold stress while their mobility is strongly decreased).

Most importantly, however, all investigated compositions fulfilled the requirements of more than 200% strain at any given time during the ageing experiments. This property is important in relation to a product's reliability

and its lifetime, in order to make sure that DE products do not experience mechanical failure as a first failure mode.

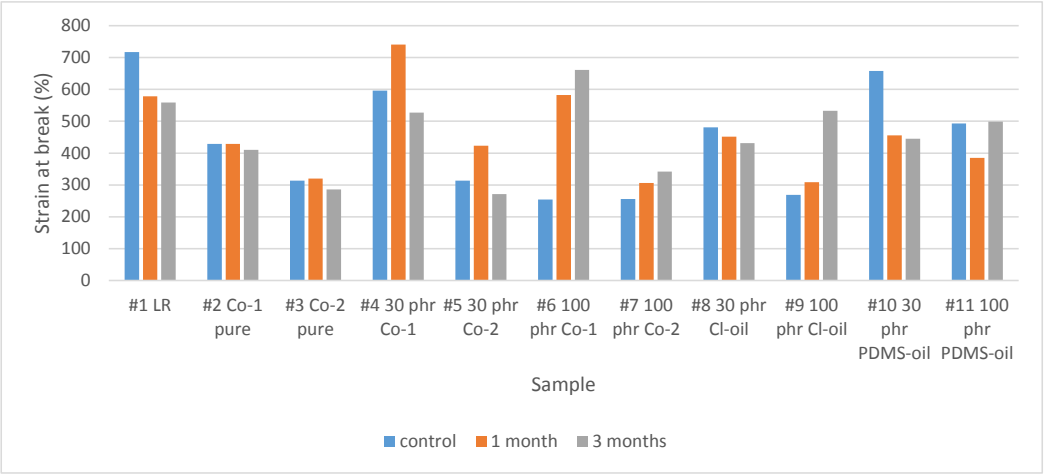

Figure 3. Strain at breaking before and after ageing for one and three months.

Tensile strengths, before and after ageing, for one and three months are shown in Figure 4, and the results are summarised further in Table 5.

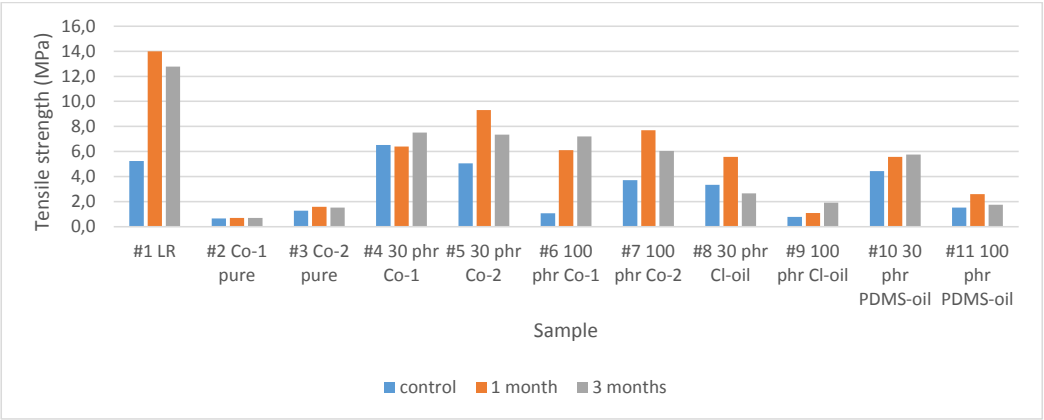

Figure 4. Tensile strengths from the ageing experiments.

There is no clear pattern between tensile strength and ageing, although most samples seem to experience increased tensile strength after one month of strain ageing, after which tensile strength decreases at further ageing for three months. This may be due to two phenomena occurring simultaneously. The first phenomenon is most likely small siloxanes and residual solvent leaving the elastomers[41]. This has previously been shown to significantly increase the Young's modulus and tensile strength of stretched elastomers.[37] When the surface of an elastomer is broken upon straining, small molecules, consisting mainly of cyclic siloxanes, which are bi-products from the initial polymer synthesis, and residual solvent are able to diffuse out of the elastomer.

The migration and evaporation of volatiles significantly hardens the elastomers, which can also be seen in Figure 5, where Young's moduli as a function of the strain timeframe are shown. The phenomenon is particularly evident for sample 1 (pure commercial elastomers LR3043/50), sample 5 (LR3043/50 + 30 phr Co-2), sample 6 (LR3043/50 + 100 phr Co-1), sample 7 (LR3043/50 + 100 phr Co-2) and sample 8 (LR3043/50 + 30 phr chloro-oil), all of which show significant increases in tensile strength and Young's moduli after one month of straining. After three months, tensile strength as well as Young's moduli dropped for most of the samples that showed increased values after one month. This is due to ageing effects, whereby properties deteriorate after long-term straining. Sample 6 (LR3043/50 + 100 phr Co-1), however, does not show any ageing effects after three months, and all samples with oils show a decreased Young's modulus after three months of strain. It is clear that samples containing oils exhibit similar behaviours, namely initial stiffening, due to the evaporation of small molecules, followed by ageing, which deteriorates mechanical properties. Most samples with copolymers also follow this trend, albeit not to the same extent.

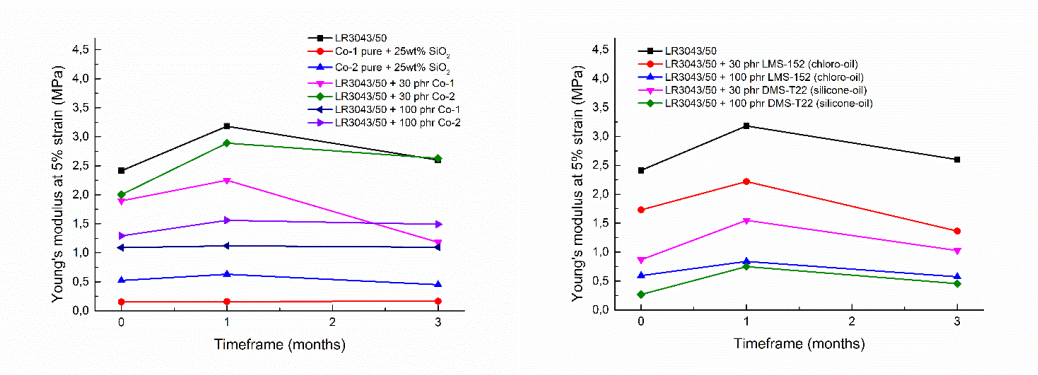

Figure 5. Young's modulus at 5% strain after ageing for one and three months for left: Samples with copolymers and right: samples with oils.

Furthermore, the effect of oil concentration on mechanical properties upon ageing can be seen in Figure 6, where stress-strain curves for pure LR3043/50 and LR3043/50 containing 30 and 100 phr oil are shown. Overall, the commercial elastomer LR3043/50 maintains its mechanical properties. After one month of ageing, hardening is seen in the fact that the volatiles, which act as plasticisers, have left the elastomer and the ultimate strain has reduced. After three months, there is no further significant ageing beyond what happened at one month. It is clear that sample 11, which contains 100 phr PDMS-based silicone oil, behaves differently upon ageing than pure LR3043/50 and the low-oil concentration (30 phr) sample. The high concentration sample clearly ages more than the low concentration sample, where only minor differences in stress-strain behaviour are observed compared to the reference sample LR3043/50. The 30 phr sample, however, slightly hardens continuously throughout the three months, though the maximum extension of >650% is lost within the first month. The chloropropyl-functional oil-containing samples behave somewhat differently to the PDMS-based silicone oil-containing samples. Contrary to its PDMS-based silicone oil counterpart, the 10 phr chloropropyl-functional silicone softens after ageing, and a degree of extension is lost. The 100 phr chloropropyl-functional oil sample behaves differently to all of the other oil samples after three months of ageing. As the only sample, both its tensile strength and maximum strain increase after ageing. Chloropropyl-functional and PDMS-based silicone oil thus behave differently in the silicone matrix upon long-term straining, which might be due to the chloropropyl-functional silicone oil not having the same affinity for reinforcing silica particles in the elastomer

as the PDMS-based silicone oil does. Therefore, silica particles in the chloropropyl-functional oil-containing samples are not affected by silicone oil and are plasticised to the same extent as the PDMS-based oil samples. Thus, silica particles are able to reinforce the network even better after age straining, since the chloropropyl-functional oil has had time to diffuse away from the silica particles (and probably phase-separate, to some extent) during the ageing experiment. Overall, it is clear that oil content plays a role in the ageing of silicone elastomers, and it is evident that high concentrations of silicone oils should be avoided for DEs with a desired long lifetime, due to significantly reduced mechanical properties and the tendency toward strain-softening behaviour over time – as observed most obviously for the 100 phr chloropropyl-functional silicone oil sample.

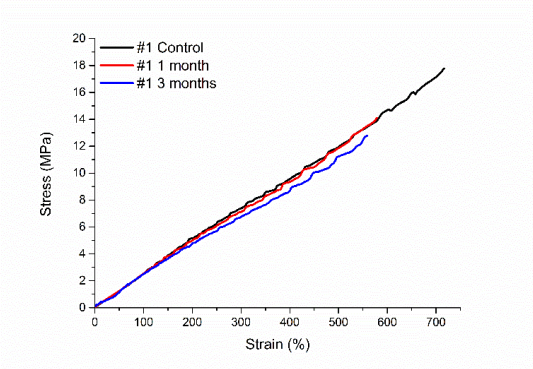

Stress-strain curve for #1, LR3043/50

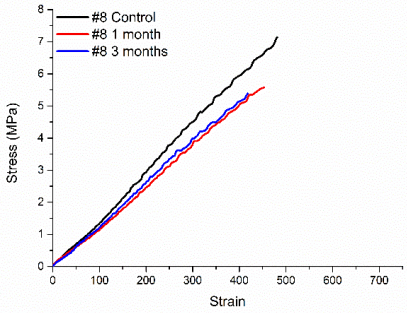

Stress-strain curve for #8, LR3043/50+ 30 phr chloropropyl-functional silicone oil

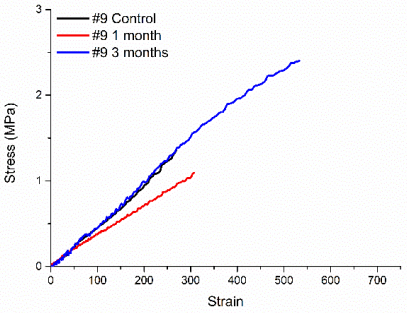

Stress-strain curve for #9 LR3043/50+ 100 phr chloropropyl-functional silicone oil

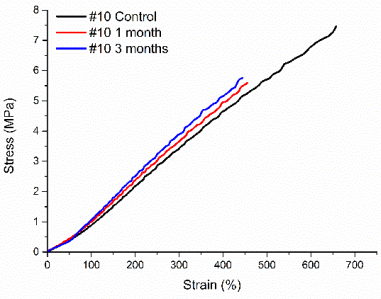

Stress-strain curve for #10 LR3043/50+ 30 phr PDMS-based silicone oil

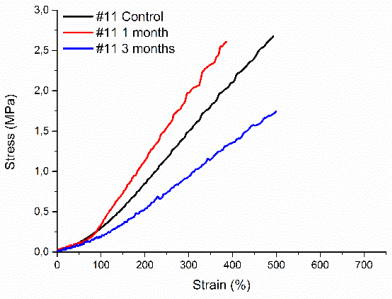

Stress-strain curve for #11 LR3043/50+ 100 phr PDMS-based silicone oil

Figure 6. Stress strain curves, before and after ageing of samples with oils.

For samples containing copolymers, the trend in stress-strain-related ageing is not so obvious (all results can be found in the supporting information), since elastomers based on pure Co-1 or Co-2 do not age significantly upon straining for one or three months. This may be due to these samples' inherent softness and lower filler content. LR3043/50 samples with copolymers all age to some extent, whereby some age strongly and others

only slightly. One of the samples with the most interesting behaviour is sample 4 (LR3043/50 + 30 phr Co-1), which fails completely after ageing (both one and three months), as seen in Figure 7, since it starts to show strain-softening behaviour and significantly reduced tensile strength.

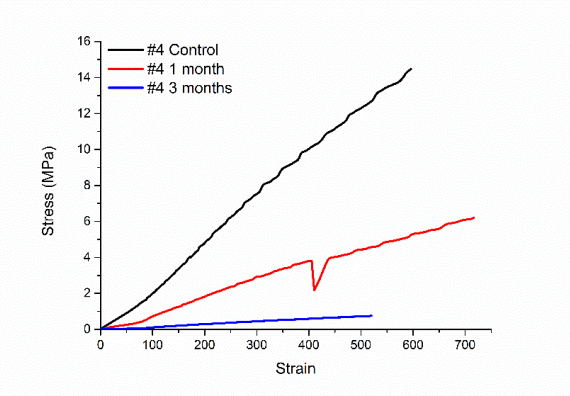

Figure 7. Stress-strain curves, before and after ageing, for sample #4 ((LR3043/50 + 30 phr Co-1).

Sample 6, which contains 100 phr Co-1, also dramatically changes properties over time, albeit in a positive way this time, since its tensile strength and maximum strain increase significantly. This may again be due to the chloropropyl-functional nature, which acts in a similar way to the 100 phr chloropropyl-functional silicone oil sample. Sample 7, which contains 100 phr Co-2, also gains in both tensile strength and maximum strain after ageing, but it loses its strain-hardening behaviour after three months of ageing, and its Young's modulus is constant up to its breaking point at a strain of approximately 325%.

3.3 Properties after ageing experiments: breakdown properties

Since the mechanical properties of samples containing copolymers and oils were all affected in one way or another by the strain-ageing experiments, it is also expected that the dielectric breakdown strength of the samples will be affected. The average dielectric breakdown strength from eight breakdown tests on each sample is shown in Figure 8 and summarised further in Table 5.

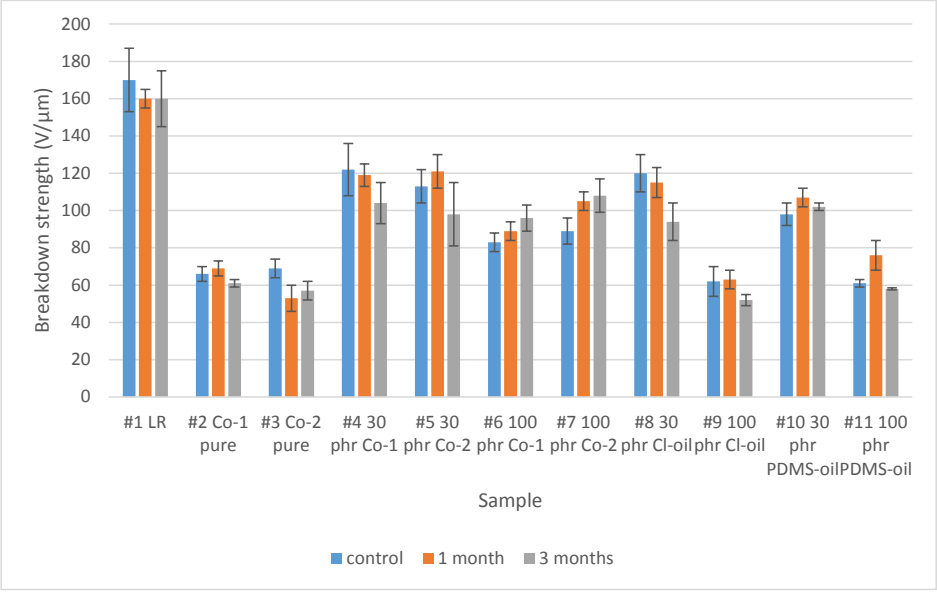

Figure 8. Dielectric breakdown strengths, before and after the ageing experiments.

Within the bounds of experimental uncertainty, all samples roughly maintain their breakdown strength after ageing. There is, however, a trend for decreasing breakdown strengths after three months of ageing, expect for samples 6 (100 phr Co-1) and 7 (100 phr Co-2). These decreasing and increasing trends closely follow the detected changes in Young's moduli upon ageing.

In order to investigate the effect of ageing experiments on breakdown distribution, Weibull analyses were performed. Weibull is one of the most used methods for lifetime analysis and can furthermore provide information about the homogeneity and electrical reliability of an elastomer.

The Weibull distribution function from Equation 1 can be linearised to give:

$$ln[-ln(1 - F(E_B))] = \beta \cdot \ln(E_B) - \beta \cdot \ln(\eta) \qquad (3)$$

The shape parameter, β, is then equal to the slope of the regressed line. It is desirable to have as large a β-value as possible, since this means that the breakdown values fall within a narrow range of voltages. A high β-value also gives an indication about homogeneity at the microscale, as the breakdown strength measurement is very sensitive to imperfections. η should also be as high as possible and is determined from the distribution at which 63% of the samples have broken down. The Weibull distribution results with β, η and a linear regression value (r^2) are shown in

Table ***4***, whereas the Weibull probability plots from which the parameters have been determined can be found in the supporting information. The probability plot for LR3043/50 after three months of ageing shows two distributions, whereas the control sample and the sample after one month of ageing only show one distribution. This indicates that three months of ageing destroys locally the properties of the LR3043/50 network and reduces local breakdown strength. Many of the samples containing chloropropyl functionality show peculiar breakdown behaviour in the Weibull probability plots, with two clearly separated distributions signifying two breakdown processes. As an example of this behaviour, the Weibull plot for sample 5 (LR3043/50 + 30 phr Co-2), after one month of ageing, is shown in Figure 9. This indicates that breakdown in these samples occurs specifically as a result of the presence of the chloropropyl groups and less because of actual defects. Chloropropyl groups may act as local 'defects' in the samples, perhaps owing to the agglomeration of the polar chloropropyl groups.

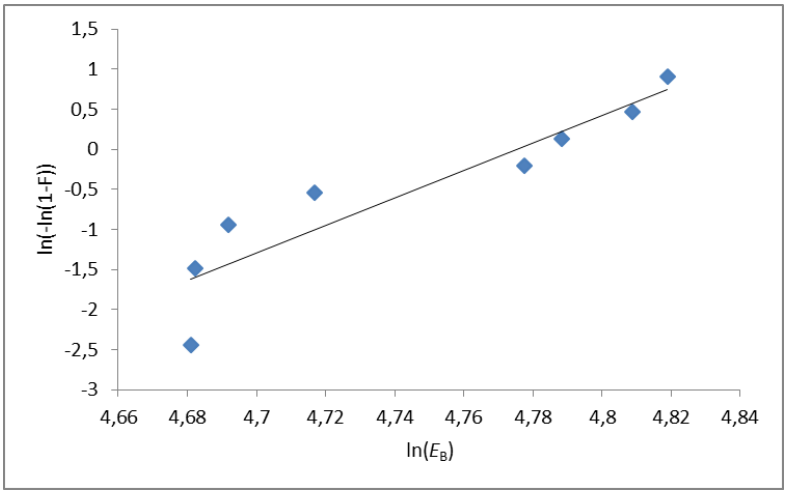

Figure 9. Weibull probability plot for #5 LR3043/50 + 30 phr Co-2 after one month of ageing.

Table 4. Weibull parameters and r^2, before and after the ageing experiments. Red numbers indicate decreasing values compared to the control, and green numbers indicate increasing values in this regard.

		Scale (η) (V/μm)			Shape (β)			r^2		
No	Composition	control	one month	three months	control	one month	three months	control	one month	three months
#1	LR3043/50	183	158	167	11	53	11	0.76	0.95	0.89
#2	Co-1 pure + 25 wt% SiO_2	68	66	62	20	14	41	0.95	0.87	0.66
#3	Co-2 pure + 25wt% SiO_2	71	56	59	16	9	12	0.79	0.84	0.91
#4	LR3043/50 + 30 phr Co-1	127	119	109	11	19	11	0.75	0.95	0.75
#5	LR3043/50 + 30 phr Co-2	117	118	106	15	20	6	0.76	0.85	0.95
#6	LR3043/50 + 100 phr Co-1	85	82	100	19	25	13	0.82	0.88	0.98
#7	LR3043/50 + 100 phr Co-2	92	104	112	15	41	13	0.81	0.86	0.89
#8	LR3043/50 + 30 phr LMS-152 (chloro-oil)	124	114	99	13	31	9	0.97	0.87	0.97
#9	LR3043/50 + 100 phr LMS-152 (chloro-oil)	65	61	53	8	26	23	0.88	0.88	0.82
#10	LR3043/50 + 30 phr DMS-T22 (silicone-oil)	101	108	103	16	63	51	0.97	0.91	0.92
#11	LR3043/50 + 100 phr DMS-T22 (silicone-oil)	62	73	58	26	27	123	0.97	0.63	0.78

The Weibull distribution parameters show that strain-ageing experiments affect the reliability of the tested samples negatively as the scale parameter for most samples decreases. On the other hand, it can be seen from the shape parameters that most samples benefit from one month of ageing, since this leads to increases in β. This is probably due to the aforementioned removal of volatiles, which leads to more homogenous elastomers and higher Young's moduli. After three months of ageing, only four samples maintain this positive effect of volatile removal, and true ageing effects have therefore set in. Furthermore, r^2, the linear regression goodness-of-fit value, decreases after three months of ageing for approximately half of the samples with no clear trend.

3.4 Properties after the ageing experiments: figure of merit

The figures of merit, normalised to the reference elastomer LR3043/50 before and after the ageing experiments, are shown in Table 5. It is evident that the predicted performance of most elastomers improves after one month of aging, since normalised figure of merit values increase due to the small siloxanes and or solvent that have evaporated away from the elastomers and have thus increased dielectric breakdown strength. After three months of ageing, samples with high concentrations of oils (sample 9 and 11) show decreased predicted performance as a result of true ageing effects. Again, high concentrations of free species in the elastomers are shown to decrease overall DE properties significantly over time. The other samples' figures of merit after three months do not seem to follow any specific trend.

Table 5. Summary of properties, before and after the ageing experiments. Red numbers indicate decreasing values compared to the control, and green numbers indicate increasing values in this regard.

No	Composition	Thickness (µm)			Breakdown (V/µm)			Y @ 5% strain (MPa)			Tensile strength (MPa)			Strain @ break (%)			Normalised figure of merit		
		control	one month	three months	control	one month	three months	control	one month	three months	control	one month	three months	control	one month	three months	control	one month	three months
#1	LR3043/50	49	52	52	181±6	160±5	160±15	2.41	3.18	2.60	5.23	14.0	12.8	717	578	559	1	1	1
#2	Co-1 pure + 25 wt% SiO_2	80	76	82	66±4	69±4	61±2	0.54	0.16	0.17	0.65	0.70	0.70	429	429	410	3.7	6.4	4.0
#3	Co-2 pure + 25wt% SiO_2	113	153	140	69±5	53±7	57±5	0.52	0.63	0.45	1.27	1.59	1.52	314	320	286	1.3	1.0	1.4
#4	LR3043/50 + 30 phr Co-1	75	83	80	122±14	119±6	104±11	1.90	2.25	1.18	6.51	6.40	7.50	596	741	527	0.7	0.9	1.1
#5	LR3043/50 + 30 phr Co-2	106	86	106	113±9	121±9	98±17	2.00	2.89	2.63	5.06	9.30	7.34	314	423	271	0.7	0.8	0.5
#6	LR3043/50 + 100 phr Co-1	80	77	73	83±5	89±5	96±7	1.09	1.12	1.10	1.06	6.10	7.19	254	582	661	0.6	1.1	1.0
#7	LR3043/50 + 100 phr Co-2	129	111	87	89±7	105±5	108±9	1.29	1.56	1.49	3.71	7.70	6.04	256	306	342	0.6	1.2	1.1
#8	LR3043/50 + 30 phr LMS-152 (chloro-oil)	78	77	82	120±10	115±8	94±10	1.73	2.22	1.36	3.34	5.57	2.65	481	452	431	1.0	1.2	1.1
#9	LR3043/50 + 100 phr LMS-152 (chloro-oil)	96	101	101	62±8	63±5	52±3	0.60	0.84	0.57	0.78	1.08	1.91	269	309	533	1.0	1.2	1.0
#10	LR3043/50 + 30 phr DMS-T22 (silicone-oil)	99	75	71	98±6	107±5	102±2	0.87	1.55	1.03	4.43	5.56	5.76	658	456	445	0.9	1.0	1.1
#11	LR3043/50 + 100 phr DMS-T22 (silicone-oil)	94	71	85	61±2	76±8	58±0.5	0.27	0.75	0.46	1.51	2.60	1.74	493	385	499	1.1	1.1	0.8

4. Conclusion

Soft silicone elastomers were prepared by using a strong commercial elastomer, LR3043/50, mixed with a choice of cross-linkable chloropropyl-functional copolymers, chloropropyl-functional silicone oil or PDMS-based silicone oil. Elastomer samples with different concentrations of soft fillers were subjected to static straining of 60% for up to three months, and characteristic dielectric elastomer properties, such as Young's modulus, strain at breaking and dielectric breakdown strength, were analysed before and after the strain ageing experiments. The results showed that adding soft functional fillers to the LR3043/50 elastomer influenced its properties after ageing. One month of strain seemed to benefit most compositions, since small volatiles were allowed to escape from the elastomers during straining. This phenomenon enhanced the Young's moduli, tensile strength and strain at breaking, as well as dielectric breakdown strength, for the majority of the samples. After three months of straining, true ageing effects were seen for most of the samples, although some samples, such as those containing chloropropyl groups, seemed to benefit from three months of strain treatment, with significantly increased Young's moduli, strain at breaking and breakdown strengths as a consequence. This might be due to the migration of chloropropyl groups away from silica particles which are then able to reinforce the elastomers significantly. High concentrations of oils, whether chloropropyl-functional or PDMS-based, should be avoided, since this induces significantly reduced breakdown strengths and mechanical stability, both before and after strain ageing.

5. Acknowledgements

The authors gratefully acknowledge the financial support of the Danish Council for Independent Research, Innovationsfonden Denmark and the Ministry of Education of Malaysia and Universiti Malaysia Pahang.

6. References

[1] Pelrine R, Kornbluh R, Pei Q and Joseph J 2000 High-speed electrically actuated elastomers with strain greater than 100% *Science* **287** 836–9

[2] Madsen F B, Daugaard A E, Hvilsted S and Skov A L 2015 The current state of silicone-based dielectric elastomer transducers *Macromol. Rapid Commun.* n.a.

[3] Kollosche M, Stoyanov H, Ragusch H, Risse S, Becker a. and Kofod G 2010 Electrical breakdown in soft elastomers: Stiffness dependence in un-pre-stretched elastomers *2010 10th IEEE Int. Conf. Solid Dielectr.* 1–4

[4] Sommer-Larsen P and Larsen A L 2004 Materials for dielectric elastomer actuators *Proc. SPIE* **5385** 68–77

[5] Vudayagiri S, Junker M D and Skov A L 2013 Factors affecting surface and release properties of thin polydimethylsiloxane films *Polym. J.* **45** 871–8

[6] Kussmaul B, Risse S, Kofod G, Waché R, Wegener M, McCarthy D N, Krüger H and Gerhard R 2011 Enhancement of dielectric permittivity and electromechanical response in silicone elastomers: molecular grafting of organic dipoles to the macromolecular network *Adv. Funct. Mater.* **21** 4589–94

[7] Racles C, Cazacu M, Fischer B and Opris D M 2013 Synthesis and characterization of silicones containing cyanopropyl groups and their use in dielectric elastomer actuators *Smart Mater. Struct.* **22** 104004

[8] Racles C, Alexandru M, Bele A, Musteata V E, Cazacu M and Opris D M 2014 Chemical modification of polysiloxanes with polar pendant groups by co-hydrosilylation *RSC Adv.* **4** 37620

[9] Racles C, Bele A, Dascalu M, Musteata V E, Varganici C D, Ionita D, Vlad S, Cazacu M, Dünki S J and Opris D M 2015 Polar–nonpolar interconnected elastic networks with increased permittivity and high breakdown fields for dielectric elastomer transducers *RSC Adv.* **5** 58428–38

[10] Madsen F B, Daugaard A E, Hvilsted S, Benslimane M Y and Skov A L 2013 Dipolar cross-linkers for PDMS networks with enhanced dielectric permittivity and low dielectric loss *Smart Mater. Struct.* **22** 104002

[11] Madsen F B, Javakhishvili I, Jensen R E, Daugaard A E, Hvilsted S and Skov A L 2014 Synthesis of telechelic vinyl/allyl functional siloxane copolymers with structural control *Polym. Chem.* **5** 7054–61

[12] Madsen F B, Daugaard A E, Fleury C, Hvilsted S and Skov A L 2014 Visualisation and characterisation of heterogeneous bimodal PDMS networks *RSC Adv.* **4** 6939–45

[13] Ha S M, Yuan W, Pei Q, Pelrine R and Stanford S 2006 Interpenetrating Polymer Networks for High-Performance Electroelastomer Artificial Muscles *Adv. Mater.* **18** 887–91

[14] Ha S M, Yuan W, Pei Q, Pelrine R and Stanford S 2007 Interpenetrating networks of elastomers exhibiting 300% electrically-induced area strain *Smart Mater. Struct.* **16** S280–7

[15] Brochu P, Stoyanov H, Niu X and Pei Q 2013 All-silicone prestrain-locked interpenetrating polymer network elastomers: free-standing silicone artificial muscles with improved performance and robustness *Smart Mater. Struct.* **22** 055022

[16] Yu L, Madsen F B, Hvilsted S and Skov A L 2015 High energy density interpenetrating networks from ionic networks and silicone *Proc. SPIE* **9430** 94300T – 1–94300T – 11

[17] Yu L, Madsen F B, Hvilsted S and Skov A L 2015 Dielectric elastomers, with very high dielectric permittivity, based on silicone and ionic interpenetrating networks *RSC Adv.* **5** 49739–47

[18] Goff J, Sulaiman S and Arkles B 2015 High elongation silicone elastomers derived from dual functional siloxane macromonomers *ACS Boston 2015*

[19] Carpi F, Gallone G, Galantini F and De Rossi D 2008 Silicone–Poly(hexylthiophene) Blends as Elastomers with Enhanced Electromechanical Transduction Properties *Adv. Funct. Mater.* **18** 235–41

[20] Liu H, Zhang L, Yang D, Ning N, Yu Y, Yao L, Yan B and Tian M 2012 A new kind of electro-active polymer composite composed of silicone elastomer and polyethylene glycol *J. Phys. D. Appl. Phys.* **45** 485303

[21] Risse S, Kussmaul B, Krüger H and Kofod G 2012 Synergistic improvement of actuation properties with compatibilized high permittivity filler *Adv. Funct. Mater.* **22** 3958–62

[22] Madsen F B, Yu L, Hvilsted S and Skov A L 2015 Super soft silicone elastomers with high dielectric permittivity *Proc. SPIE* **9430** 94301D – 1–94301D – 14

[23] Vudayagiri S, Zakaria S, Yu L, Hassouneh S S, Benslimane M and Skov A L 2014 High breakdown-strength composites from liquid silicone rubbers *Smart Mater. Struct.* **23** 105017

[24] Carpi F and De Rossi D 2005 Improvement of Electromechanical Actuating Performances of a Silicone Dielectric Elastomer by Dispersion of Titanium Dioxide Powder *IEEE Trans. Dielectr. Electr. Insul.* **12** 835–43

[25] Tian M, Wei Z, Zan X, Zhang L, Zhang J, Ma Q, Ning N and Nishi T 2014 Thermally expanded graphene nanoplates/polydimethylsiloxane composites with high dielectric constant, low dielectric loss and improved actuated strain *Compos. Sci. Technol.* **99** 37–44

[26] Quinsaat J E Q, Alexandru M, Nueesch F A, Hofmann H, Borgschulte A and Opris D M 2015 Highly stretchable dielectric elastomer composites containing high volume fraction of silver nanoparticles *J. Mater. Chem. A* **3** 14675–85

[27] Quinsaat J E Q, Nüesch F A, Hofmann H and Opris D M 2013 Dielectric properties of silver nanoparticles coated with silica shells of different thicknesses *RSC Adv.* **3** 6964–71

[28] Opris D M, Molberg M, Walder C, Ko Y S, Fischer B and Nüesch F A 2011 New silicone composites for dielectric elastomer actuator applications in competition with acrylic foil *Adv. Funct. Mater.* **21** 3531–9

[29] Zakaria S, Morshuis P H F, Benslimane M Y, Yu L and Skov A L 2015 The electrical breakdown strength of prestretched elastomers with and without sample volume conservation *Smart Mater. Struct.* **24** 55009

[30] Gatti D, Haus H, Matysek M, Frohnapfel B, Tropea C and Schlaak H F 2014 The dielectric breakdown limit of silicone dielectric elastomer actuators *Appl. Phys. Lett.* **104** 052905

[31] Tröls A, Kogler A, Baumgartner R, Kaltseis R, Keplinger C, Schwödiauer R, Graz I and Bauer S 2013 Stretch dependence of the electrical breakdown strength and dielectric constant of dielectric elastomers *Smart Mater. Struct.* **22** 104012

[32] Huang J, Shian S, Diebold R M, Suo Z and Clarke D R 2012 The thickness and stretch dependence of the electrical breakdown strength of an acrylic dielectric elastomer *Appl. Phys. Lett.* **101** 122905

[33] Suo Z 2010 Theory of dielectric elastomers *Acta Mech. Solida Sin.* **23** 549–78

[34] Zhao X, Hong W and Suo Z 2007 Electromechanical hysteresis and coexistent states in dielectric elastomers *Phys. Rev. B - Condens. Matter Mater. Phys.* **76** 134113

[35] Carpi F, Anderson I, Bauer S, Frediani G, Gallone G, Gei M, Graaf C, Jean-Mistral C, Kaal W, Kofod G, Kollosche M, Kornbluh R, Lassen B, Matysek M, Michel S, Nowak S, O'Brien B, Pei Q, Pelrine R, Rechenbach B, Rosset S and Shea H 2015 Standards for dielectric elastomer transducers *Smart Mater. Struct.* **24** 105025

[36] Rosset S, Maffli L, Houis S and Shea H R 2014 An instrument to obtain the correct biaxial hyperelastic parameters of silicones for accurate DEA modelling ed Y Bar-Cohen *Proc. SPIE* **9056** 90560M – 1–90560M – 12

[37] Zakaria S, Yu L, Kofod G and Skov A L 2015 The influence of static pre-stretching on the mechanical ageing of filled silicone rubbers for dielectric elastomer applications *Mater. Today Commun.* **4** 204–13

[38] Zhang X-M, Li H, Chen W-X and Feng L-F 2012 Rheological properties and morphological evolutions of polypropylene/ethylene-butene copolymer blends *Polym. Eng. Sci.* **52** 1740–8

[39] Madsen F B, Yu L, Daugaard A E, Hvilsted S and Skov A L 2015 A new soft dielectric silicone elastomer matrix with high mechanical integrity and low losses *RSC Adv.* **5** 10254–9

[40] Yu L, Vudayagiri S, Zakaria S, Benslimane M Y and Skov A L 2014 Filled liquid silicone rubbers: possibilities and challenges ed Y Bar-Cohen *Proc. SPIE* **9056** 90560S

[41] Brook M A, Saier H U, Schnabel J, Town K and Maloney M 2007 Pretreatment of liquid silicone rubbers to remove volatile siloxanes *Ind. Eng. Chem. Res.* **46** 8796–805

Supplementary Information (SI) for Appendix D

Mechanical and electrical ageing effects on the long-term stretching of silicone dielectric elastomers with soft fillers

#1 LR3043/50

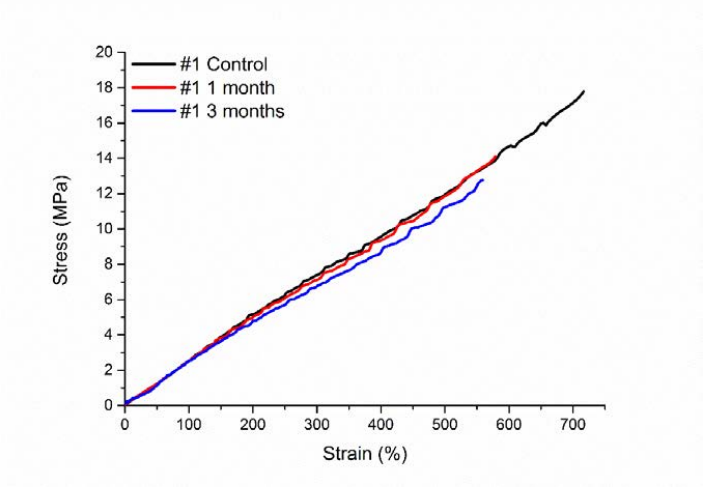

Figure S1: Stress-strain curves for #1 LR3043/50.

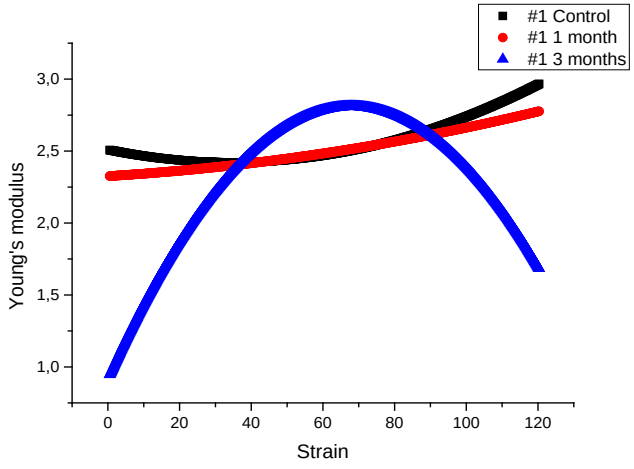

Figure S2: Young's modulus as function of strain for #1 LR3043/50.

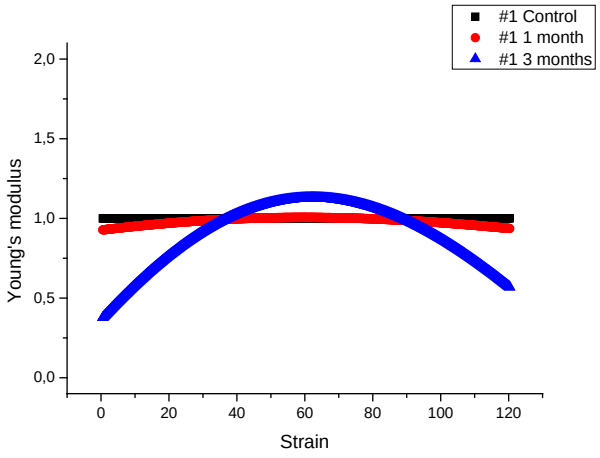

Figure S3: Normalized Young's modulus as function of strain for #1 LR3043/50.

Table S1: Measured breakdown data for #1 LR3043/50 control.

No	Control			1 month			3 months		
	Thickness	Breakdown voltage	Breakdown	Thickness	Breakdown voltage	Breakdown	Thickness	Breakdown voltage	Breakdown
	[µm]	[V]	[V/µm]	[µm]	[V]	[V/µm]	[µm]	[V]	[V/µm]
1	47	8160	173.6	50	7600	152	52	6690	128.7
2	47	8280	176.2	50	7710	154.2	49	7310	149.2
3	46	8190	178.04	50	7750	155	50	7550	151
4	49	8890	181.4	50	7840	156.8	51	8560	167.8
5	46	8390	182.4	50	7850	157	51	8600	168.6
6	48	9050	188.5	50	7900	158	50	8580	171.6
7	47	8900	189.4	50	8010	160.2	50	8600	172
8				48	7790	162.3	51	8820	172.9

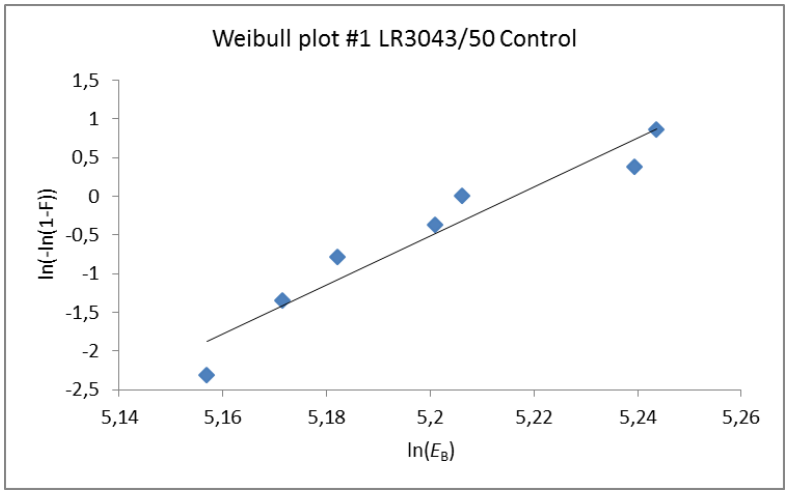

Figure S4: Weibull plot for #1 LR3043/50 control.

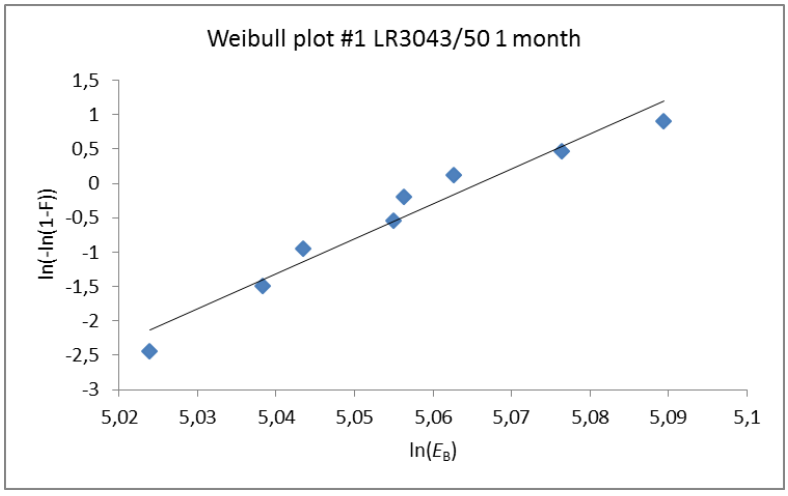

Figure S5: Weibull plot for #1 LR3043/50 after ageing for 1 month.

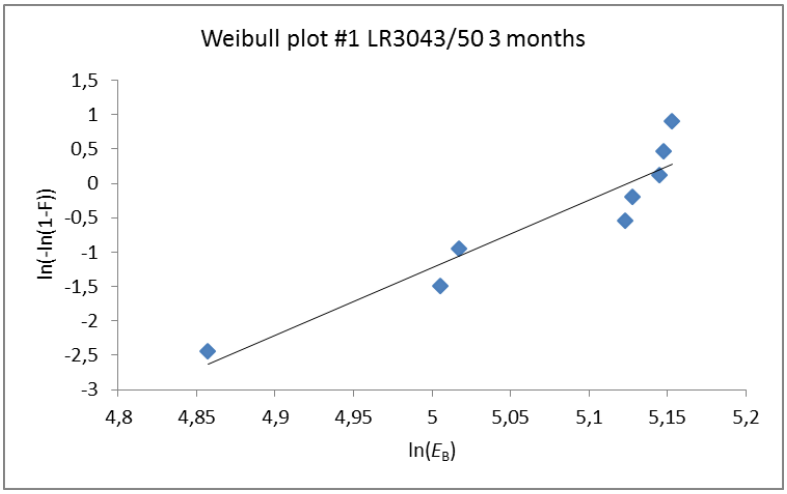

Figure S6: Weibull plot for #1 LR3043/50 after ageing for 3 months.

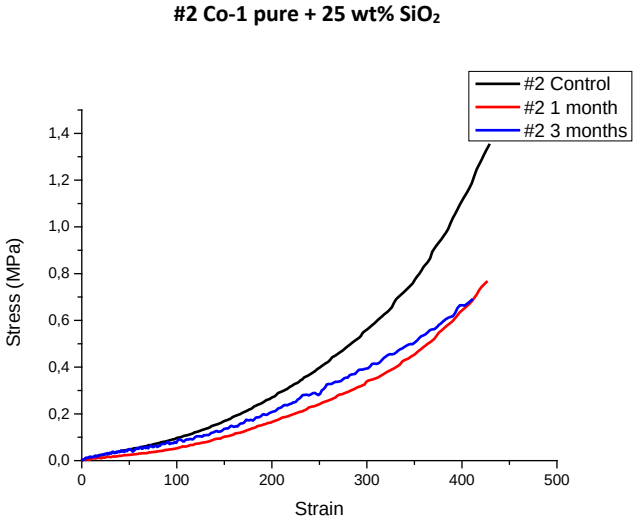

Figure S7: Stress-strain curves for #2 Co-1 pure.

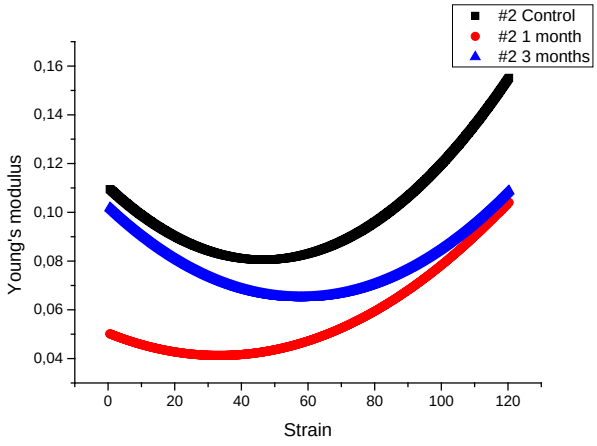

Figure S8: Young's modulus as function of strain for #2 Co-1 pure.

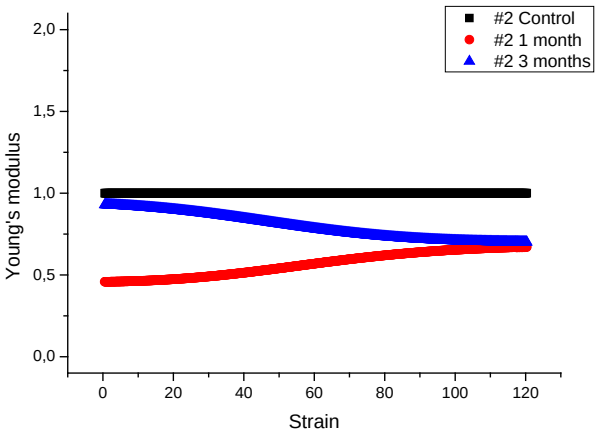

Figure S9: Normalized Young's modulus as function of strain for #2 Co-1 pure.

Table S2: Measured breakdown data for #2 Co-1 pure.

No	Control			1 month			3 months		
	Thickness	Breakdown voltage	Breakdown	Thickness	Breakdown voltage	Breakdown	Thickness	Breakdown voltage	Breakdown
	[µm]	[V]	[V/µm]	[µm]	[V]	[V/µm]	[µm]	[V]	[V/µm]
1	78	4700	60.3	75	4310	57.5	82	4840	59.0
2	78	4820	61.8	75	5160	57.5	80	4880	59.0
3	79	5200	65.8	74	5010	59.6	81	4890	60.4
4	77	5080	65.9	73	4350	60.1	80	4850	60.6
5	79	5250	66.5	75	4510	65.8	79	4810	60.9
6	78	5240	67.2	74	4870	67.7	80	5250	61.0
7	77	5360	69.6	75	5340	68.8	80	4890	61.1
8	78	5590	71.7	75	5020	71.2	81	4820	65.6

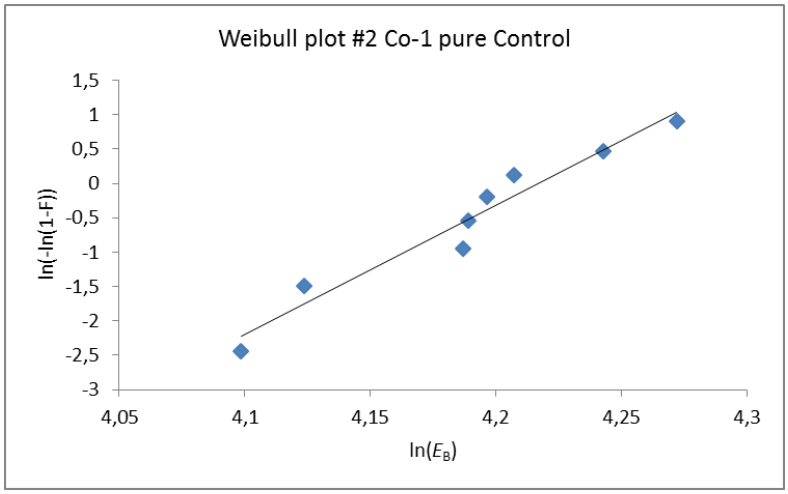

Figure S10: Weibull plot for #2 Co-1 pure control.

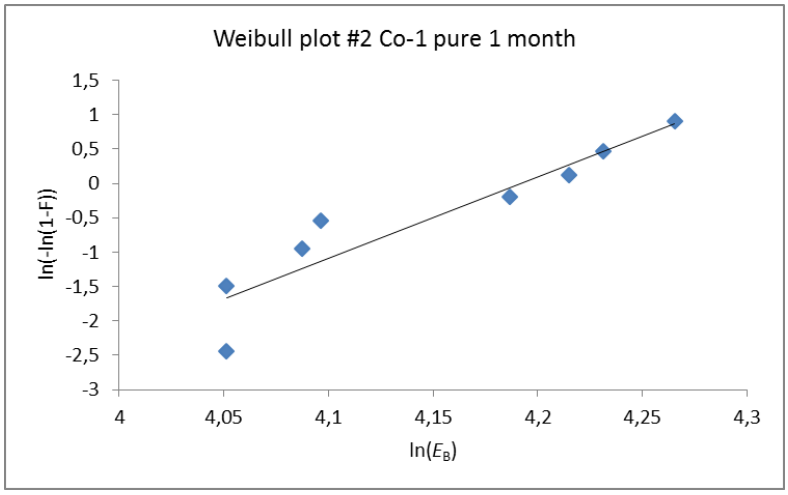

Figure S11: Weibull plot for #2 Co-1 pure 1 after 1 month of ageing.

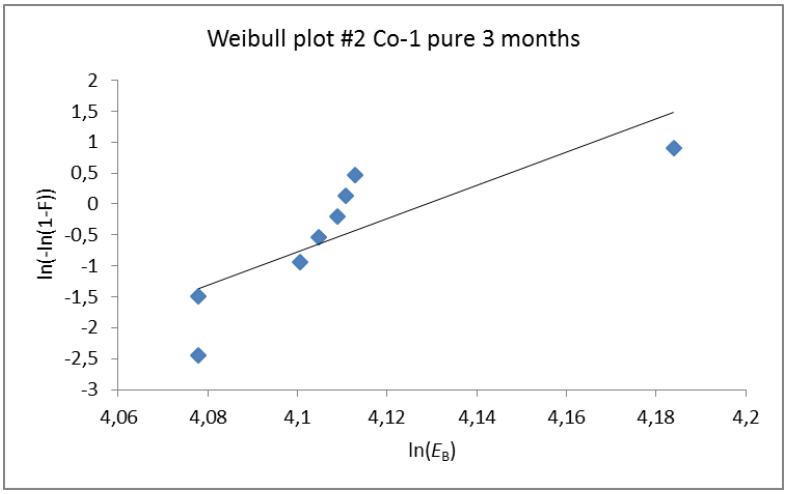

Figure S12: Weibull plot for #2 Co-1 pure 1 after 3 months of ageing.

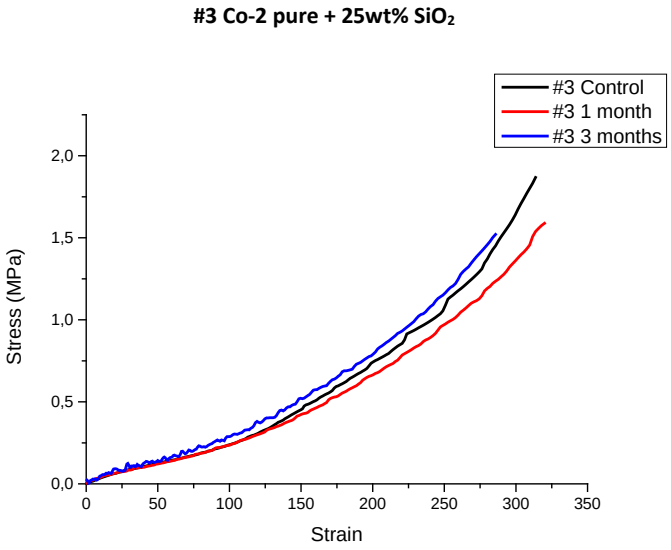

Figure S13: Stress-strain curves for #3 Co-2 pure.

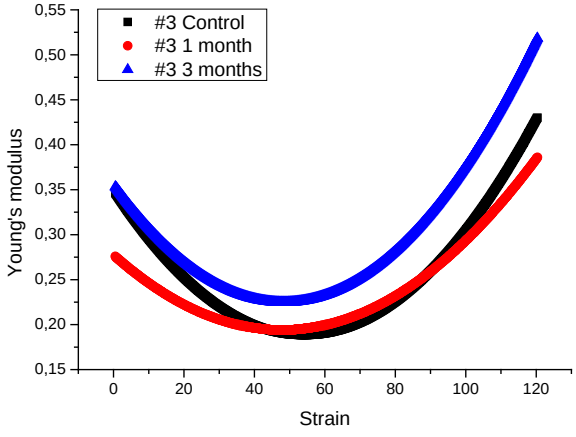

***Figure** S14: Young's modulus as function of strain for #3 Co-2 pure.*

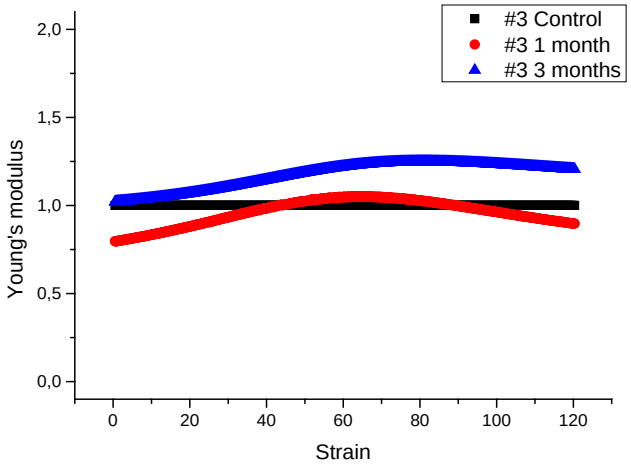

Figure S15: Normalized Young's modulus as function of strain for #3 Co-2 pure.

Table S3: Measured breakdown data for #3 Co-2 pure.

No	Control			1 month			3 months		
	Thickness	Breakdown voltage	Breakdown	Thickness	Breakdown voltage	Breakdown	Thickness	Breakdown voltage	Breakdown
	[µm]	[V]	[V/µm]	[µm]	[V]	[V/µm]	[µm]	[V]	[V/µm]
1	111	7150	64.4	152	6870	45.2	138	7020	50.9
2	111	7160	64.5	150	7080	47.2	139	7120	51.2
3	109	7050	64.7	148	7020	47.4	137	7230	52.8
4	109	7280	66.8	145	7060	48.7	139	7890	56.8
5	111	7750	69.8	145	7670	52.9	139	8060	57.9
6	109	7640	70.1	152	8710	57.3	139	8580	61.7
7	111	8490	76.5	148	9430	63.7	140	8690	62.1
8	109	8460	77.6	148	9450	63.9	139	8960	64.5

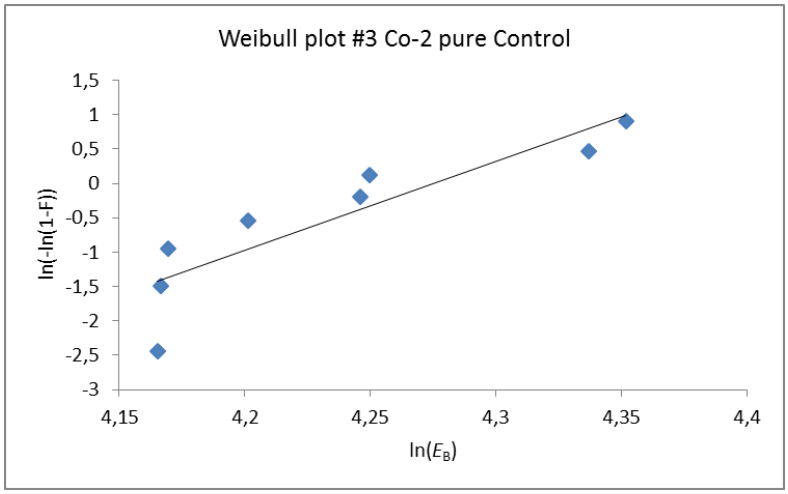

Figure S16: Weibull plot for #3 Co-2 pure control.

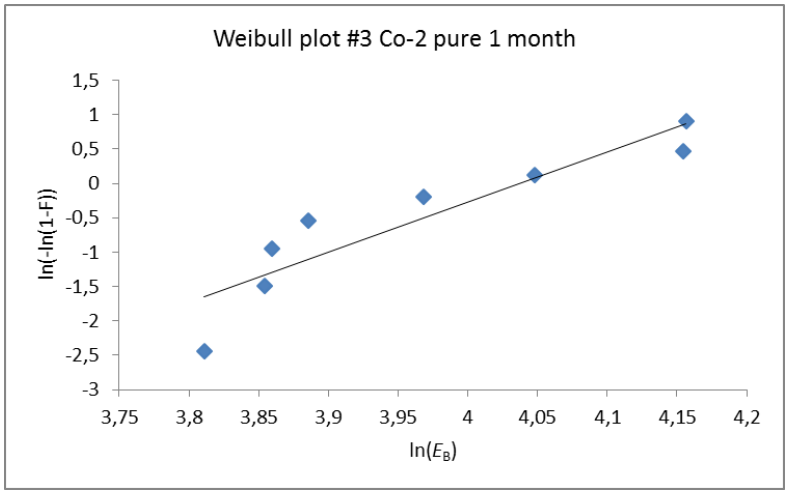

Figure S17: Weibull plot for #3 Co-2 pure after 1 month of ageing.

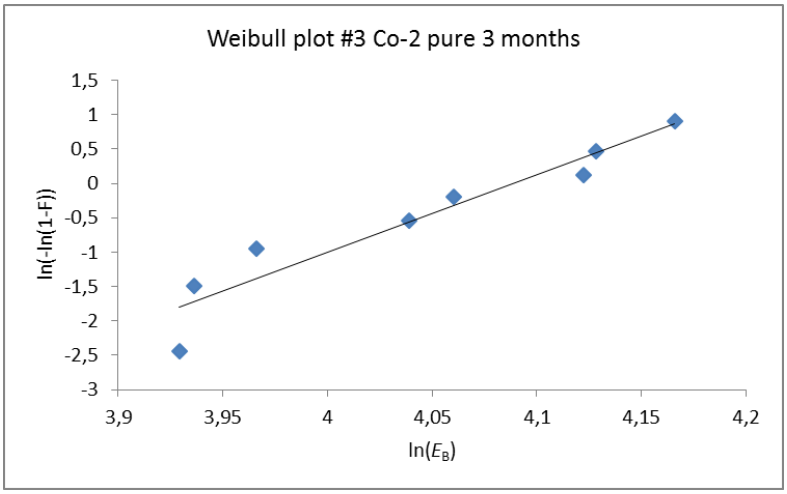

Figure S18: Weibull plot for #3 Co-2 pure after 3 months of ageing.

#4 LR3043/50 + 30 phr Co-1

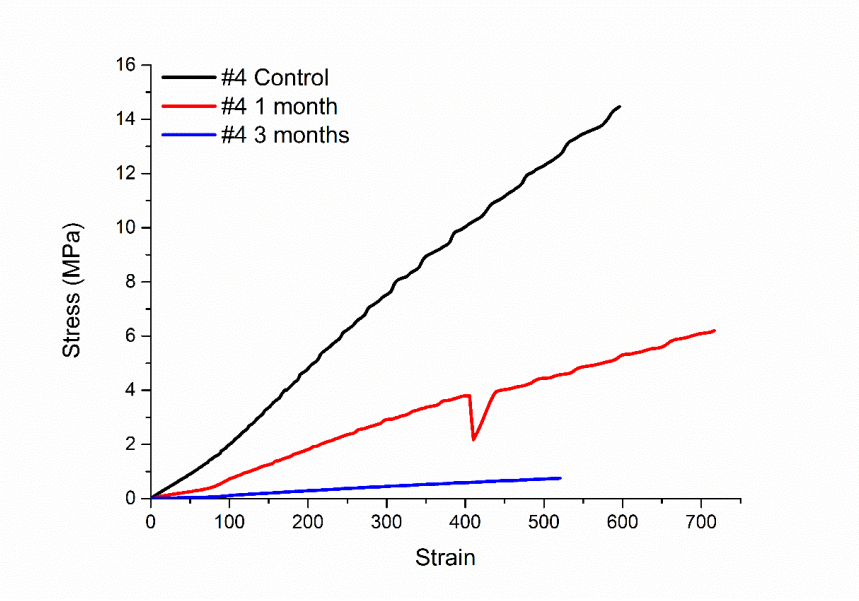

Figure S19: Stress strain curve for #4 LR3043/50 + 30 phr Co-1.

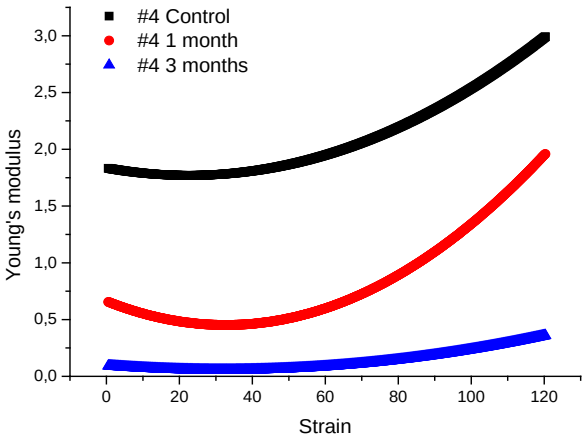

Figure S20: Young's modulus as function of strain for #4 LR3043/50 + 30 phr Co-1.

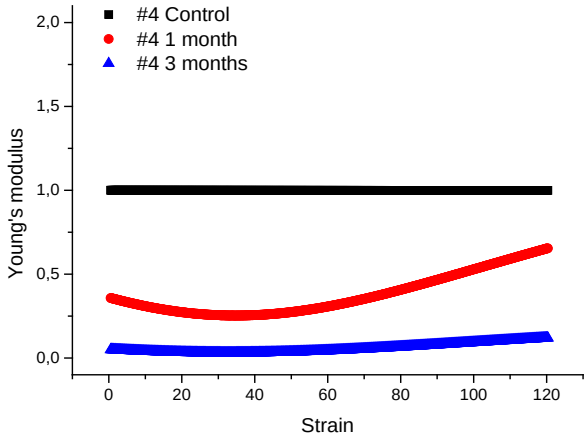

Figure S21: Normalized Young's modulus as function of strain for #4 LR3043/50 + 30 phr Co-1.

Table S4: Measured breakdown data for #4 LR3043/50 + 30 phr Co-1.

No	Control			1 month			3 months		
	Thickness	Breakdown voltage	Breakdown	Thickness	Breakdown voltage	Breakdown	Thickness	Breakdown voltage	Breakdown
	[µm]	[V]	[V/µm]	[µm]	[V]	[V/µm]	[µm]	[V]	[V/µm]
1	74	7910	106.9	81	8650	106.8	79	6770	85.7
2	73	8020	109.9	82	8900	108.5	79	6790	85.9
3	74	8580	115.9	81	9210	113.7	79	8490	107.5
4	74	8640	116.8	81	9240	114.1	80	8800	110
5	73	8640	118.4	81	9560	118.0	79	8730	110.5
6	74	8800	118.9	79	9590	121.4	79	8750	110.8
7	74	10190	137.7	79	9790	123.9	79	8790	111.3
8	73	11160	152.9	79	9830	124.4	79	8860	112.2

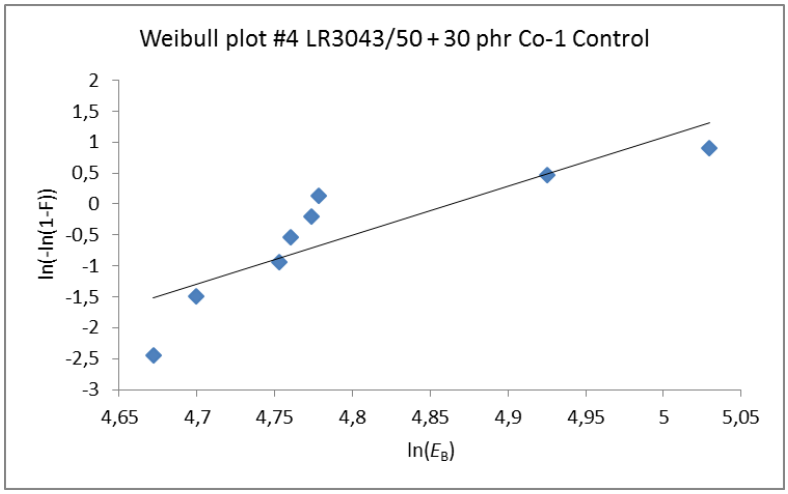

Figure S22: Weibull plot for #4 LR3043/50 + 30 phr Co-1 control.

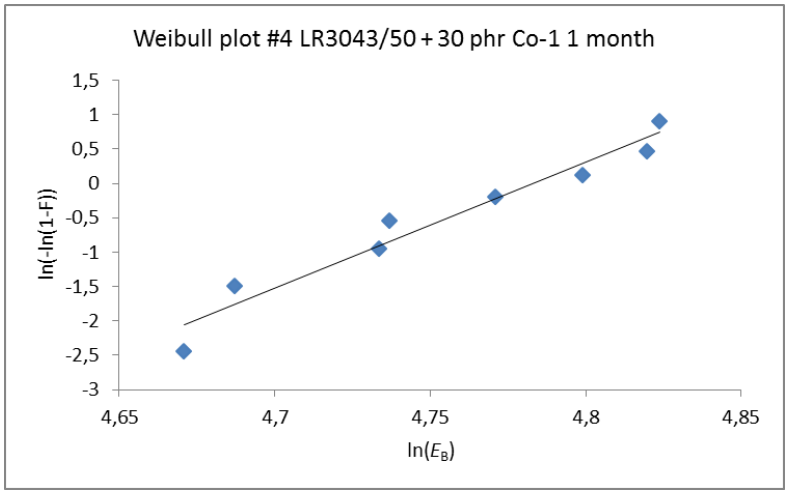

Figure S23: Weibull plot for #4 LR3043/50 + 30 phr Co-1 after ageing for 1 month.

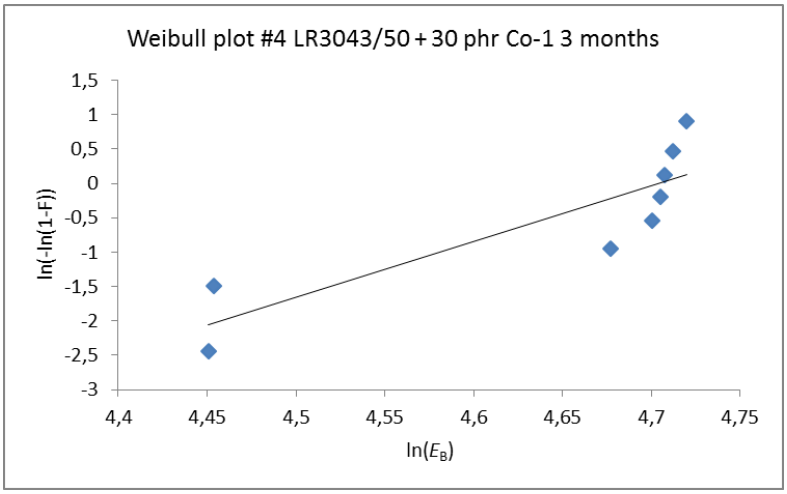

Figure S24: Weibull plot for #4 LR3043/50 + 30 phr Co-1 after ageing for 3 months.

#5 LR3043/50 + 30 phr Co-2

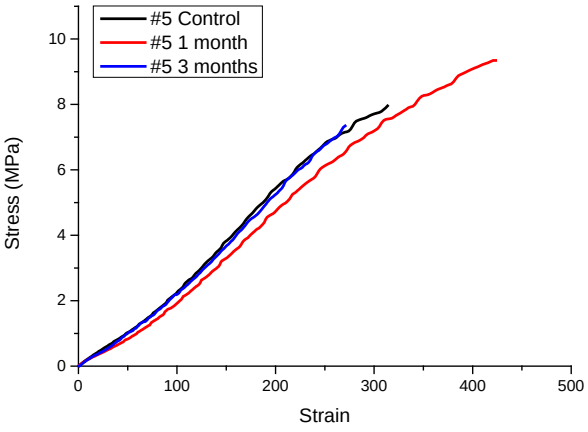

Figure S25: Stress-strain curves for #5 LR3043/50 + 30 phr Co-2.

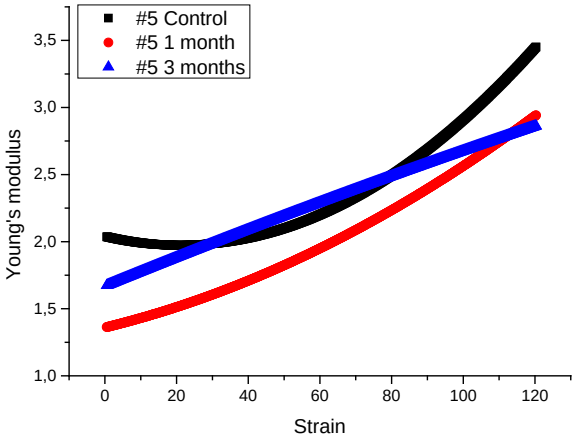

Figure S26: Young's modulus as function of strain for #5 LR3043/50 + 30 phr Co-2.

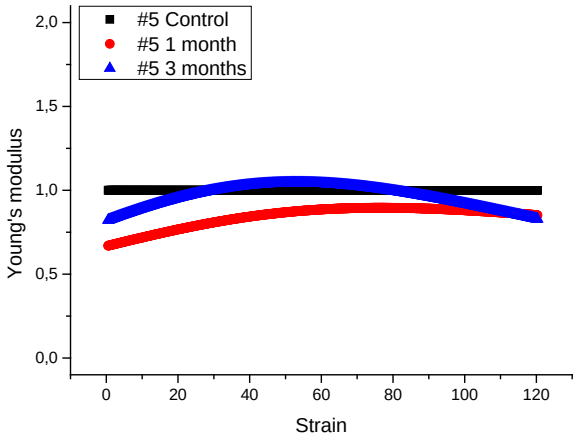

Figure S27: Normalized Young's modulus as function of strain for #5 LR3043/50 + 30 phr Co-2.

Table S5: Measured breakdown data for #5 LR3043/50 + 30 phr Co-2.

No	Control			1 month			3 months		
	Thickness	Breakdown voltage	Breakdown	Thickness	Breakdown voltage	Breakdown	Thickness	Breakdown voltage	Breakdown
	[µm]	[V]	[V/µm]	[µm]	[V]	[V/µm]	[µm]	[V]	[V/µm]
1	104	10770	103.6	85	9170	107.9	103	7170	69.6
2	101	10670	105.6	85	9180	108	107	8210	76.7
3	103	10900	105.8	85	9270	109.1	103	8980	87.2
4	101	10800	106.9	82	9170	111.8	102	10270	100.7
5	103	11320	109.9	83	9860	118.8	104	11000	105.8
6	101	12530	124.1	83	9970	120.1	105	11930	113.6
7	104	13010	125.1	81	9930	122.6	105	12080	115.0
8	104	13090	125.9	81	10030	123.8	103	12040	116.9

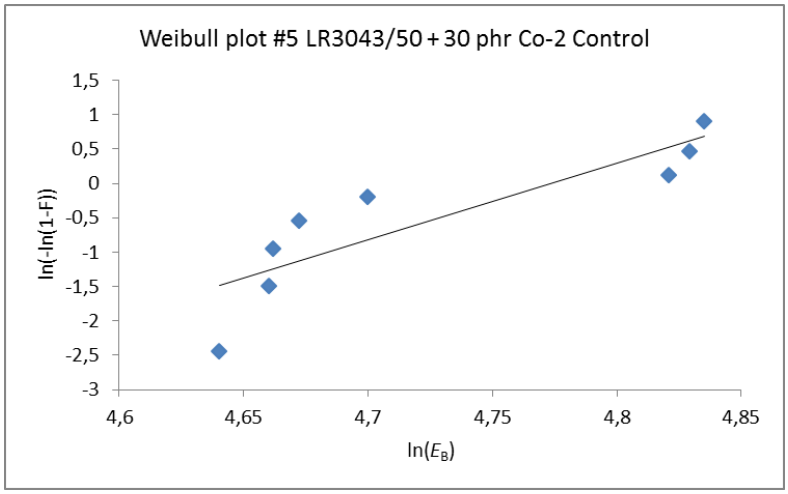

Figure S28: Weibull plot for #5 LR3043/50 + 30 phr Co-2 control.

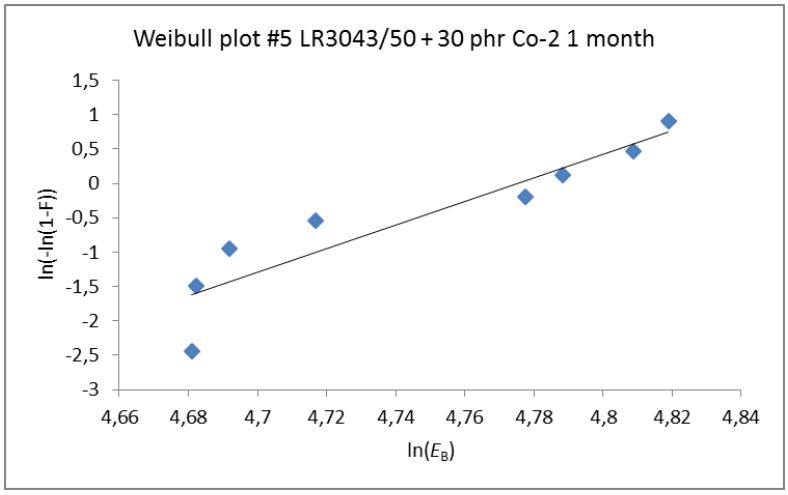

Figure S29: Weibull plot for #5 LR3043/50 + 30 phr Co-2 after 1 month of ageing.

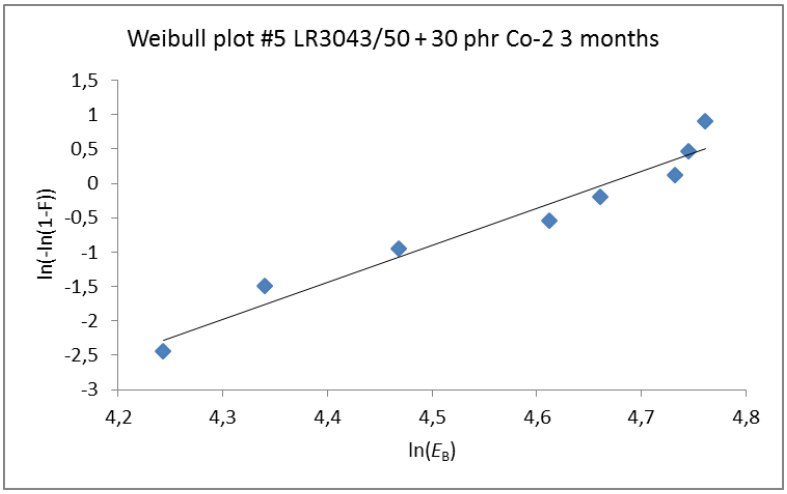

Figure S30: Weibull plot for #5 LR3043/50 + 30 phr Co-2 after 3 months of ageing.

#6 LR3043/50 + 100 phr Co-1

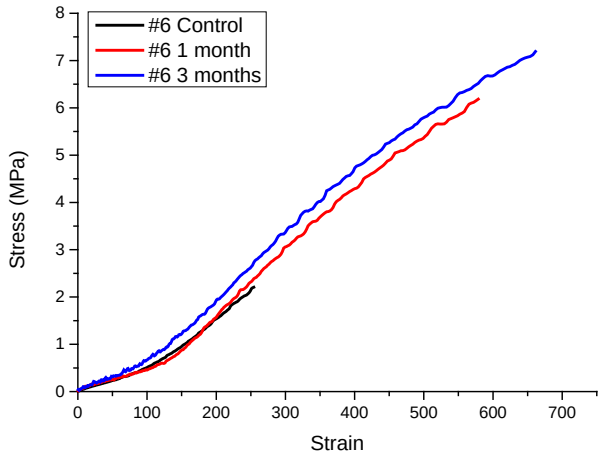

Figure S31: Stress-strain curves for #6 LR3043/50 + 100 phr Co-1.

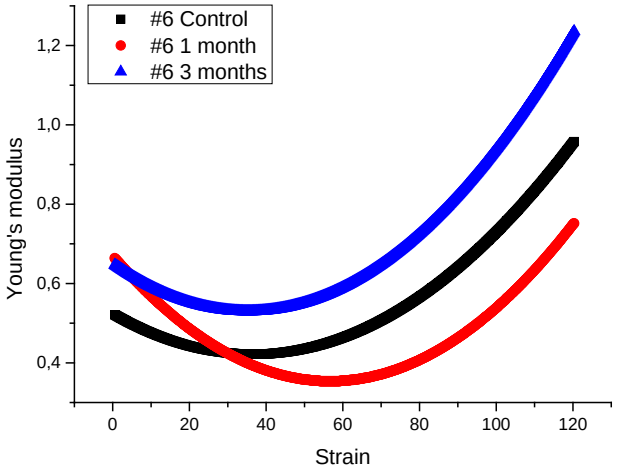

Figure S32: Young's modulus as function of strain for #6 LR3043/50 + 100 phr Co-1.

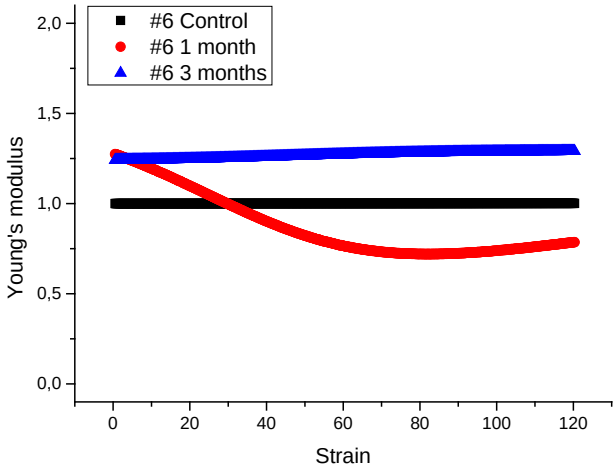

Figure S33: Normalized Young's modulus as function of strain for #6 LR3043/50 + 100 phr Co-1.

Table S6: Measured breakdown data for #6 LR3043/50 + 100 phr Co-1.

No	Control			1 month			3 months		
	Thickness	Breakdown voltage	Breakdown	Thickness	Breakdown voltage	Breakdown	Thickness	Breakdown voltage	Breakdown
	[µm]	[V]	[V/µm]	[µm]	[V]	[V/µm]	[µm]	[V]	[V/µm]
1	78	6060	77.7	73	5520	75.6	73	6010	82.3
2	77	6050	78.6	73	5520	75.6	73	6540	89.6
3	79	6220	78.7	71	5500	77.5	71	6570	92.5
4	79	6280	79.5	71	5650	79.6	71	6700	94.4
5	77	6450	83.8	76	6320	83.2	70	6960	99.4
6	78	6660	85.4	75	6250	83.3	70	7130	101.9
7	78	6940	88.9	76	6380	83.9	71	7360	103.7
8	77	7130	92.6	76	6420	84.5	72	7530	104.6

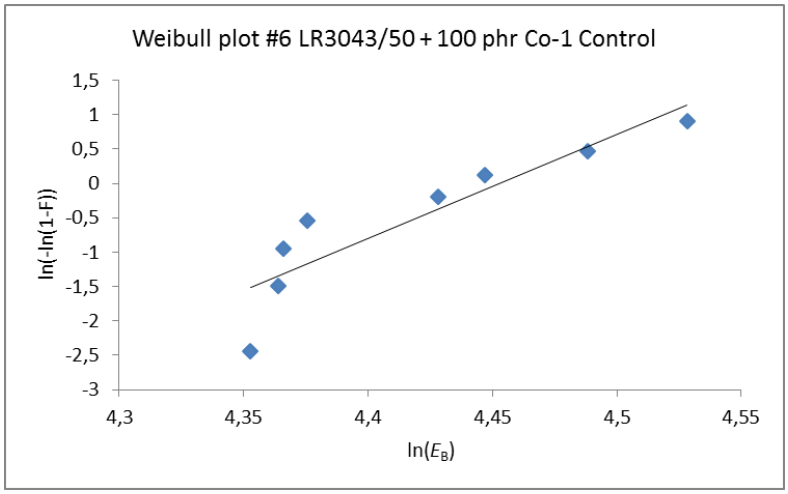

Figure S34: Weibull plot for #6 LR3043/50 + 100 phr Co-1 control.

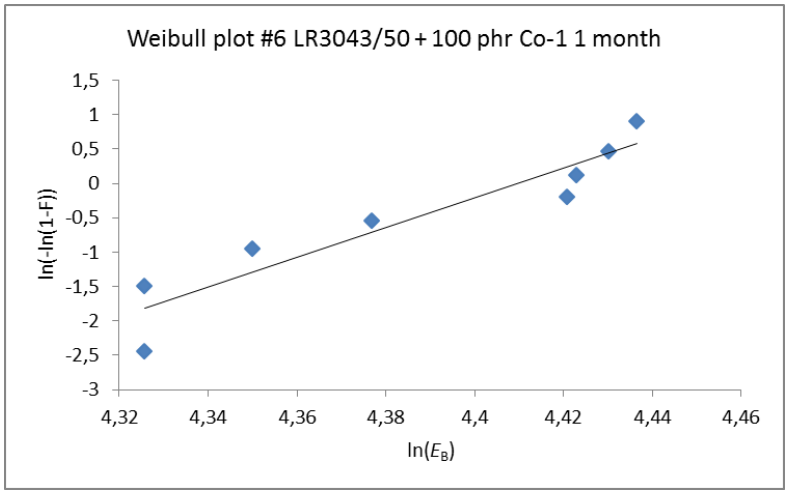

Figure S35: Weibull plot for #6 LR3043/50 + 100 phr Co-1 after 1 month of ageing.

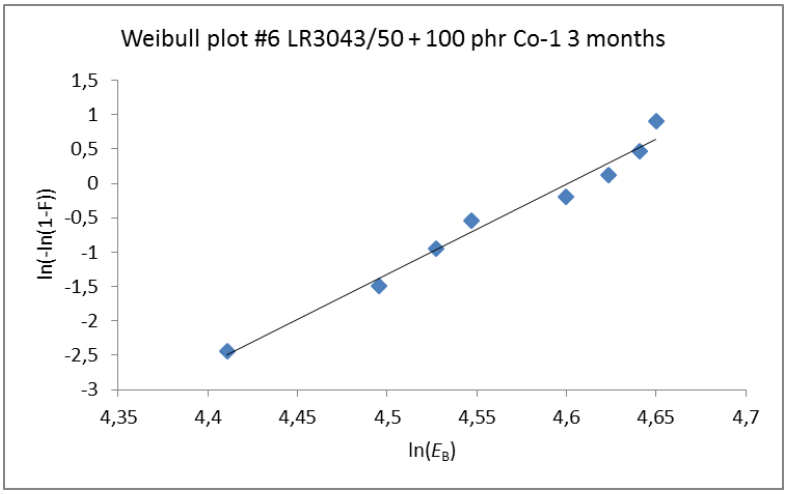

Figure S36: Weibull plot for #6 LR3043/50 + 100 phr Co-1 after 3 months of ageing.

#7 LR3043/50 + 100 phr Co-2

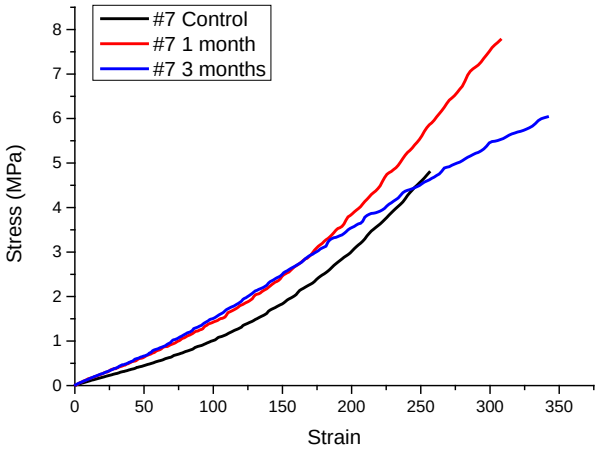

Figure S37: Stress-strain curves for #7 LR3043/50 + 100 phr Co-2.

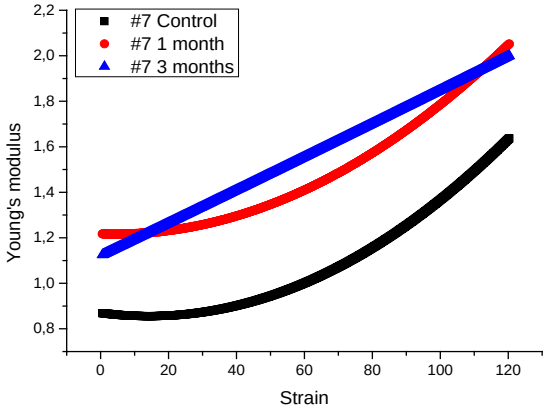

Figure S38: Young's modulus as function of strain for #7 LR3043/50 + 100 phr Co-2.

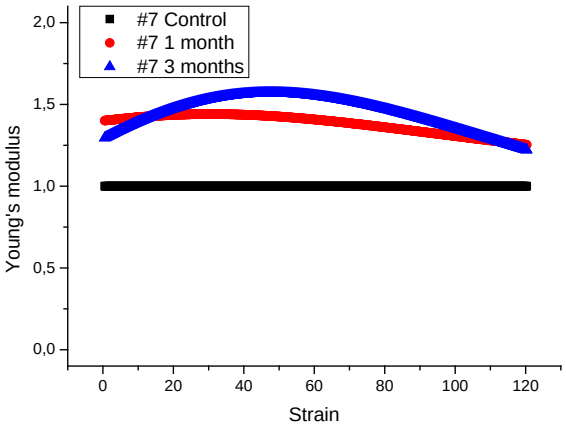

Figure S39: Normalized Young's modulus as function of strain for #7 LR3043/50 + 100 phr Co-2.

Table S7: Measured breakdown data for #7 LR3043/50 + 100 phr Co-2.

No	Control			1 month			3 months		
	Thickness	Breakdown voltage	Breakdown	Thickness	Breakdown voltage	Breakdown	Thickness	Breakdown voltage	Breakdown
	[µm]	[V]	[V/µm]	[µm]	[V]	[V/µm]	[µm]	[V]	[V/µm]
1	126	10230	81.2	110	10850	98.6	85	7530	88.6
2	128	10440	81.6	107	10580	98.8	85	8690	102.2
3	126	10310	81.8	108	10940	101.3	85	9080	106.8
4	126	11290	89.6	109	11360	104.2	83	9190	110.7
5	127	11450	90.2	109	11450	105.0	86	9590	111.5
6	126	11380	90.3	109	11480	105.3	84	9680	115.2
7	127	11770	92.7	109	11480	105.3	86	9930	115.5
8	125	12870	102.9	109	11490	105.4	84	9700	115.5

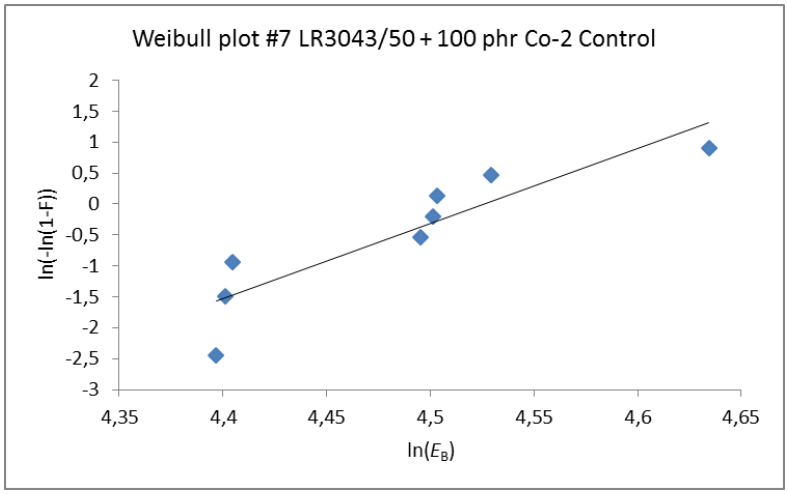

Figure S40: Weibull plot for #7 LR3043/50 + 100 phr Co-2 control.

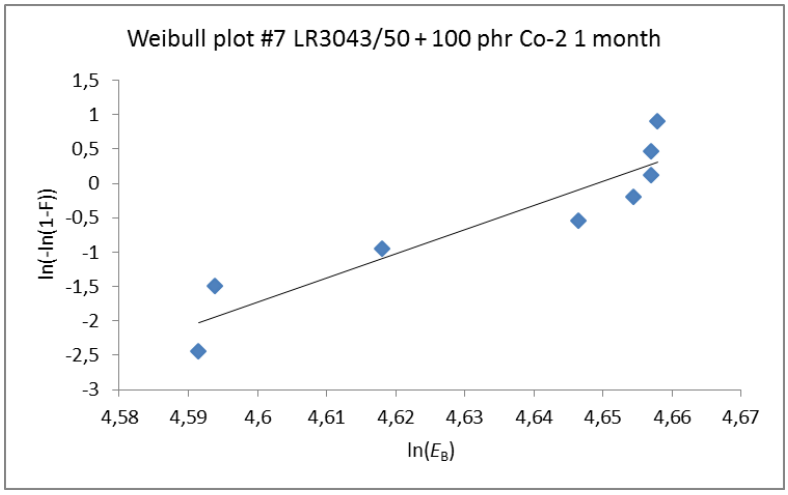

Figure S41: Weibull plot for #7 LR3043/50 + 100 phr Co-2 after 1 month of ageing.

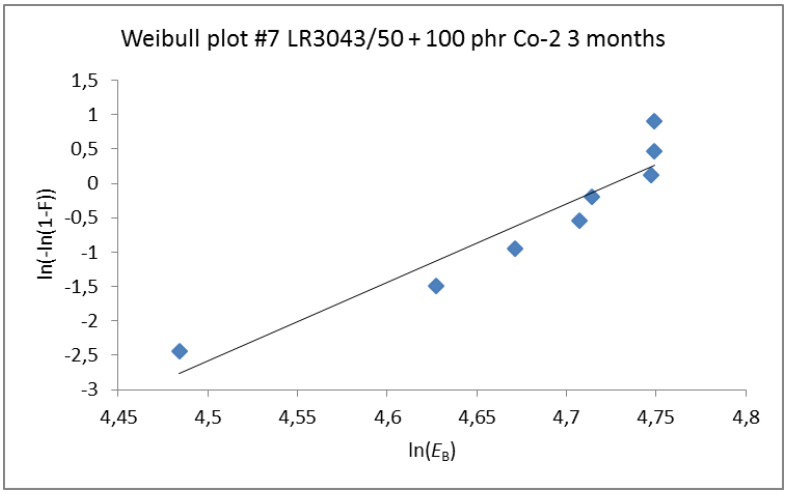

Figure S42: Weibull plot for #7 LR3043/50 + 100 phr Co-2 after 3 months of ageing.

#8 LR3043/50 + 30 phr LMS-152 (chloro-oil)

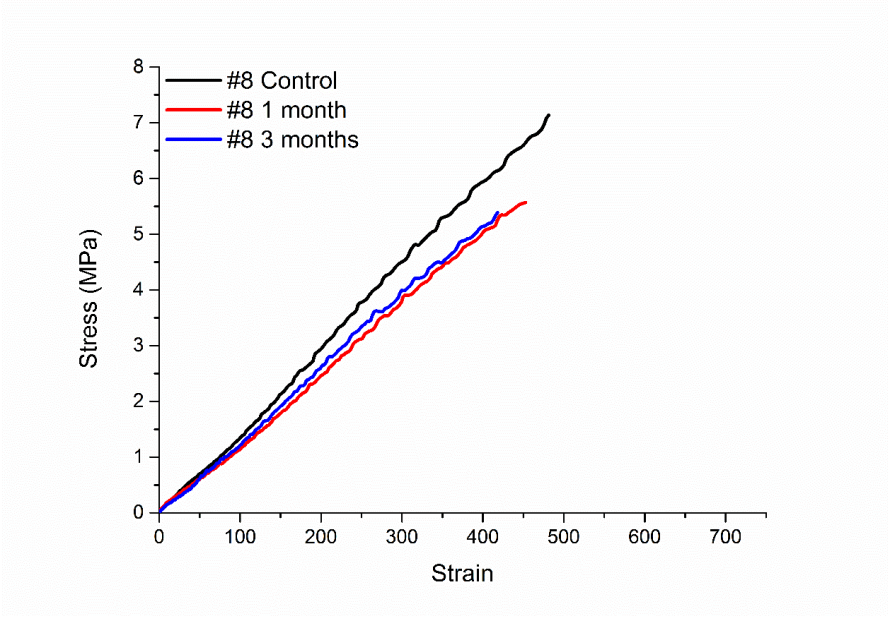

Figure s43: Stress-strain curves for #8 LR3043/50 + 30 phr LMS-152.

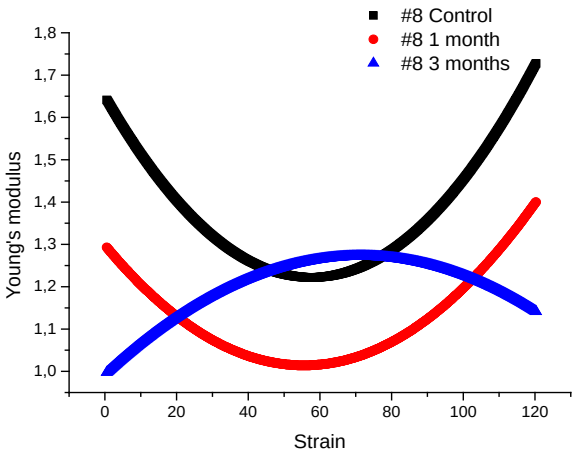

Figure S44: Young's modulus as function of strain for #8 LR3043/50 + 30 phr LMS-152.

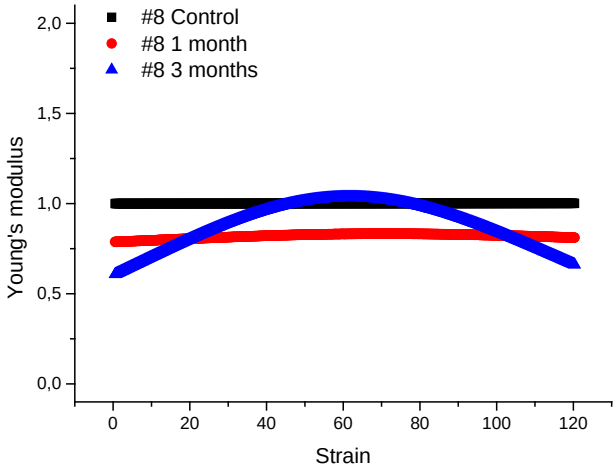

Figure S45: Normalized Young's modulus as function of strain for #8 LR3043/50 + 30 phr LMS-152.

Table S8: Measured breakdown data for #8 LR3043/50 + 30 phr LMS-152.

No	Control			1 month			3 months		
	Thickness	Breakdown voltage	Breakdown	Thickness	Breakdown voltage	Breakdown	Thickness	Breakdown voltage	Breakdown
	[µm]	[V]	[V/µm]	[µm]	[V]	[V/µm]	[µm]	[V]	[V/µm]
1	74	7570	102.3	76	7950	104.6	81	6120	75.6
2	74	8300	112.2	74	7950	107.4	79	6410	81.1
3	76	8900	117.1	72	8070	112.1	79	7190	91.0
4	73	8590	117.7	71	8130	114.5	80	7650	95.6
5	73	8750	119.9	75	8630	115.1	83	8170	98.4
6	75	9530	127.1	71	8170	115.1	81	8110	100.1
7	75	9570	127.6	75	8650	115.3	80	8280	103.5
8	75	10190	135.9	75	8670	115.6	83	8890	107.1

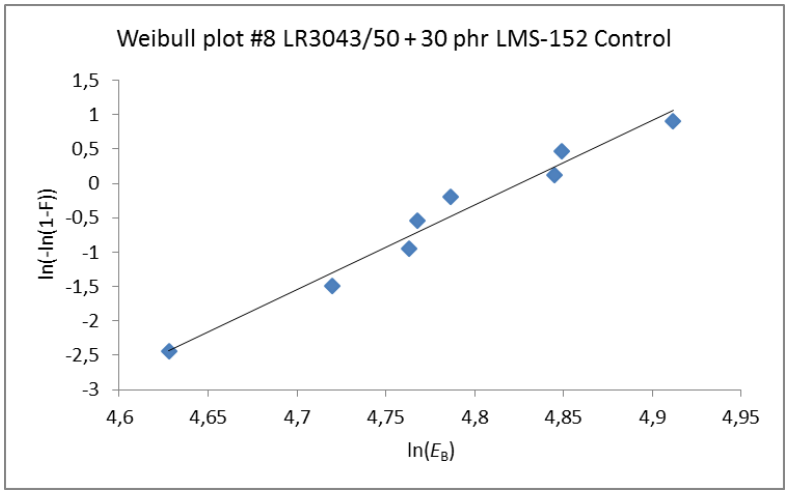

Figure S46: Weibull plot for #8 LR3043/50 + 30 phr LMS-152 control.

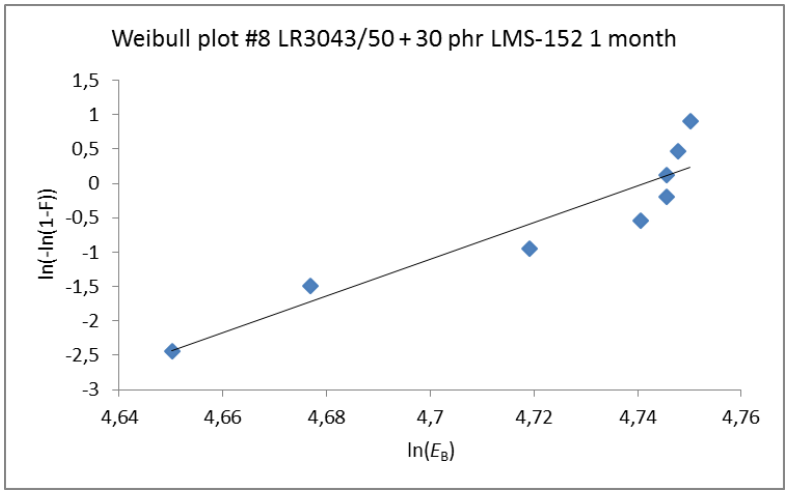

Figure S47: Weibull plot for #8 LR3043/50 + 30 phr LMS-152 after 1 month of ageing.

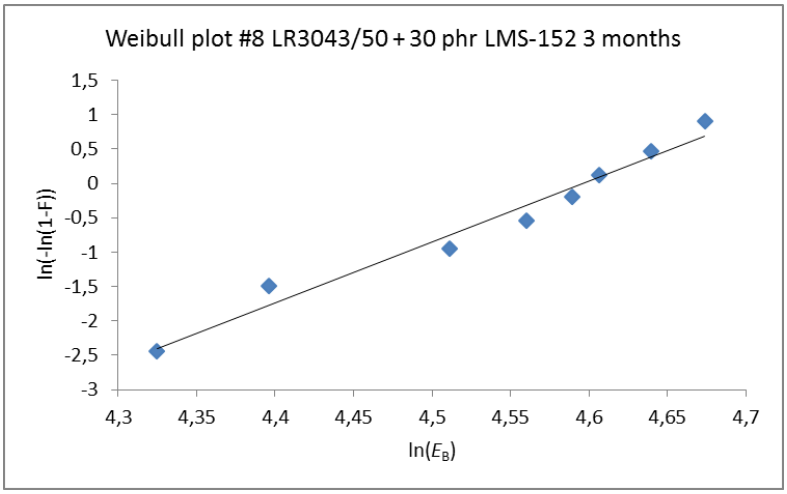

Figure S48: Weibull plot for #8 LR3043/50 + 30 phr LMS-152 after 3 months of ageing.

#9 LR3043/50 + 100 phr LMS-152 (chloro-oil)

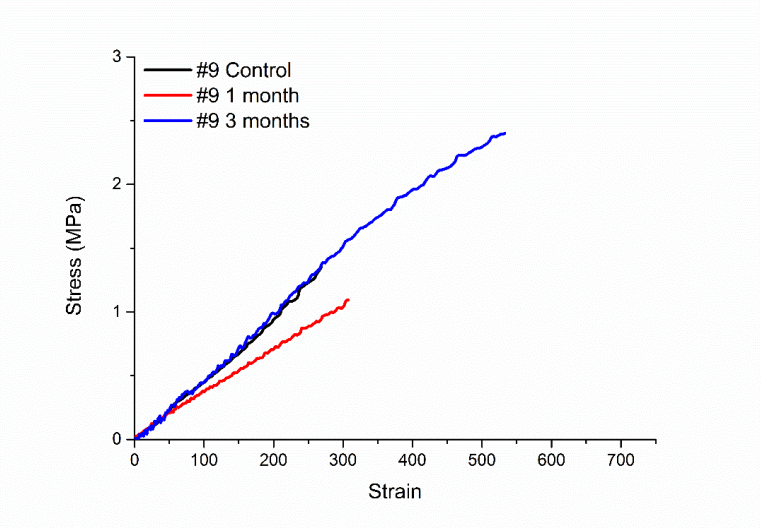

Figure S49: Stress-strain curves for #9 LR3043/50 + 100 phr LMS-152.

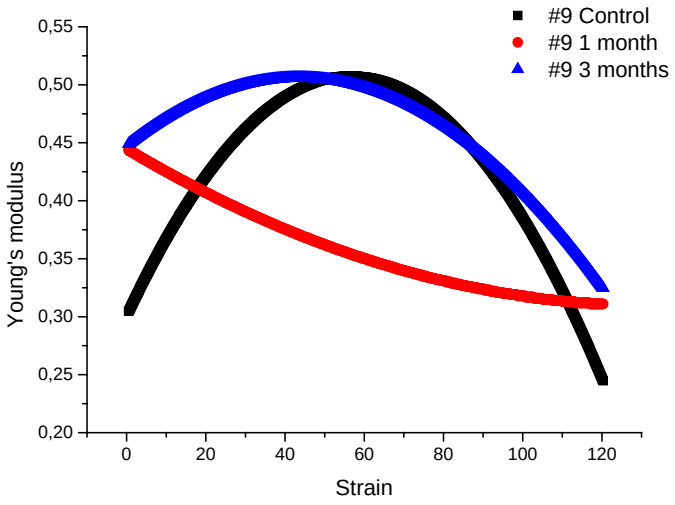

Figure S50: Young's modulus as function of strain for #9 LR3043/50 + 100 phr LMS-152.

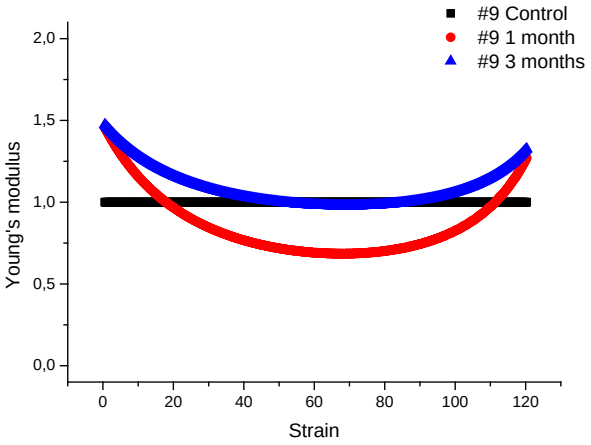

Figure S51: Normalized Young's modulus as function of strain for #9 LR3043/50 + 100 phr LMS-152.

Table S9: Measured breakdown data for #9 LR3043/50 + 100 phr LMS-152.

No	Control			1 month			3 months		
	Thickness	Breakdown voltage	Breakdown	Thickness	Breakdown voltage	Breakdown	Thickness	Breakdown voltage	Breakdown
	[µm]	[V]	[V/µm]	[µm]	[V]	[V/µm]	[µm]	[V]	[V/µm]
1	94	4940	52.6	96	5400	56.3	99	4800	48.5
2	93	4930	53.0	100	5690	56.9	100	5040	50.4
3	93	5060	54.4	96	5500	57.3	98	4980	50.8
4	92	5380	58.5	96	5590	58.2	100	5130	51.3
5	95	6140	64.6	97	5760	59.4	99	5080	51.3
6	92	5950	64.7	98	6060	61.8	102	5340	52.4
7	91	6410	70.4	99	6130	61.9	101	5480	54.3
8	92	7000	76.1	97	6140	63.3	99	4800	48.5

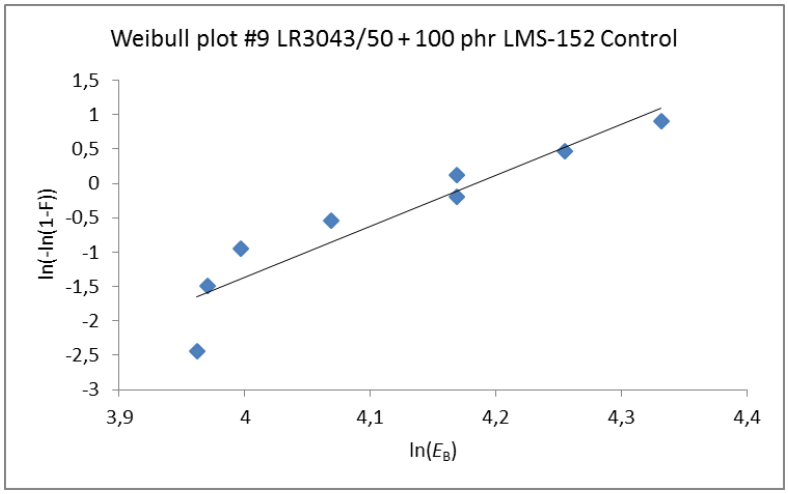

Figure S52: Weibull plot for #9 LR3043/50 + 100 phr LMS-152 control.

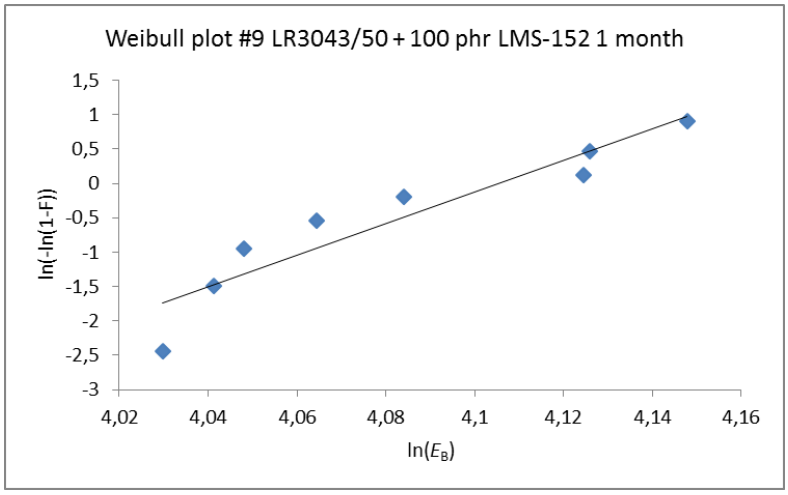

Figure S53: Weibull plot for #9 LR3043/50 + 100 phr LMS-152 after 1 month of ageing.

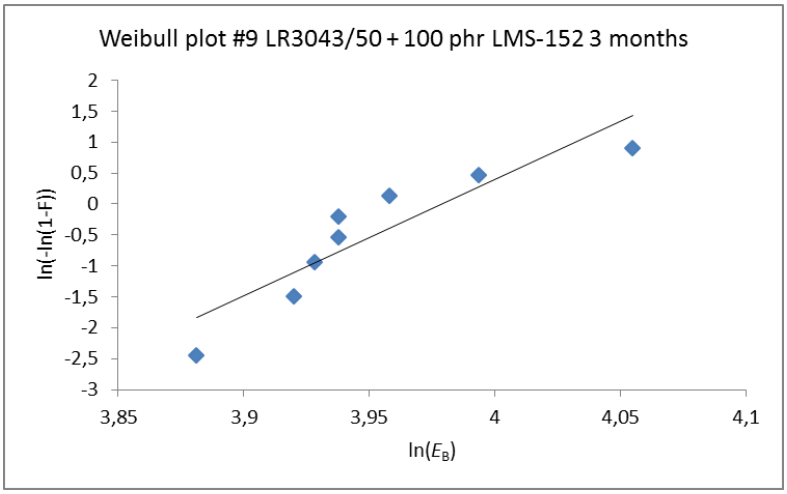

Figure S54: Weibull plot for #9 LR3043/50 + 100 phr LMS-152 after 3 months of ageing.

#10 LR3043/50 + 30 phr DMS-T22 (silicone-oil)

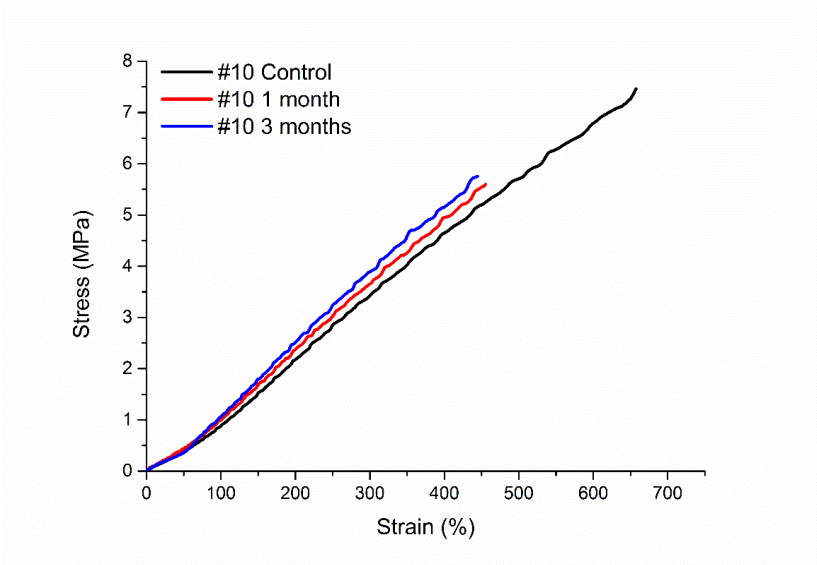

Figure S55: Stress-strain curves for #10 LR3043/50 + 30 phr DMS-T22.

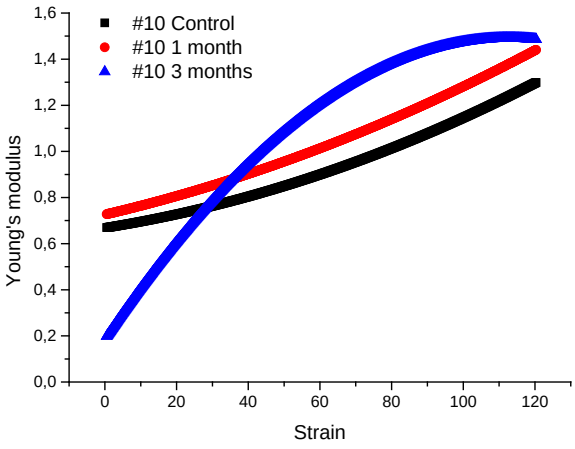

Figure S56: Young's modulus as function of strain for #10 LR3043/50 + 30 phr DMS-T22.

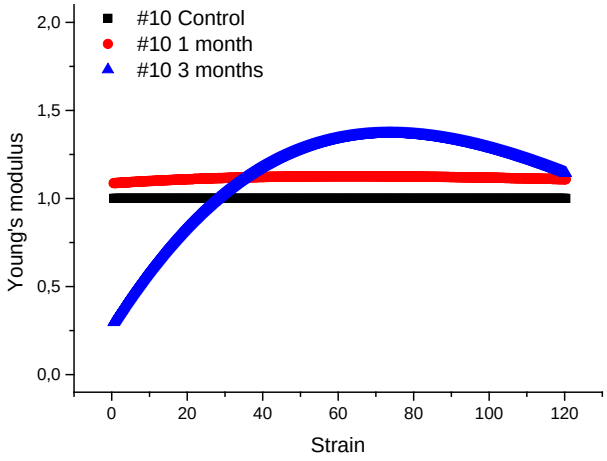

Figure S57: Normalized Young's modulus as function of strain for #10 LR3043/50 + 30 phr DMS-T22.

Table S10: Measured breakdown data for #10 LR3043/50 + 30 phr DMS-T22.

No	Control			1 month			3 months		
	Thickness	Breakdown voltage	Breakdown	Thickness	Breakdown voltage	Breakdown	Thickness	Breakdown voltage	Breakdown
	[µm]	[V]	[V/µm]	[µm]	[V]	[V/µm]	[µm]	[V]	[V/µm]
1	96	8490	88.4		7400	100	72	7120	98.9
2	95	8800	92.6	74	7630	103.1	69	6910	100.1
3	95	8980	94.5	70	7330	104.7	72	7310	101.5
4	97	9320	96.1	71	7570	106.6	72	7310	101.5
5	94	9330	99.3	71	7590	106.9	72	7340	101.9
6	96	9850	102.6	70	7530	107.6	68	7120	104.7
7	94	9930	105.6	71	7670	108.0	68	7120	104.7
8	94	10160	108.1	72	7840	108.9	70	7360	105.1

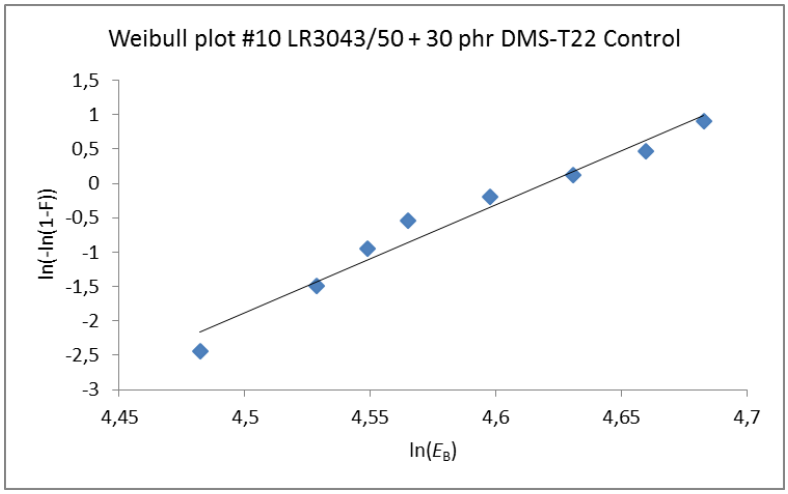

Figure S58: Weibull plot for #10 LR3043/50 + 30 phr DMS-T22 control.

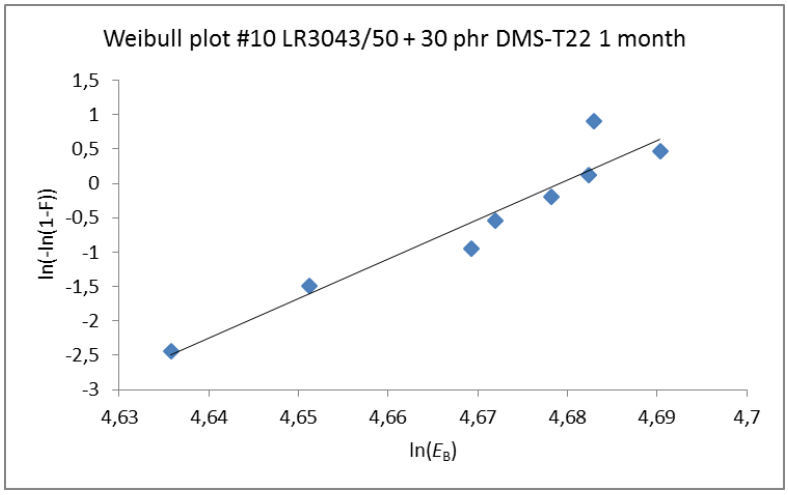

Figure S59: Weibull plot for #10 LR3043/50 + 30 phr DMS-T22 after 1 month of ageing.

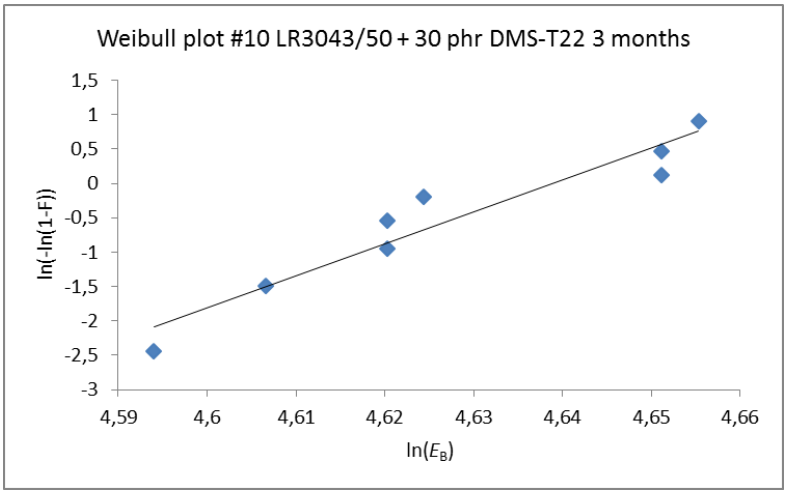

Figure S60: Weibull plot for #10 LR3043/50 + 30 phr DMS-T22 after 3 months of ageing.

#11 LR3043/50 + 100 phr DMS-T22 (silicone-oil)

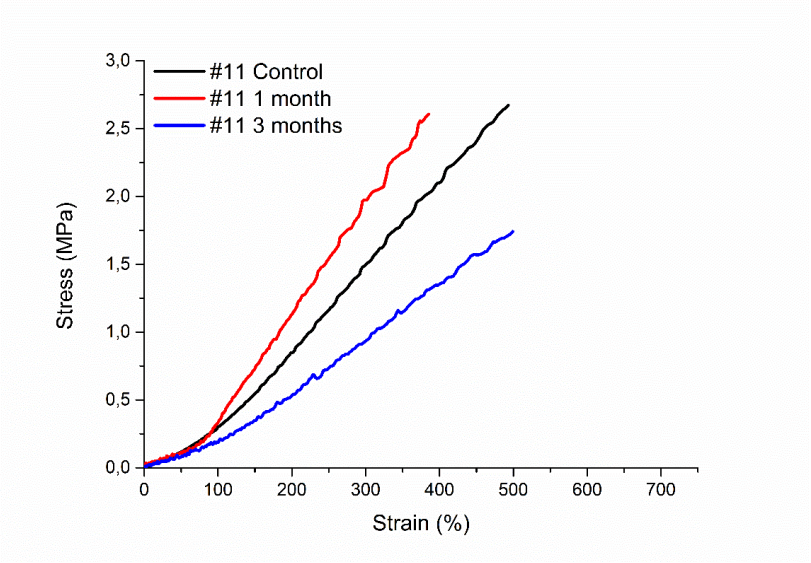

Figure S61: Stress-strain curves for #11 LR3043/50 + 100 phr DMS-T22.

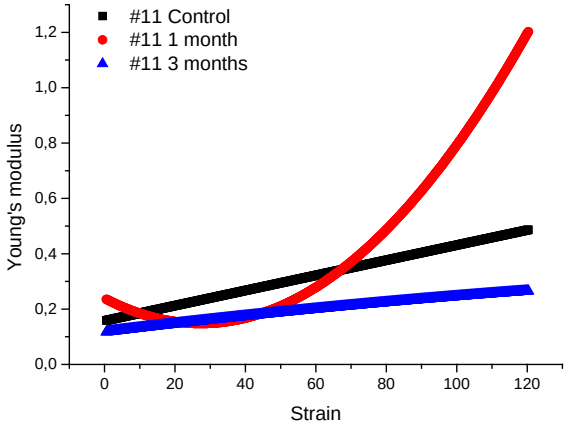

Figure S62: Young's modulus as function of strain for #11 LR3043/50 + 100 phr DMS-T22.

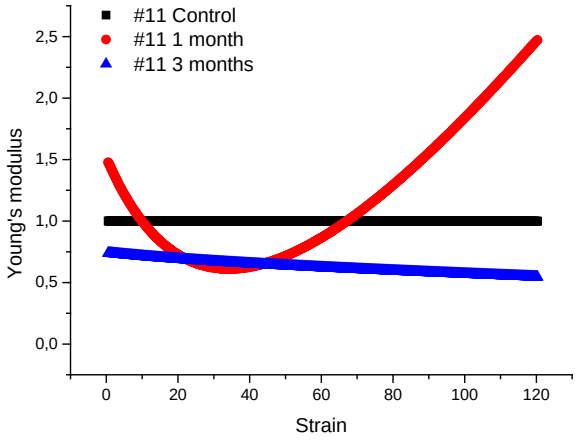

Figure S63: Normalized Young's modulus as function of strain for #11 LR3043/50 + 100 phr DMS-T22.

Table S11: Measured breakdown data for #11 LR3043/50 + 100 phr DMS-T22.

No	Control			1 month			3 months		
	Thickness	Breakdown voltage	Breakdown	Thickness	Breakdown voltage	Breakdown	Thickness	Breakdown voltage	Breakdown
	[µm]	[V]	[V/µm]	[µm]	[V]	[V/µm]	[µm]	[V]	[V/µm]
1	91	5060	55.6	70	4770	68.1	86	4890	56.9
2	91	5340	58.7	68	4720	69.4	84	4890	58.2
3	92	5530	60.1	70	4870	69.6	84	4890	58.2
4	94	5670	60.3	70	4870	69.6	84	4890	58.2
5	91	5630	61.9	70	4890	69.9	86	5010	58.3
6	94	5830	62.0	68	4780	70.3	84	4910	58.5
7	92	5760	62.6	67	5040	75.2	84	4930	58.7
8	91	5780	63.5	70	5520	78.9	84	4930	58.7

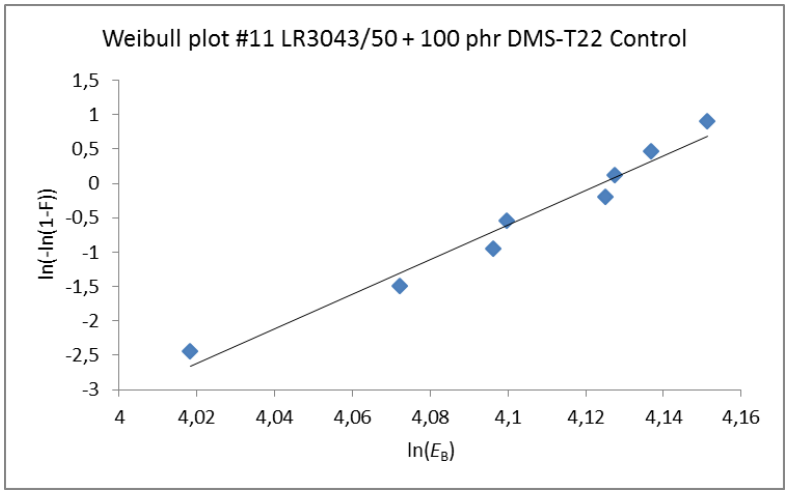

Figure S64: Weibull plot for #11 LR3043/50 + 100 phr DMS-T22 control.

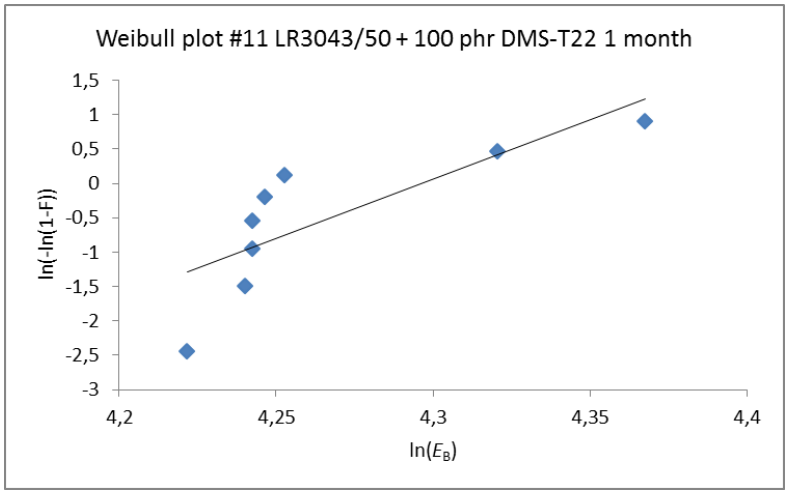

Figure S65: Weibull plot for #11 LR3043/50 + 100 phr DMS-T22 after 1 month of ageing.

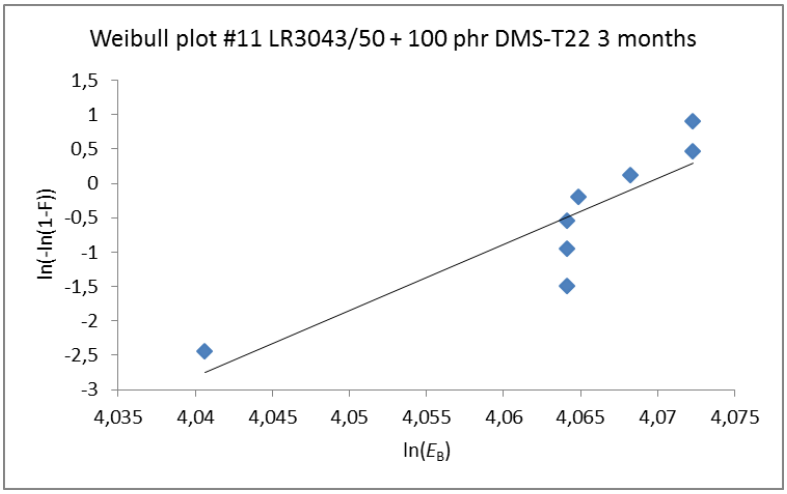

Figure S66: Weibull plot for #11 LR3043/50 + 100 phr DMS-T22 after 3 months of ageing.

APPENDIX E:

Post-curing as an effective means of ensuring the long-term reliability of PDMS thin films for dielectric elastomer applications

Zakaria S, Madsen FB and Skov AL

Macromolecular Materials and Engineering

2015

DOI: 10.1002/marc.((insert number)) ((or ppap., mabi., macp., mame., mren., mats.))

Full Paper

Post-curing as an effective means of ensuring the long-term reliability of PDMS thin films for dielectric elastomer applications

Shamsul Zakaria, Frederikke Bahrt Madsen and Anne Ladegaard Skov*

S. Zakaria, Dr. F. B. Madsen, Prof. A. L. Skov
Danish Polymer Centre, Department of Chemical and Biochemical Engineering, Technical University of Denmark, Søltofts Plads, Building 227, 2800 Kgs. Lyngby, Denmark. E-mail: al@kt.dtu.dk
S. Zakaria
Faculty of Industrial Science and Technology, Universiti Malaysia Pahang, Lebuhraya Tun Razak 26300 Gambang, Pahang, Malaysia.

Polydimethylsiloxane (PDMS) elastomers may contain a small and apparently irrelevant quantity of low molecular weight siloxanes, which are by-products from polymer synthesis. However, for many applications this low amount may alter both the mechanical and the electrical properties of PDMS elastomers. Post-curing can be used to facilitate volatile removal and thus produce PDMS films with stable elastic and electrical properties over time. In this study, the effect of post-curing was investigated for commercial silicone elastomer thin-films as a means of improving long-term elastomer film reliability. The Young's moduli and electrical breakdown strengths of commercial (silica-reinforced) PDMS elastomer films, with and without additional 35 parts per hundred rubber (phr) titanium dioxide (TiO_2), were investigated after high-temperature (200°C) post-curing for various timespans. The elastomers were found to contain less than 2% of volatiles (significantly higher for TiO_2-filled samples), but nevertheless a strong effect from post-curing was observed. The young's moduli as well as the strain-dependent behaviour were found to change significantly upon post-curing treatment. Furthermore, the determined dielectric breakdown parameters from Weibull analyses showed

that greater electrical stability and reliability could be achieved by post-curing the PDMS films before usage, and this method therefore paves a way towards more reliable dielectric elastomers.

1. Introduction

Silicone elastomers are used widely in various applications because of their many favourable properties, including their inherent softness, combined with low viscous dissipation as well as their temperature stability, which usually ranges from -100°C to more than 200°C.[1] Due to their softness and elasticity, combined with their electrically insulating properties, silicone elastomers are one of the most used materials for dielectric elastomers (DEs), which can be employed in various products, such as lightweight and linear transducers, either in the form of generators (converting mechanical energy into electrical energy) or actuators (converting electrical energy into mechanical energy). This DE technology holds great promise due to the possibility of noiseless transduction, large strains and low energy consumption, and so DE-based products are currently being commercialised.[2] The optimisation of the silicone elastomers – mainly with respect to obtaining increased dielectric permittivity and thus increased energy density – is manifested through various approaches, such as the covalent grafting of high-permittivity moieties,[3–6] interpenetrating networks,[7–11] blending in high-permittivity oils[12,13] and creating silicone elastomer composites with high-permittivity fillers such as metal oxides.[14,15] However, all modifications, to date, have resulted in one or more drawbacks. Very commonly, not only is the dielectric breakdown strength of the DE reduced, but also the overall lifetime of the silicone elastomer itself may be significantly altered. The lifetime and reliability of DEs are now more important than ever, especially with the emergence of the first commercial products. The reliability of the developed silicone DE transducers depends on the type of material used, fabrication techniques[16], product design as well as transducer operating conditions, including the applied frequency, the amplitude of the applied voltage and any pre-straining of the elastomer. However, the reliability of optimised/modified silicone elastomers is very often ignored, perhaps due to their reputation of being the most reliable material for DEs ever since SRI investigated various elastomer materials in the early 1990s.[17] They showed that the acrylic double-adhesive VHB 4910, produced by 3M, was the

best-performing elastomer with respect to actuation strain at a given applied voltage and outperformed silicone-based elastomers over short time scales. Silicone elastomers, however, were shown to possess significantly faster actuation responses (in the order of milliseconds), greater reliability as well as negligible viscous loss compared to VHB.[17] However, an important and often ignored factor in filled silicone elastomers especially is the Mullins effect, i.e. the experienced maximum-strain dependency of the elastic properties (stress-softening). Precautions against these issues, however, can be taken.[18]

Silicone polymers are synthesised through the equilibration polymerisation of low molecular weight linear and cyclic siloxanes in the presence of acid or base catalysts. One disadvantage of this process is the formation of undesired by-products caused by a premature chain termination reaction and unreacted cyclic oligomers.[19] These residues are mobile within the resulting silicone elastomers, and under certain conditions they outgas to the elastomer's surface or any device interface, thus leading to contamination. Siloxane oligomers from the polymerisation process are a main contributor to silicone outgassing;[20] nonetheless, they are compatible with the silicone elastomer matrix and may have very low vapour pressures, so the outgassing process is often very slow indeed. The performance of many silicone elastomer-based devices is often reduced by outgassing,[21] which changes the mechanical properties of elastomers, such as their tear strength and maximum elongation, due to the loss of a plasticising effect from the oligomers.[20] If the silicone elastomer is intended for use in human-contact products such as medical applications, post-curing is mandatory in order to exclude outgassing in the final product. Post-curing, however, is tedious and therefore generally avoided. In post-curing, the volatiles from the cross-linked silicone are normally removed by diffusion and evaporation at a higher temperature than the curing temperature. The rate at which this development proceeds depends on the physical and chemical properties of the utilised silicone as well as on the geometry and the design of devices (for example the thickness and total surface area).[20] Rothka et al. [22] investigated the effect of post-curing on the outgassing of silicone

elastomers, which were initially post-cured for 4 hours at 204°C, resulting in a 2.7% mass loss. Subsequently, the post-cured silicone elastomers were treated at 177°C for 20 hours, and the observed mass loss was then less than 0.5%. In comparison, with no post-curing the mass loss at 177°C for 24 hours was in the order of 4% (about eight times greater). It is thus evident that post-curing is a key parameter in respect to outgassing.

Several methods to produce silicone elastomers with improved electromechanical properties have been developed, with the addition of fillers, such as metal oxides, being the most commonly investigated due to the ease of elastomer formulation. Incorporating rigid fillers into silicone elastomers, though, changes intrinsic mechanical behaviour such as the Mullins effect, as discussed earlier. In a previous study we showed that non-post-cured elastomers with significant amounts of filler showed significant loss of tension over time upon pre-straining to 120% for 3 months.[23]

Brook et al.[20] reported that post-curing increases the Young's moduli of silicone elastomers. Since the dielectric breakdown strength of silicone elastomers is strongly dependent on the Young's modulus, dielectric breakdown strength is also very likely affected by post-curing.[24] Long-term mechanical and electrical reliability should be achievable if silicone elastomers are post-cured before they are used in DE applications. Therefore, this study focuses on two types of silicone elastomers commonly utilised as DE materials, namely commercial silicone elastomers, one with and one without an additional 35 phr permittivity-enhancing filler (TiO_2), in order to investigate the effect of post-curing on the mechanical and electrical stability of DEs. The study was carried out by heating the cured silicone elastomers at 200°C for 0, 5, 30, 60, 120 and 240 minutes subsequent to the initial curing procedure. Most commonly used curing conditions for addition-cure silicone elastomers are ~120°C for 10-30 minutes. The resulting mechanical and electrical properties of the various samples were then measured. To our knowledge the effect of post-curing on, for example, dielectric breakdown strength has not been

investigated previously, since the fraction of volatiles is so low (usually stated to be 1-2% by the elastomer supplier) that it has – so far – seemed irrelevant.

2. Experimental Section

2.1. Materials

Four different compositions of commercial silicone, with and without permittivity-enhancing filler, were investigated. The pristine elastomers were Elastosil RT625 A/B and Elastosil LR3040/30 A/B from Wacker Chemie AG. Elastosil RT625 A/B is a room-temperature vulcanising (RTV) elastomer, supplied as a two-part system. The utilised mixing ratio of parts A and B is 9:1. Elastosil LR3040/30 A/B is a high-viscosity liquid silicone rubber (LSR) which is also supplied as a two-part system. The utilised mixing ratio of parts A and B was 1:1, as recommended by the supplier. Both commercial elastomers are naturally filled with SiO_2. The solvent OS-20 (an ozone-safe, volatile methylsiloxane fluid) was obtained from Dow Corning and was added in order to achieve a suitable viscosity for film coating. The OS-20 was added to the silicone formulation, as it also facilitates filler dispersion and thus produces more homogenous elastomer films.

The composites consist of the abovementioned elastomers compounded with hydrophobic titanium dioxide (TiO_2) R420 from Sachtleben Chemie, with an average primary particle size of 250 nm. The particles were added in quantities of 35 parts per hundred rubber (phr), equating to a mass fraction of 26% in the final composite. The OS-20 was added to both silicone formulations with TiO_2. For clarity, the commercial silicone films will be referred to as *pristine* PDMS films, and composites containing additional 35 phr TiO_2 will be referred to as *filled* PDMS elastomers.

2.2. Sample preparation

Thin films were prepared based on the procedures described by Skov et al. [25] and as summarised below. Part B of the elastomer, some solvent and filler (in the case of the filled elastomer) were mixed by a DAC 150FVZ SpeedMixer (Hauschild Co.) at 3000 rpm. After 5 minutes of mixing, part A of the material was added and mixed for another 5 minutes at 2000 rpm. Glass plates were coated with the premixes, using a thin-film 3540 bird applicator from Elcometer. The films were cured in an oven for 5 minutes at 75ºC and subsequently for 10 minutes at 115ºC. The prepared films were removed from the glass plates before post-curing was carried out in a ventilated oven at 200°C for 0 (control), 5, 30, 60, 120 and 240 minutes. The thicknesses of the prepared films were around 52-105 µm. Finally, the films were stored between 50 µm-thick ethylene-tetrafluorethylene (ETFE) foils, and kept in a desiccator until use.

2.3. Methods

The volatile content measurements were performed on 150 x 50 mm PDMS films with thicknesses of 52-105 µm. The weights of the PDMS films before and after 240 minutes of post-curing were taken, and the weight loss percentages of the volatiles were then calculated. The differential scanning calorimetry (DSC) analysis was performed with a TA Discovery DSC in an air atmosphere ranging from -90 to 100°C and at a heating rate of 10°C/min. The thermogravimetric analysis (TGA) was performed with a TA Discovery TGA. The films were heated in an air atmosphere up to 700°C and the heating rate was 10 °C/min. Uniaxial extensional rheology was performed to determine the Young's modulus at different strains. Rectangular strips of approximately 6 mm x 20 mm and 52-105 µm in thickness were prepared for the measurements, which were carried out by using an ARES-G2 with Sentmanat extensional rheology 2 (SER2) geometry. The SER2 has rotary clamps which are basically two cylinders winding up the sample, thus a step-wise increasing load can be applied and the

corresponding elongations can be measured. The test specimen was elongated uniaxially at a steady Hencky strain rate of 0.001 (s^{-1}). Young's moduli were obtained from the tangent of the stress-strain curves from 0 to 130% strains. Breakdown measurements were performed on an in-house-built device based on international standards (IEC 60243-1 (1998) and IEC 60243-2 (2001)), and the film thicknesses (which can be found as supporting information) were determined with a Leica DMLB microscope replete with a USB Thorlabs 2.0 digital camera. The distance between the two spherical electrodes (with diameters of 20 mm) was set according to sample thickness with a micrometre stage and gauge. An indent of less than 3% of sample thickness was added to ensure that the spheres were in contact with the sample. A step-wise increasing voltage was applied (50-100 V/step) at a rate of 0.5-1.0 steps/s. Each sample was subjected to 10 breakdown measurements, and an average of the values was stated as the breakdown strength of the sample. Furthermore, Weibull analysis was performed on the 10 breakdown measurements to determine shape (β) and scale (η) parameters. Linear viscoelasticity for all samples was measured using an ARES-G2 rheometer (TA Instruments) set to a controlled strain mode, at 0.5% strain and with frequency sweeps from 100 Hz to 0.01 Hz at ambient temperature, using a parallel-plate geometry of 25 mm in diameter. The elastomer samples for LVE measurements were 25 mm in diameter and 0.5-1.3 mm thick. Frequency sweeps of the samples were measured at different post-cure times (0, 5, 30, 60, 120 and 240 minutes). Time sweeps were performed on samples, A, B, C and D at 0 and 240 minutes of post-curing at a temperature of 200°C for 480 minutes at a constant strain (0.5%) and frequency (1 Hz). Temperature sweeps were likewise performed on these samples, using a temperature ramp mode within a temperature range of 20-200°C at a constant strain (0.5%) and frequency (1 Hz).

3. Results and Discussion

Four different silicone elastomer compositions were tested in post-cure experiments, namely the two commercial elastomers RT625 and LR3040/30 as well as RT625 with 35 phr TiO_2 and LR3040/30 filled with 35 phr TiO_2. The TiO_2 particles were mixed into the elastomer premixes (using a SpeedMixer) before curing together with solvent, in order to facilitate proper mixing and film-casting. After the initial cure, which was carried out at 75ºC for 5 minutes and subsequently at 115ºC for 10 minutes, the prepared films were removed from the glass plates, following which post-curing was carried out at 200°C for 0 (control), 5, 30, 60, 120 and 240 minutes.

The content of volatiles in the samples was measured by examining the weight of the samples before and after the post-curing treatment at 200°C for 5, 30, 60, 120 and 240 minutes. The results were calculated in terms of actual loss as a percentage as well as loss relative to the pure elastomer matrix for samples containing TiO_2. The results are also shown in **Table 1** and **Figure 1**.

From the results in Table 1 and Figure 1, it is clear that post-curing filled elastomers results in a higher mass loss of volatiles compared to the two pristine silicone elastomers. During film preparation, solvent and other volatiles may be adsorbed by the TiO_2 particles, and thus these strongly influence the diffusion of volatiles during the initial cure. In principle the solvent utilised for the filled samples should have been completely removed during curing, but from the results in Table 1 it is clear that the cured samples with TiO_2 contain a higher fraction of volatiles. This again illustrates the importance of post-curing especially for silicone elastomers with high filler content. It is also clear that outgassing depends not only on sample geometry, but also, to a large extent, on sample composition. It can also be seen from Figure 1 that most

of the outgassing occurs after approximately 60 minutes, and thereafter only minor outgassing is taking place.

A determination of the content of volatiles in the films before and after post-curing was undertaken using thermogravimetric analysis (TGA). **Figure 2** shows TGA thermograms of the four elastomers after 0 and 240 minutes of post-curing, respectively.

A time of 240 minutes was chosen as the maximum post-curing time, as this is a commonly required treatment for thick silicone elastomers.[20] Samples without post-curing show significant weight loss from room temperature to the first degradation process (around 350^{o}C) in the order of 3-5%. In comparison, samples which have been extensively post-cured show significantly smaller weight loss over the same temperature range, as the volatiles inside the elastomer films have been effectively removed during the post-curing process. The TGA thermograms for all samples post-cured at the different timespans can be found as supporting information.

The effect of post-curing on thermal transition behaviour in elastomers was examined by differential scanning calorimetry (DSC). All thermograms for samples post-cured at different timespans can be found as supporting information. An exothermic peak is observed for both the post-cured and the non-post-cured PDMS films during cooling, which corresponds to crystallisation processes taking place in the films. During heating, an endothermic peak is observed, which corresponds to the crystallites melting. The temperatures for which crystallisation and melting occur are denoted by T_c and T_m, respectively. The DSC results indicate that post-curing causes only a marginal effect on T_m. The results also indicate that the pristine PDMS films (*A* and *B*) exhibit lower T_c upon post-curing. Inversely, upon post-curing, the TiO_2-filled PDMS films have higher than or similar T_c to their non-post-cured counterparts. The high filler content in the filled samples thus greatly influences the thermal behaviour of the

PDMS films. The glass transition temperatures, T_g, do not change significantly after post-curing.

From the obtained results – so far – it is obvious that outgassing is to be expected if post-curing is omitted during film fabrication. Thus, changes in the mechanical properties of the elastomer films over time are expected. In order to investigate these changes in mechanical properties with post-curing time, the Young's modulus as a function of strain for the different samples was measured before and after post-curing for different timespans. **Figure 3** shows the Young's modulus at 5% strain as a function of post-curing time. The Young's moduli at 5% strain are furthermore summarised in **Table 2** together with their percentage-wise increase induced by the post-cure. As seen in Figure 3 and Table 2, the Young's moduli of the control samples of the two pristine elastomers are in the same order of magnitude. After post-curing, the Young's moduli, however, have increased to different extents. RT625 experienced a maximum increase of 68% following 120 minutes of post-curing, while LR3040/30 experienced a maximum increase in the Young's modulus of 108% after 240 minutes of post-curing. LR3040/30 thus becomes significantly stiffer than RT625 over time despite it containing a lower percentage of volatiles. This also means that LR3040/30 will change more over time than RT625 if the post-curing of samples is not performed prior to use as DEs. As seen in Figure 3 and Table 2, elastomers with TiO_2 experience a dramatic increase in the Young's modulus compared to the pristine elastomers. This is expected when adding hard fillers to a silicone elastomer. Nevertheless, the samples do not experience similar increases despite having similar initial Young's moduli, possibly due to a difference in the composition of the two elastomers RT625 and LR3040/30. Upon post-curing, the two elastomers with TiO_2 also show different behaviour. The modulus of RT625 + 35 phr TiO_2 increases by more than 200% after post-curing, which thus has a dramatic effect upon the mechanical properties of the filled RT625. LR3040/30 + 35 phr TiO_2 show a modulus increase of 100%, which is comparable to what was experienced by

its pristine counterpart. Furthermore, it applies to all samples that increase in Young's modulus levels after 120 minutes of post-curing.

Figure 4 illustrates stress-strain behaviour up to 130% strain of elastomers before and after post-curing for 240 minutes. The stress-strain curves clearly illustrate the stiffening effect of post-curing, which is especially pronounced for elastomers with TiO_2 fillers.

Figure 5 shows the Young's moduli and normalised Young's moduli as a function of strain after different post-curing timespans for the pristine PDMS films RT625 and LR3040/30. Normalised Young's moduli ($Y_n(s)$) are calculated from $Y_n(s) = \frac{Y(s)}{Y_0(s)}$, where $Y(s)$ is the Young's modulus for post-cured elastomer films at a given strain, and Y_0 is the corresponding Young's modulus for the non-post-cured samples at the same strain. The effect of post-curing on the pristine elastomers is illustrated in Figure 5. Both investigated pristine elastomers show identical behaviour with increased Young's moduli during increased post-curing periods. The pristine elastomers both exhibit significant strain-softening up to approximately 70% strain, following which strain-hardening effects sets in. This characteristic property of silicone elastomers leads to a local minimum in the Young's modulus as a function of strain. Strain-hardening is particularly favourable in the context of avoiding the electro-mechanical instability (EMI) phenomenon which occurs when local Maxwell pressure exceeds the compressive stress of the elastomer[27–29]. The normalised Young's modulus plots (Figure 5 b)) show that LR3040/30 benefits on this occasion from post-curing, since the curves become more strain-hardening. The effect is less pronounced for RT625.

Young's moduli and normalised Young's moduli as functions of strain for RT625 and LR3040/30 with 35 phr TiO_2 are shown in **Figure 6**. The two different TiO_2-filled elastomers show very different responses in the Young's modulus as a function of strain. Filled LR3040/30 shows significantly more strain-hardening and softening behaviour than filled RT625, while

the normalised Young's moduli plots as functions of strain (Figure 6 b)) also illustrate the different behaviours between the two elastomers. After post-curing the filled RT625 exhibits more strain-dependent effects than the non-post-cured control sample. LR3040/30, on the other hand, experiences very different effects. After post-curing for longer than 5 minutes, the curves change shapes from concave to convex, with a peak maximum at approximately 85% strain. This phenomenon is only seen for the filled LR3040/30 elastomer and can be attributed to the high filler content within the elastomer. Up to a certain strain the elastomer exhibits stress-hardening behaviour where after stress-softening sets in due to the high filler content, which in turn induces significant Mullins effects such as the rupture of filler clusters and the separation of weak polymer chains from the fillers.[30] The strain-hardening that is experienced after post-curing up to approximately 80% strain is, as mentioned previously, beneficial in the context of avoiding EMI. Post-curing therefore improves this failure mode of filled DEs.

Figure 7 shows the storage modulus and loss (tan δ) as a function of temperature at a constant strain and frequency. It can be seen that all samples experience the same behaviour, to a greater or lesser extent. After post-curing, all materials have become significantly stiffer, as illustrated by the increase in storage modulus. Before post-curing, all samples experience a temperature-independent storage modulus, whereas thereafter the storage modulus drops as a function of temperature. Since the modulus drop is more pronounced for samples with high filler content, it may be ascribed to polymer-filler interactions such as the relaxation of polymer chains surrounding the fillers. Thus, for these samples polymer-filler interactions are more pronounced than entropic elasticity, which would have led to storage modulus increases in line with increasing temperatures.[31] The losses are seen to decrease when the temperature increases, meaning that the samples become less dissipative at increasing temperatures. In the supporting information, time and frequency sweeps for different post-cure timespans can be found for all samples. These results confirm that samples become stiffer after post-curing and that no 'actual'

post-curing (further cross-linking) takes place during the process, since the loss factor does not decrease thereafter.

Since post-curing changes the Young's moduli of elastomers, dielectric breakdown strength may also be affected, as the breakdown strength of DE films has been found previously to scale linearly – or even exponentially – with the Young's modulus.[14,24] Table 2 shows dielectric breakdown strength and Young's moduli at 5% strain at different post-cure times. Dielectric breakdown strength as a function of Young's moduli at 5% strain is furthermore shown in **Figure 8**. As expected, the breakdown strengths of elastomer samples increase as the Young's moduli increase. For both types of pristine elastomers a maximum increase of 16-17% is obtained following post-curing, which means that post-curing effectively increases the dielectric breakdown strength of commercial DE films. Furthermore, the results show that the breakdown strength of heavily filled PDMS elastomers increases to a greater extent than for the pristine elastomers. The filled elastomers both experience an increase in breakdown strength of 33-34%, which is almost two-fold higher than for the pristine elastomers. This means that heavily filled elastomers benefit to a very great extent from post-curing.

An analysis was performed in order to investigate the effect of post-curing elastomer films on dielectric breakdown strength distribution. The Weibull distribution is one of the most commonly used methods in lifetime analysis and can provide insights into the electrical reliability of an elastomer. The breakdown data points (E_B) are therefore fitted to the Weibull cumulative distribution function, $F(E_B)$:

$$F(E_B) = 1 - exp\left(-\frac{E_B}{\eta}\right)^{\beta} \quad (1)$$

which can be linearised to give:

$$ln[-ln(1 - F(E_B))] = \beta \cdot ln(E_B) - \beta \cdot ln(\eta) \quad (2)$$

The Weibull shape parameter, β, is equal to the slope of the regressed line. Different β values lead to noticeable effects on lifetime distribution, and β is also required to be as large as possible, such that the measured breakdown strengths all fall within a narrow range of voltages. This is furthermore an indication of homogeneity on the microscale. The Weibull scale parameter, η, which is determined from the distribution at which 63% of the films have broken down electrically, should be as high as possible and locate distribution along the scale. **Table 3** shows the Weibull distribution results with β, η and linear regression (r^2) in a probability plot for control samples and 240 min of post-cured films. The results show that post-curing significantly increases the reliability of the tested elastomer films as the scale and the shape parameters increase. This improvement is, amongst other things, attributed to the increase in the Young's modulus of the PDMS films upon post-curing.[24] Post-curing also extensively removes the volatiles that contribute to modulus inhomogeneities and defects which are introduced during film preparation.[20] Furthermore, since r^2, the linear regression goodness-of-fit values become closer to 1, and the breakdown data thus become better fitted to the Weibull distribution after post-curing. This again indicates that elastomers become more homogenous after post-curing, since small-molecule inhomogeneities have been removed.

Figure 9 and **Figure 10** show the cumulative probability of failure, from which shape and scale parameters as well as r^2 have been determined. It is clear from Figure 9 that sample B, before post-curing, experiences breakdown behaviour, with two clearly separated distributions signifying two breakdown processes. The first part of the data points is most likely due to small defects and filler agglomeration in the highly filled LR3040/30, whereas the second part of the data point distribution represents 'true' breakdown processes. This behaviour is significantly smaller after post-curing, thereby indicating that post-curing eliminates some of the causes of early breakdown phenomena, which can also be seen from the shape and scale parameters as well as the r^2 values. The same behaviour can be seen for the TiO_2-filled samples in Figure 10,

where both elastomers experience two breakdown distributions before post-curing, and where the behaviour is significantly reduced thereafter.

4. Conclusions

Four samples with different compositions were prepared, namely a commercial RTV elastomer, RT625, a commercial LSR elastomer, LR3040/30, and the two mentioned elastomers with additional 35 phr added TiO_2. Important properties in relation to dielectric elastomers were measured before and after post-cure treatment at 200°C for up to 240 minutes. This included the effect of post-curing on thermal properties, elastic/mechanical properties and dielectric breakdown strength. This study shows that even commercial silicone elastomers require post-curing for mechanical and electrical stability. This is an overlooked feature of silicone elastomers utilised in dielectric elastomers. The two commercial elastomers (RTV and LSR) both show improved strength over the post-curing period. This phenomenon can be ascribed to the evaporation of volatiles and other residues from the PDMS films at high temperatures. In other words, the elastomer will not provide constant actuation over time if it is not ensured that all volatiles have been removed beforehand. The removal of volatiles is furthermore favourable, as it increases electrical breakdown strength and thus enhances the reliability of the elastomer.

Supporting Information

Supporting Information is available from the Wiley Online Library or from the author

Acknowledgements: The authors gratefully acknowledge financial support offered by the Ministry of Education of Malaysia and Universiti Malaysia Pahang. The Danish Council for Independent Research and Innovationsfonden Danmark are acknowledged for additional funding.

Keywords: ageingelastomers, mechanical properties, silicones, thin films

REFERENCES

[1] J. E. Mark, *Silicon-Based Polymer Science: A Comprehensive Resource*, American Chemical Society, Oxford University Press, United Kingdom, **1990**.

[2] P. Brochu, Q. Pei, *Macromol. Rapid Commun.* **2010**, *31*, 10–36.

[3] S. J. Dünki, Y. S. Ko, F. A. Nüesch, D. M. Opris, *Adv. Funct. Mater.* **2015**, *25*, 2467–2475.

[4] F. B. Madsen, L. Yu, A. E. Daugaard, S. Hvilsted, A. L. Skov, *Polymer* **2014**, *55*, 6212–6219.

[5] B. Kussmaul, S. Risse, G. Kofod, R. Waché, M. Wegener, D. N. McCarthy, H. Krüger, R. Gerhard, *Adv. Funct. Mater.* **2011**, *21*, 4589–4594.

[6] F. B. Madsen, I. Javakhishvili, R. E. Jensen, A. E. Daugaard, S. Hvilsted, A. L. Skov, *Polym. Chem.* **2014**, *5*, 7054–7061.

[7] L. Yu, F. B. Madsen, S. Hvilsted, A. L. Skov, *RSC Adv.* **2015**, *5*, 49739–49747.

[8] C. Tugui, G. T. Stiubianu, M. Iacob, C. Ursu, A. Bele, S. Vlad, M. Cazacu, *J. Mater. Chem. C* **2015**, *3*, 8963–8969.

[9] S. M. Ha, W. Yuan, Q. Pei, R. Pelrine, S. Stanford, *Smart Mater. Struct.* **2007**, *16*, S280–S287.

[10] S. M. Ha, M. Wissler, R. Pelrine, S. Stanford, G. Kovacs, Q. Pei, *Proc. SPIE* **2007**, *6524*, 652408–652408–10.

[11] P. Brochu, H. Stoyanov, X. Niu, Q. Pei, *Smart Mater. Struct.* **2013**, *22*, 055022.

[12] F. Carpi, G. Gallone, F. Galantini, D. De Rossi, *Adv. Funct. Mater.* **2008**, *18*, 235–241.

[13] F. B. Madsen, L. Yu, P. S. Mazurek, A. L. Skov, *Unpublished* **2015**.

[14] S. Vudayagiri, S. Zakaria, L. Yu, S. S. Hassouneh, M. Benslimane, A. L. Skov, *Smart Mater. Struct.* **2014**, *23*, 105017.

[15] G. L. Wang, Y. Y. Zhang, L. Duan, K. H. Ding, Z. F. Wang, M. Zhang, *J. Appl. Polym. Sci.* **2015**, *132*, 42613.

[16] S. Vudayagiri, M. D. Junker, A. L. Skov, *Polym. J.* **2013**, *45*, 871–878.

[17] F. Carpi, D. De Rossi, R. Kornbluh, R. Pelrine, P. Sommer-Larsen, *Dielectric Elastomers as Electromechanical Transducers: Fundamentals, Materials, Devices, Models and Applications of an Emerging Electroactive Polymer Technology*, Elsevier Ltd, Oxford UK, **2008**.

[18] S. Rosset, L. Maffli, S. Houis, H. R. Shea, *Proc. SPIE* **2014**, *9056*, 90560M–1–90560M–12.

[19] W. Noll, *Chemistry and Technology of Silicones*, Academic, New York, **1968**.

[20] M. A. Brook, H. U. Saier, J. Schnabel, K. Town, M. Maloney, *Ind. Eng. Chem. Res.* **2007**, *46*, 8796–8805.

[21] R. M. Villahermosa, A. D. Ostrowski, in *Proc. SPIE 7069, Opt. Syst. Contam. Eff. Meas. Control* (Ed.: S.A. Straka), International Society For Optics And Photonics, **2008**, pp. 706906–706906–10.

[22] J. Rothka, R. Studd, K. Tate, D. Timpe, *Outgassing of Silicone Elastomers.*, ArlonSilicone Technology Division, ISC., **2000**.

[23] S. Zakaria, L. Yu, G. Kofod, A. Ladegaard, **n.d.**

[24] M. Kollosche, H. Stoyanov, H. Ragusch, S. Risse, a. Becker, G. Kofod, *2010 10th IEEE Int. Conf. Solid Dielectr.* **2010**, 1–4.

[25] A. L. Skov, S. Vudayagiri, M. Benslimane, *Proc. SPIE* **2013**, *8687*, 86871I–86871I–8.

[26] M. Benslimane, H.-E. Kiil, M. J. Tryson, *Proc. SPIE* **2010**, *7642*, 764231–764231–11.

[27] X. Zhao, Z. Suo, *Phys. Rev. Lett.* **2010**, *104*, 1–4.

[28] D. Gatti, H. Haus, M. Matysek, B. Frohnapfel, C. Tropea, H. F. Schlaak, *Appl. Phys. Lett.* **2014**, *104*, 052905.

[29] K. H. Stark, C. G. Garton, *Nature* **1955**, *176*, 1225–1226.

[30] A. Dorfmann, R. W. Ogden, *Int. J. Solids Struct.* **2004**, *41*, 1855–1878.

[31] A. M. Stricher, R. G. Rinaldi, C. Barrès, F. Ganachaud, L. Chazeau, *RSC Adv.* **2015**, *5*, 53713–53725.

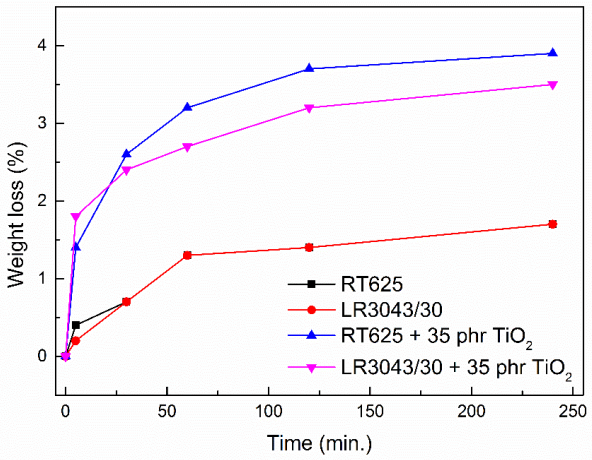

Figure 1. Weight loss as a function of post-cure time.

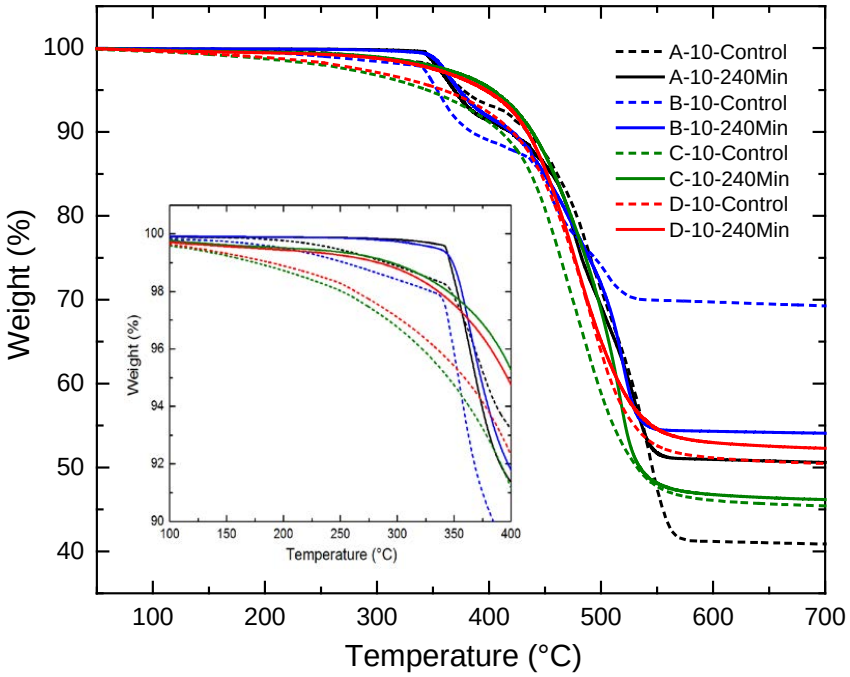

Figure 2. TGA thermograms for the investigated pristine and filled PDMS elastomer films with and without post-curing treatment. Heating rate of 10°C/min in air atmosphere. (A = RT625, B = LR3040/30, C = RT625 + 35 phr TiO_2, D = LR3040/30 + 35 phr TiO_2).

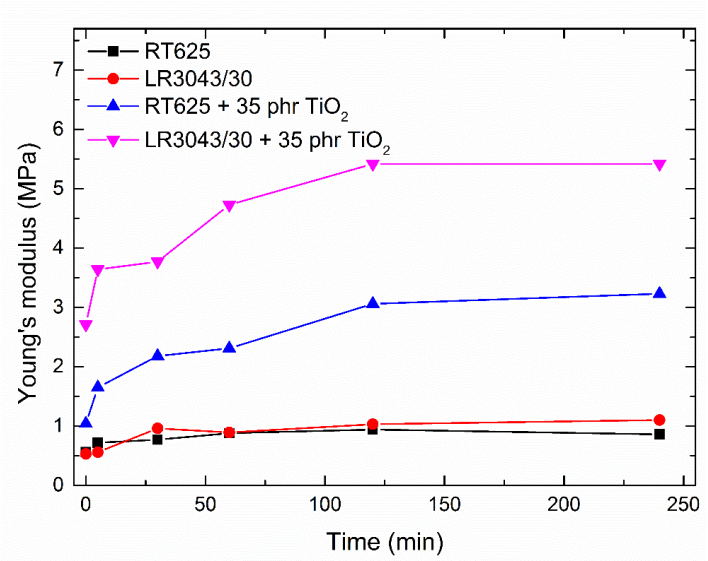

Figure 3. Young's modulus at 5% strain as a function of post-cure time.

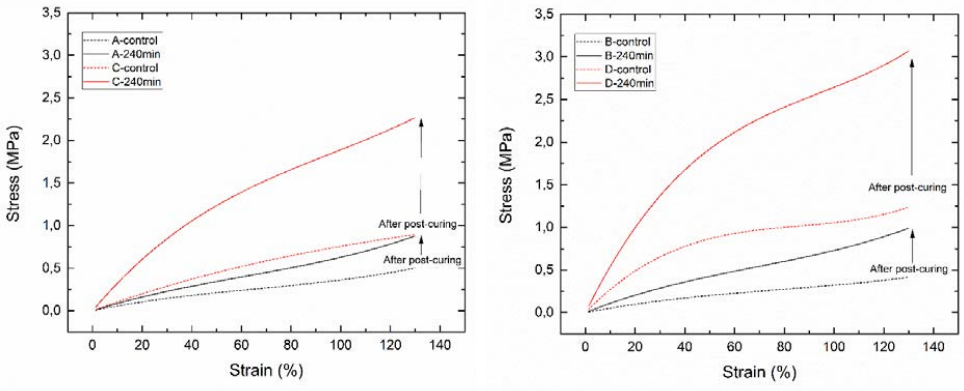

Figure 4. Stress-strain curves for left: pristine RT625 (A) and RT625 with 35 phr TiO_2 (C) and right: pristine LR3040/30 (B) and LR3040/30 with 35 phr TiO_2 (D).

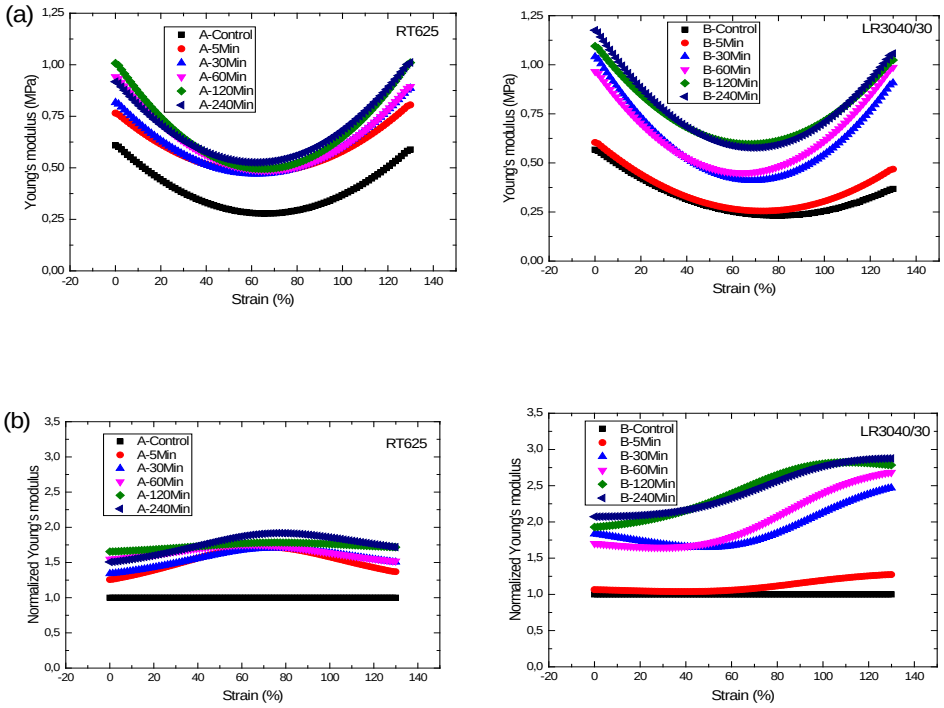

Figure 5. Young's modulus (a) and normalised Young's modulus (b) as a function of strain at different post-curing periods for the pristine PDMS films (A = RT625 and B = LR3040/30).

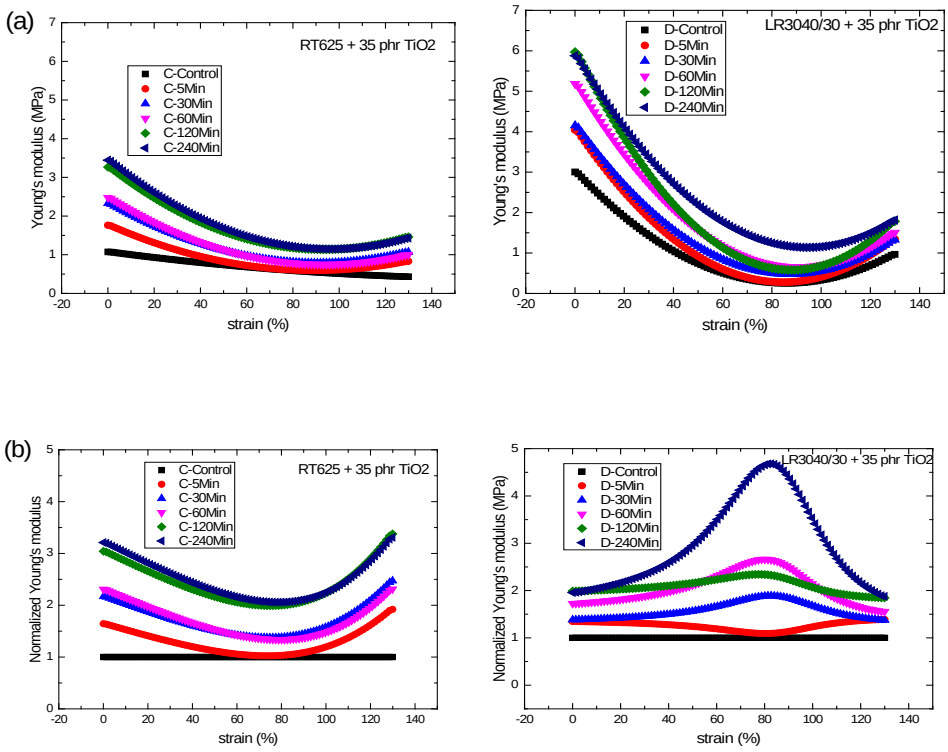

Figure 6. Young's modulus (a) and a normalised Young's modulus (b) as a function of strain at different post-curing periods for the filled PDMS films (C = RT625 + 35 phr TiO_2 and D = LR3040/30 + 35 phr TiO_2).

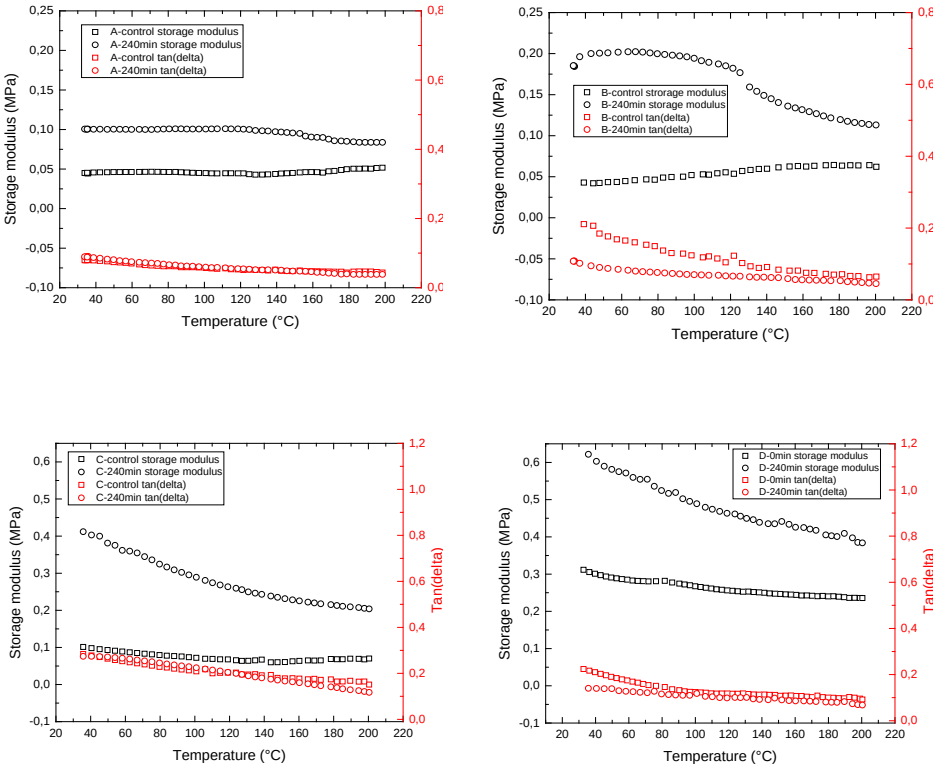

Figure 7. Storage modulus and loss (tan δ) as a function of temperature before and after 240 minutes of post-curing for (A = RT625, B = LR3040/30, C = RT625 + 35 phr TiO_2 and D = LR3040/30 + 35 phr TiO_2).

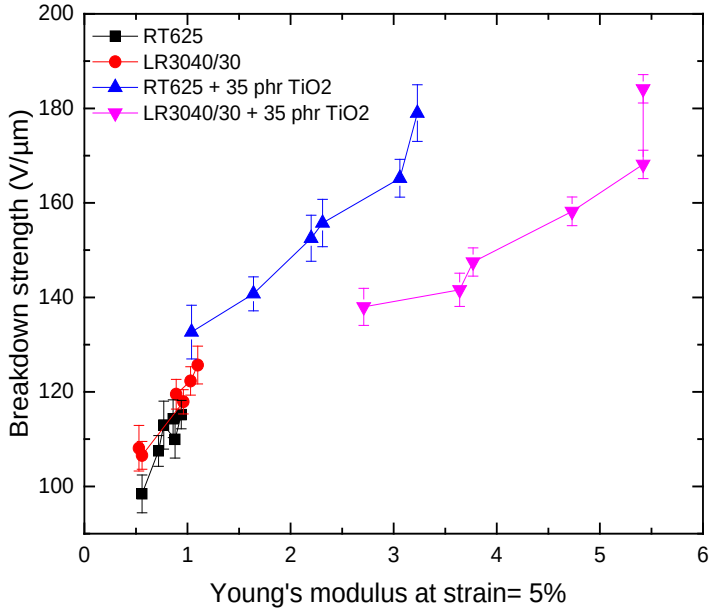

Figure 8. Breakdown strength as a function of the Young's modulus for the PDMS films. The Young's moduli for all tested samples are presented according to elevated post-curing periods at 0-control, 5 mins, 30 mins, 60 mins, 120 mins and 240 mins.

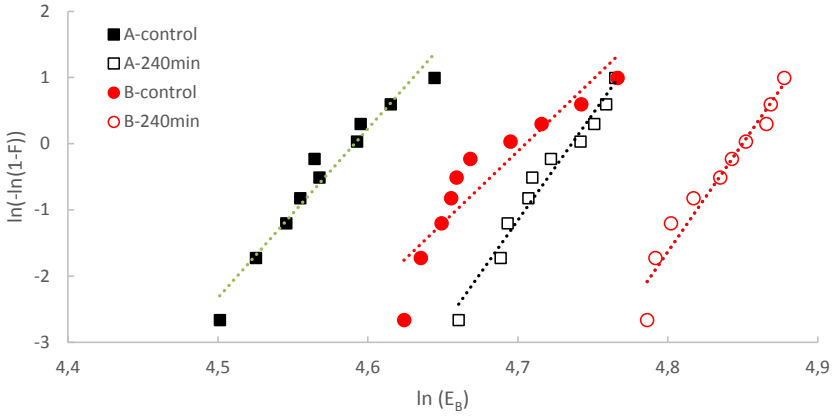

Figure 9. Cumulative probability of pristine PDMS film failure before and after post-curing (A=RT625 and B=LR3040/30).

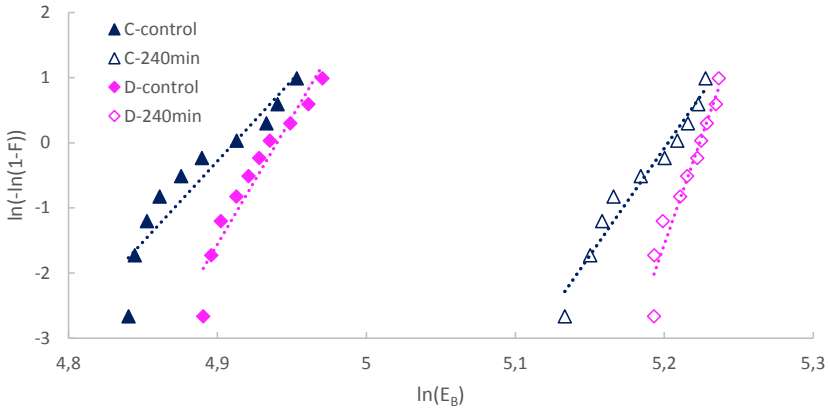

Figure 10. Cumulative probability of filled PDMS film failure before and after post-curing (A= RT625 + 35 phr TiO_2 and B= LR3040/30 + 35 phr TiO_2).

Table 1: Weight loss of PDMS elastomer films after post-curing for 5, 30, 60, 120 and 240 minutes. The weight loss of samples with TiO_2 is furthermore calculated relative to the commercial elastomer (by excluding the TiO_2 mass) for easy comparison with pure commercial elastomers.

Sample ID	**Materials**	**5 min.**		**30 min.**		**60 min.**		**120 min.**		**240 min.**	
		Loss (%)	Loss relative to elastomer matrix (excluding filler) (%)	Loss (%)	Loss relative to elastomer matrix (excluding filler) (%)	Loss (%)	Loss relative to elastomer matrix (excluding filler) (%)	Loss (%)	Loss relative to elastomer matrix (excluding filler) (%)	Loss (%)	Loss relative to elastomer matrix (excluding filler) (%)
A	RT625	0.4	0.4	0.7	0.7	1.0	1.0	1.1	1.1	1.2	1.2
B	LR3040/30	0.2	0.2	0.7	0.7	1.3	1.3	1.4	1.4	1.7	1.7
C	RT625 + 35 phr TiO_2	1.4	1.9	2.6	3.6	3.2	4.4	3.7	4.9	3.9	5.3
D	LR3040/30 + 35 phr TiO_2	1.8	2.4	2.4	3.2	2.7	3.7	3.2	4.3	3.5	4.7

Table 2: Dielectric breakdown data and Young's moduli at 5% strain for different post-cure times (A = RT625, B = LR3040/30, C = RT625 + 35 phr TiO_2, D = LR3040/30 + 35 phr TiO_2).

Sample ID	Post-cure time (min)	Breakdown strength (V/µm)	Increase in breakdown strength compared to control (%)	Thickness (µm)	Breakdown voltage (V)	Y at 5% strain (MPa)	Increase in Young's modulus compared to control (%)
A-Control	0	98±4	-	69	6791	0.56	-
A-5Min	5	107±3	9.2	69	7419	0.72	28.6
A-30Min	30	112±5	14.3	68	7683	0.77	37.5
A-60Min	60	109±4	11.2	67	7368	0.88	57.1
A-120Min	120	115±3	17.3	67	7718	0.94	67.9
A-240Min	240	114±4	16.3	66	7545	0.86	53.6
B-Control	0	108±5	-	70	7566	0.53	-
B-5Min	5	106±3	-1.9	69	7353	0.56	5.7
B-30Min	30	117±3	8.3	68	8018	0.96	81.1
B-60Min	60	119±3	10.2	68	8126	0.89	67.9
B-120Min	120	122±3	13.0	67	8195	1.03	94.3
B-240Min	240	126±4	16.7	67	8421	1.10	107.5
C-Control	0	133±6	-	53	7031	1.04	-
C-5Min	5	140±4	5.3	53	7460	1.65	58.7
C-30Min	30	152±5	14.3	53	8083	2.18	109.6
C-60Min	60	155±5	16.5	52	8098	2.31	121.2
C-120Min	120	165±4	24.1	52	8591	3.06	194.2
C-240Min	240	179±6	34.6	52	9305	3.23	210.6
D-Control	0	138±4	-	65	8911	2.71	-
D-5Min	5	141±4	2.2	65	9205	3.64	34.3
D-30Min	30	147±3	6.5	65	9586	3.77	39.1
D-60Min	60	158±3	14.5	63	9967	4.73	74.5
D-120Min	120	168±3	21.7	63	10593	5.42	100
D-240Min	240	184±3	33.3	63	11790	5.42	100

Table 2. Weibull parameters and r^2 for the control and 240-minute post-cured films.

Parameter	scale (η) (V/µm)		shape (β)		r^2	
	Before post-cure	After post-cure 240 min	Before post-cure	After post-cure 240 min	Before post-cure	After post-cure 240 min
A(RT625)	99	114	27	33	0.95	0.97
B(LR3040/30)	110	127	26	34	0.85	0.94
C(RT625 + 35 phr TiO_2)	135	182	28	34	0.88	0.96
D(LR3040/30 + 35 phr TiO_2)	140	186	42	71	0.92	0.93

Supporting Information

for *Macromol. Mater. Eng.*, DOI: 10.1002/mame.2013#####

Post-curing as an effective means of ensuring the long-term reliability of PDMS thin films for dielectric elastomer applications

Shamsul Zakaria, Frederikke Bahrt Madsen and Anne Ladegaard Skov*

Supplementary Information (SI) for Appendix E

Post-curing as an effective means of ensuring the long-term reliability of PDMS thin films for dielectric elastomer applications

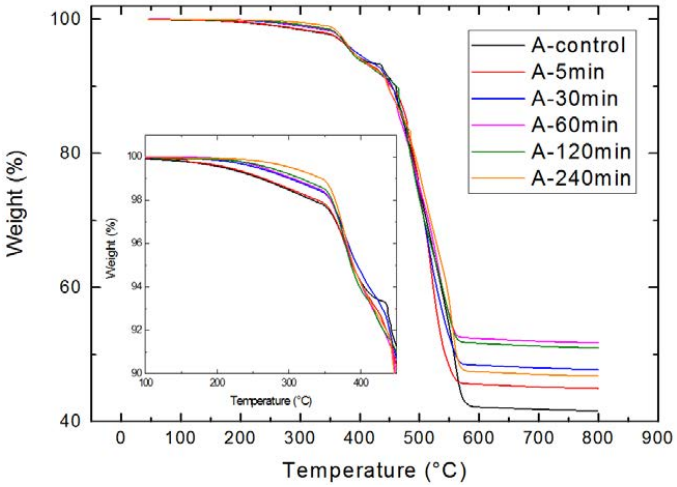

Figure S1: TGA thermograms for RT625 (A) before and after post-cure at different timespans.

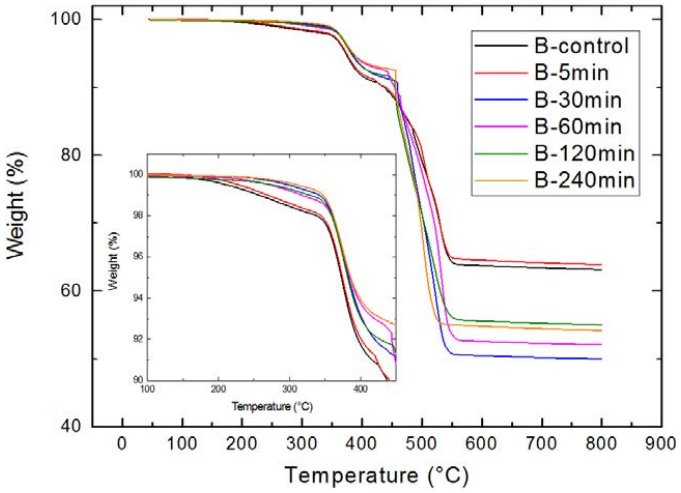

Figure S2: TGA thermograms for LR3040/30 (B) before and after post-cure at different timespans.

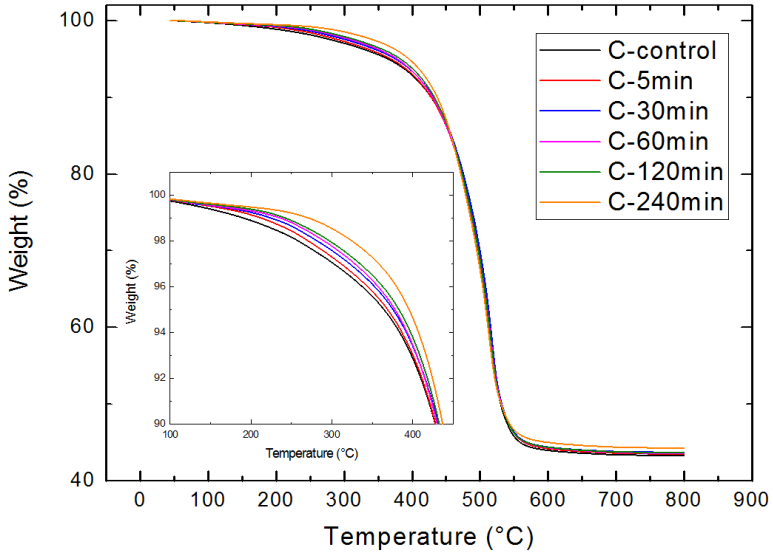

Figure S3: TGA thermograms for RT625 + 35 phr TiO_2 (C) before and after post-cure at different timespans.

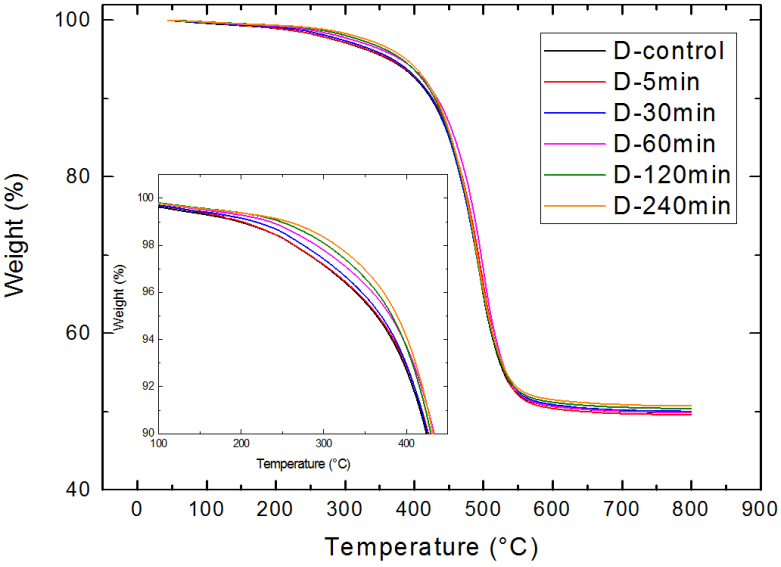

Figure S4: TGA thermograms for LR3040/50 + 35 phr TiO_2 (D) before and after post-cure at different timespans.

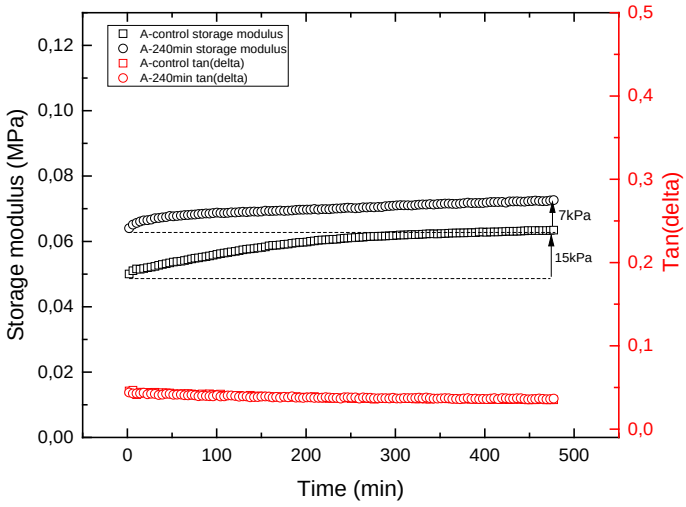

Figure S5: Storage modulus and loss (tan δ) as function of time for RT625 (A) before and after post-cure.

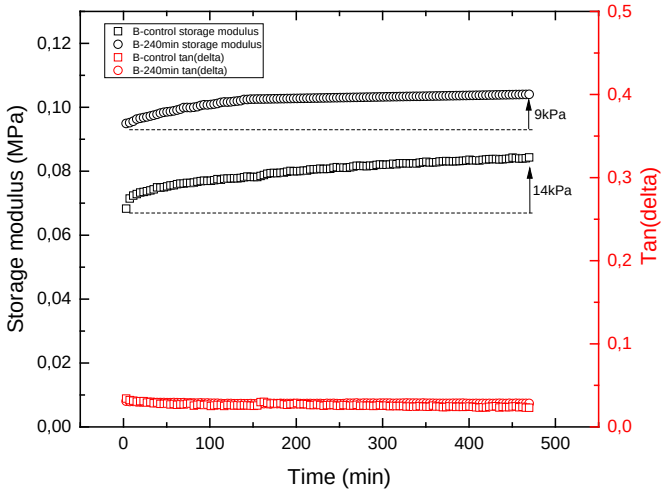

Figure S6: Storage modulus and loss (tan δ) as function of time for LR3040/30 (B) before and after post-cure.

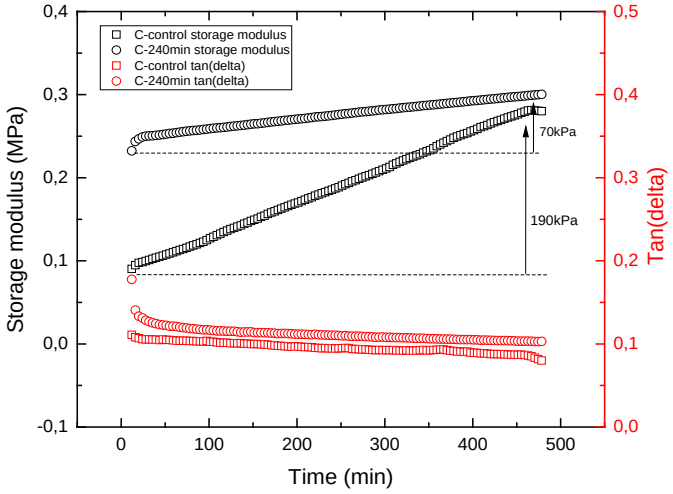

Figure S7: Storage modulus and loss (tan δ) as function of time for RT625 + 35 phr TiO_2 (C) before and after post-cure.

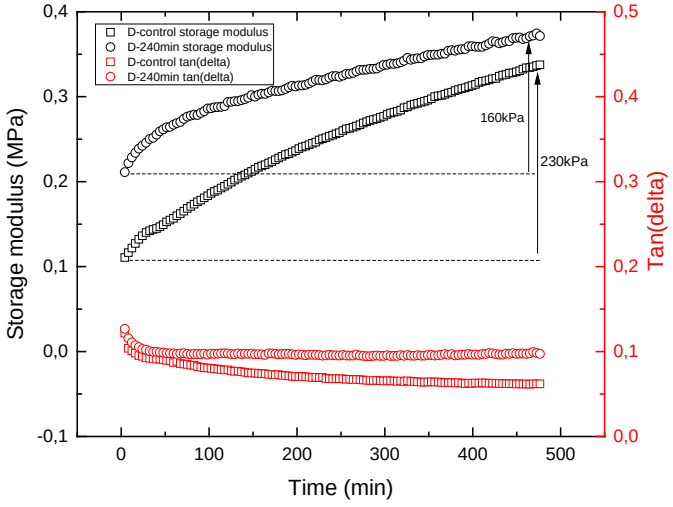

Figure S8: Storage modulus and loss (tan δ) as function of time for LR3040/30 + 35 phr TiO_2 (D) before and after post-cure.

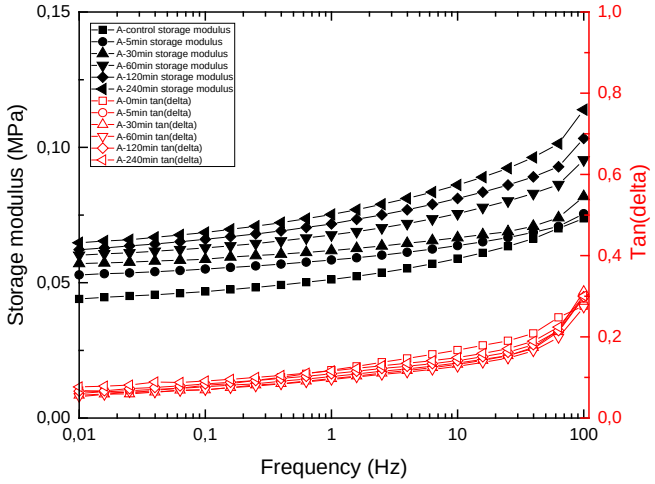

Figure S9: Storage modulus and loss (tan δ) as function of frequency for RT625 (A) before and after post-cure.

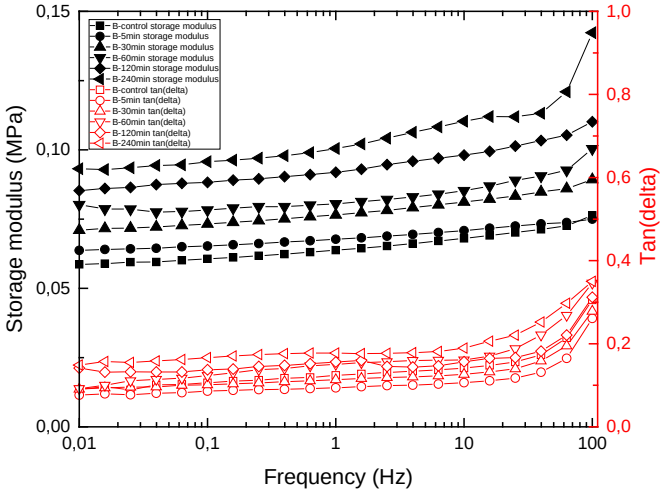

Figure S10: Storage modulus and loss (tan δ) as function of frequency for LR3040/30 (B) before and after post-cure.

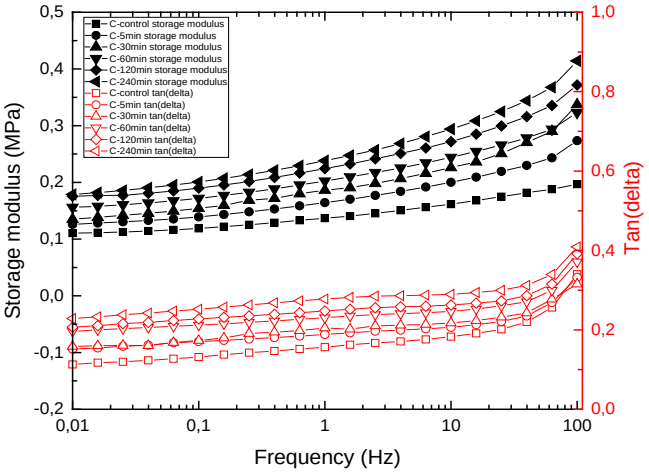

Figure S11: Storage modulus and loss (tan δ) as function of frequency for RT625 + 35 phr TiO_2 (C) before and after post-cure.

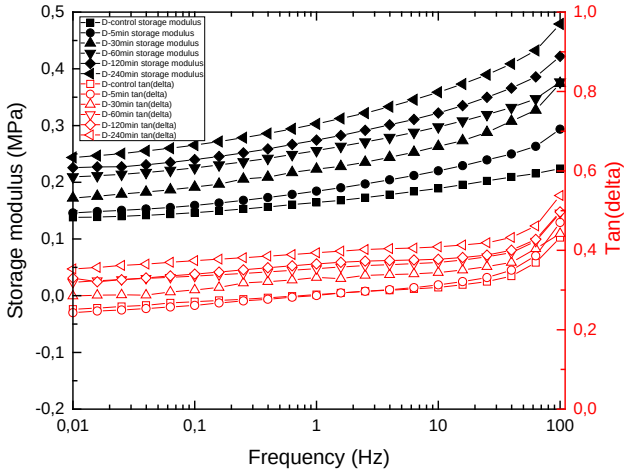

Figure S12: Storage modulus and loss (tan δ) as function of frequency for LR3040/30 + 35 phr TiO_2 (D) before and after post-cure.

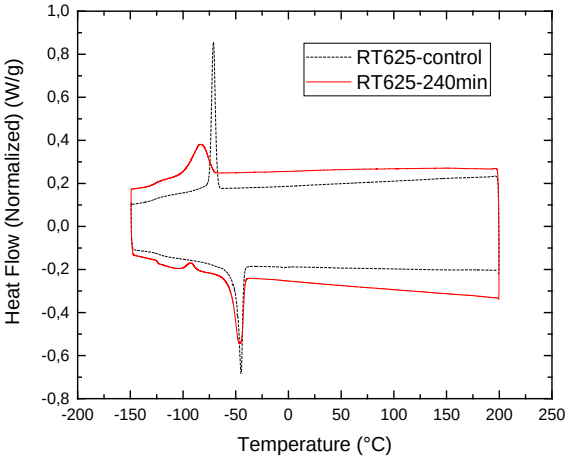

Figure S13: DSC thermograms for RT625 (A) before and after post-cure for 240 minutes.

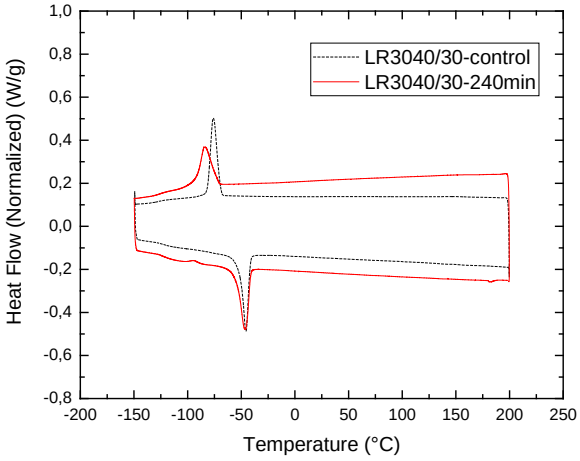

Figure S14: DSC thermograms for LR3040/30 (B) before and after post-cure for 240 minutes.

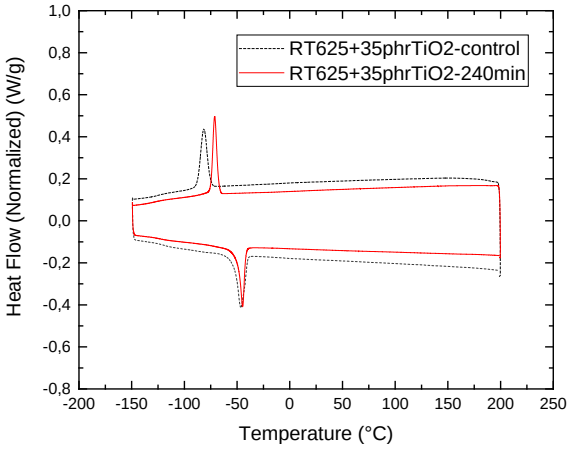

Figure S15: DSC thermograms for RT625 + 35 phr TiO_2 (C) before and after post-cure for 240 minutes.

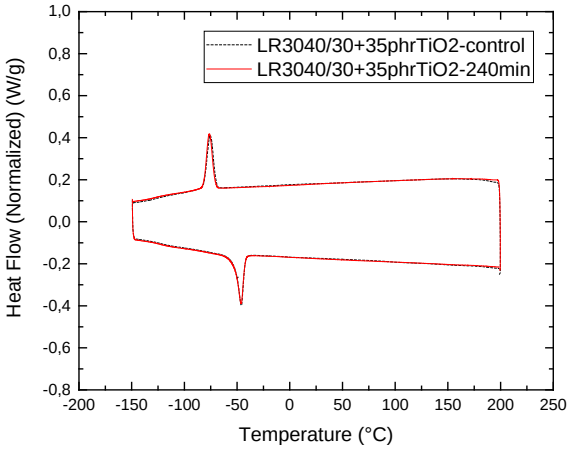

Figure S16: DSC thermograms for LR3040/30 + 35 phr TiO_2 (D) before and after post-cure for 240 minutes.

Table S1: The thicknesses and the breakdown strengths of all tested films.

	RT625 (sample A)		LR3040/30 (sample B)		RT625+35 phr TiO_2 (sample C)		LR3040/30+35 phr TiO_2 (sample D)	
Time (min)	Thickness (μm)	Breakdown strength (V/μm)	Thickness (μm)	Breakdown strength (V/μm)	Thickness (μm)	Breakdown strength (V/μm)	Thickness (μm)	Breakdown strength (V/μm)
0	69	98±4	70	108±5	53	133±6	65	138±4
5	69	107±3	69	106±3	53	140±4	65	141±4
30	68	112±5	68	117±3	53	152±5	65	147±3
60	67	109±4	68	119±3	52	155±5	63	158±3
120	67	115±3	67	122±3	52	165±4	63	168±3
240	66	114±4	67	126±4	52	179±6	63	184±3

The Danish Polymer Centre
Department of Chemical and Biochemical Engineering
Technical University of Denmark
Søltofts Plads, Building 227
DK – 2800 Kgs. Lyngby
Denmark

Phone: +45 45 25 68 01
Web: kt.dtu.dk/english/Research/DPC